Schweizerische Eidgenossenschaft
Confédération suisse
Confederazione Svizzera
Confederaziun svizra

FFG
Promoting Innovation.

Final report dated 31 May 2023

Underground Sun Conversion – Flexible Storage

USC – Flex Store

Source: ©RAG Austria AG 2021

Smart Energy Systems ERA-Net

Location: Vienna and Bern
Date: 31 May 2023

Publisher:
RAG Austria AG
Energie 360° AG

Supporting Agency Austrian Project Partners:
Austrian Research Promotion Agency FFG
Sensengasse 1, A-1090 Vienna, Austria
www.ffg.at

Supporting Agency Swiss Project Partners:
Swiss Federal Office of Energy SFOE, Energy Research and Cleantech
Pulverstrasse 13, CH-3063 Ittigen, Switzerland
www.bfe.admin.ch

Subsidy recipients:
RAG Austria AG
Schwarzenbergplatz 16, A-1010 Vienna, Austria
www.rag-austria.at/

University of Natural Resources and Life Sciences BOKU, IFA-Tulln
Konrad Lorenz Strasse 20, A-3430 Tulln, Austria
www.boku.ac.at/en/ifa-tulln

Verein WIVA P&G
Magazingasse 7, A-4020 Linz, Austria
www.wiva.at/

Energie 360° AG
Aargauerstrasse 182, CH-8010 Zurich, Switzerland
www.energie360.ch

University of Bern, Institute of Geological Sciences
Baltzerstrasse 3, CH-3012 Bern, Switzerland
www.geo.unibe.ch

Eastern Switzerland University of Applied Sciences OST, IET Institute for Energy Technology
Oberseestrasse 10, CH-8640 Rapperswil SG, Switzerland

Empa, Urban Energy Systems
Ueberlandstrasse 129, CH-8600 Dubendorf, Switzerland
www.empa.ch

Editors:
Benedikt Hasibar, RAG Austria AG, benedikt.haisbar@rag-austria.at
Daniel Sidler, Energie 360° AG, daniel.sidler@energie360.ch

Authors:
Hannes Konegger, BOKU, hannes.konegger@boku.ac.at
Andreas Loibner, BOKU, andreas.loibner@boku.ac.at
Niels Waldmann, BOKU, niels.waldmann@boku.ac.at
Artur Zaduryan, BOKU, artur.zaduryan@boku.ac.at
Maria Zeiser, BOKU, maria.zeiser@boku.ac.at
Martin Rüdisüli, Empa, martin.Ruedisueli@empa.ch
Robin Mutschler, Empa, robin.Mutschler@empa.ch
Daniel Sidler, Energie 360° AG, daniel.sidler@energie360.ch
Meret Boggiano, Energie 360° AG, meret.boggiano@energie360.ch
Andreas Kunz, Energie 360° AG, andreas.kunz@energie360.ch
Zoe Stadler, OST, zoe.stadler@ost.ch
Fiona Hauser, OST, fiona.hauser@ost.ch
Imre Antalfy, OST, imre.antalfy@ost.ch
Robin Leonhard, OST, robin.leonhard@ost.ch
Markus Pichler, RAG Austria AG, markus.pichler@rag-austria.at
Benedikt Hasibar, RAG Austria AG, benedikt.haisbar@rag-austria.at
Stephan Bauer, RAG Austria AG, stephan.bauer@rag-austria.at
Daniela B. van den Heuvel, University of Bern, daniela.vandenheuvel@geo.unibe.ch
Larryn W. Diamond, University of Bern, larryn.diamond@geo.unibe.ch
Ferdinando Musso Piantelli, University of Bern, ferdinando.musso@geo.unibe.ch
Philippos Garefalakis, University of Bern, philippos.garefalakis@geo.unibe.ch

FFG project coordinators:
Gertrud Aichberger

SFOE project coordinators:
Michael Moser, michael.moser@bfe.admin.ch
Valentin Gischig, valentin.gischig@bfe.admin.ch

FFG contract number: 879311
SFOE contract number: SI/502072-01

Zusammenfassung

Der Ausbau der erneuerbaren Stromproduktion bewirkt, dass die Produktion und die Nachfrage mit Strom bezüglich Zeit, Menge und Leistung zunehmend divergiert. Dadurch ist der Bedarf nach unterschiedlichen Energiespeicherlösungen gegeben. Die saisonale Energiespeicherung in Form von erneuerbaren Gasen wird neben den Formen für kurz- und mittelfristige Speicherbedürfnisse eine wichtige Rolle spielen. Im Kontext von Power-to-Gas kombiniert das Projekt Underground Sun Conversion - Flexible Storage erneuerbare Methanproduktion mit großvolumiger Energiespeicherung. Die dabei verwendete Geo-Methanisierung wandelt in unterirdischen Lagerstätten H_2 und CO_2 in CH_4 um. Die Ermittlung der für eine Umsetzung wichtigen Betriebsparameter auf technischer, mikrobiologischer und systemischer Ebene, sowie die konzeptionelle Einbettung in das übergeordnete Energiesystem und Infrastruktur, als auch die Anforderungen an die Geologie waren dazu zu tätigen. Im Rahmen dieses Projektes wurden die Potenziale und Möglichkeiten der Geo-Methanisierung erarbeitet und erprobt. Ein besonderer Fokus liegt dabei auf dem flexiblen Betrieb von Underground Sun Conversion, einschließlich konzeptioneller Überlegungen, der Suche nach geologisch und infrastrukturell optimalen Standorten sowie dem tatsächlichen Betrieb der Geo-Methanisierung im Feld und in begleitenden Versuchen im Labormaßstab.

In den Feldversuchen konnte die sichere Speicherung und Umwandlung von H_2 und CO_2 in einem unterirdischen Reservoir demonstriert werden. Darüber hinaus wurde eine Steigerung der Konversionsraten in Methan durch die Verwendung bestimmter Betriebsmodi erreicht. Dies wird durch Ergebnisse aus Laborexperimenten gestützt. Hier konnten die ablaufenden Reaktionen, die beteiligten Mikroorganismen und die Randbedingungen der Geo-Methanisierung näher beschrieben werden.

Variationen der Betriebsparameter führen zu unterschiedlichen Betriebskonzepten der Underground Sun Conversion. Die drei Vielversprechendsten wurden ausgeführt und im Detail betrachtet. Besonderes Augenmerk wurde dabei auf das flexible Zusammenspiel mit einem zukünftigen Energiesystem gelegt. Hinsichtlich der Einbettung der Underground Sun Conversion in dieses Umfeld zeigen verschiedene Szenarien das Potenzial sowohl für die Schweiz als auch für Österreich. Für die Schweiz wurden zahlreiche vielversprechende Standorte für die Realisierung einer Underground Sun Conversion-Anlage identifiziert, die an die notwendige Infrastruktur (erneuerbare Stromproduktion, Gasnetz, CO_2-Quelle) angeschlossen sind. Ob diese Standorte alle geologischen Kriterien erfüllen, muss durch kommerzielle Erkundungen nachgewiesen werden. Zusätzlich wurden drei Anwendungsfälle für Underground Sun Conversion – Flexible Storage entwickelt, die als Produkt- und Sektorenkopplungsdienst dienen.

Die erzielten Ergebnisse bilden die Grundlage für die Skalierung der Technologie. Mit der Kombination von Speicherung und Umwandlung im Kontext von Power-to-Gas kann Underground Sun Conversion – Flexible Storage einen wichtigen Beitrag zur saisonalen Energiespeicherung und damit zur Energiewende leisten.

<u>Wichtigste Ergebnisse:</u>

- Nachweis der sicheren unterirdischen Speicherung von H_2 und CO_2 und Optimierung des Geo-Methanisierungsprozesses
- Definition von betrieblichen Randbedingungen und Entwicklung von Anwendungen der Technologie Underground Sun Conversion
- Identifikation von explorierbaren Standorten für die Geo-Methanisierung
- Einbettung von Underground Sun Conversion – Flexible Storage in künftige Energiesystemszenarien

Résumé

Le développement de la production d'électricité renouvelable a pour conséquence une augmentation de la demande d'électricité divergent de plus en plus en termes de temps, de quantité et de puissance. Il en résulte des besoins de différentes solutions de stockage d'énergie. Le stockage saisonnier de l'énergie sous forme de gaz renouvelable devient, à part d'autres besoins de stockage à court et moyen terme. Dans le cadre du power-to-gas, le projet Underground Sun Conversion - Flexible combine la Storage associe la production de méthane renouvelable et le stockage d'énergie à grande échelle. La La géométhanisation utilisée transforme dans des réservoirs souterrains le H2 et du CO2 en CH4. Déterminer les paramètres importants pour une mise en œuvre paramètres d'exploitation au niveau technique, microbiologique et systémique, ainsi que l'intégration conceptuelle dans le système énergétique général et les infrastructure, ainsi que les exigences en matière de géologie est fait. Dans le cadre de ce projet, les potentiels et les possibilités de la géométhanisation ont été élaborées et testées. Une attention particulière a été portée à la flexibilité des operation de l'Underground Sun Conversion - Flexible Storage, y compris les considérations conceptuelles, la localisation de sites géologiquement et optimale en termes d'infrastructures, ainsi que les opérations réelles de géométhanisation dans le terrain et lors d'essais d'accompagnement à l'échelle du laboratoire.

Les tests réalisés sur cette installation ont permis de démontrer la sécurité du stockage et de la conversion de H_2 et de CO_2 dans un réservoir souterrain, en reproduisant les conditions réelles à grande échelle. De plus, l'utilisation de certains modes d'exploitation a permis d'obtenir une augmentation des taux de conversion en méthane. Ceci est étayé par les résultats d'expériences en laboratoire. Les réactions qui se produisent, les micro-organismes impliqués et les conditions marginales de la géo-méthanisation ont pu y être décrits plus en détail. Des concepts d'installations interagissant avec des installations aériennes et souterraines ont été développés, et les trois plus prometteurs ont été examinés en détail. Une attention particulière a été accordée à la flexibilité de l'interaction avec un futur système énergétique. En ce qui concerne l'intégration de la géo-méthanisation dans le futur système énergétique, différents scénarios de système montrent le potentiel aussi bien pour la Suisse que pour l'Autriche. Pour la Suisse, de nombreux sites prometteurs ont été identifiés pour la mise en œuvre d'une installation souterraine de conversion solaire, qui sont accessibles à l'infrastructure nécessaire (production d'électricité renouvelable, réseau de gaz, source de CO_2). La question de savoir si ces sites remplissent tous les critères géologiques doit être prouvée par une exploration commerciale. De plus, trois cas d'application pour l'Underground Sun Conversion – Flexible Storage ont été développés afin de démontrer de manière exemplaire le potentiel des produits et des services, notamment dans le domaine du couplage sectoriel.

Les résultats obtenus constituent la base de la mise à l'échelle de la technologie. En combinant le stockage et la conversion dans le cadre du Power to Gas, l'Underground Sun Conversion – Flexible Storage peut apporter une contribution importante au stockage saisonnier de l'énergie et donc à la transition énergétique.

Principaux résultats :

- Démonstration de la sécurité du stockage souterrain de H_2 et de CO_2 et optimisation du processus de géo-méthanisation.
- Définition des conditions limites d'exploitation et développement des applications de la technologie d'Underground Sun Conversion
- Identification de sites explorable pour géo-méthanisation.
- Intégration d'Underground Sun Conversion dans les scénarios des systèmes énergétiques futurs.

Summary

Seasonal energy storage in forms of renewable gases will play an important role in future energy systems. As the expansion of renewable electricity production means that production and demand do not coincide sufficiently in terms of time, amplitude and magnitude, the need for different energy storage solutions is given. Besides short-term energy storage, seasonal storage of energy in forms of gas will play an important role. In the context of Power-to-Gas, Underground Sun Conversion - Flexible Storage combines renewable methane production with large-scale underground energy storage. The used process of geo-methanation describes the conversion of H_2 and CO_2 to CH_4 in underground reservoirs. In order to enable implementation on a commercial scale, some topics need to be further addressed. These concern operating parameters at the technical, microbiological, and systemic level as well as the embedding in the higher-level energy system, the underlying geology, and the associated infrastructure. In the course of this project the potential and possibilities for Underground Sun Conversion were elaborated and tested. A special focus is set on the flexible operation of an Underground Sun Conversion system, including conceptional considerations, the search for optimal locations in terms of geology and infrastructure as well as the actual operation of geo-methanation in field, accompanied by laboratory-scale research.

In the field tests, the safe storage and conversion of H_2 and CO_2 in an underground reservoir was demonstrated. In addition, an increase in conversion rates was achieved through the use of certain operation modes. This is supported by results from laboratory experiments. Here, the reactions taking place, the microorganisms involved, and the boundary conditions of geo-methanation could be further described.

Variations in the operating parameters result in different operation concepts of Underground Sun Conversion. The three most promising ones were developed and considered in detail. Particular emphasis was placed on their flexible interaction with a future energy system. Regarding the embedding of Underground Sun Conversion into this environment, different system scenarios show the potential for Switzerland as well as for Austria. For Switzerland, numerous promising locations for the implementation of an Underground Sun Conversion facility were identified, which are accessible to the necessary infrastructure (renewable electricity production, gas network, CO_2 source). Whether these sites fulfil all geological criteria needs to be proven by commercial exploration. Additionally, three use cases for Underground Sun Conversion – Flexible Storage were developed, serving as product and sector coupling service.

The results obtained will form the basis for scaling the technology. With the combination of storage and conversion in the context of Power-to-Gas, Underground Sun Conversion – Flexible Storage can make an important contribution to seasonal energy storage and thus to the energy transition.

Main findings:

- Demonstration of safe underground storage of H_2 and CO_2 and optimization of the geo-methanation process
- Definition of operational boundary conditions and development of applications of the Underground Sun Conversion technology
- Identification of explorable locations for geo-methanation in Switzerland
- Embedding Underground Sun Conversion in future energy system scenarios

Table of Content

1 Introduction

1.1 Background information and current situation

Interseasonal Energy Storage is increasing in its anticipated importance for the energy-supply-system for Europe. Concerning electricity, the Federal Electricity Commission (ElCom) for instance, raises concerns regarding increasing import risks. Within its report, ElCom strongly recommends to not to exceed yearly electricity imports of ten (10) TWh. This is due to a foreseen increase of imports in all of Switzerland's neighboring countries at similar times as Switzerland would need to (*ElCom*, 2021), which hints at the scale of the problem in the heart of Europe and its transmission system.

While electricity and scarcity thereof in especially winters to come, the demand for renewable gas is increasing rapidly. Austria is as of this year demanding a domestic production of renewable gas in the year 2030 of 7.5 Terrawatthours. The corresponding legislative procedures are ongoing at the time of writing this report. The fact, that there are discussions of this kind at all, and that the proposal of the government is including a quota with sanctions for utilities who miss those, speaks at the same time for an increasing demand for renewable gas as a mean to decarbonize economies.

During the course of this project, the seemingly given implicitness of secure, stable and cheap energy supply has been shaken in our societies. Energy, as the year of 2022 has clearly demonstrated, is not merely a vital commodity for the functioning of economies, but rather a prerequisite for stable political and societal environments within industrialized nations and unions.

Energy storage with the ability to store large amounts of energy over a timespan of at least months therefore does have a strategical value. This strategic viewpoint was evaluated in the present project, the implications and possibilities of the outlined possibilities are nevertheless inescapably to be drawn. What is researched though, is the potential for the generation of renewable gas by giving an estimation on the surplus of electricity, compared to the deficits at other times of this supply.

1.2 Purpose of the project

The project aims to explore an inter-seasonal energy storage technology for its potentials and limitations. By doing so, the project embeds the technology as an option in a socio-economic and political frame in order to contribute to a sustainable, reliable and secure energy future relying on renewable production.

Converting excess power in H_2, adding CO_2, storing the two feed gases and converting those to methane while in an underground storage, geo-methanation may contribute to this goal. Given its large scale of storage area, boundary conditions are examined as well as the future need from the energy system's standpoint. The geological potential for underground storage outside of depleted gas-fields is researched by screening the geology of Switzerland. As no technology will be able to be implemented without a positive economic outlook, these aspects are covered as well with a focus on entirely new storages.

Working through a feedback loop in between of Austrian and Swiss partners, models and operation-modes of the test facilities were adapted to the indicated boundaries of flexibility regarding feed-gas-ratios, pressures, and temperatures.

Together with the need owners, the systemic potential and projected shortcomings, and the economic feasibility of a large-scale application of the technology is examined. This includes ongoing talks with the respective organizations responsible for certifying the produced renewable gas on the test-side and the common understanding for the requirements to trade these certificates independently of the underlying commodity across borders and registries. Social, legal, and regulative acceptance of such a process is examined with Switzerland in mind and backed by practical experiences in Austria.

1.3 Objectives

In preparation of the project, the tasks and their respective objectives were assigned to work packages. In addition, deliverables were scheduled and KPI defined where appropriate. Those objectives were reached in quality and time. This report is a mean to disseminate the achieved knowledge and results and represents a condensed form of the common work, the necessary iterations in between of all partners and plausibility checks in the field and across the project. The KPI and a summary on conclusions and findings can be found in chapter 7.

In short, the objectives of the project can be stated as follows:

- Define cautionary boundary conditions of the metagenomic microbiome and its adaption then exposed to different reservoir conditions and gas compositions;
- Specify simulation-requirements, operations-concepts and establish operational flexibility while replicating findings on the test facility;
- Estimation of costs for a green-field installation for geo-methanation, while defining use cases for need owners for inter-seasonal storage;
- Determine potential and needs for inter-seasonal storage in Switzerland compared to Austria, map inputs for geo-methanation over time and locations;
- Locate potential storage sites in Switzerland and estimate exploration costs.

2 Investigation on microbial activities during Geo-Methanation

2.1 Introduction

2.1.1 Overview on the microbial potential in natural gas storages

Natural gas in underground gas reservoirs has formed either via thermogenic or biogenic processes. The USC-FlexStore project investigates the potential of traditional and newly established natural gas storages for the sustainable production of renewable methane in a circular economy framework. It may be assumed, that the respective microbes responsible for the production of methane are contained in such reservoirs and hence be accessible as inducible biocatalysts.

Based on molecular methods such as 16S rRNA gene analyses (Woese and Fox, 1977), the impressive microbial biodiversity in reservoir brine originating from unaffected underground gas reservoirs has previously been described (Kimura et al., 2010). For the purpose of description, the resolved microbial community contained in the reservoir brine collected from the scientific field test facility (SFTF) in Lehen is depicted in figure 2-1 and forms the basis for a subsequent description of the key metabolic processes and microbes involved in geo-methanation.

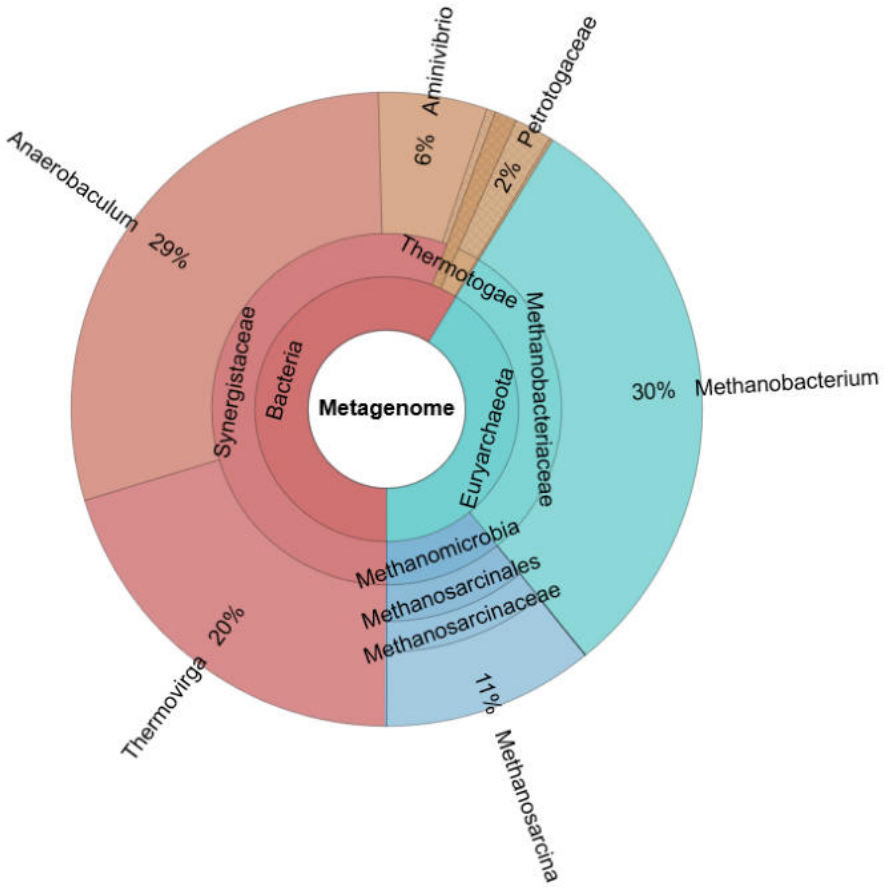

Figure 2-1: Most abundant microbial genera occurring in formation water of the SFTF in Lehen prior to the start of the USC-FlexStore project as determined via Illumina's MiSeq DNA sequencing and bioinformatic analysis of the 16S rRNA gene. The taxonomic profile is based on 114.559 quality filtered and merged sequencing reads.

2.1.2 Archaea

Of central interest for geo-methanation are archaea, one of the three domains of life as introduced by the pioneering work Carl Richard Woese (Woese and Fox, 1977). All known methanogens to date belong to the phylum of Euryarchaeota, which further can be subdivided into more phylogenetic taxa. The initial microbial consortium in the SFTF was particularly enriched, up to 41% of all detected taxa, in the anaerobic genera *Methanobacterium* and *Methanosarcina*, both known for the generation of methane (Thauer et al., 2008).
Species belonging to the genus *Methanobacterium* convert both hydrogen (H_2) and carbon dioxide (CO_2) to methane and use this reaction as their main source of metabolic energy. This biochemical pathway is called **hydrogenotrophic methanogenesis (HM)** and is given in equation 2-1.

Equation 2-1: Hydrogenotrophic methanogenesis (HM): $CO_2 + 4\ H_2 \rightarrow CH_4 + 2\ H_2O$; $\Delta G^{o'} = -131$ kJ/mol

Members of the genus *Methanosarcina* are more versatile in terms of their methanogenic substrate spectrum and have previously been reported as the dominating methanogens contributing most to global microbial methane production. For instance, *Methanosarcina barkeri* may utilize CO_2 and H_2, methanol, methylamines and/or acetate to generate CH_4. However, this versatility comes at a cost of higher maintenance expenses (e.g., for the replication of the bigger genome in comparison to *Methanobacterium* species) and hence arising disadvantages in specific selective environments: It may be speculated at this point, that *Methanobacterium sp.* may outcompete *Methanosarcina sp.* when being fed high quantities of both H_2 and CO_2. Two alternative methanogenic reactions of *Methanosarcina* are summarized in equation 2-2 and 2-3, namely **acetoclastic (AM) and methylotrophic methanogenesis (MM)**, respectively (Kurth et al., 2020).

Equation 2-2: Acetoclastic methanogenesis (AM): $CH_3COO^- + H^+ \rightarrow CH_4 + CO_2$; $\Delta G^{o'} = -36$ kJ/mol
Equation 2-3: Methylotrophic methanogenesis (MM): $4\ CH_3OH \rightarrow CO_2 + 3\ CH_4 + 2\ H_2O$; $\Delta G^{o'} = -107$ kJ/mol

Methanogenic archaea prefer to grow at neutral to slightly alkaline pH values in a wide range of different temperature regimes. Several physiological and ecological aspects were previously investigated in the context of anaerobic digestion and biogas applications, which delivered valuable information for the implementation of a Geo-Methanation process. Most notably, it was reported that volatile fatty acids (VFAs) such as acetate, butyrate or propionate inhibit methanogenesis (Wang et al., 2009).

2.1.3 Bacteria

The remaining 59% of all detected taxa could be assigned to the domain of bacteria. As with archaea, bacteria are extremely divers in terms of their metabolisms and may conduct a huge variety of different reactions to generate energy.
Since geo-methanation primarily interferes with the local carbon pool in underground gas storages, the following paragraph will focus on the respective microbial pathways involved with the cycling of carbon. As a starting point, another chemolithotrophic, derived from the Greek terms 'lithos' (rock) and 'troph' (consumer), pathway may be highlighted.
Homo-acetogenesis requires both H_2 and CO_2 to produce acetate (CH_3COO^-), which may serve as a building block for cellular growth or potentially for the synthesis of more complex organic molecules in a process called chain elongation. The generation of acetate is catalyzed by certain anaerobic acetogenic bacteria, typically belonging to the genera *Acetobacterium* or *Morella* (Steger et al., 2017). In comparison to methanogenic archaea, homo-acetogens tend to thrive at lower pH values and seem to tolerate higher concentrations of VFAs such as acetate. As apparent from the chemical reaction

equation given in equation 2-4, a direct competition with hydrogenotrophic methanogens for the gaseous substrates CO_2 and H_2 becomes obvious.

Equation 2-4: $2\ CO_2 + 4\ H_2 \rightarrow CH_3COO^- + H^+ + 2\ H_2O;\ \Delta G^{o'} = -95$ kJ/mol

A quick comparison of the tabulated thermodynamic yields of both hydrogenotrophic methanogenesis and homo-acetogenesis as determined by the standard Gibbs free energy at physiological conditions ($\Delta G^{o'}$) indicates a slight energetic advantage for hydrogenotrophic methanogenesis. The competitive character of both previously mentioned reaction pathways (Kotsyurbenko et al., 2001) will be further elucidated in the upcoming section describing the outcomes of the conducted reactor experiments.

The majority of bacteria detected prior to the start of the field test trial belong to the genus of *Anaerobaculum*, which has recently been reclassified to *Acetomicrobium* (Hania et al., 2016). As indicated by the higher-level taxonomic assignment to the family of *Synergistaceae*, these bacteria synergistically interact with other microbes in order to propagate. Most notably, *Acetomicrobium* has been described to be proficient of **Syntrophic Acetate Oxidation (SAO)**, a biochemical pathway which converts acetate to H_2 and CO_2. The reaction equation is given in equation 2-5:

Equation 2-5: $CH_3COO^- + H^+ + 2\ H_2O \rightarrow 2\ CO_2 + 4\ H_2;\ \Delta G^{o'} = +95$ kJ/mol

This process can be considered as 'reverse homo-acetogenesis' and requires an external source of energy for the reaction to occur. As commonly occurring in biochemistry, the required Gibbs free energy gets supplied via coupling to another, more energy-yielding reaction. Indeed, syntrophic associations between SAO-bacteria and hydrogenotrophic methanogens have been reported earlier at specific environmental conditions (Schnuerer et al., 1999). This type of associations will be referred to as **SAO-HM**. From this perspective it may be emphasized that the generation of acetate (according to equation 2-4) in underground gas storages is no energetic dead end, but that microbes of both domains of life are competent re-utilize acetate towards methane (as outlined in equation 2-2 and 2-5).

Prior to the start of the field test of USC-FlexStore another anaerobic bacterial genus, namely *Thermovirga*, was richly abundant. This genus has been associated with sulfur reduction and alternative fermentative pathways and might have enriched due to the most recent history of the underground gas reservoir. Previously, the same reservoir has been exposed to limited amounts of both H_2 and CO_2 within the framework of the predecessor FFG project Underground Sun Conversion. Minimal concentrations of hydrogen sulfide could be detected in the produced gas at the beginning of the field trial, which steadily declined in later phases of the trial. Throughout USC-FlexStore, hydrogen sulfide production further ceased, which may be explained on basis of depleted sulfur or sulfate sources in the formation (see chapter 3.2.2). Two upcoming publications will further investigate the extent of sulfur metabolism and other aforementioned metabolic pathways by the means of comparative metagenomic data analysis.

2.1.4 Outline of activities

The work focus of partner BOKU during the first project year revolved around revisiting insights linked to experiments of the predecessor FFG flagship project Underground Sun Conversion (USC), the collection of field data and samples from the scientific field test facility (SFTF) in Lehen plus other reservoirs, as well as the setup and conduction of high-pressure reactor experiments.

Due to apparently slow gas conversion rates in the SFTF at the beginning of the project, a thorough literature study was anticipated to identify potential factors limiting the observed *in situ* geo-methanation potential. Previous and most recent field data was evaluated and brought into context with laboratory experiments of the USC project to provide a recommended course of action for the activities outlined in the chapter 'geo-methanation. The further progression of the field trial was monitored at a short interval, confirming a steady and considerable increase of microbial activity as quantified via ATP measurements in the well 'LESP-001A' of the SFTF at the end of the first project year.

Formation water samples from the ongoing field experiment could be collected during five independent sampling events throughout the project to provide the basis for realizing milestone A, namely the establishment of a methanogenic consortium, which has been adapted to off-stoichiometric gas mixtures. Hydrochemical and molecular-biological analyses of the water samples were conducted, and ultimately selected reservoir brines were used as inocula for two major series of reactor experiments.

Considerable efforts were taken to adapt and improve the preexisting high-pressure bioreactor infrastructure, in particular the Confined Core Reactors (CCR), which were central to more realistic geo-methanation experiments involving non-stoichiometric gas mixtures applied close to reservoir conditions. Thermic treatment and subsequent washing steps were carried out to minimize and control viable biomass in the reactors prior to the inoculation with reservoir brine of the 'Nussdorf-W-002' well. This particular reservoir brine was selected for inoculation of the CCR to mitigate a potential risk of process failure due to high concentrations of VFAs in the reservoir brine of the SFTF by that time. Subsequently, the microbial community was exposed to substrate gas to initiate the adaptation towards *in vitro* geo-methanation. The adaptation phase, hence the establishment of a methanogenic microbial consortium, was finished by January 2022. Subsequently, extensive experimental geo-methanation series were started involving both stoichiometric and non-stoichiometric gas mixtures. A continuous enhancement of methanogenic activities could be observed and data for the computation of reaction rates for two formation water samples from two different wells, 'Nussdorf-W-002' and 'LESP-001-A', was collected. Methanogenic reaction rates at optimal conditions were reported to the project consortium in March 2023.

Furthermore, *in silico* sequence simulations were conducted and interpreted to select for optimal sequencing techniques to be used in the metagenomic sequencing campaign of two selected reactor experiments. DNA extraction methods were reassessed and optimized to provide sufficient material for shotgun metagenomic sequencing. The analysis and interpretation of metagenomic data is highly complicated and thorough reporting of the results will occur in the framework of two scientific articles. Extra efforts were invested to develop a molecular assay based on quantitative PCR involving two selected functional markers, to approximate the biochemical potential of the microbial community for methanogenesis and acetogenesis. This method may be applied as a timely and low-cost monitoring tool to assess the current state of the observed geo-methanation system.

2.2 Materials, Methods

2.2.1 Sampling of formation brine

We presume that reservoir brine accumulating in the wellbore tubing constitutes a representative sample of water from the respective sandstone formation. Brine was sampled in collaboration with RAG Austria AG and RED Drilling & Services GmbH using a customized bailer (4.42 meters length, 2.5 L volume), which was cleaned with pressurized steam and decontaminated with 70% ethanol. After two minutes of exposure time to ethanol, the bailer was washed with sterile ultra-pure water and eventually flushed with Argon (purity 5.0, Messer Austria) prior to running it into the well. Brine withdrawn from the reservoir was then transferred to autoclaved gas tight glass bottles (Pyrex®) filled with Argon. All manipulations of sampled reservoir brine were carried out under aseptic and anaerobic (oxygen-free atmosphere) conditions. Hydrochemical measurements were conducted at the sampling site, namely pH, EC (electrical conductivity) and ATP measurements (2nd Generation ATP® Testing, LuminUltra Technologies Ltd., Canada) to proxy for microbial activity. Samples for DNA extraction, TC and HPLC were processed at the laboratory in Tulln upon arrival. All withdrawn samples were cooled down to 4 °C and stored in the dark until further usage.
In total, five sampling events at the SFTF 'LESP-001A' as well as 'LEH-002' in Lehen (April, June and September 2021, March and October 2022) and two sampling events at an unaffected observation well 'Nussdorf-W-002' (April 2021 and October 2022) were realized. Two further sampling events took place at two different sites, investigating the microbial composition of underground gas and oil storages from a more general perspective.

2.2.2 Substrate Gas Mixtures

Gas mixtures and pure gases were provided by Messer Austria GmbH. The custom-made gas mixtures were ordered in “Labline” quality and were certified according to ISO 6141:2015 “Gas analysis - Contents of certificates for calibration gas mixtures” by the manufacturer. Argon 5.0 high purity gas was used for reactor purging and leakage testing. The addition “5.0” denotes a purity of 99.999 Vol.% and was necessary to provide anoxic conditions for the experiments. In the following, the simple abbreviation “Argon” is used for the high purity argon gas.
Four different feed gases were used and are listed in table 2-1. Pressure values are described either in bar(a), defining absolute pressures or bar(g), defining relative gauge pressure respectively.

Table 2-1: Used gas mixtures in Messer Austria GmbH “Labline” quality (purity ‘5.0’) and corresponding gas certificates, ± 2% relative deviation.

		[% v/v]		
H_2 target	**H_2 actual**	**CO_2 target**	**CO_2 actual**	**Carrier gas**
10.0	9.6	0.5	0.5	Argon
10.0	10.0	2.5	2.5	Argon
40.0	40.3	10.0	10.0	Argon
80.0	80.0	20.0	20.0	-

2.2.3 Wellbore Simulation Reactors (WSR)

This simplified reactor system was employed to understand the fundamental principles of geo-methanation and to further inform later experimental designs applied to the more comprehensive CCR system which mimics reservoir conditions in a more realistic way. Therefore, only reservoir brine originating from the unaffected observation well ‘Nussdorf-W-002’ without additional rock material was introduced to the WSR and gas conversion experiments started for the screening of most optimal process conditions and the identification of critical boundaries.
Two WSR were engineered by MAL Metallbau GmbH Austria and manufactured by S.K.M. GmbH Austria. To withstand potential corrosion, an austenitic steel alloy (1.4571 – X6CrNiMoTi17-12-2, AISI 316Ti) and a rubber Viton seal (75° shore, Neotecha GmbH) were used. The reactors were specified to a maximum operating pressure of 26 bar(g) and temperature of 45 °C. The total internal volume per reactor was calculated to 1.2 L with an inner diameter of 101 mm and height of 140 mm. A schematic technical drawing of a WSR can be seen in the following figure 2-2.

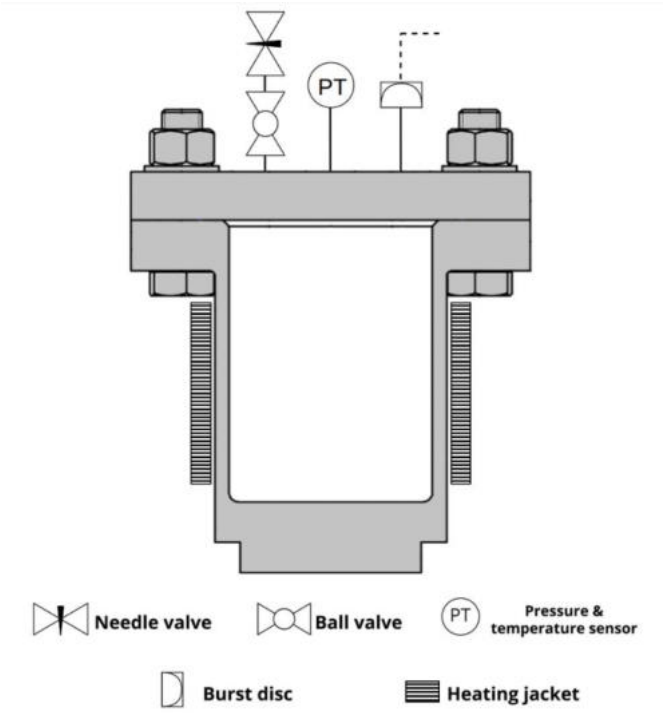

Figure 2-2: Sketch of the mini reactor with installed sensors, valves, bursting disc and heating jacket. TÜV Austria approval was renewed in February 2022, assuring that the system is safe to operate at the conditions specified.

Both reactors were equipped with a digital PA-33 X combined temperature and pressure sensor (KELLER AG, Winterthur, Switzerland) directly connected into each top flange lid via a G ¼" port. The measuring pressure range was 0 – 100 bar(g) and temperature range of -10 °C to 80 °C with an accuracy of ± 0.1% FS (Full Scale). The reactors were heated with custom made heating sleeves (Mikanitheizband 114 mm, 50 W) made by "carlo" Loysch GmbH Austria. For insulation, two layers of sheep wool (DAEMWOOL, Naturdämmstoffe GmbH & Co KG) and a housing made from XPS (extruded polystyrene foam) boards (Austrotherm GmbH) were used.
The **digital control and data logging** unit was set up in house and comprised a CompactLogix, 16DI, 16DO, 24VDC PS and CompactLogix ASCII Interface Modul (Routeco GesmbH, Austria). The PLC (programmable logic controller) was coded in "RS Logix" and further connected to "FactoryTalk" (Rockwell Automation) for data logging and visualization.
For sampling and feeding operation the reactors were equipped with a ball valve (HOKE® GYROLOK® 7122G6YMM, Crane Holdings, Co) followed by a needle valve (HOKE® GYROLOK® 1711G6YMM, Crane Holdings, Co) on top. Both valves as well as all connectors were made from high-quality steel (AISI 316) and were mounted into the second G ¼" port. A bursting disc with an opening pressure of 38.5 bar(g) at 47 °C (Type B18r35-01, Berstscheiben Schlesinger GmbH, Austria) was installed in the G ½" port and connected to an off-gas line to comply to legal safety regulations.

2.2.4 Confined Core Reactors (CCR)

One important characteristic of the Confined Core Reactor (CCR) system, in comparison to the previously described WSR, is the installed porous rock core which should resemble the gas carrying rock encountered in a natural gas reservoir. The one-meter long rock cores were tailored to fit into the reactor casing to leave a minimum of remaining vacant gas volume. Since different gas components exhibit different diffusion patterns in water-saturated porous rocks (Bauer, 2021), a gas-tight sealing was applied at the lateral surface of the porous core matrix and the outlet side of the CCR to account for arising concentration differences along the horizontal axis of the reactor.

Gray Berea sandstone, which is widely used for scientific applications in the oil and gas industry, was selected for the mounting into the CCR. Berea consists mainly of quartz and comparably small shares of calcite (as shown in table 2-2), with an average gas permeability of 200 – 315 mD, a brine permeability of 60 – 10 mD and a porosity of 19 – 21 %, as specified by Kocurek Industries, USA. Considering a homogenous porosity of 20%, the calculated free pore volume of approximately 1.6 L (diameter = 101 mm, length = 1002 mm) allowed for an adequate volume for both gas and liquid samplings.

Table 2-2: Mineralogical composition of Grey Berea sandstone as specified by Kocurek Industries.

[wt%]	Quartz	Albite	Calcite	Dolomite	Hermatite	Kaolinite	Illite	Chlorite	Total clay	Accessory minerals
Gray Berea	87	3	2	0	0	6	2	0	8	No data

The dimensions of the CCR were defined according to the length and diameter of the acquired Berea sandstone cores. The reactors were designed by MAL Metallbau GmbH Austria with an inner diameter of 101 mm, a length of 1002 mm (final internal reactor volume of 9 L) and manufactured by S.K.M. GmbH Austria from high-quality stainless-steel alloy (1.4571 – X6CrNiMoTi17-12-2, AISI 316Ti). Sealing rings for both flanges were made from Viton (75° shore, Neotecha GmbH). The maximum pressure and temperature for each CCR was specified with 50 bar(g) and 50 °C, respectively. A schematic technical drawing of a CCR can be seen in the following figure 2-3.

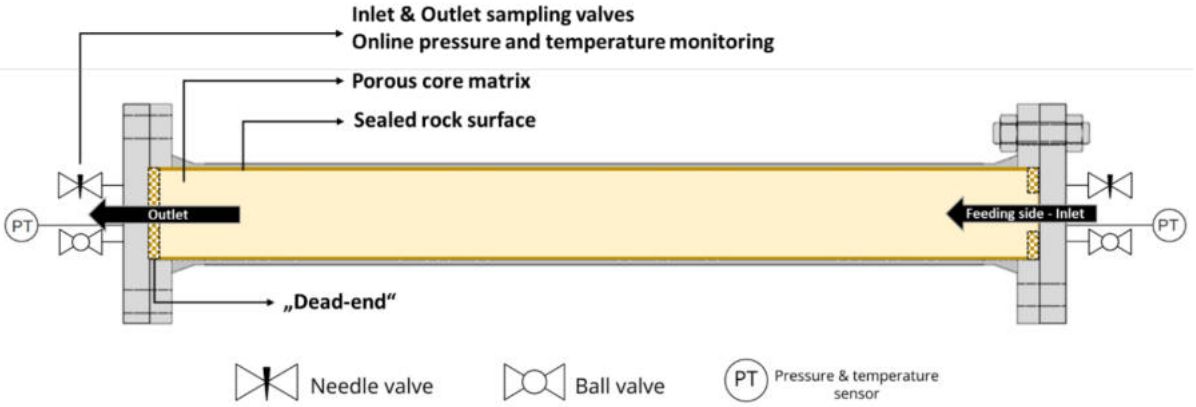

Figure 2-3: Schematic drawing of a Confined Core Reactor with attached periphery such as valves and sensors. Injection of feed gases always occurred at the same end of the reactor, labelled Inlet. Gas and liquid samples were withdrawn at the Inlet and Outlet sides to investigate the effects of arising substrate gradients proximal and distal of the injection side.

Each CCR was equipped with two digital PA-33 X sensors (KELLER AG, Winterthur, Switzerland) with a pressure range of 0 – 100 bar(g) and temperature range of -10 °C to 80 °C. The sensors were directly attached to each flange (Inlet & Outlet side) via a G ¼" port. Temperature measurement at the flanges showed a certain offset and was not appropriate for the feedback-controlled heating setup due to an inhomogeneous temperature distribution. For more precise temperature monitoring and controlling, two additional temperature sensors (RS PRO PT100 2 mm x 10 mm, RS Components GmbH) were attached to the outer shell between the flange lids and used for heating control and monitoring.
The digital control and data logging unit was set up in house and comprised a CompactLogix, 16DI, 16DO, 24VDC PS and CompactLogix ASCII Interface Modul (Routeco GesmbH, Austria). The PLC (programmable logic controller) was coded in "RS Logix" and further connected to "FactoryTalk" (Rockwell Automation) for data logging and visualization. All three reactors were heated with custom made heating-bands (Teflon Konstantheizband, 180 W) by "carlo" Loysch GmbH Austria. The 6 m

heating band was attached between the two flange lids with a winding distance of approximately 50 mm. Sheep wool (DAEMWOOL, Naturdämmstoffe GmbH & Co KG) was used for the inner layer and a reflective thermal insulation mattress for the outer layer thermal insulation.
Needle valves (HOKE® GYROLOK® 1711G6YMM, Crane Holdings, Co.) and ball valves (HOKE® GYROLOK® 7122G6YMM, Crane Holdings, Co.) were directly connected to the G ¼" ports on the inlet and outlet side of the reactors. ATEX Zone 2 classified solenoid valves (ASCO™ Series E262K080SGV00F8, Emerson Electric Co., Austria) were used for automatic gas feeding operation and were implemented into the digital control interface. Additionally, all reactors were equipped with a burst disc (type WBs-SUM-4-G, Type B18r35-01, Berstscheiben Schlesinger GmbH, Austria) fixed to the G ½" port on the inlet flange and connected to a safety tubing system for gas release to the exterior. The burst disc was specified for a burst pressure of 60 - 70 bar(g) at 47 °C. All described valves, adapters and piping were made from high quality steel (AISI 316).

2.2.5 Measurement of available gas volume in CCR

Knowledge of the available free gas volume in the employed CCR is critical for the computation of geo-methanation rates plus the assessment of quantitative information on the biocatalytic process. Hence the available pore space in the CCR was determined with a thermal mass flow meter (SFAH-5U-Q6S-PNLK-PNVBA-L1, Festo SE & Co. KG, Germany) and Argon gas of the purity 5.0 (Messer Gase, Austria). For a faithful measurement of the available gas volume after the fed-batch experiments, remaining reactor brine was discharged from each CCR by repetitively using a gas pressure gradient of 10 bar(g) against ambient pressure until no further liquid was released from the reactors. The dry CCRs were then filled with Argon gas up to either 10 or 40 bar(g) and the pressurized reactor atmosphere was released through the thermal mass flow meter, which quantified the volume of Argon gas at room temperature. In order to obtain reproducible measurements at both pressure regimes, a pressure reducer (FUTURA Druckregler, G 1/4", 0,5 - 10bar, Baureihe 0, Germany) and a fine dosing valve (HOKE® GYROLOK® 1315G4Y, Milli-Mite 1300 Series, Crane Holdings, Co., USA) were installed between the reactor and the flow meter to sustain a constant input pressure to the flow meter. Five volume readings per pressure level were recorded and an average of the corresponding values was computed. Eventually the available free gas volume per CCR at ambient pressure could be determined.

2.2.6 Computation of Geo-Methanation rates

Based on the determined available free gas volume per CCR, the known volume of brine, the total pressure reading at the end of the respective fed-batch campaign and differential pressure information of all cumulative feedings, quantitative information on the molar amount of gas in the reactors could be obtained. This information was complemented with averaged GC-derived gas composition data from both the Inlet and Outlet of each CCR, which allowed the calculation of molar quantities of all educt and product gases on basis of the ideal gas law at the respective reactor temperature of 40 °C.
The required temporal information for the computation of geo-methanation rates was derived according to live pressure monitoring: For all fed-batch experiments, the relative pressure loss curve of the last feeding of each fed-batch trial was selected and the time point determined, where 95 % of the maximum observed pressure loss had occurred (t_{95}). For this timepoint, 95% consumption of all gaseous substrates was assumed, which could be correlated to quantitative information on the molar amounts of individual gas components. All pressure loss profiles were checked for plausibility in terms of their apparent relative pressure loss – for all fed-batches an exclusive hydrogenotrophic methanogenesis was assumed, which allowed to compute the expected relative pressure losses for all employed gas mixtures.
Eventually, a methane evolution rate (MER) was computed which involved the quantity of formed CH_4 per extrapolated time duration for a 100 % conversion and per free available porous gas volume.

2.2.7 Hydrochemical and product gas analyses

Electrical conductivity (EC) and pH of temperature equilibrated (25 °C) samples were measured using a HACH HQ40d multi base unit equipped with a HACH IntelliCAL PHC101 standard gel filled pH electrode and a HACH IntelliCAL CDC401 standard conductivity probe (Hach Lange GmbH, Austria). Additional pH measurements of both reservoir and reactor fluids were carried out on a FiveEasy Benchtop F20 pH/mV system equipped with a LE422 pH-Micro-Electrode (Entry-Level, 4.3 mm diameter), both Mettler-Toledo GmbH, Germany. Prior to pH measurements, all pH and EC meters were calibrated with SINGLET standard solutions (pH = 4, pH = 7, EC = 147 µS / cm) of Hach Lange GmbH, Austria.

Volatile fatty acids (VFAs) and other organic compounds in liquid samples were analyzed on a **high-pressure liquid chromatography (HPLC)** system (Agilent 1260 Infinity II series) consisting of an autosampler, isocratic pump, degasser, column oven and refractive index-detector. The injected sample volume for standards and samples was 40 µL and were separated on a Transgenomic ICSep-ICE-ION-300 column equipped with the corresponding Coregel-Ion300 guard column at an operating temperature of 45 °C. The flow rate for the mobile phase 0.01 N H_2SO_4 was 0.325 mL min^{-1} with a maximum runtime of 120 minutes. Calibration standards ranged from 10 up to 1000 mg L^{-1} and were divided into three compound groups to avoid peak overlapping.

Relevant sum parameters associated to the carbon content in the liquid samples such as **TOC** (total organic carbon), **TIC** (total inorganic carbon) and **TC** (total carbon) were determined using a TOC analyzer TOC-V CPH of Shimadzu GmbH, Germany.

Gas samples for **gas chromatography (GC)** were collected from reactor headspace using evacuated 1 L gas bags (SUPEL Inert Foil Gasbags, Art. Nr.30227-U, Sigma-Aldrich Co LLC) and were measured on an AGILENT gas chromatograph (7890A). Helium (quality 5.0, Messer Austria GmbH) was used as a mobile phase after an additional purification step (Valco Instruments Co. Inc.). To detect individual components, gas samples were split into separate streams. Stream 1 was equipped with a PlotQ15 Agilent 19095P-Q03 [15 m x 530 µm x 40 µm] and a PlotMS Agilent 19095P-MS6 column [30 m x 530 µm x 50 µm], leading to a pulsed discharge detector (PDD) for quantifying H_2, H_2S, O_2 and N_2. In stream 2, CH_4 and CO_2 were separated on a PlotQ30 Agilent 19095P-Q04 column [30 m x 530 µm x 50 µm] and detected using an FID (CO_2 reduction prior to detection using H_2 and a nickel catalyst). Each sample was analyzed twice using a split ratio of 1:25, so enlarging the calibration range to meet concentrations of all individual gas components (injection volume 2.5 µL, inlet temperature 105 °C).

2.2.8 Molecular methods

2.2.8.1. DNA extraction from reservoir brine and reactor fluids

For subsequent molecular analyses and DNA sequencing, genomic DNA (gDNA) had to be extracted from reservoir brines and reactor fluids. Since most processed fluids were relatively low in extractable DNA, an enrichment step had to be implemented for the subsequent kit extraction: A defined volume of fluid was centrifugated for precipitate separation (4000 g, 15 mins, 4 °C) and the supernatant was filtered through a 0.2 µm Cellulose Nitrate membrane filter to capture remaining cells. Both the precipitate and the corresponding filter were transferred to an extraction tube of the FastDNA Spin Kit for Soil, MP Biomedicals Germany, and 80 µL of p.a. acetone was added to disintegrate the membrane filter. The DNA extraction procedure was carried out according to default parameters specified in the manual. Quantification of the retrieved gDNA samples was carried out on the Nanophotometer NP80 spectrophotometer (Implen GmbH, Germany) and by using the Qubit dsDNA HS (High Sensitivity) Assay Kit by Thermo Fisher Scientific, Austria.

2.2.8.2. Illumina MiSeq DNA amplicon sequencing

Selected gDNA samples retrieved from DNA extraction were further prepared for amplicon sequencing of the V4 region of the 16S rRNA gene. The analysis of 16S amplicon data allows the creation of a taxonomic profile of the present microbial community along with relative abundance information, as earlier shown in Figure 2-1. For the amplification of the 1st step amplicon library, 10 µL of 2 ng/L of gDNA template were mixed with 3.6 µL DMSO, 3.2 µL H_2O, 20 µL NEBNext Ultra II Q5 Master Mix (New England Biolabs, Germany) and 1.6 µL of forward (515F (Parada et al., 2016)) and reverse primers (806R, (Apprill et al., 2015)) each at 10 µM and with added indexing sequences for library prep. The final reaction volume was 40 µL, the amplification was carried out on a SureCycler 8800 system (Agilent, USA) consisting of 30 iterative PCR cycles with 10 seconds of denaturation (98 °C), 20 seconds of annealing (55 °C) and 30 seconds of elongation (72 °C). A hot start at 98 °C and a final elongation at 72 °C for 1 min were included. All amplified 1st step libraries were quality assessed via agarose gel electrophoresis and delivered to Microsynth AG, Balgach, Switzerland for further library prep, Illumina MiSeq 2 x 300 bp (v3 chemistry) sequencing and bioinformatic amplicon analysis.

2.2.8.3. Quantitative PCR of selected functional marker genes

Real-time quantitative PCR measurements were performed in triplicates on a qTOWER3 (Analytic Jena, Germany) detection system. The amplification of the *mcrA* gene fragment (~550 bp) was performed with MLas_for (5'-GGTGGTGTMGGDTTCACMCARTA-3') and ML_rev (5'-TTCATTGCRTAGTTWGGRTAGTT-3') primer pair (Steinberg and Regan, 2008), and the amplification of the *FTHFS* gene fragment (~250 bp) was performed with fhs1_fw (5'-GTWTGGGCWAARGGYGGMGAAGG-3') and FTHFS_rev (5'GTATTGDGTYTTRGCCATACA-3') primer pair (Leaphart and Lovell, 2001; Xu et al., 2009). The qPCR assays were performed with FIREPol® EvaGreen® qPCR Supermix (Solis BioDyne, Estonia), primer concentration of 10 nM, for 40 cycles, at following conditions

Table 2-3: qPCR amplification protocol to amplify both mcrA and FTHFS marker genes

	Temperature, °C		**Time**		**Ramp speed, °C / s**	
	mcrA	*FTHFS*	*mcrA*	*FTHFS*	*mcrA*	*FTHFS*
Initial denaturation	95	95	12 min	12 min	4	4
Denaturation	95	95	20 s	15 s	3	2
Annealing	53	55	35 s	45 s	2.5	2
Elongation	72	72	1 min 10 s	1 min	2.5	2
Measurement	80		10 s		3	
Melting curve	60-95	55-95	15 s	15 s	5	5

2.3 Results and Discussion

As noted in chapter 2.1, several independent reactor trials were conducted to comprehend and characterize the geo-methanation technology from several different perspectives. As a starting point, we decided to first focus on fundamental physicochemical and biological limitations inherent to the process with respect to varying microbial activities being encountered at different environmental conditions. To describe such potential limitations, a simplified experimental setup with unaffected formation water from the well 'Nussdorf-W-002' without any additional porous rock was chosen and two experimental series were initiated in the earlier described WSR systems.
The obtained insights from these trials served as a basis for the rational definition of feeding schemes for more substantial experiments, which were carried out in our rock-bearing CCR systems. This reactor configuration closely resembles the environmental, *in situ* conditions in natural gas reservoirs and was therefore selected for gas conversion experiments, which provided data for the computation of methanogenic rates.

2.3.1 Identification of key factors affecting geo-methanation

Findings of the predecessor project of USC-FlexStore, Underground Sun Conversion, indicated that the ratio of ongoing methanogenic and homo-acetogenic activities may directly be linked to the operational mode applied to the bioreactors, in particular to the administered partial pressures of introduced substrate gases and the time of exposure. Previously we could observe, that methanogenic conversion rates were receding and homo-acetogenic process became apparent, when critical threshold concentrations of introduced substrate gases were reached for a prolonged timespan (Bauer, 2021). The continuous accumulation of acetate led to accompanying detrimental effects on methanogenic conversion rates and severely impaired long-term process stability. In an effort to avoid and bypass such unfavorable dynamics during the bioprocess, an alternative operational mode for geo-methanation was anticipated.

2.3.1.1. Operational modes in geo-methanation

In earlier reactor trials during the Underground Sun Conversion project, batch injections introducing high partial pressures of gaseous substrates such as H_2 and CO_2 at stoichiometric (for methanogenesis) ratios were pursued. Microbial communities in the respective reactors were instantly confronted with a high abundance of available substrates, which allowed both hydrogenotrophic methanogenic and homo-acetogenic processes to occur simultaneously. A continuation of this feeding scheme at short time intervals led to a batch-wise increase of acetate concentrations and a consequential reduction in methanogenic activities over a longer period (Wang et al., 2009). Despite the fact, that the accumulated acetate could be re-mobilized via acetotrophic pathways to generate methane at distinct process conditions, it needs to be emphasized that the observed reaction speed was slow and hence not suitable for an industrial-scale application of geo-methanation. To our understanding, higher methanogenic conversion rates in geo-methanation may be feasible, when central **homeostatic boundary conditions** are not being exceeded and long-term net acetate turnover equals zero.
Instead of injecting large quantities of substrate gases at once (= batch operation), we propose to limit the feeding quanta to smaller portions and repeatedly inject at given time intervals (= **fed-batch operation**). Such an operational mode would also be more in line with the proposed central advantage of the geo-methanation technology, namely to properly respond to the volatile generation of excess renewable energy (Rüdisüli et al., 2023).

2.3.1.2. Fed-Batch geo-methanation with ‘lean’ and ‘rich’ substrate gas mixtures

The previously suggested fed-batch feeding scheme was applied to an experimental series involving formation water ‘Nussdorf-W-002’, originating from an observation wellbore of the 7Fields reservoir which has not been affected by exogenous injections of H_2 and CO_2. The microbial community in the sampled formation water may therefore be considered mostly representative for natural gas reservoirs in the molasse basin and thus in need of metabolic adaptation to initiate a successful geo-methanation campaign. Therefore, 2x 750 mL of formation water was transferred to two WSRs operated at 40 °C, which had been decontaminated, rinsed with autoclaved water and brought to an anaerobic atmosphere prior to the transfer. As earlier mentioned, no rock cores were introduced to this setup. With the scope of slowly reestablishing the metabolism of the dormant (4 °C storage after sampling) microbial community, natural gas was introduced to the WSRs to reconstitute *in situ* conditions for a duration of 10 days.

To eventually induce geo-methanation processes in the WSRs with formation water, three consecutive batch feedings with a non-stoichiometric gas mixture containing 10% (v/v) H_2, 0.5 % (v/v) CO_2 in Argon at 5 bar(g) for a duration of 10 days were performed. In all of the three individual batch runs, conventionally called ‘*cycles*’, CH_4 production could be detected. Most interestingly, the molar amount of formed CH_4 clearly exceeded the amount of introduced, exogenous CO_2, which implies the presence of alternative carbon sources in the observed system, which could be mobilized for methanogenesis. A more detailed discussion of this and other phenomena will be provided in an upcoming scientific article, which is currently in preparation.

After initiating methanogenic processes in both WSRs, a **fed-batch campaign with a lean stoichiometric gas-mixture** containing 10 % (v/v) H_2, 2.5 % (v/v) CO_2 in Argon at 5 bar(g) per feeding was started. The used gas mixture introduced partial pressures of $p(H_2)$ = 0.5 bar(g) and $p(CO_2)$ = 0.125 bar(g) per feeding cycle, which were processed for a duration of 7 days each. In total four feedings were carried out, summing up to a total duration of 28 days for the complete fed-batch campaign. The choice for the relatively small amounts of introduced H_2 and CO_2 could be explained on basis of low biomass and hence biocatalyst concentrations being present in the system before the start of the experiment. Thus, the limitation of substrates may be considered a preventative measure to not overload the system with gaseous substrates to induce unfavorable homo-acetogenesis.

An informative and simple way to live monitor the ongoing gas conversions in WSRs or other reactor systems is via pressure measurements. A closer look at equation 2-1 and 2-4 outlines, that both hydrogenotrophic and homo-acetogenic conversions are accompanied by a pressure drop, which can be accounted to the consumption of gaseous substrates from the atmosphere. Illustrating the example of exclusive hydrogenotrophic methanogenesis, five mole of substrate gases get converted to one mole of product gas, resulting in a pressure loss down of $1/5^{th}$ (= 20 %) of the initial pressure. The relative pressure loss for exclusive homo-acetogenesis with stoichiometric gas mixtures (4:1 ratio for H_2:CO_2) on the other hand is smaller, since residual H_2 remains in the system as derivable via equation 2-4. For the earlier outlined fed-batch feeding campaign in the WSRs, a relative pressure loss of 10 % (p_t/p_0 = 0.1) may be presumed, if all substrate gases were entirely converted to CH_4. Figure 2-4 depicts the averaged relative pressure losses of all individual feeding cycles (A – first feeding to D – last feeding) for both WSRs. The shown relative pressure loss curves were normalized to account only for the injected feeding gas quantum of the respective cycle (p_0 = top up feeding pressure ≈ 5 bar(g)).

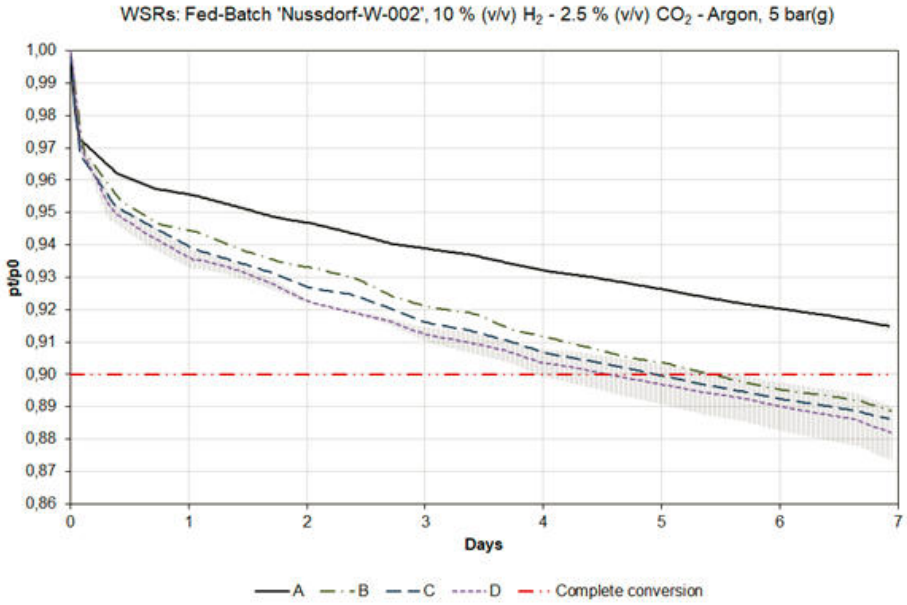

Figure 2-4: Normalized relative pressure loss curves of a fed-batch feeding campaign with 'Nussdorf-W-002' formation brine involving gas mixture 10 % (v/v) H_2, 2.5 % (v/v) CO_2 in Argon at 5 bar(g) per feeding. The standard deviations for both the first and last feeding cycles are given (n = 2). The horizontal line at p_t/p_0 = 0.90 represents the maximum theoretical pressure loss per feeding cycle, if exclusive hydrogenotrophic methanogenesis is assumed.

The relative pressure loss curves of all feeding cycles combined show ongoing gas conversions to the expected range indicative for hydrogenotrophic methanogenesis. Notably, the relative pressure loss of the initial feeding cycle A was not as pronounced as the ones for the later feeding cycles B-D. It might be assumed, that not the entire provided substrate was consumed until the end of cycle A and hence was further introduced to feeding cycle B. Additionally, the apparent gas conversion speed as derived from the curvature of the pressure loss curves is steadily accelerating between the individual feeding cycles. The most likely explanation for this observation is the continuous increase of biomass in the reactors during the fed-batch, which has also been supported by higher concentrations of extractable gDNA from reactor brine at the end of the fed-batch campaign in comparison to the start samples.

At the end of the fed-batch conversion, gas samples were withdrawn from the WSRs and the gas composition was analyzed, as summarized in table 2-4. Evidently, nearly all CO_2 in the reactor systems was consumed and CH_4 was produced. However, only 63 % of the molar carbon contained in CO_2 (= 15.2 mmol) was converted to CH_4, additionally considerable amounts of H_2 remained in the WSRs. The HPLC profile of withdrawn liquid samples revealed a moderate increase of acetate from 100 mg/L at the start of the fed-batch to 138 mg/L at the end of it, which corresponds to an increase of 0.26 mmol of acetate. The pH in the system slightly dropped from 9.2 to 9.0 units.

Table 2-4: Computed cumulative molar mass of injected gas and measured averaged molar quantities of H_2, CO_2 and CH_4 at the end of the fed-batch series in the WSRs, which involved the gas mixture 'lean' containing 10 % (v/v) H_2, 2.5 % (v/v) CO_2 in Argon.

Fed-Batch 'lean'	**H_2 [mmol]**	**CO_2 [mmol]**	**CH_4 [mmol]**
∑ Feedings	65.4 ± 1.5	15.2 ± 0.4	n.d.
End	12.8 ± 3.6	0.1 ± 0.0	9.7 ± 0.7

The provided data indicates that the bulk of CO_2 was converted to CH_4, however also acetate was generated to a minor extent. An acceleration of the gas conversion process became obvious, which may be due to increasing biomass in the system, which would also explain the share of missing carbon in the total carbon balance of the system. The introduced formation water 'Nussdorf-W-002' originated from an observation probe of the 7fields reservoirs and hence has never been in contact to exogenous substrate gases. Therefore, a strong accumulation of biomass in response to the initial injection of H_2 and CO_2 may be expected.

Directly after completing the fed-batch campaign involving the lean gas mixture, another fed-batch conversion series was started in both WSRs involving a gas mixture with a substrate concentration four times higher than before. Similar to the prior **fed-batch process, 5 bar(g) of the rich gas mixture containing 40 % (v/v) H_2, 10 % (v/v) CO_2 in Argon** was repetitively injected into the WSRs, however the interval between the feedings was doubled to 14 days to allow for the complete consumption of the introduced substrates. The used gas mixture introduced partial pressures of $p(H_2)$ = 2 bar(g) and $p(CO_2)$ = 0.5 bar(g) per feeding cycle. In total four feedings were conducted with a total experimental run time of 56 days. As previously, the total pressure and the temperature were live monitored and liquid samples for various analyses were withdrawn at the end of the fed-batch trial.

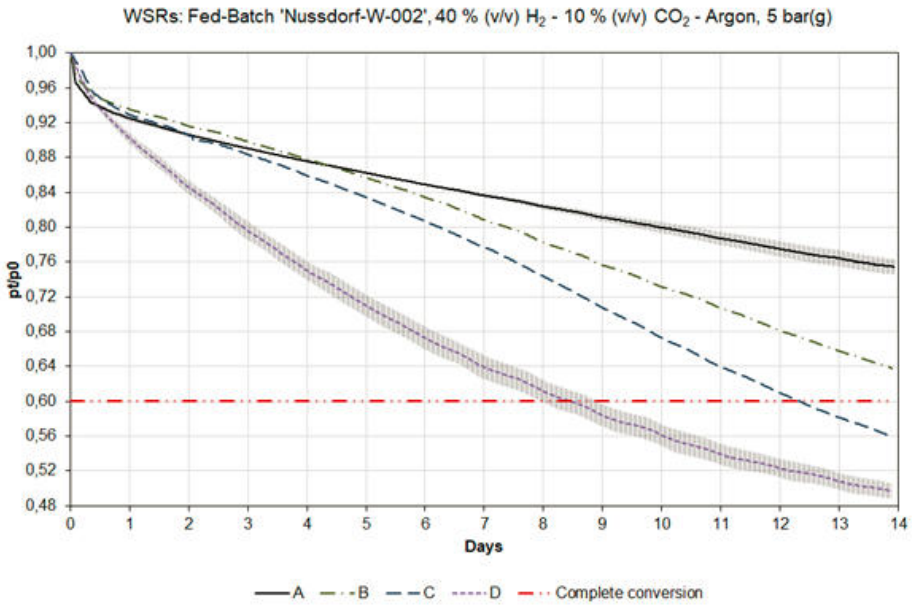

Figure 2-5: Normalized relative pressure loss curves of a fed-batch feeding campaign with 'Nussdorf-W-002' formation brine involving gas mixture 40 % (v/v) H_2, 10 % (v/v) CO_2 in Argon at 5 bar(g) per feeding. The standard deviations for both the first and last feeding cycles are given (n = 2). The horizontal line at p_t/p_0 = 0.60 represents the maximum theoretical pressure loss per feeding cycle, if exclusive hydrogenotrophic methanogenesis is assumed.

The relative pressure loss curves shown in figure 2-5 demonstrate ongoing gas conversion in both WSRs throughout the fed-batch experiment. Similar to the fed-batch campaign with the lean gas mixture (Figure 2-4), the first feeding cycles with the rich substrate gas mixture revealed smaller relative pressure losses than all later cycles. Remarkably, the relative pressure loss curve of the first feeding cycle, A, followed a linear reaction kinetic, which may imply that the gas conversion process was running at the maximum speed for the given microbial biomass in the system in analogy to Michaelis-Menten kinetics (Johnson and Goody, 2011). The curves of the subsequent feeding cycles B and C both show progressive acceleration in reaction rates as indicated by the increasing steepness of the relative pressure loss curves, in particular during the second half of the respective conversion cycles. This tendency may again be attributed to ongoing biomass growth in the WSRs in response to the rich abundance of gaseous substrates. The assumption of ongoing biomass growth was also reflected in the yields of extractable gDNA, which increased by 45 % during the fed-batch with the rich gas mixture. The relative pressure loss curve of the last feeding cycle D graphically illustrates, that the apparent nature of the conversion kinetic eventually shifted to follow a first order rate law, which introduces a concentration dependency of the reaction rate. The cumulative decrease in relative pressure in the WSRs over all feeding cycles does not fully account for an exclusive complete hydrogenotrophic methanogenic conversion to methane. To understand the carbon fluxes in the given system, both gas and liquid samples were withdrawn and analyzed.

Table 2-5: Computed cumulative molar mass of injected gas and measured averaged molar quantities of H_2, CO_2 and CH_4 at the end of the fed-batch series in the WSRs, which involved the gas mixture 'rich' containing 40 % (v/v) H_2, 10 % (v/v) CO_2 in Argon.

Fed-Batch 'rich'	H_2 [mmol]	CO_2 [mmol]	CH_4 [mmol]
∑ Feedings	250.6 ± 1.9	58.9 ± 0.4	n.d.
End	20.6 ± 1.6	0.5 ± 0.1	45.7 ± 0.3

Obtained gas chromatography data as shown in table 2-5 demonstrate, that ~99 % of all CO_2 was consumed by the end of the fed-batch process. On the contrary, about 92 % of the available H_2 was metabolized during the same time, indicating modest homo-acetogenic processes might have occurred during the gas conversion. The methanogenic yield considerably improved during this fed-batch campaign in comparison to the experiments with the lean gas mixtures. Instead of 63 % as with earlier trials, now 77 % of the totally introduced carbon could be converted to CH_4.
The HPLC profile of the withdrawn samples revealed a neglectable increase in acetate concentrations in the reactor brine from 138 mg/L to 146 mg/L, other VFAs could not be detected. The pH value in the reactors continued to decrease from pH 9 down to pH 8.5.

Overall, it may be concluded, that the fed-batch campaign involving the rich gas mixture containing 40 % (v/v) H_2, 10 % (v/v) CO_2 in Argon generated almost exclusively CH_4 as its end product. The microbial community adapted to the feeding campaign by growth processes, which fixed CO_2 for anabolic processes, as also substantiated by increases in extractable gDNA yields. The shape of the relative pressure loss curve of the last feeding in figure 2-5 implies, that the fed-batch campaign did not completely finish by the time of the final sampling, which could explain the residual H_2 in the headspace gas and the slightly elevated acetate levels in the reactor brine: It may be hypothesized at this point, that both hydrogenotrophic methanogenesis and homo-acetogenesis take place simultaneously (Kotsyurbenko et al., 2001) during the fed-batch feedings. After all CO_2 is depleted from the headspace via both microbial pathways, the residual H_2 in the WSRs could serve as an electron donor for acetotrophic, methanogenic processes, if the extractable Gibbs free energy exergonically facilitates this reaction. The synthesis of intermediary acetate might therefore be considered for the proper implementation of geo-methanation in the field. To further elucidate the role of acetate, subsequent experiments were conducted to demonstrate the effects of higher substrate concentrations and insufficient conversion times on the yields of both hydrogenotrophic methanogenesis and homo-acetogenesis.

2.3.1.3. The long-term effects of excessive substrate gas feeding on geo-methanation

After establishing a predominantly methanogenic microbial community in both WSRs via fed-batch feeding operations, the pre-conditioned mixed culture was exposed to excessive amounts of both H_2 and CO_2. The intention of this experiment was to demonstrate the inherent dynamics of the microbial carbon cycle and how elevated partial pressures of substrate applied for several weeks affect the progression of geo-methanation and its stability. Two WSRs containing 'Nussdorf-W-002' reservoir brine with a highly-active methanogenic consortium were selected for two consecutive batch injections with a substrate gas mixture containing 80 % (v/v) H_2 and 20 % (v/v) CO_2 at 20 bar(g). This resulted in partial pressures of $p(H_2)$ =16 bar and $p(CO_2)$ = 4 bar per injection in each WSR. The brine used for this experiment was pre-treated identically to that in fed-batch campaigns described in the preceding chapter, however the initial acetate concentrate was higher (745 mg/L). Nevertheless, both WSRs were predominantly methanogenic directly before the start of the two consecutive batch injections, which had

a runtime of 28 days each. Headspace gas samples were taken after each batch injection, before the WSRs were flushed with Argon to remove residual H_2 and CO_2 and subsequently refilled with new substrate gas to 20 bar(g). Liquid samples for HPLC analyses and pH readings were collected before the first injection and at the end of the second batch conversion.

Table 2-6: Computed molar masses of injected substrates and measured averaged molar quantities of H_2, CO_2 and CH_4 at the end of each of the two batch injections into the WSRs (n = 2), which involved a gas mixture containing 80 % (v/v) H_2 and 20 % (v/v) CO_2 applied at 20 bar(g). Each batch conversion lasted for a duration of 28 days.

		H_2 [mmol]	CO_2 [mmol]	CH_4 [mmol]
1st Batch	Start	553.6 ± 12.0	140.2 ± 2.7	0.3 ± 0.1
	End	468.1 ± 30.8	93.6 ± 6.8	12.5 ± 7.5
2nd Batch	Start	578.7 ± 7.0	141.2 ± 1.8	n.d.
	End	485.5 ± 2.7	108.3 ± 1.8	4.1 ± 4.1

The compiled gas composition measurement results of both individual batch injections (see table 2-6) reveal an incomplete gas conversion as indicated by the high concentrations of residual gaseous educts. Most interestingly, an over-stoichiometric consumption of CO_2 with regards to hydrogenotrophic methanogenesis became apparent in both batches, as deduced from the molar ratios of H_2 to CO_2. A complete conversion of both substrates to CH_4 exclusively via hydrogenotrophic methanogenesis would result in a 4:1 ratio of consumed H_2 to CO_2, respectively (compare with equation 2-1). On the other hand, this ratio for an exclusively homoacetogenic conversion is 2:1 H_2:CO_2, respectively (compare with equation 2-4). Considering the sum of consumed H_2 and CO_2 from both batch injections and computing the ratio of utilized H_2 to CO_2, a ratio of 2.2:1 becomes evident, suggesting predominantly homo-acetogenic conversions to take place in the WSRs. Additionally, the limited generation of CH_4 after the first batch injection further seized during the course of the second batch, which may imply the subtle manifestation of an inhibition of methanogenesis in the WSRs. A more detailed view on the assessed hydrochemical parameters compiled in table 2-7 further depicts a substantial shift towards acidic conditions, accompanied by an enormous increase of acetate in the reactor brine.

Table 2-7: Selected hydrochemical parameters of reactor brine samples withdrawn from WSRs (n = 2) before and after the start of two consecutive batch injections with a gas mixture containing 80 % (v/v) H_2 and 20 % (v/v) CO_2 applied at 20 bar(g).

	pH [/]	Acetic acid [mg L^{-1}]	Formic acid [mg L^{-1}]
Start: 1st Batch	8.4 ± 0.1	745 ± 193	14 ± 1
End: 2nd Batch	5.0 ± 0.1	4915 ± 195	72 ± 13

Strikingly, the continuous long-term exposure of the previously methanogenic WSRs to gas containing high partial pressures of H_2 and CO_2 induced a functional shift of the microbial community to homo-acetogenesis. Unfavorably, methanogenic activities ceased at the specified conditions, initiating a self-enhancing process which holds the potential to terminally abort first methanogenic and eventually homo-acetogenic processes, in analogy to failed anaerobic digestion processes (D. T. Hill et al., 1987).

The provided data suggests that the long-term exposure of the methanogenesis-competent microbial community of the well 'Nussdorf-W-002' to excessive amounts of H_2 and CO_2 gases (in 4:1 stoichiometric ratio, respectively) leads to the accumulation of acetate in the given system. If high levels of the gaseous substrates are sustained for longer time periods, the affinity towards homo-acetogenic pathways continuously rises, resulting in a consequential interruption of methanogenic processes (D. T. Hill et al., 1987; Wang et al., 2009). For monitoring purposes during geo-methanation, the ratio of consumed H_2/CO_2 may be considered to approximate the extent of both methanogenic and homo-acetogenic processes. It needs to be emphasized that acetate also serves as a methanogenic substrate which may be re-utilized for the generation of CH_4. Acetotrophic reactions are common in analogous anaerobic digestion processes but under heavily thermodynamic regulation (Dolfing et al., 2008), which directly corresponds to the concentrations / partial pressures of substrate and product gases in the observed system.

To our understanding, the formation of intermediary acetate during geo-methanation cannot be completely prevented, thus an efficient bioprocess which utilizes acetate for CH_4 production must be anticipated to sustain physiological conditions for the proper functioning of methanogenesis. The practicability of such a process was demonstrated in our CCR and is described in chapter 2.3.2.1. In the following, the applicability of an in-house developed molecular assay to quantify the extent of potential methanogenesis and homo-acetogenesis is described.

2.3.1.4. Molecular assay to assess the extent of acetogenic and methanogenic processes

Within the framework of USC-FlexStore, a molecular biological assay based on quantitative real-time polymerase chain reaction technique (qPCR) was under development. In contrast to conventional end-point PCR, qPCR allows for quantification of a target DNA sequence in the sample. Briefly, in qPCR a fluorescence signal is measured in real-time that is directly proportional to the number of target DNA molecules generated via the PCR amplification. This amplification is performed in consecutive cycles; theoretically, the amount of target is doubled every cycle of amplification. When the fluorescent signal rises above the fluorescence threshold (Figure 2-6, horizontal black line), the Ct values (Figure 1, intersections of sample amplification curves (colored curves) and the fluorescence baseline) are obtained, which are directly proportional to the number of target gene copies in the original sample. The more target material in the original sample (Figure 2-6, "target input" section), the smaller the resulting Ct value

.

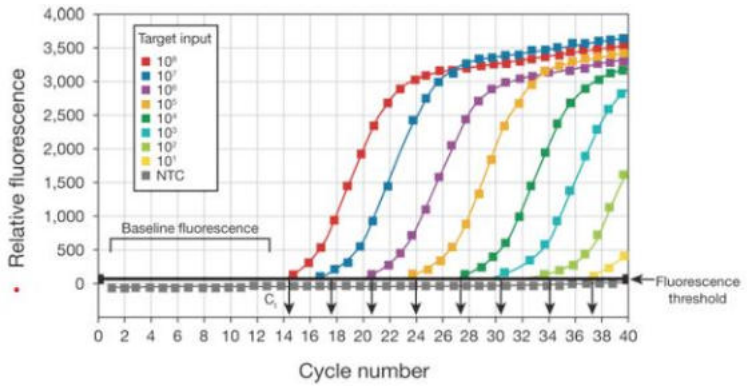

Figure 2-6: Relative fluorescence (y axis) vs. cycle number (x axis). Amplification plots are created when the fluorescent signal from each sample is plotted against cycle number; therefore, amplification plots represent the accumulation of product over the duration of the real-time PCR experiment. The samples used to create the plots in this figure (Thermo Fisher Scientific Inc., 2014) are a dilution series of the target DNA sequence.

In microbial ecology applications of qPCR, the target genetic material typically is the *marker gene*: a gene involved in a specific metabolic pathway and shared across diverse microbial groups that employ this metabolism. For methanogenesis, the established marker gene is *mcrA* (encoding the methyl coenzyme M reductase subunit alpha), and for homo-acetogenic metabolism the marker gene is *FTHFS* (encoding for formyltetrahydrofolate synthetase). Quantification of these marker genes allows to evaluate the significance and dynamics of the respective metabolisms in the total metabolic network of the community. Furthermore, establishing ratios between values obtained for methanogenesis and acetogenesis and comparing them at varying conditions allows to evaluate the impact of these conditions on the metabolic behaviour of the community on the biomolecular level. The following expression

$$\frac{Ct1m}{Ct1a} / \frac{Ct2m}{Ct2a}, \qquad \textbf{Equation 2-6}$$

where “Ct1m” is the Ct value for methanogenesis at condition 1, “Ct1f” - for homoacetogenesis at condition 1, “Ct2m” - for methanogenesis at condition 2, “Ct2f” - for homoacetogenesis at condition 2, allows to obtain and compare these ratios. If the resulting value is below 1, total metabolism of the community shifted towards acetogenesis; if the resulting value is above 1, the total metabolism of the community shifted towards methanogenesis

The described analysis was applied to evaluate two samples as a proof-of-concept:

METH (Figure 2-7, blue triplicate): DNA extracted from Nussdorf brine incubated at 10% H_2 / 2.5% CO_2, which demonstrated predominantly methanogenic conversions,
ACET (Figure 2-7, red triplicate): DNA extracted from Nussdorf brine incubated at 80% H_2 / 20% CO_2, which is expected to promote homo-acetogenesis (compare with table 2-6).

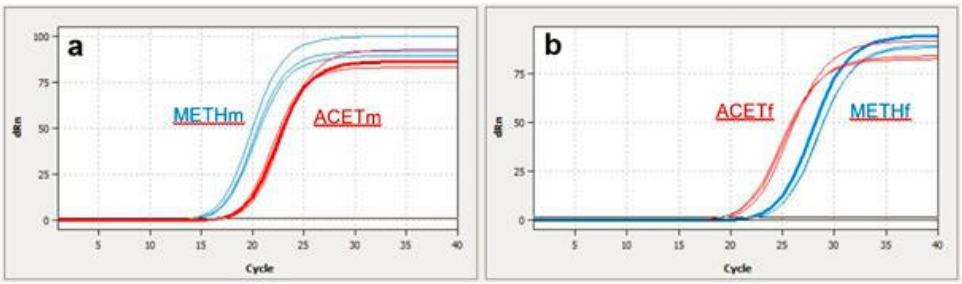

Figure 2-7: Amplification curves of target genes mcrA and FTHFS in samples a) METH (blue curves – methanogenic setting), and b) ACET (red curves – homo-acetogenic setting). All qPCR amplifications were carried out as technical triplicates:

The mean Ct values (calculated from technical triplicates) are presented in table 2-8:

Table 2-8: Mean Ct values of qPCR amplification of mcrA (methanogenesis marker gene) and FTHFS (acetogenesis marker gene) at two conditions: METH (methanogenic condititions) and ACET (acetogenic conditions)

	METH	ACET
mcrA	14.53	16.89
FTHFS	22.47	19.38

After equation 2-6, the desired ratio may be calculated as follows: (METHm/METHf)/(ACETm/ACETf) = (14/22.47)/(16.89/19.38) = **0.74**

The value obtained is below 1, which suggests that the total metabolism of the community shifted towards acetogenesis in response to the series of treatments provided in between. This is in good agreement with the observed decrease in methane generation (Table 2-6) and measured acetate accumulation in the reactor brine (Table 2-7) in response to the injection of 80 % (v/v) H_2 and 20 % (v/v) CO_2 at 20 bar(g).

Additionally, a ratio may be established between the same marker gene across the two samples (given that input DNA amount has been normalized) via the following expression:

$$\frac{METHm}{ACETm}; \frac{METHa}{ACETa} \quad \textbf{Equation 2-7}$$

From this ratio it can be determined whether the share of a certain metabolism in the total metabolism of the community has increased (value >1) or decreased (value <1). For methanogenesis, the value calculated is **0.86**, suggesting a decrease in methanogenic activity, whereas for acetogenesis it is **1.16**, suggesting an increase of acetogenesis in the total metabolism of the community. Note that while these calculations may appear to suffice an identical enquiry as compared to the ratio obtained via calculation of equation 2-6, a scenario may be imagined where both metabolisms decrease over the course of the evaluated period, but one decreases less and the other decreases more, e.g., both values obtained are >1. In this case, it may still be further determined that, within the share of the community that employ the two compared metabolisms, a shift has occurred towards the metabolism with the larger value (that is still below 1).

However, the following consideration must be taken in account. The so-called amplification efficiency – the “completeness” of doubling of the target material during each cycle – will affect the resulting Ct values. If the amplification efficiency is outside of the recommended range of 90%-110%, the Ct values obtained are not considered optimal (Ruijter et al., 2013). Several ways exist to estimate amplification efficiency (Brankatschk et al., 2012). Here, the LinRegPCR methodology (Ramakers et al., 2003) was employed to obtain the following efficiency values (Table 2-9):

Table 2-9: Amplification efficiency values for amplification of mcrA (methanogenesis marker gene) and FTHFS (acetogenesis marker gene) at two conditions: METH (methanogenic conditions) and ACET (acetogenic conditions)

	METH	ACET
mcrA	85%	88%
FTHFS	89%	85%

On the one hand, these amplification efficiency values are slightly below the recommended range. On the other, they are comparable to each other, therefore an interpretation of resulting Ct values is possible. However, additional optimization of the method is required to reproducibly obtain desired amplification efficiencies.
Furthermore, the method described above has been developed on the level of DNA content of the sample. Finer time-resolution into metabolic processes may be obtained by surveying the community on the level of gene expression (RNA gene transcripts), for which the method is extended to RNA extraction, RNA reverse transcription to cDNA and the following qPCR evaluation of the targets from the obtained cDNA pool. The RNA part of the total method, along with final optimization of the DNA-based qPCR, is being developed in the framework of the follow-up project “Carbon-Cycle Economy Demonstration” (C-CED).

2.3.2 Geo-Methanation experiments in CCR with rock cores

All previously described gas conversion experiments were conducted at relatively low total pressures (up to 20 bar(g)) and without the involvement of rock material. This highly simplified experimental setup does not resemble the environmental conditions *in situ*, but allows to investigate fundamental dynamics inherent to geo-methanation. To establish a more realistic understanding of the microbial processes occurring in the formation, a more comprehensive reactor system (CCR) was operated. Each of these reactors carries a 1 m long sealed porous sandstone, saturated with microbially-active formation brine. In contrast to the WSR, the CCR exhibits a comparable surface-area-to-volume ratio to the porous reservoir rock, which allows the computation of more realistic methanogenic conversion rates. Additionally, the contained sandstone introduces some pH buffering capacity due to possible rock-liquid interactions, which may affect the dynamics of the microbial metabolisms. To assess methanogenic conversion rates, two sets of fed-batch conversion experiments in CCR involving two different formation brines (originating from 'Nussdorf-W-002' and 'LESP-001A', the SFTF in Lehen) were conducted. For illustrative purposes, the public report of USC-FlexStore only highlights the obtained results for the experimental series involving the formation brine of the SFTF in Lehen. Prior to the start of the fed-batch trial, accumulated acetate from previous experiments had to be depleted from both CCR.

2.3.2.1. The fate of acetate – a potential substrate for methanogenesis

Potential acetate accumulation during geo-methanation does not strictly correspond to an irreversible loss of energy due to the conversion of H_2 and CO_2 to dissolved acetate in formation brine. At distinct conditions, acetate serves as a prevalent substrate for methanogenic processes, either by direct acetoclastic methanogenesis (equation 2-2) or via syntrophic acetate oxidation in association with hydrogenotrophic methanogenesis (equation 2-1 and 2-5).

The following CCR experiments were devised to demonstrate the consumption of acetate and other VFAs for the synthesis of CH_4. As a starting point, CCR filled with 'LESP-001A' formation brine with acetate concentrations ranging between 2.5 and 4 g/L were subjected to a fed-batch process to assess methanogenic reaction rates for the aforementioned reaction pathway. For this purpose, a non-stoichiometric gas mixture containing 10 % (v/v) H_2, 0.5 % (v/v) CO_2 in Argon was selected for the injection into two pretreated CCRs. The pretreatment of the reactors was intended to condition the microbial community for acetate oxidation and involved two batch injections with the respective non-stoichiometric gas mixture at 5 bar(g) for 16 days and subsequently 10 bar(g) for 8 days. The following fed-batch campaign consisted of four consecutive fillings at 10 bar(g) each and lasted for 28 days.

The obtained normalized relative pressure loss curves for the fed-batch experiment are given in Figure 2-8. It needs to be emphasized, that a complete methanation of all exogenous CO_2 with H_2 would correspond to a maximum apparent relative pressure loss of 2 % (0.5 mol CO_2 reacts with 2 mol of H_2 to generate 0.5 mol of CH_4). However, throughout the fed-batch process considerably higher relative pressure losses were detected in both CCRs, which converged at later stages to values of about 10 %. The most plausible explanation for this observation might be related to the introduced excess of H_2, which could serve as an electron donor for hydrogenotrophic methanogenesis on basis of emerging CO_2 from acetate oxidation (compare with both equation 2-2 and 2-5). The observed variance in pressure development as indicated by the error bars was considerably higher during this experiment as with the earlier described fed-batches which were operated in the WSR (relate to both Figure 2-4 and Figure 2-5). One factor contributing to this high variance might be the difference in acetate concentrations between CCR1 and CCR2. At equilibrium conditions, higher acetate concentrations evoke higher concentrations of H_2 and CO_2 in the gas phase, which in return could positively stimulate methanogenic reaction rates by first-order kinetics (Johnson and Goody, 2011).

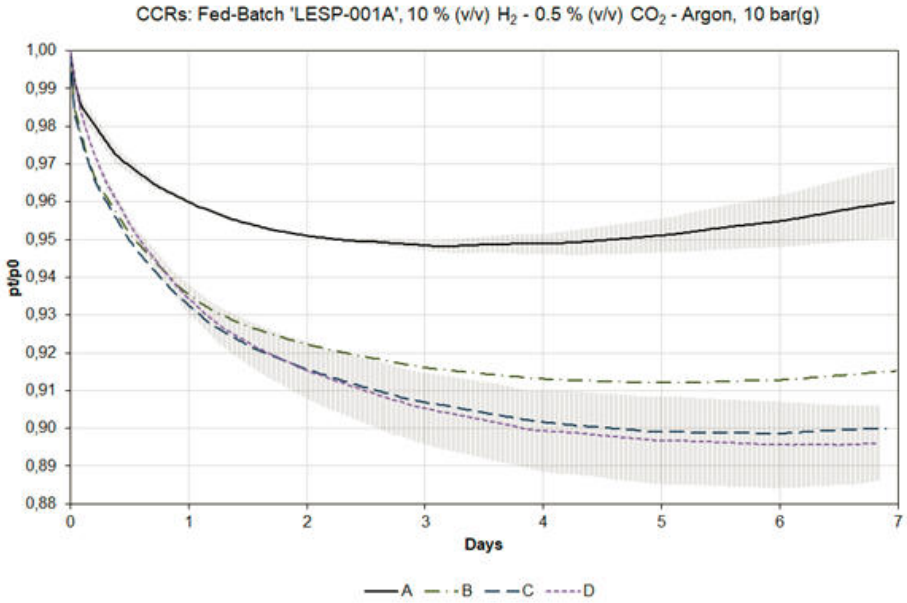

Figure 2-8: Normalized relative pressure loss curves of a fed-batch feeding campaign with 'LESP-001A' formation brine in CCR involving non-stoichiometric gas mixture 10 % (v/v) H_2, 0.5 % (v/v) CO_2 in Argon at 10 bar(g) per feeding. The standard deviations for both the first and last feeding cycles are given (n = 2). In total four chronologically sorted curves are shown, curve A relating to the first feeding and curve D relating to the last feeding of the Fed-Batch.

The deflection of the pressure curve corresponding to the first feeding (A) in Figure 2-8 shows an increase in reactor pressure and hence implies the production of gas during this stage of operation. This trend remains visible throughout every individual feeding of the entire fed-batch campaign, however with weakening emergence. The damping of observed gas production at later stages of the fed-batch might be due to both decreasing acetate concentration in the system and feedback inhibition via accumulation of CH_4. To gain further insights on the occurring processes in the CCR, liquid samples were withdrawn at the start and at the end of the fed-batch campaign and analyzed. A summary of the most relevant hydrochemical parameters is compiled in table 2-10.

Table 2-10: Selected hydrochemical parameters at the start and end of a fed-batch experiment involving non-stoichiometric gas mixture 10 % (v/v) H_2, 0.5 % (v/v) CO_2 in Argon in CCR1 and CCR2. Liquid samples were withdrawn at both the Inlet and the Outlet side of each CCR.

			pH [/]	Acetic acid [mg L^{-1}]	Formic acid [mg L^{-1}]	Butyric acid [mg L^{-1}]	i-Butyric acid [mg L^{-1}]
CCR 1	**Inlet**	Start	6.8	3100	33	599	65
		End	7.8	874	35	198	63
	Outlet	Start	7.1	2595	33	315	52
		End	7.4	3343	36	391	56
CCR 2	**Inlet**	Start	7.1	3795	32	488	227
		End	7.9	1907	n.d.	443	254
	Outlet	Start	7.1	3660	33	482	238
		End	7.7	3617	33	496	236

As a brief reminder, Figure 2-3 shows two possible sampling points at each end of the CCR – the Inlet and the Outlet. Gas injections into the CCR are accomplished via the Inlet side, which consequentially leads to higher partial pressures of substrate gases at this side in comparison to the Outlet side which is about 1 m apart. The hydrochemical data of table 2-10 reveals a consistent increase in pH for CCR1 and CCR2 at both reactor sides. One explanation for the pH shift towards more alkaline conditions may be the utilization of acetate or other VFAs from reactor brine. Indeed, a substantial decrease in acetate levels could be detected at the Inlet sides of both CCR. Nonetheless, CCR1 showed a minor increase of acetate concentration at its Outlet side, which currently cannot be explained.

Generally, it must be stated that acetate concentrations do considerably vary between different sides of the CCR. Consequentially, a reliable quantification of the total acetate or VFA pools was not feasible for both CCRs, which in return complicated the computation of methanogenic conversion rates. However, an alternative mode of methanogenic rate computation was anticipated (see chapter 2.2.6) which relied on assessed gas chromatography (table 2-11), void gas volume per CCR and pressure data.

Table 2-11: Gas composition of process gas samples withdrawn from both the Inlet and Outlet side of each CCR after completion of fed-batch involving a non-stoichiometric gas mixture containing 10 % (v/v) H_2, 0.5 % (v/v) CO_2 in Argon.

			H_2 [% (v/v)]	CO_2 [% (v/v)]	CH_4 [% (v/v)]
	CCR1	Inlet	0.29	n.d.	3.16
		Outlet	0.34	0.01	2.73
	CCR2	Inlet	n.d.	0.01	4.08
		Outlet	n.d.	0.03	4.31

Taking a closer look at the compiled gas composition data of the withdrawn gas samples, an almost complete consumption of both H_2 and CO_2 in both CCRs becomes evident. Residual traces of H_2 could still be detected at both the Inlet and Outlet side of CCR1, which might suggest that either the gas conversion process did not completely finish up to the point of sampling. On the contrary, no residual H_2 could be detected in CCR2, intriguingly traces of CO_2 could still be measured at both sides of the reactor.

Gas samples withdrawn from both CCR attested for predominant methanogenic activities. The amount of formed CH_4 clearly exceeded the amount of CH_4 which could theoretically be ascribed to the introduced exogenous CO_2.

Considering the data presented in Figure 2-8, table 2-10 and table 2-11, it may be concluded that acetate was consumed via methanogenic processes at the specified conditions. Due to the inhomogeneous distribution of acetate throughout the CCR, no accurate statements on the extent of acetate utilization can be made. However, an averaged methanogenic evolution rate (MER) for the illustrated fed-batch experiment involving the respective non-stoichiometric gas mixture could be computed on basis of the described method in chapter 2.2.6 with a determined t_{95} = 3.89 days:

MER = 0.089 ± 0.028 m^3 CH_4 * m^3 pore space $volume^{-1}$ * day^{-1}

It needs to be emphasized that the given methanogenic conversion rate is merely valid for the specified condition (acetate levels, 10 bar(g) feeding batches of the non-stoichiometric gas mixture and the given feeding interval). Due to the endergonic nature of the acetate oxidation process, variations of the process conditions e.g., applied partial pressures of both gaseous substrates, are expected to widely affect the biocatalytic conversion rate due to potential product inhibition. To stimulate optimal rates of acetate oxidations towards H_2 and CO_2, a limitation of both molecules in the given system should be anticipated according to Le Chatelier's principle.

2.3.2.2. Efficient geo-methanation with 'lean' stoichiometric gas mixtures in CCRs (SFTF)

Based on preliminary experimental data obtained during the predecessor project Underground Sun Conversion (Bauer, 2021), an inhibitory effect of extensively accumulated acetate and VFAs on geo-methanation rates during geo-methanation was presumed. This relationship was clearly proven with WSR experiments highlighted in chapter 2.3.1.3, which revealed an almost entire abolition of methanogenesis when reaching a critical acetate concentration of 4915 mg/L at pH 5. However, CCR experiments with formation brine containing acetate concentrations of > 2.5 g/L demonstrated the reproducible methanogenic utilization of acetate to CH_4 when applying a non-stoichiometric gas mixture at limited pressures. In comparison to gas conversion experiments from earlier projects involving stoichiometric gas mixtures at neglectable acetate concentrations in the CCRs, the progression of the gas conversion for the shown acetotrophic feeding scenario involving non-stoichiometric gas mixtures (Figure 2-8) was considerably slower. To assure economically-feasible, performant and robust Geo-Methanation, the generation and relatively slow subsequent re-utilization of acetate should be prevented. Hence, an evaluation of critical process boundaries in CCR experiments involving stoichiometric gas mixtures was pursued.

In the following fed-batch campaign we continued the operation of both CCR used earlier and assessed relevant process metrics when using a stoichiometric gas mixture containing 10% (v/v) H_2, 2.5 % (v/v) CO_2 in Argon. Similar to the prior fed-batch, 10 bar(g) of this gas mixture were injected. However, the feeding interval was shortened to 6 days, summing up to a total runtime of 24 days. The recorded averaged, relative pressure loss curves are depicted in figure 2-9.

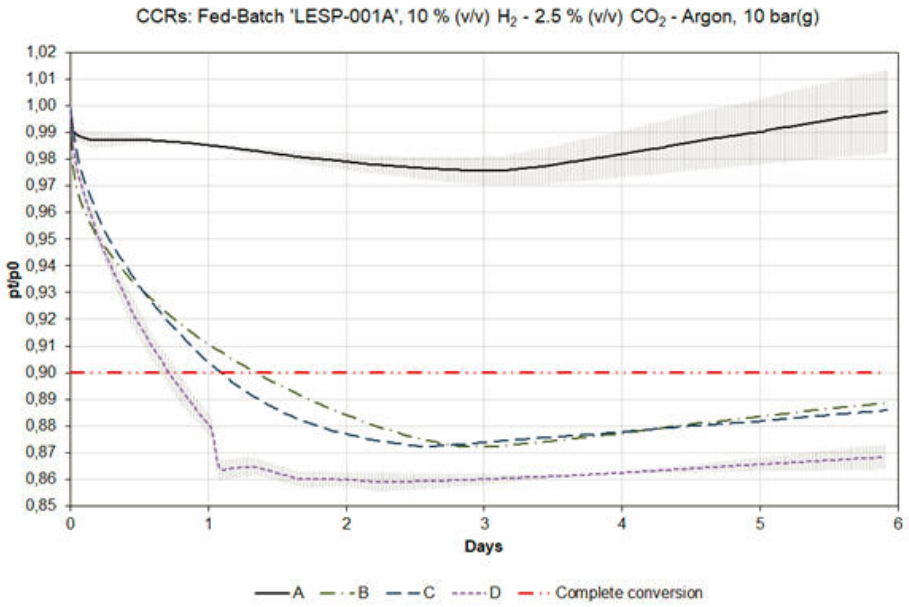

Figure 2-9: Normalized relative pressure loss curves of a fed-batch feeding campaign with 'LESP-001A' formation brine in CCR involving gas mixture 10 % (v/v) H_2, 2.5 % (v/v) CO_2 in Argon at 10 bar(g) per feeding. The standard deviations for both the first and last feeding cycles are given (n = 2). The horizontal line at p_t/p_0 = 0.90 represents the maximum theoretical pressure loss per feeding cycle, if exclusive hydrogenotrophic methanogenesis is assumed. In total four chronologically sorted curves are shown, curve A relating to the first feeding and curve D relating to the last feeding of the Fed-Batch.

Similar to CCR experiments involving the non-stoichiometric gas mixture (Figure 2-8), a strong tendency for gas formation becomes apparent for both CCR, particularly during the first feeding cycle as indicated by curve 'A'. This does not come as a surprise, since both CCRs still contained high levels of acetate and other VFAs at the start of the experiment (table 2-10). Once again, a damping of the observed gas production at later stages of the fed-batch becomes obvious. The increasing steepness of the relative pressure loss curves during the early phases of the feeding cycles imply accelerating reaction rates over the course of the fed-batch campaign. Curve 'D' contains an artifact shortly after day 1, which can be ascribed to a temporal power cut which occurred during this time.

Table 2-12: Selected hydrochemical parameters at the start and end of a fed-batch experiment involving stoichiometric gas mixture 10 % (v/v) H_2, 2.5 % (v/v) CO_2 in Argon in CCR1 and CCR2. Liquid samples were withdrawn at both the Inlet and the Outlet side of each CCR.

			pH [/]	Acetic acid [mg L^{-1}]	Formic acid [mg L^{-1}]	Butyric acid [mg L^{-1}]	i-Butyric acid [mg L^{-1}]
CCR 1	**Inlet**	Start	7.8	874	35	198	63
		End	7.7	34	n.d.	n.d.	n.d.
	Outlet	Start	7.4	3343	36	391	56
		End	6.8	3246	n.d.	350	19
CCR 2	**Inlet**	Start	7.9	1907	n.d.	443	254
		End	7.7	789	n.d.	209	192
	Outlet	Start	7.7	3617	33	496	236
		End	7.6	1574	n.d.	380	173

The hydrochemical data derived from samples withdrawn at the start and the end of the series compiled in Table 2-12 reveals a net decrease in acetate and other VFA concentrations during the fed-batch involving the stoichiometric 'lean' gas mixture. Furthermore, the pH values remained constant in both CCRs except for a minor decrease in pH at the Outlet side of CCR1. Overall, this data implies a stable operation of geo-methanation utilizing both H_2 and CO_2 as well as acetate at the given conditions.

Table 2-13: Gas composition of process gas samples withdrawn from both the Inlet and Outlet side of each CCR after completion of fed-batch involving a stoichiometric gas mixture 'lean' containing 10 % (v/v) H_2, 2.5 % (v/v) CO_2 in Argon.

			H_2 [% (v/v)]	CO_2 [% (v/v)]	CH_4 [% (v/v)]
	CCR1	Inlet	0.01	0.17	2.95
		Outlet	0.05	0.08	2.89
	CCR2	Inlet	0.03	0.30	4.59
		Outlet	0.05	0.29	4.73

Additionally, gas samples were withdrawn at both the Inlet and Outlet of each CCR after the completion of the Fed-Batch. The gas composition data of table 2-13 demonstrates an almost entire consumption of H_2 from both CCRs. Larger quantities of CO_2 remained in the gaseous phase, in particular obvious for CCR2, implying the presence of acetotrophic processes which generate both carbon dioxide and CH_4. The latter compound was formed extensively in both CCRs, however similar to the gas composition data in table 2-11 CCR2 showed a higher methanogenic activity in comparison to CCR1. Again, the recorded data was used for the computation of methanogenic evolution rates (MER) based on the relative pressure loss curve of the last feeding cycle 'D' for the respective conditions:

$$\underline{\textbf{MER}} = 0.355 \pm 0.021\ m^3\ CH_4 * m^3\ \text{pore space volume}^{-1} * day^{-1}$$

The computed MER for the fed-batch campaign employing stoichiometric gas mixture 'lean' with reservoir brine from the SFTF in Lehen is highly affected by ongoing acetotrophic processes, leading to a probable overestimation of the apparent methanogenic conversion rate. An exclusive assignment of

generated CH_4 to exclusive hydrogenotrophic methanogenesis is not possible in this specific case, since the total extent of acetate and other VFA depletion in the CCRs cannot be determined. An averaged conversion time (t_{95}) was computed to be 1.07 days. For validation of the described computational approach applied to acetotrophic conditions, the gas composition at the lowest measured pressure in the reactor was determined during a subsequent batch conversion conducted at the same conditions, showing an almost entire consumption of both H_2 and CO_2 from the gas phase at this time point (data not shown). Hence it may be concluded, that the point of the lowest apparent pressure in the reactor also corresponds to the point where all gaseous substrate was consumed, provided that no homo-acetogenesis is occurring.

2.3.2.3. Efficient geo-methanation with 'rich' stoichiometric gas mixtures in CCRs (SFTF)

The outcome of the fed-batch series involving the stoichiometric 'lean' gas mixture attested for robust geo-methanation in both CCRs due to absent VFA accumulation and over stoichiometric CH_4 generation. One economic limitation of geo-methanation is the huge energy demand for pumps to inject and circulate gases in the reservoir. One approach to increase the efficiency of the overall process would be to reduce the share of carrier gas during injection. Therefore, the following fed-batch campaign strives to evaluate the applicability of gas mixtures containing higher shares of H_2 and CO_2.

After accomplishing the conversion trials with the stoichiometric 'lean' gas mixture, both CCRs with reactor brine originating from the SFTF in Lehen were subjected to another fed-batch campaign involving a substrate gas mixture containing 40 % (v/v) H_2, 10 % (v/v) CO_2 in Argon, referred to as 'rich'. Four successive feedings with 10 bar(g) of the 'rich' gas-mixture were initiated every 7 days, summing up to a total runtime of 28 days.

The online pressure monitoring during the Fed-Batch campaign employing the 'rich' gas mixture (as depicted in figure 2-10) shows a minor gas formation tendency in the late phase of the first feeding cycle. Once again, this slight increase in reactor pressure towards the end of the feeding cycle most probably relates back to ongoing microbial gas production from acetate. In contrast to the two previous fed-batches in the CCRs, the intrinsic tendency for gas formation declines, most likely due to lower acetate concentrations in both reactors. All subsequent feeding cycles exhibited a similar progression, as judged upon by the comparable deflections of the relative pressure loss curves. The apparent gas conversion rates accelerated from feeding cycle to feeding cycle, as indicated by the increasing steepness of the relative pressure loss curves. The observed relative pressure losses of all cumulated feedings stand in good agreement with the theoretical relative pressure loss of 40 %, as indicated by the red line in Figure 2-10.

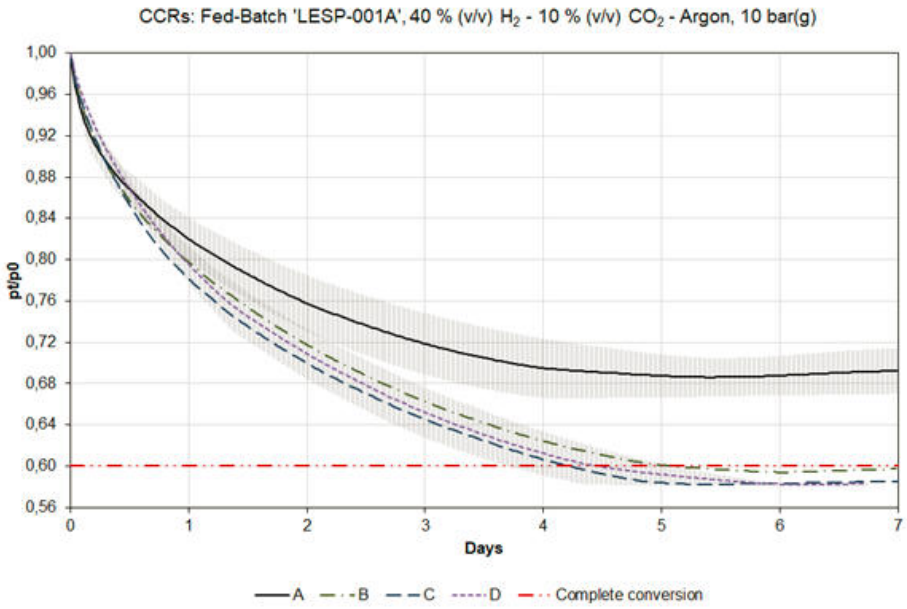

Figure 2-10: Normalized relative pressure loss curves of a fed-batch feeding campaign with 'LESP-001A' formation brine in CCR involving gas mixture 40 % (v/v) H_2, 10 % (v/v) CO_2 in Argon at 10 bar(g) per feeding. The standard deviations for both the first and last feeding cycles are given (n = 2). The horizontal line at p_t/p_0 = 0.60 represents the maximum theoretical pressure loss per feeding cycle, if exclusive hydrogenotrophic methanogenesis is assumed. In total four chronologically sorted curves are shown, curve A relating to the first feeding and curve D relating to the last feeding of the Fed-Batch.

Reactor brine samples were taken at the beginning and the end of the fed-batch experiment and used for in-house analyses. A summary of selected hydrochemical parameters is given in table 2-14. Overall, it may be concluded that all determined VFA levels were receding over the course of the experiment. Also, pH values were maintained in a range which is beneficial for methanogenesis. The presented data suggests, that stable and efficient geo-methanation is feasible with the applied feeding scheme involving gas mixtures containing higher shares of both H_2 and CO_2.

Table 2-14: Selected hydrochemical parameters at the start and end of a fed-batch experiment involving stoichiometric gas mixture 40 % (v/v) H_2, 10 % (v/v) CO_2 in Argon in CCR1 and CCR2. Liquid samples were withdrawn at both the Inlet and the Outlet side of each CCR.

			pH [/]	Acetic acid [mg L^{-1}]	Formic acid [mg L^{-1}]	Butyric acid [mg L^{-1}]	i-Butyric acid [mg L^{-1}]
CCR 1	Inlet	Start	7.6	246	n.d.	20	n.d.
		End	7.5	145	n.d.	n.d.	n.d.
	Outlet	Start	6.6	3013	n.d.	355	21
		End	6.9	2610	n.d.	301	20
CCR 2	Inlet	Start	7.6	686	n.d.	129	146
		End	7.8	382	n.d.	45	48
	Outlet	Start	7.4	896	n.d.	275	150
		End	7.8	251	n.d.	46	41

Further information could be gathered via gas chromatography: According to the presented gas composition data in table 2-15, nearly all gaseous substrates were converted to CH_4. Besides traces of H_2 in both CCRs, carbon dioxide could be detected in both reactors, which most likely originates from acetate oxidation processes as described earlier.

Table 2-15: Gas composition of process gas samples withdrawn from both the Inlet and Outlet side of each CCR after completion of a fed-batch experiment involving a stoichiometric gas mixture 'rich' containing 40% (v/v) H_2, 10 % (v/v) CO_2 in Argon.

			H_2 [% (v/v)]	CO_2 [% (v/v)]	CH_4 [% (v/v)]
	CCR1	Inlet	0.01	0.40	10.63
		Outlet	0.03	0.25	11.60
	CCR2	Inlet	0.14	0.43	12.26
		Outlet	0.01	0.36	12.36

The aggregated data of the previous analyses attests for stable and efficient geo-methanation at the given conditions. Despite the increase in substrate concentrations by the factor of four in comparison to the 'lean' gas mixture, no accumulation of VFAs could be detected over the course of the experiment. Based on the determined free pore space volume, the gas composition and pressure data, an averaged methane evolution rate could be computed:

$$\underline{\textbf{MER}} = 0.167 \pm 0.025\ m^3\ CH_4 * m^3\ \text{pore space volume}^{-1} * \text{day}^{-1}$$

Based on the live pressure monitoring throughout the last conversion cycle, an averaged t_{95} = 4.25 days could be determined for the computation of the MER. Due to limited gas formation in the reactors according to the relative pressure profile, the calculated value gives a good estimate on methanogenic reaction rates, which predominantly feed on gaseous products.

The analysis of additional DNA sequencing data from selected WSR and CCR experiments is currently ongoing and will be the subject of two upcoming scientific publications authored by members of the BOKU team.

2.4 Conclusion

geo-methanation offers a means to convert renewable energy to a chemical energy carrier, i.e. green methane, fully compatible with the existing gas infrastructure. The translocation of this conversion process into the underground by using natural gas storage facilities should provide the high capacity needed for seasonal energy conservation which is associated with the de-fossilation of the global energy supply.

Certain factors may affect the success of the geo-methanation process in a suitable reservoir, most importantly the partial pressures of substrate gases and the pH. Analysis of microbial and physico-chemical characteristics prevailing in the reactor and monitoring of process parameters provides information on potential and ongoing microbial pathways. The ratio of consumed H_2/CO_2 is informative to estimate the extent to which competing pathways such as homo-acetogenesis and hydrogenotrophic methanogenesis are present and potentially active. Furthermore, molecular monitoring tools based on quantitative PCR of selected functional marker genes allow us to estimate the genetic abundance of the aforementioned pathways.

To achieve and maintain high methanation efficiency, the supply of substrate gases needs to be balanced properly since several microbial processes are competing for the same substrates. An increased partial pressure of carbon dioxide will reduce the pH in the reactor system which will favor homo-acetogenesis. According to literature, the optimal pH range for homo-acetogens is between 5 – 5.5, while methanogenesis operates best in a range from 6.5 – 7.5 (Ishak et al., 2022). Establishing a pCO_2 of 4 bar in the experimental series using only reservoir brine without drill cores, resulted in a drop of pH to a value of 5.0 and the accumulation of 4.9 g/L of acetate. It must be noted though, that the presence of sufficient buffer capacity allows for a stable operation of the process at comparable pCO_2. This was previously demonstrated in the predecessor project Underground Sun Conversion, where a robust geo-methanation process operated at pCO_2 of 3 bar could be maintained in reactors containing rock cores of the Haller series (Bauer, 2021). Given the fact that the buffer capacity existing in the reservoir needs to be assessed in a side specific manner, the first measure to control the pH in the reservoir is limiting the amount of carbon dioxide that is injected. Different operational modes of geo-methanation have been investigated in a number of reactor experiments mimicking reservoir conditions. Out of them, fed-batch operation turned out to be an appropriate reactor setting not prone to process failure. Therefore, it is most recommended for the field application of geo-methanation, which stands in good agreement with the strategic scope of this technique to compensate for the volatile mode of energy generation and to provide high-capacity for energy storage for seasonal balance. Fed-batch experiments employed two separate formation brines of different geological origin and two gas mixtures with varying H_2 and CO_2 contents. Methane evolution rates for all tested gas mixtures were in a range between 0.08 and 0.35 m^3 CH_4 * m^3 pore space $volume^{-1}$ * day^{-1}.

Another option to keep pCO_2 and pH low, is “diluting” the substrate gases by using a carrier gas such as natural gas. This may seem to be a costly and inefficient possibility. But it has to be considered that also for conventional sub-surface gas storage, it is technically necessary to maintain a certain minimum pressure in the storage (cushion gas). Carrier gas could be used to meet this requirement in the case of gas storage combined with geo-methanation. Still, we consider fed-batch operation as the more cost-efficient and viable mode for converting green hydrogen and carbon dioxide to renewable methane.

Accumulation of acetate as a consequence of applying too high partial pressures of substrate is not necessarily a total loss of energy. We demonstrated a way to deplete the acetate pool and re-stimulate methanogenesis. This was accomplished by the means of involving a non-stoichiometric gas mixture

with 10 % (v/v) H_2 and 0.5 % (v/v) CO_2. For the depletion of acetate and other VFAs during CCR experiments with ‘Nussdorf-W-002' formation brine, a gas mixture containing 10 % (v/v) H_2 in Argon was succesfully used. It must be mentioned though, that we observed comparably low reaction rates and long recovery times at the outlined non-stoichiometric feeding scenarios. The utilization of non-stoichiometric gas mixtures with relatively low H_2 contents in comparison to CO_2 (e.g., a 2:1 ratio respectively) was not further anticipated due to consequential biasing towards unwanted homo-acetogenic processes. Consequently, it is recommended to prevent excessive intermediate acetate production by establishing a subsurface environment that channels hydrogen towards methanogenesis rather than the competing microbial pathway.

2.5 Abbreviations

$\Delta G^{o'}$	Standard Gibbs free energy at physiological conditions
AM	Acetoclastic Methanogenesis
ATP	Adenosine TriphosPhate
BOKU	Universität für BOdenKUltur (University of Natural Resources and Life Sciences)
cDNA	Complementary DesoxyriboNucleic Acid
CH_3COO^-	Acetate
CH_3OH	Methanol
CH_4	Methane
CO_2	Carbon-Dioxide
CCR	Confined Core Reactors
Ct	Cycle threshold
DNA	DesoxyriboNucleic Acid
EC	Electrical Conductivity
FFG	ForschungsFörderungsGesellschaft (Austrian Research Promotion Agency)
GC	Gas Chromatography
gDNA	genomic DesoxyriboNucleic Acid
H_2	Hydrogen
H_2O	Water
H_2S	Hydrogen Sulfide
H_2SO_4	Sulfuric Acid
HM	Hydrogenatrophic Methanogenesis
HPLC	High Performance Liquid Chromatography
ISO	International Organization for Standardization
kJ	Kilojoule
mD	milliDarcy
MER	Methane Evolution Rate
MM	Methylotrophic Methanogenesis
mm	Millimeter
N_2	Nitrogen
n.d.	Not detected
nM	Nanomolar
O_2	Oxygen
p.a.	Pro analysi
pCO_2	Partial Pressure CO_2
PCR	Polymerase Chain Reaction
pH	Acidity
PLC	Programmable Logic Controller
PDD	Pulsed Discharge Detector
rRNA	ribosomal RiboNucleic Acid
SAO	Syntrophic Acetate Oxidation
SFTF	Scientific field test facility
t_{95}	Time at which 95% of the maximum relative pressure loss was observed
TC	Total Carbon
TIC	Total Inorganic Carbon
TOC	Total Organic Carbon
VFA	Volatile fatty acids
v/v	Volume per volume
W	Watt
WSR	Wellbore Simulation Reactor
wt%	Mass fraction
qPCR	quantitative real-time Polymerase Chain Reaction

2.6 References

Apprill, A., McNally, S., Parsons, R., Weber, L., 2015. Minor revision to V4 region SSU rRNA 806R gene primer greatly increases detection of SAR11 bacterioplankton. Aquat. Microb. Ecol. 75, 129–137. https://doi.org/10.3354/ame01753

Bauer, S., 2021. Underground Sun Conversion: Renewable energy storage and conversion by in-situ biological methanation in porous Underground gas reservoirs (No. 855231, FFG). RAG Austria AG, Vienna.

Brankatschk, R., Bodenhausen, N., Zeyer, J., Bürgmann, H., 2012. Simple Absolute Quantification Method Correcting for Quantitative PCR Efficiency Variations for Microbial Community Samples. Appl. Environ. Microbiol. 78, 4481–4489. https://doi.org/10.1128/AEM.07878-11

D. T. Hill, S. A. Cobb, J. P. Bolte, 1987. Using Volatile Fatty Acid Relationships to Predict Anaerobic Digester Failure. Trans. ASAE 30, 0496–0501. https://doi.org/10.13031/2013.31977

Dolfing, J., Larter, S.R., Head, I.M., 2008. Thermodynamic constraints on methanogenic crude oil biodegradation. ISME J. 2, 442–452. https://doi.org/10.1038/ismej.2007.111

Hania, W.B., Bouanane-Darenfed, A., Cayol, J.-L., Ollivier, B., Fardeau, M.-L., 2016. Reclassification of Anaerobaculum mobile, Anaerobaculum thermoterrenum, Anaerobaculum hydrogeniformans as Acetomicrobium mobile comb. nov., Acetomicrobium thermoterrenum comb. nov. and Acetomicrobium hydrogeniformans comb. nov., respectively, and emendation of the genus Acetomicrobium. Int. J. Syst. Evol. Microbiol. 66, 1506–1509. https://doi.org/10.1099/ijsem.0.000910

Ishak, M.A.M., Ani, A.Y., Syed Ismail, S.N.A., Ali, M.L.M., Ahmad, R., 2022. Conversion of biomass to biofuels, in: Value-Chain of Biofuels. Elsevier, pp. 49–67. https://doi.org/10.1016/B978-0-12-824388-6.00005-1

Johnson, K.A., Goody, R.S., 2011. The Original Michaelis Constant: Translation of the 1913 Michaelis–Menten Paper. Biochemistry 50, 8264–8269. https://doi.org/10.1021/bi201284u

Kimura, H., Nashimoto, H., Shimizu, M., Hattori, S., Yamada, K., Koba, K., Yoshida, N., Kato, K., 2010. Microbial methane production in deep aquifer associated with the accretionary prism in Southwest Japan. ISME J. 4, 531–541. https://doi.org/10.1038/ismej.2009.132

Kotsyurbenko, O.R., Glagolev, M.V., Nozhevnikova, A.N., Conrad, R., 2001. Competition between homoacetogenic bacteria and methanogenic archaea for hydrogen at low temperature. FEMS Microbiol. Ecol. 38, 153–159. https://doi.org/10.1111/j.1574-6941.2001.tb00893.x

Kurth, J.M., Op den Camp, H.J.M., Welte, C.U., 2020. Several ways one goal — methanogenesis from unconventional substrates. Appl. Microbiol. Biotechnol. 104, 6839–6854. https://doi.org/10.1007/s00253-020-10724-7

Leaphart, A.B., Lovell, C.R., 2001. Recovery and Analysis of Formyltetrahydrofolate Synthetase Gene Sequences from Natural Populations of Acetogenic Bacteria. Appl. Environ. Microbiol. 67, 1392–1395. https://doi.org/10.1128/AEM.67.3.1392-1395.2001

Parada, A.E., Needham, D.M., Fuhrman, J.A., 2016. Every base matters: assessing small subunit rRNA primers for marine microbiomes with mock communities, time series and global field samples: Primers for marine microbiome studies. Environ. Microbiol. 18, 1403–1414. https://doi.org/10.1111/1462-2920.13023

Ramakers, C., Ruijter, J.M., Deprez, R.H.L., Moorman, A.F.M., 2003. Assumption-free analysis of quantitative real-time polymerase chain reaction (PCR) data. Neurosci. Lett. 339, 62–66. https://doi.org/10.1016/S0304-3940(02)01423-4

Rüdisüli, M., Mutschler, R., Teske, S.L., Sidler, D., van den Heuvel, D.B., Diamond, L.W., Orehounig, K., Eggimann, S., 2023. Potential of renewable surplus electricity for power-to-gas and geo-methanation in Switzerland. Int. J. Hydrog. Energy 48, 14527–14542. https://doi.org/10.1016/j.ijhydene.2022.12.290

Ruijter, J.M., Pfaffl, M.W., Zhao, S., Spiess, A.N., Boggy, G., Blom, J., Rutledge, R.G., Sisti, D., Lievens, A., De Preter, K., Derveaux, S., Hellemans, J., Vandesompele, J., 2013. Evaluation of qPCR curve analysis methods for reliable biomarker discovery: Bias, resolution, precision, and implications. Methods 59, 32–46. https://doi.org/10.1016/j.ymeth.2012.08.011

Schnuerer, A., Zellner, G., Svensson, B.H., 1999. Mesophilic syntrophic acetate oxidation during methane formation in biogas reactors. FEMS Microbiol. Ecol. 29, 249–261. https://doi.org/10.1111/j.1574-6941.1999.tb00616.x
Steger, F., Rachbauer, L., Windhagauer, M., Montgomery, L.F.R., Bochmann, G., 2017. Optimisation of continuous gas fermentation by immobilisation of acetate-producing Acetobacterium woodii. Anaerobe 46, 96–103. https://doi.org/10.1016/j.anaerobe.2017.06.010
Steinberg, L.M., Regan, J.M., 2008. Phylogenetic Comparison of the Methanogenic Communities from an Acidic, Oligotrophic Fen and an Anaerobic Digester Treating Municipal Wastewater Sludge. Appl. Environ. Microbiol. 74, 6663–6671. https://doi.org/10.1128/AEM.00553-08
Thauer, R.K., Kaster, A.-K., Seedorf, H., Buckel, W., Hedderich, R., 2008. Methanogenic archaea: ecologically relevant differences in energy conservation. Nat. Rev. Microbiol. 6, 579–591. https://doi.org/10.1038/nrmicro1931
Thermo Fisher Scientific Inc., 2014. Real-time PCR handbook. Waltham, USA.
Wang, Y., Zhang, Y., Wang, J., Meng, L., 2009. Effects of volatile fatty acid concentrations on methane yield and methanogenic bacteria. Biomass Bioenergy 33, 848–853. https://doi.org/10.1016/j.biombioe.2009.01.007
Woese, C.R., Fox, G.E., 1977. Phylogenetic structure of the prokaryotic domain: The primary kingdoms. Proc. Natl. Acad. Sci. 74, 5088–5090. https://doi.org/10.1073/pnas.74.11.5088
Xu, K., Liu, H., Du, G., Chen, J., 2009. Real-time PCR assays targeting formyltetrahydrofolate synthetase gene to enumerate acetogens in natural and engineered environments. Anaerobe 15, 204–213. https://doi.org/10.1016/j.anaerobe.2009.03.005

2.7 Contact Details

University of Natural Resources and Applied Life Sciences, Vienna

Ao.Univ.Prof. Dr.nat.techn. Andreas Paul LOIBNER

Konrad-Lorenz-Straße 20, 3430 Tulln an der Donau, Austria

+43 1 47654 97470

andreas.loibner@boku.ac.at

https://short.boku.ac.at/H97400-GeoBio-en

Main Author:

Hannes KONEGGER

Contributing Authors:

Niels WALDMANN

Artur ZADURYAN

Maria ZEISER

3 Geo-methanation in porous reservoirs

3.1 Introduction

Initially filled with natural gas and depleted during gas production, porous reservoirs have been in use for the storage of natural gas for decades. Besides natural gas, in the near future also H_2 will play a significant role serving as energy carrier and storage medium. The storage of natural gas enriched with H_2 within a porous reservoir has been demonstrated in field tests within the research project "Underground Sun Storage" ("USS")while the subsurface storage of 100 % H_2 will be demonstrated within the project "Underground Sun Storage 2030" ("USS2030") (https://www.uss-2030.at/en/). During the project "Underground Sun Conversion" it was proven, that a porous reservoir is suitable not only for the safe storage, but also for the conversion of H_2 and CO_2 to methane (Pichler, 2021). For this purpose, natural gas enriched with H_2, and CO_2 is injected into the reservoir, where methanogenic archaea convert these feed-gases to CH_4 and water (see equation 3-1) in a process called geo-methanation (see figure 3-1).

Equation 3-1 $$4H_2 + 1CO_2 <-> 1\,CH_4 + 2H_2O$$

These microorganisms are endemic to the reservoir and were involved in the original natural gas generation when the reservoir and its surrounding cap rock was deposited. More details to the microbial consortia can be found in chapter 2.

Based on this prove of concept the field experiments in "Underground Sun Conversion – Flexible Storage" were set up to further understand the overall process and optimize parameters for a reliable conversion with high rates. A major focus was set on the demonstration and investigation of flexible operating modes, as this flexibility will be needed in a future energy system. This includes the injection of different feed-gas ratios to figure out the limits and optima for geo-methanation.

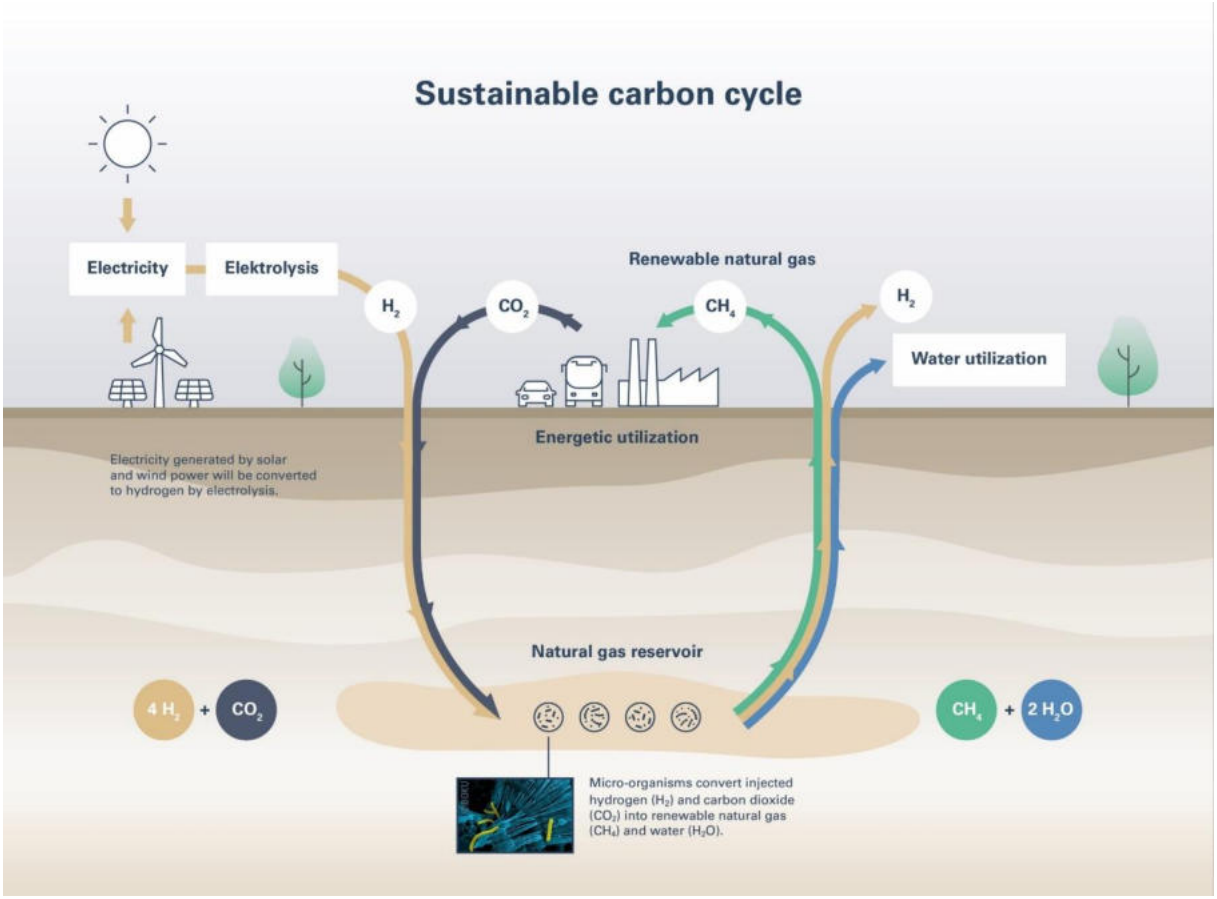

Figure 3-1: Scheme of the Underground Sun Conversion process, where H_2 and CO_2 are converted to CH_4 and water.

In general, there are today two kinds of subsurface structures that can be used for the storage of natural gas. One being artificially generated salt caverns and the other being naturally occurring porous structures. Salt caverns can be ruled out for geo-methanation as the high salinity inhibits microbial growth to a certain extent. The porous reservoirs are divided into depleted gas reservoirs and aquifer storages, the difference being that the former one has already been filled with gas and the later one is filled with water.

Both structures can potentially contain methane generating microbes which have been deposited in the subsurface along with the sandy material making up the reservoir. During the Underground Sun Conversion project, a thorough screening of RAG's own reservoirs as well as an internal literature review on the potential of subsurface formations to act as geo-methanation reactors has been done. So far, every gas reservoir in RAG's assets that was tested contained a microbial consortium able to metabolize hydrogen and carbon dioxide into methane. As a rule of thumb all subsurface reservoirs worldwide that contain gas of biogenic origin can be used as geo-methanation facilities. These make up about 20% of the known gas reservoirs in the world summing up to roughly 15 trillion Nm³ of volume (Rice, 1992).

The physico-chemical parameters of a reservoir required for geo-methanation are determined by the physiology of the methanogenic archaea. According to laboratory experiments this means a temperature window between 35 °C to 70 °C and a salinity below 4.4M and a pH-value between 6 and 9. The pressure might also have an influence on microbial growth, but this is not yet fully understood and needs further investigation (Dopffel et.al. 2021).

These parameters can be seen as given as soon as a reservoir is chosen for Underground Sun Conversion. Other parameters, which can be adapted during operation, have a major influence on the overall process. These include operation modes, injection/withdrawal rates, shut-in times and feed-gas composition. Depending on the available number of wells different operation modes can be applied for the geo-methanation process:

- Batch mode

A gas mixture is injected into the reservoir and stored for a predefined amount of time, before it is withdrawn. For this mode one well is sufficient, each additional well can increase the performance. While this mode involves the least effort, it also offers little room for influence during operation.

- Cycle mode

For this mode at least two wells are necessary. While a gas mixture is injected into one well, at the other one gas is withdrawn and recycled to the first well. At this point additional H_2/CO_2 can be admixed, increasing the flexibility and opportunities for influence on the overall process. Also, the continuous gas flow enables the injected gas to reach as large an area of the reservoir as possible. This increases methanation rates, more methanogenic archaea are supplied with feed gases.

The feed gas composition plays a significant role, as it directly influences the production rates of microbial consortia responsible for geo-methanation (methanogenesis). On the one hand, geo-methanation rates themselves are highest with a certain H_{2in}/CO_{2in} ratio. On the other hand, methanogenesis may also be accompanied by other microbial reactions such as acetogenesis. Microorganisms following these competing pathways are favoured with certain H_{2in}/CO_{2in} ratios and may lead to a loss of H_2 or in worst case an acidification of the reservoir. More information on these microbial pathways can be found in chapter 2.

3.2 Materials, Methods

3.2.1 Field test site

A depleted gas reservoir situated within the assets of RAG Austria AG in Upper Austria is used to act as a field test site. This reservoir was already used for field experiments for the projects “Underground Sun Storage” (“USS”) and “Underground Sun Conversion” (“USC”). Figure 3-2 and figure 3-3 give a schematic overview of the main package units and an aerial view of the field test site, respectively.

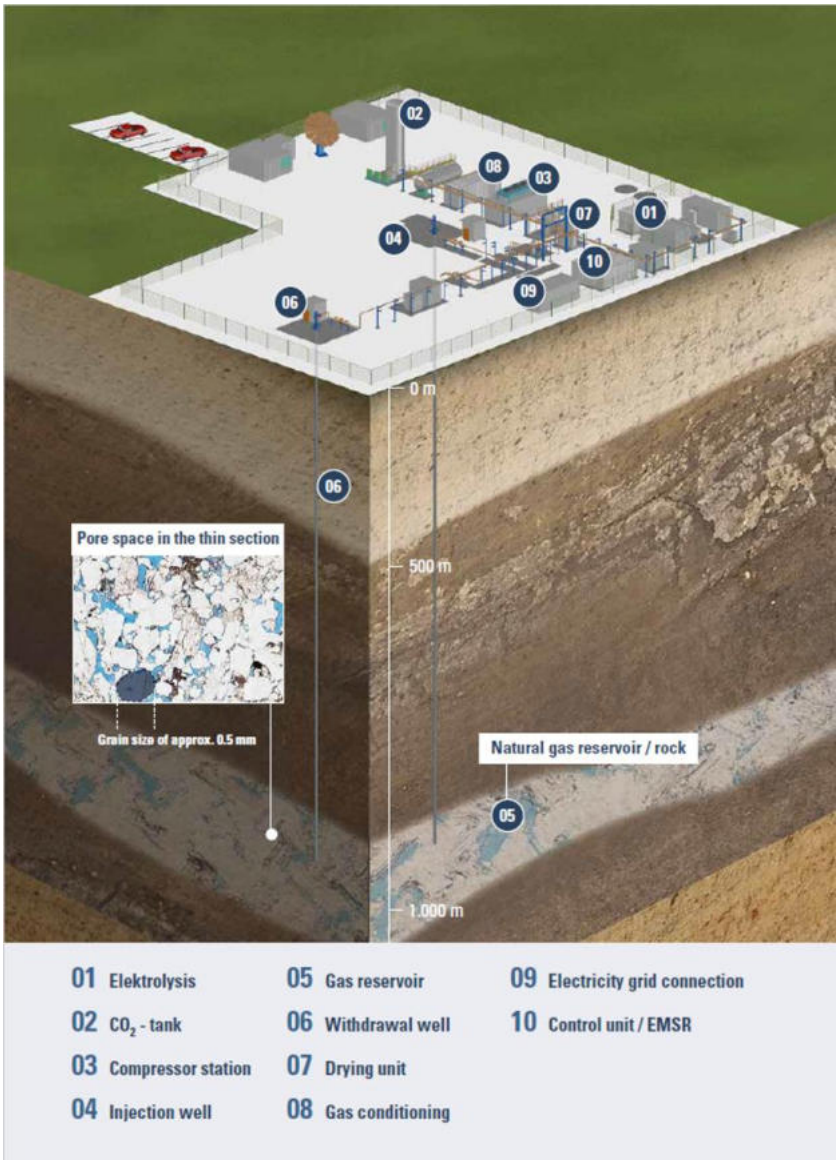

Figure 3-2: Schematics of the Underground Sun Conversion Facility

A few facts and figures:

- Electrolysis: 500 kW alkaline
- CO_2 logistics: 18 t buffer tank; liquid CO_2 via trailer from bioethanol production
- Compressor: piston compressor
- Drying unit: silica drying
- Gas conditioning: membrane technology
- Gas Chromatography
- Wells:
    - LEH-002A – original production well, recompleted for energy storage purposes
    - LESP-001A – well for cycle operation mode

Figure 3-3: Aerial view of the field test site

3.2.2 Reservoir characterization

The reservoir rock is a litharenitic sandstone with a weakly carbonated non-cemented matrix. This sandstone body is enclosed by clay rock and lies isolated in the shallower layers of the molasse zone (Haller series) at a vertical depth of 1,023 meters. The initial pressure in the reservoir was 107 bar(a). The permeability is up to 2000 mD [millidarcy] as was confirmed by SCAL (special cores analysis). The temperature of the gas reservoir is about 40 °C. It is a sweet gas deposit with low reservoir brine salinity (14,000 mg/l NaCl) that has a pH value of ~6-6,5. Communication with other layers or an active aquifer can be excluded due to the volumetric behavior of the reservoir during the depletion phase. Previously to the projects Underground Sun Storage and Underground Sun Conversion the reservoir was depleted down to a pressure of 19 bar(a). Any communication with adjacent layers or a larger water body would have resulted in an increase of this pressure or significant water production at the end of the production phase. The overall gas production from the reservoir was roughly 4,7 million Nm³ of natural gas with another 1,8 million Nm³ that remained. One part of the remaining gas, the cushion gas, in this case describes natural gas that is on the one hand used to keep the pressure above a certain operation point in order to provide the necessary flowrates when producing from the reservoir. On the other hand, there is always gas that is irrecoverable as it is kept in the reservoir by capillary forces. In total this means a gas volume of approximately 6,5 million Nm³ which makes the reservoir especially small when compared to commercial gas storages which usually contain gas volumes of more than 200 million Nm³.

The reservoir parameters are very well comparable to the parameters of RAG's commercial gas storages, but the volume is much smaller which makes operation and monitoring much easier thus providing a test opportunity but with justifiable effort.

3.2.2.1. Well LEH-002

The Lehen gas reservoir initially was produced by only one well which is the well LEH-002. When drilled in 2007 the well hit the target reservoir in the Haller Series at a beneficial position with a good connection to the overall gas volume and a low water saturation in the near wellbore region. The well hit the target reservoir at a depth of 1023 mTVD (vertical depth) which corresponds to a length of the wellbore of 1145 mMD (measured depth) which means, that the well path is slightly slanted. The well LEH-002 was used as an injection and production well for USS. In that project the well had been exposed to hydrogen for almost one year (2015 – 2016). In order to rule out any negative effects due to the injection of hydrogen the well had an initial assessment of its integrity previously to the start of hydrogen injection. CBL (Cement Bond Log for detection of microfractures in the cement) and USIT (Ultra Sonic Integrity Tool for detection of corrosion of the casing) measurements have been performed before and after the project to monitor any changes that might indicate damage to the well components due to hydrogen exposure. A new completion (Tubing, SSSV, Packers) was inserted into the well to also have a clean baseline for monitoring changes. It was also taken out after the project was finished and sent back to the manufacturer for testing. The investigation didn't yield any evidence, that physical or chemical changes had happened to the well during the USS project. More details can be found in the final report of the project Underground Sun Conversion (USC) (Pichler, 2021).

3.2.2.2. Well LESP-001A

A second well (LESP-001A) was drilled during the USC project. It was necessary to enable cycling of gas through the reservoir as was planned in the project and also delivered additional insight to the geological situation of the reservoir. When drilling the well LESP-001A also reservoir- and cap rock cores have been drilled out of the formation to have material available for integrity testing of the reservoir as well as in-situ materials for microbial laboratory experiments. This way it was possible to have experimental conditions as close as possible to real reservoir conditions.
Unfortunately, during testing of the new well it became apparent, that the connection between the two wells was not good enough to conduct subsurface cycle experiments. However, on the positive side the second well provided the opportunity to do more and faster testing within the same reservoir and with only minimal interference between the compartments leading to important findings regarding microbial distribution in a porous reservoir.

3.2.3 Operation modes

3.2.3.1. Batch experiments

As mentioned above, two modes of operation have been executed in the field-test. One being the batch experiments and the other being the modified cycle experiments. Batch-experiments are performed at well LEH-002 as it has the bigger operational volume. A gas mixture consisting of hydrogen, carbon dioxide and natural gas is injected into the well and stored there for a predefined amount of time. Afterwards it is withdrawn and the differences in gas composition are recorded and analysed. In addition, the gas from the batch is cycled to the well LESP-001A to act as carrier gas (hydrogen and natural gas) for the experiments conducted in this part of the reservoir.

The two batches conducted during USC-FlexStore consisted of a gas mixture containing up to 10 vol. % H_2 and up to 1.3 vol. % of CO_2. The further reduction in cycle volume compared to the USC project and the low number of batches are due to the fact that the LESP-001A is clearly the more microbial active well and LEH-002 was mostly used for storage of the carrier gas and for flow behaviour experiments. Table 3-1 gives an overview about the batches that have been performed. A detailed discussion of the batches will follow in chapter 3.3.

Table 3-1: Short description of performed batches at well LEH-002

Batch	Volume moved in and out [Nm³]	Findings
BATCH I	600.000	Gas Mixture: Injection of constant H_2 ratio (10 vol. %) and changing CO_2 concentration (0.3 – 1.3 vol. %). Equilibration of CO_2 throughout the batch. Hydrogen accumulation around the wellbore no longer influenced by mixing with original gas
BATCH II	715.000	Conversion: No injection of additional CO_2 therefore further slow conversion of the CO_2 in the cushion gas and minor decrease in hydrogen concentration. H_2S generation no longer apparent as no more SO_4 can be detected in the reservoir brine.

3.2.3.2. Modified Cycle experiments

It became already apparent during the USC project that although both wells have very good performance parameters their subsurface connection is not sufficient to sustain a continuous cycle operation within the reservoir. As laboratory experiments showed that gas movement is an important factor for the efficiency of the geo-methanation process it was therefore decided to cycle the gas at the surface by withdrawing from one well and injecting into the other. While this provides movement to the gas it is still no full substitute to subsurface cycling as the gas cannot use the whole reservoir volume, and therefore the whole microbial consortium for conversion. The highest converting areas are in this case located around the wellbores where flow speed is highest and fresh feed gas is readily available.

What also plays a role is the fact that hydrogen and carbon dioxide do not move through the reservoir at the same speed. Hydrogen has a higher mobility and therefore tends to spread further into the reservoir than carbon dioxide. This means that the dispersive forces defining the flow do lead to some mixing of the hydrogen bearing gas mixture with the gas that is already in the reservoir. Diffusion on the other hand does not seem to have an influence on the distribution of hydrogen throughout the reservoir (see also Figure 3-7). In addition, the water solubility of carbon dioxide is higher than that of hydrogen meaning that it will readily dissolve in the pore water near the wellbore but will only slowly reach further into the reservoir. Apart from these physical challenges, the microbes responsible for the geo-methanation are not homogenously distributed throughout the reservoir.

Therefore, the modus for cycling gas in the reservoir was changed in a way that the gas injected in LEH-002 contained hydrogen and only minor amounts of CO_2 (up to 1.3 vol. %). In a second step this gas was withdrawn from LEH-002 and mixed with additional CO_2 (up to 2.3 vol. %) and injected into LESP-001A where it was converted. Thus, the operation in Lehen actually tested a most likely scenario for a future energy system where carbon dioxide is continuously available, and hydrogen is provided from a storage as its production will be more fluctuating.

3.2.4 Result values for geo-methanation

3.2.4.1. H_2/CO_2 ratio

- Input ratio (H_{2in}/CO_{2in})

The H_{2in}/CO_{2in} ratio in the feed gas directly influences the microbial processes inside the reservoir. This is one of the most important parameters for actively controlling the microbial processes in the reservoir.

- Converted ratio (H_{2conv}/CO_{2conv})

The H_{2conv}/CO_{2conv} ratio indicates the overall main reaction(s) of a single experiment or a series of experiments since different ratios can be attributed to different reactions (see chapter 2). These result values are essential to find out which experimental conditions support which microbial reactions.

3.2.4.2. Methane evolution rate (MER)

The MER gives the volume of methane produced (Nm^3) per used pore space (m^3) and day (d) (unit: [$Nm^3\ m^{-3}\ d^{-1}$]). It can be calculated either via an increase in methane volume, or via a decrease in CO_2 and/or H_2 volume. In order to strengthen the validity of the results, all three calculation methods were performed and compared.

3.2.5 Material & corrosion testing

Several corrosion tests for the materials used were already performed in course of the projects “Underground Sun Storage” and “Underground Sun Conversion”. The main outcome of these tests was, that no change in corrosion behaviour between natural gas and natural gas mixed with H_2/CO_2 was observed (Trautmann, 2020; Rockmann and Lubenau, 2021). For further confirmation of these results, corrosion control coupons (CCC) were installed in the gas path of the plant and within the well and their degree of corrosion was determined.

3.3 Results and Discussion

3.3.1 Overall Performance of the plant

Within this project 2 major batches of natural gas mixed with up to 10 vol. % H_2 and up to 1.3 vol. % CO_2 were injected into the larger reservoir compartment LEH-002. Using these gas batches 32 modified cycle experiments were performed, 16 in each LEH-002 and LESP-001A. With every withdrawal and injection of gas volumes from/to the reservoir conclusions could be drawn about the processes and reactions in the reservoir. With every field test performed more operational experience is generated. This concerns the subsurface as well as the surface facilities, from electrolysis to gas conditioning.

3.3.2 Reservoir integrity and productivity

From the literature and laboratory experiments concerns were raised that an extended period of microbial activity in the reservoir might lead to exponential growth of theses microbes and therefore a loss in pore volume and permeability. In addition, the injection of CO_2 was also anticipated to cause some issues as it would change the pH value of the reservoir brine thus leading to dissolution of the calcareous minerals in the rock matrix. A thorough monitoring program was conducted during the project prevent such effects to go unnoticed. Subsurface pressure and temperature measurements have been done continuously throughout the project to monitor for changes in reservoir productivity or temperature changes that might be a signal for chemical reactions. Furthermore, water samples have been taken regularly to check for changes in the composition of the reservoir brine as well as the pH of the fluid.

The temperature monitoring in the reservoir of Lehen started already in 2014 when the USS project was started. The initial reservoir temperature is at ~40°C, but the monitored temperature shows only 39,5 °C. The reason for this is that the temperature needs to be monitored within the wellbore which is always slightly cooler than the reservoir itself. During injection the monitored temperatures are even lower as the injected gas has a temperature of 20°C and does not fully heat up before reaching the reservoir. During production the actual reservoir temperature can be monitored although it is also influenced by the injected cool gas. Overall, at the well LEH-002 the average temperature stayed constant during all projects so far which suggests that no sudden chemical reactions do happen within its part of the reservoir. This is further supported by the fact that no sand production does occur which would be an indication for dissolution of carbonates. At well LESP-001A the temperature started to slowly drop as the project progressed. This can be explained by the reservoir geometry. Where LEH-002 is well connected to the reservoir and has a calculated turn over volume of ~2 Mio. Nm³ the volume connected to LESP-001A is only about 0,08 Mio. Nm³. This smaller volume is naturally cooled down much faster (Figure 3-4).

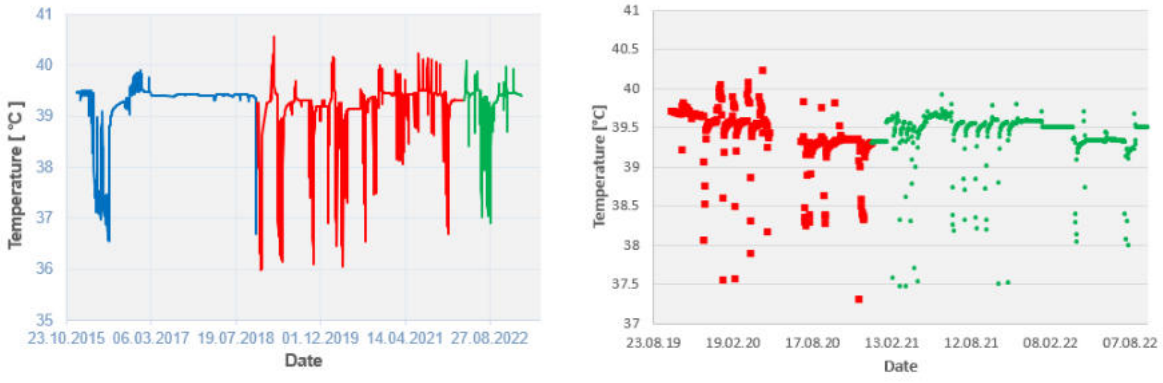

Figure 3-4: Temperature development in the wells LEH-002 (left) and LESP-001A (right). The blue color is the period of the USS project, the red color indicates the USC project, and the green color is the USC-

FlexStore project. The LEH-002 on average shows no changes in reservoir temperature. At LESP-001A the temperature started to drop as the smaller volume connected to the well is cooled down much faster.

Focusing on the reservoir productivity and the volumetric integrity flow tests as well as P/z analysis have been conducted to monitor the volume within the reservoir and the pressure development during injection and withdrawal. Ideally, each injection and withdrawal cycle would follow one curve at the P/z chart which would indicate no changes. However, in the case of Lehen the P/z chart started to shift towards the left during the USC and also during the USC-FlexStore project which can either indicate a decrease in volume or some kind of inflow (water, gas). The first shift happened after the first cycle of the USC project was performed. This coincides with the first injection into the well LESP-001A which although not well connected does influence the overall pressure behaviour of the reservoir (Figure 3-5). A second shift happened in between the USC and USC-FlexStore project and could be related to the break itself. The reservoir does not only consist of clean sandstone but has also some silty areas that are not very well connected (see LESP-001A). This means that gas needs some time to migrate into these areas and also time to migrate out of these areas. It is therefore assumed that the second shift is a product of gas inflow from tighter regions. This is further supported by the pressure gradient monitored during injection and withdrawal which is only shifted but stays exactly parallel. A smaller volume would be indicated by a steepening of the slope. Although the graphical solution is only a rough estimate it would still indicate significant changes in the reservoir volume. It is therefore concluded that the porosity and permeability of the reservoir rock did not significantly change during the USC-FlexStore project.

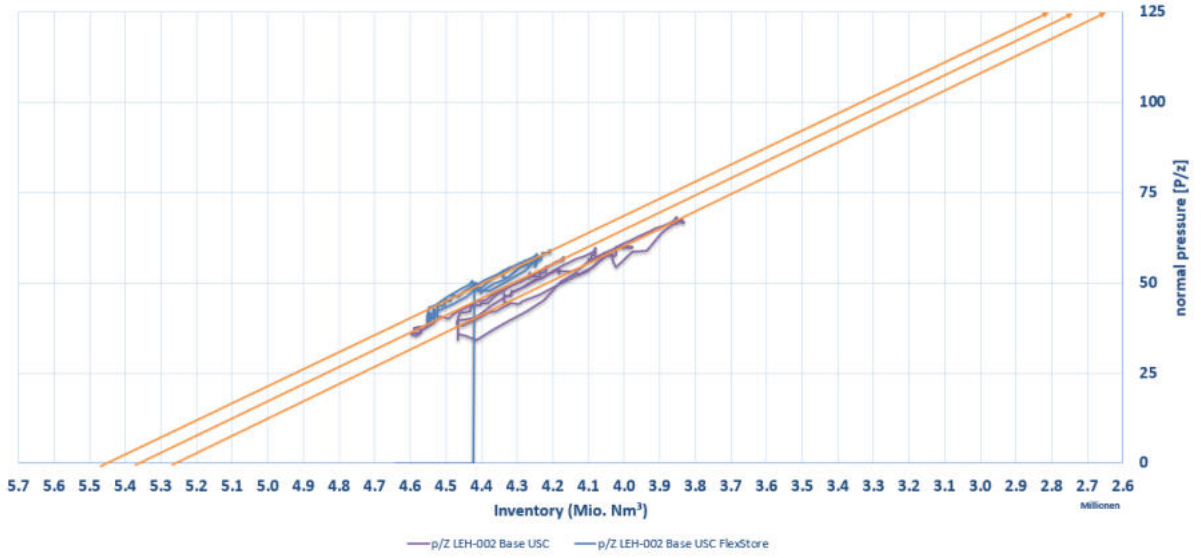

Figure 3-5: P/z plot for well LEH-002. The gradient of the research cycles is shifted towards the left but does not change its slope which suggests that the overall volume of the reservoir is not changed by the geo-methanation.

The same graph was prepared for the LESP-001A. There no clear trend can be monitored due to the small volume and a stronger influence from in- and outflow of water and gas. To get an idea on changes in the near wellbore region, pressure transient analysis (PTA) has been performed after each cycle. Here, no indication of changing permeability or productivity of the well could be monitored. As this well is microbially more active, exponential growth or parameter changes due to biochemical reactions would have been more pronounced than in LEH-002. As no changes could be found it can be deduced that the microbial activity in LESP-001A has no negative impact on the reservoir behaviour.

Two important aspects for storing non fossil gases in the subsurface have also been monitored during the USC-FlexStore project. It has already been discussed above that the pH value of the reservoir brine has been monitored throughout the project. At the start of the USC project, the water in both wells showed a pH value of ~8 which corresponds to the work over fluid that had been used for preparing the wells for the project. These values have changed in the meantime as reservoir brine has been sucked into the wellbore each time the reservoir has been depleted during storage operations. Especially, LESP-001A which is anticipated to be closer to the aquifer has seen a water production of almost 3 m^3 at the surface during the project. As not all the water is produced to the surface, some of the reservoir brine has stayed in the wellbore. This can also be seen when taking water samples at different depths as the work over fluid is much denser and does not readily mix with the reservoir brine. Monitoring samples have therefore only been taken in the shallowest regions of the water column in both wells. For well LESP-001A the pH value decreased down to 6 – 6,5 which very well corresponds to the original reservoir brine. For well LEH-002 the pH value decreased further reaching a level of 5,8. The difference is again assumed to be a product of microbial activity. While the fluid in well LEH-002 has almost no microbial activity due to a growth inhibiting work over fluid the fluid in well LESP-001A shows significant microbial activity. Thus, in LESP-001A the dissolved CO_2 is probably converted and therefore not changing the pH where else it does decrease the pH of the fluid in well LEH-002 (pH carbonic acid is 5,5). This effect however seems to be limited to the wellbore itself as the permeability around well LEH-002 did slightly decrease. If the pH would have decreased throughout the reservoir dissolution would have happened which would have increased the permeability. I should be noted that the water production does not correspond with the converted gas as the water volume generated via geo-methanation is negligible in comparison to the water volume already contained in the pores. It can be summarized that the injection and dissolution of CO_2 into the reservoir does not influence the integrity of the reservoir rock and the productivity of the reservoir.

The second important aspect discussed in the literature is the generation of H_2S via sulphur reducing bacteria. The Lehen reservoir contains the mineral pyrite that could be utilized for this process (Dopffel et.al, 2021). In addition, the original reservoir brine contained 15 mg/l of SO_4 which could also be used by the microbes to generate H_2S. Figure 3-6 shows the H_2S levels in the injected and withdrawn gas of the microbially more active well LESP-001A. It can clearly be seen that H_2S levels decreased at the beginning of the project but started to increase again when fresh CO_2 was injected into the reservoir. Even then a decrease can be monitored which suggests that H_2S generation is somehow limited. This limitation is anticipated to correspond with the reservoir brine as at the end of the project no more SO_4 could be detected in the reservoir brine. The pyrite which could be a possible sulphur source can only be dissolved at pH values below 3 and should thus stay stable in the reservoir. Another interesting observation is that H_2S levels tend to increase as soon as free water production starts in the well. This is especially prominent at day 385 where water production was forced from the well (high rates at low pressure) to get fresh reservoir brine into the wellbore for laboratory testing. From this it can be assumed that most H_2S is dissolved into the reservoir brine and not present in the gas phase. During the whole USC-FlexStore operation only 0,45 kg (corresponding to 0,35 ppm/Nm^3) of H_2S were withdrawn from the reservoir suggesting that H_2S generation during geo-methanation and during geological storage of hydrogen in one of RAG's gas reservoirs is not a major issue.

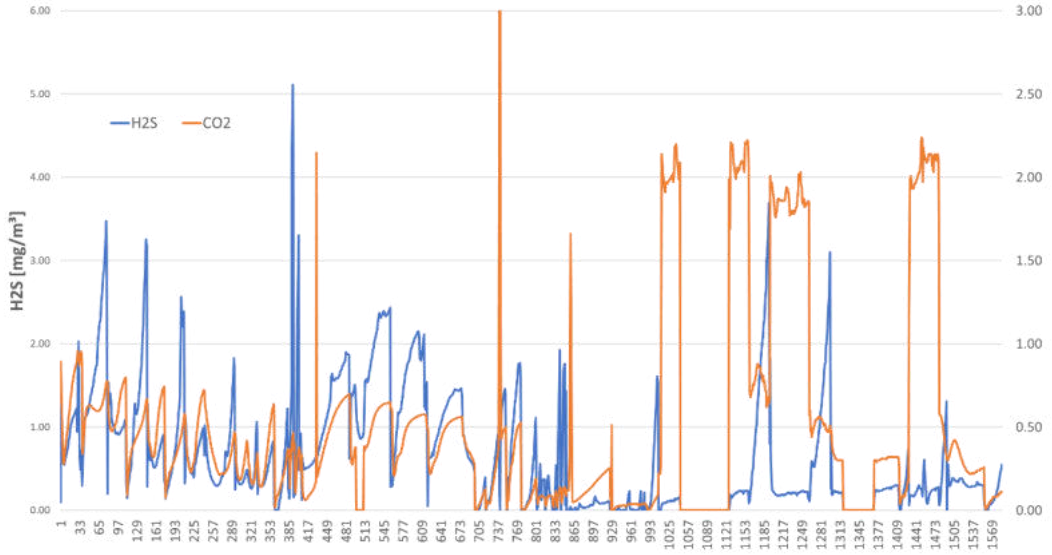

Figure 3-6: CO_2 and H_2S levels in the gas stream of well LESP-001A. The 4 spikes at the end of the project correspond with the optimized injection cycles of the USC-FlexStore project where two thirds of injected CO_2 could be converted within three weeks respectively

3.3.3 Gas mixing in the reservoir

It is important for the geo-methanation process to have a stoichiometric gas mixture distributed through the reservoir and especially in those regions where microbial activity is highest. As USC-FlexStore aimed on increasing the flexibility of the geo-methanation process different gas mixtures have been injected into the reservoir which were both stoichiometric and off stoichiometric. One thing that should be learned from the project was whether non uniform gas mixtures that are injected into a gas reservoir would equilibrate when stored. Figure 3-7 shows the carbon dioxide level during operation of Batch I in the well LEH-002. The injection of a gas mixture containing 10 vol. % of hydrogen from day 950 to day 1380 was done with different shares of carbon dioxide to see the effect of gas equilibration in the reservoir. As can be seen during withdrawal there was still some suggestion of a plateau, but the withdrawn mixture had a quite uniform carbon dioxide level. It should be noted that from 1760 Nm³ of carbon dioxide injected 1330 Nm³ were again withdrawn so conversion alone is not the reason for the equilibration. This is an important finding for future geo-methanation operations as it suggests that non-stoichiometric mixtures can be injected into the reservoir where they will equilibrate thus giving more flexibility to the process. Especially when comparing the anticipated fluctuating hydrogen production and the continuous carbon dioxide generation it is beneficial to not have the necessity to be only able to work with stoichiometric mixtures.

Figure 3-7: Carbon dioxide levels during operation of Batch I in well LEH-002

Another question that is even more relevant for the storage of hydrogen is whether or not the injected gas does mix with the cushion gas. As is described above the injected gas does mix very well which is probably related to dispersive flow that is especially relevant near the wellbore were flow speeds are highest. Further in the reservoir diffusive flow should be the driving mechanism for fluid mixing. During the USC and the USC-FlexStore projects it could be seen that the smaller volume operated around well LESP-001A is fully influenced by injected gas and no longer contains any cushion gas to mix with (Figure 3-8). Therefore, a relatively homogenous gas mixture was produced from this well in most cycles.

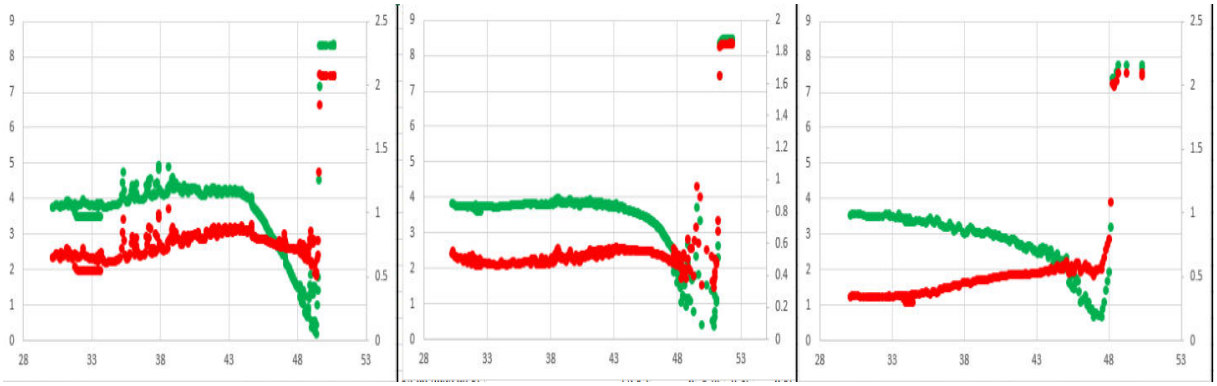

Figure 3-8: Hydrogen and carbon dioxide levels during withdrawal from well LESP-001A after three weeks of shut in. Hydrogen on the left y-axis (green) is decrease roughly stoichiometrically compared to carbon dioxide on the right y-axis (red). Except for the first volumes produced from the near wellbore regions the gas mixture tends to be homogenously distributed.

For well LEH-002 operating a bigger volume mixing of cushion gas and injected gas could be monitored. Not considering conversion the hydrogen levels tended to decrease towards the end of the withdrawal phase reaching a range of 2 – 6 vol. % of hydrogen in the withdrawn gas. One batch performed during USC even produced some of the cushion gas to get an idea of how far the hydrogen had migrated into it. A gradient calculation based on this cushion gas withdrawal revealed that about 6-8% of the injected hydrogen had migrated into the cushion gas. This effect is however assumed to be unique to the Lehen reservoir as its geometry (thin homogenous sand) supports mixing of injected gas and original gas. Figure 3-9 shows the last batch of the USC-FlexStore project where after the initial near wellbore volumes were withdrawn a quite uniform hydrogen distribution could be monitored.

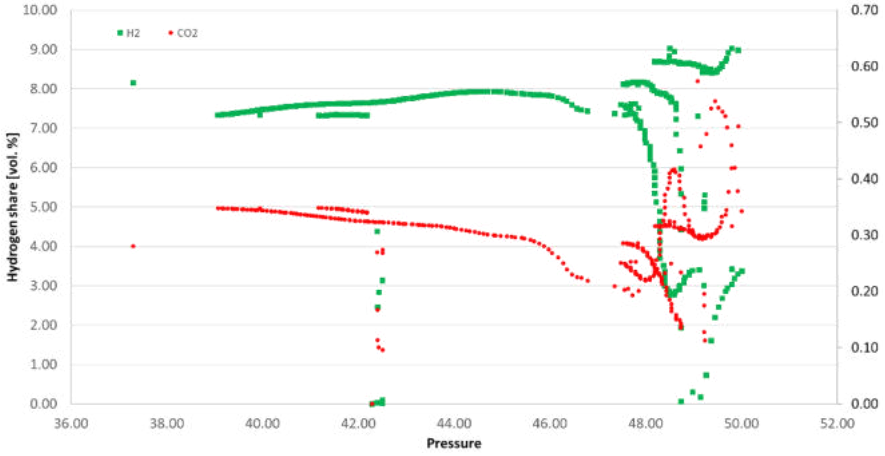

Figure 3-9: Hydrogen and carbon dioxide levels in Batch II of the USC-FlexStore project. The chaotic pattern at the beginning of the withdrawal is due to gas cycled in from well LESP-001A previously to the start of the withdrawal phase.

For carbon dioxide the mixing effect is not so pronounced which is on the one hand because the share of carbon dioxide in the injected gas is comparably low and on the other hand because there is already carbon dioxide present in the reservoir from the cushion gas.

3.3.4 Modified cycle experiments on geo-methanation LESP

Due to its higher microbial activity the smaller compartment “LESP-001A” (LESP) was used for the modified cycle experiments. These were the main field tests regarding the further development of geo-methanation. Figure 3-10 shows the resulting MER for all evaluated modified cycle experiments in LESP. A total of 16 modified cycle experiments were performed at LESP, 4 of which had to be excluded from further consideration due to technical problems (e.g., gas measurement) or insufficient gas volumes. Of the 12 remaining modified cycle experiments 2, 6, 3 and 1 were performed with an H_{2in}/CO_{2in} ratio of 20-28 (high), 6.5-12 (over-stoichiometric), 3.7-4.6 (stoichiometric) and 3-3.5 (low), respectively (Figure 3-11).

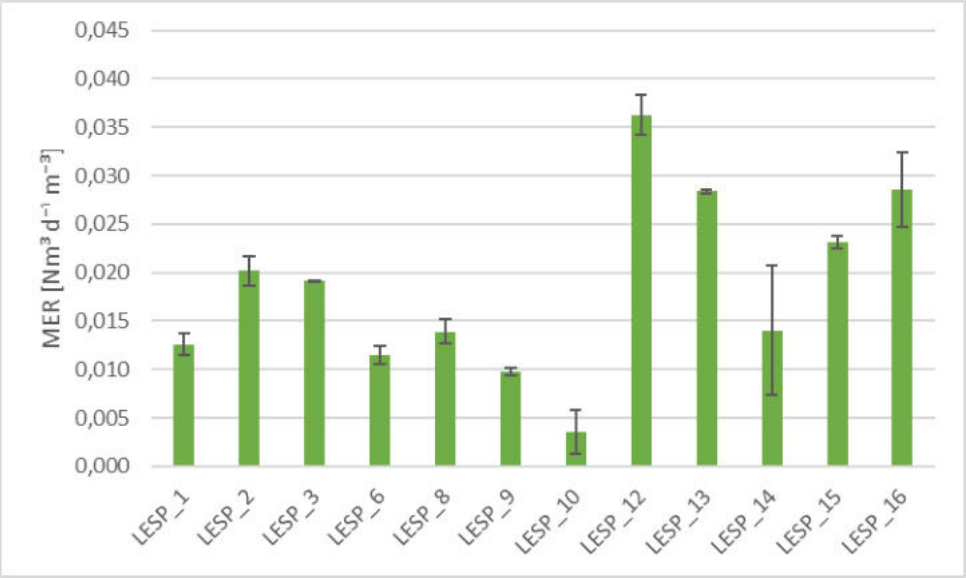

Figure 3-10: Methane evolution rate (MER, $Nm^3\ d^{-1}\ m^{-3}$) calculated via increase in methane and decrease in H_2 and CO_2 corrected by their corresponding stoichiometric factor over time and gas filled pore space for modified cycle experiments in LESP-001A. Error bars give standard deviation.

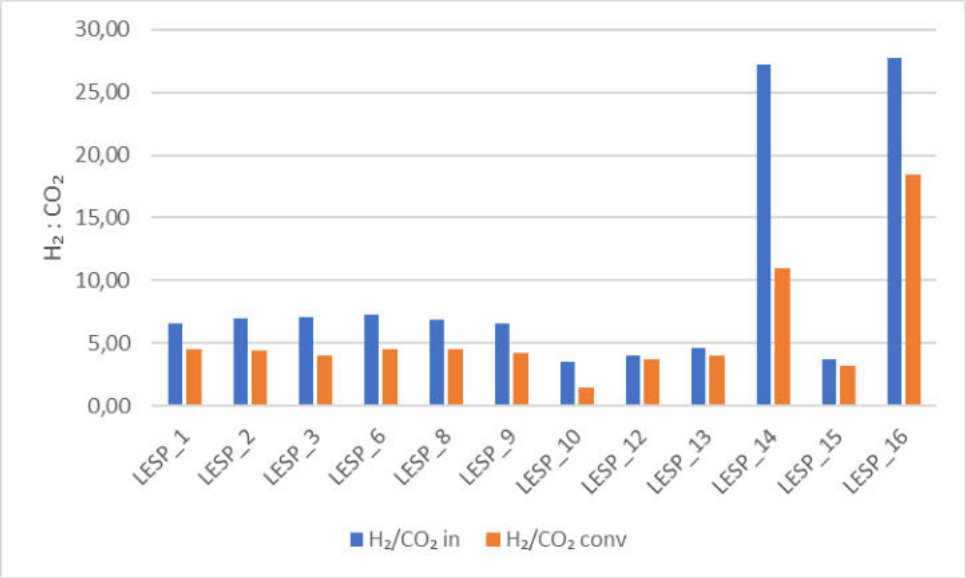

Figure 3-11: H_{2in}/CO_{2in} ratio and H_{2conv}/CO_{2conv} ratio for modified cycle experiments in LESP-001A.

It can be seen that stoichiometric H_{2in}/CO_{2in} ratios between 3.7 and 4.6 (LESP_12, LESP_13, LESP_15) lead to H_{2conv}/CO_{2conv} ratios of around 4, corresponding to the desired methanation. This is the expected output, which has already been shown in previous tests. This stoichiometric H_{2in}/CO_{2in} ratio implies a uniform injection of H_2 and CO_2. A corresponding mode of operation is possible, but severely restricts the application, as H_2 and CO_2 may be available at different times and in different quantities in the future.

But also, with over-stoichiometric H_{2in}/CO_{2in} ratios (6.5-7.5) this aimed H_{2conv}/CO_{2conv} ratio of 4 could be reached (LESP_1, LESP_2, LESP_3, LESP_6, LESP_8, LESP_9), showing the flexibility possibilities of this system. Over-stoichiometric means that more H_2 was injected than needed for the desired geo-

methanation reaction. This result has direct influence on the possible operation modes of the overall plant. As a surplus on H_2 is not harmful to the geo-methanation, at least in the range investigated, H_2 can be produced and directly stored in the reservoir in times of excess energy. Starting with a high H_{2in}/CO_{2in} ratio, CO_2 could be injected from time to time until the minimum H_{2in}/CO_{2in} ratio of 4 is reached.

Homoacetogenesis – the conversion of H_2 and CO_2 to acetate – is unwanted inside the reservoir. On the one hand it may lead to an acidification of the reservoir and thus may harm methanogenic archaea and the reservoir rock. On the other hand, it means at least a temporary loss of the energy sources used, when acetate is formed instead of CH_4. Unlike CH_4, which is extracted from the reservoir in gaseous form, the dissolved acetate remains underground and cannot be used further. Nevertheless, one run (LESP_10) under conditions beneficial for homoacetogenesis was performed to demonstrate the risk of this reaction. Here it can be seen that an H_{2in}/CO_{2in} ratio of 3,5 was low enough to result in a H_{2conv}/CO_{2conv} ratio of 1,5 and a very low MER.

This unwanted reaction of homoacetogenesis cannot be completely ruled out even under optimal operating conditions since conditions favourable for it may also occur locally in the subsurface. But as acetate can also be an educt for methanogenesis, even the acetate produced may be converted to methane in a second step. Intermediate runs with low CO_2 content were performed to test the conversion of the acetate produced to methane. A high H_{2in}/CO_{2in} ratio can benefit the conversion of volatile fatty acids, as these are used as carbon source instead of CO_2. This leads to a stabilization of pH as well as to additional CH_4 production from intermediate products, which would not be used otherwise. 2 runs with a high H_{2in}/CO_{2in} ratio of 27-28 were performed (LESP_14, LESP_16). With MERs comparable to stoichiometric and over-stoichiometric runs and high H_{2conv}/CO_{2conv} ratios, it could be shown, that another carbon source than injected CO_2 was used for methane production – most likely acetate.

Having a closer look at the modified cycle experiments with a H_{2conv}/CO_{2conv} ratio stoichiometrically correct for geo-methanation (around 4), the results give an insight to the microbial activity: Starting with a MER of 0.01 $Nm^3\ d^{-1}\ m^{-3}$ with experiment LESP_1 (H_{2conv}/CO_{2conv} ratio of 4.5) in 02/2021 and ending with a MER of 0.03 $Nm^3\ d^{-1}\ m^{-3}$ with LESP_13 (H_{2conv}/CO_{2conv} ratio of 4.1) in 11/2022, a continuous operation of the geo-methanation facility led to an increase in productivity. This can be explained on the one hand by the steadily growing operating experience, but also by the further activation of methanogenic archaea.

3.3.5 Modified cycle experiments on geo-methanation LEH

The larger compartment LEH-002 (LEH) was also used for modified cycle experiments. Moreover, it served as H_2 storage for LESP-001A. H_2 was produced in large volumes and injected to LEH-002, mixed with natural gas and small amounts of CO_2. For every run in LESP-001A, H_2-rich gas was withdrawn from LESP-001A, spiked with CO_2 and injected into LESP. This explains the strongly over-stoichiometric input H_2/CO_2 ratio. Figure 3-12 shows the resulting MER for all evaluated modified cycle experiments in LEH-002. 16 modified cycle experiments were performed in LEH-002, 7 of which had to be excluded from further consideration due to technical problems (e.g., gas measurement) or insufficient gas volumes. Of the 9 remaining modified cycle experiments 3 and 6 runs were performed with an H_{2in}/CO_{2in} ratio of 20-28 (high) and 6.5-12 (over-stoichiometric), respectively (Figure 3-13).

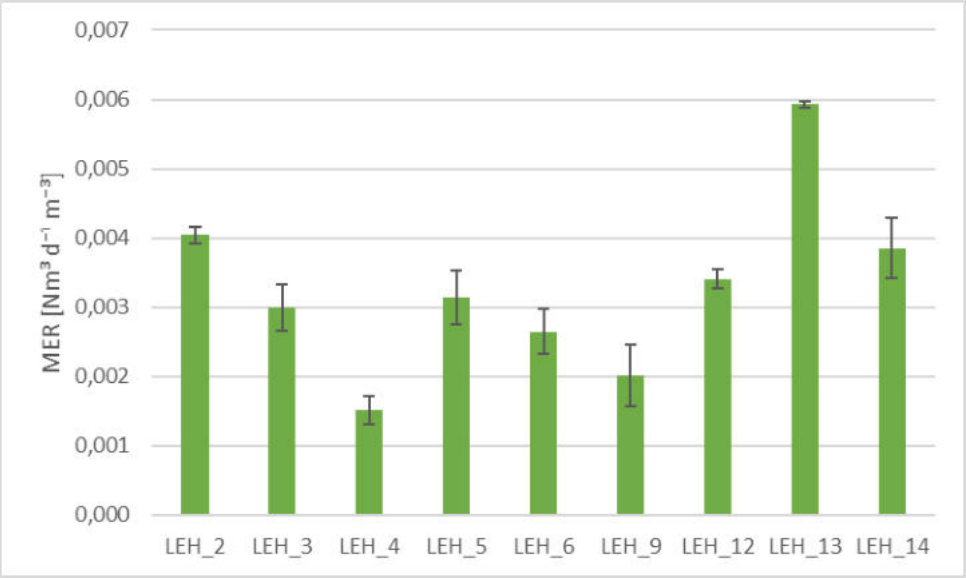

Figure 3-12: Methane evolution rate (MER, $Nm^3\ d^{-1}\ m^{-3}$) calculated via increase in methane and decrease in H_2 and CO_2 corrected by their corresponding stoichiometric factor over time and gas filled pore space for modified cycle experiments in LEH-002. Error bars give standard deviation.

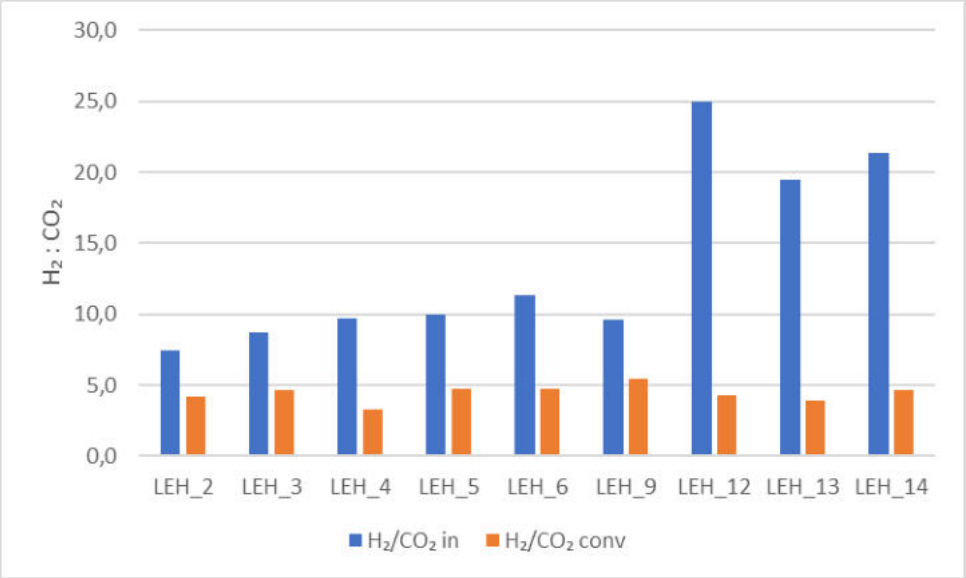

Figure 3-13: Input H_2/CO_2 ratio and H_{2conv}/CO_{2conv} ratio for modified cycle experiments in LEH-002.

It can be seen, that in all modified cycle experiments in LEH-002, both with high and over-stoichiometric H_{2in}/CO_{2in} ratio, the H_{2conv}/CO_{2conv} ratios result around 4, which corresponds with the desired reaction of methanation. Even though the MER are relatively low compared to LESP-001A, the H_{2conv}/CO_{2conv} ratios show, that methanation is the main net reaction in LEH-002 under the given circumstances. Nevertheless, the H_{2conv}/CO_{2conv} ratios vary between 3 and 5, indicating other reactions besides pure hydrogenotrophic methanogenesis. It can be assumed, that with H_{2conv}/CO_{2conv} ratios lower than 4, homoacetogenesis takes place to a certain extent. The produced acetate seems to be consumed for further methanation in runs with H_{2conv}/CO_{2conv} ratios higher than 4. The involved microbial processes are described in chapter 2.

3.3.6 Corrosion tests

To monitor corrosion in the facility, corrosion control coupons (CCC) were distributed throughout the facility at critical points (e.g., Bends, Valves, at the perforations). These were changed on regular basis and evaluated on changes in a laboratory. With a corrosion rate below 0,01 mm/a for all CCC, no differences in corrosion between the usage of natural gas and natural gas with up to 10 % H_2 and 2.5 % CO_2 could be detected. This confirms the results of earlier studies (Pichler, 2021).

3.4 Conclusion

The modified cycle experiments confirm and reinforce previous results from field and lab. Geo-methanation was well proven and input parameters optimized regarding MER. The monitoring of pressures and temperatures in the subsurface as well as the appraisal of the reservoir performance leads to the conclusion that the reservoir quality and reservoir integrity is not influenced by the storage of gaseous hydrogen and carbon dioxide. In addition, no influence of the gas used on the corrosion rates of the corrosion coupons used and thus of the overall system could be detected.

An important topic that will also get further attention in RAG's hydrogen storage projects is the gas mixing. From the tests with hydrogen bearing gas mixtures, there are indications that hydrogen mixes with the original gas near the wellbore. However, it does take quite long to migrate into the gas on the fringes of the reservoir. This might be an effect of the unique geometry of the Lehen field, but it can also be assumed that dispersive flow is responsible for mixing of gases. Diffusion seems to be a negligible effect in the porous media storage system.

The results of the modified cycle experiments with over-stoichiometric H_{2in}/CO_{2in} ratios show the flexibility possibilities of geo-methanation. Here it was shown, that also with over-stoichiometric H_{2in}/CO_{2in} ratios, methanogenesis is the main microbial reaction in the reservoir. As a surplus on H_2 is not harmful to geo-methanation, H_2 can be produced and directly stored in the reservoir in times of excess energy, while CO_2 would then be added based on its availability from time to time. This is an important input to the operational concepts considered in chapter 6.

Another crucial result especially for pure hydrogen storage is that CO_2 can be a limiting factor for geo-methanation. As soon as CO_2 is below a certain threshold, methanogenesis stops. This suggests that, as long as no CO_2 is present, H_2 can be stored in an underground reservoir, even if methanogens are present. For the storage of 100 % H_2, as demonstrated in USS2030, this is a major finding.

3.5 Abbreviations

CO_2	Carbon-Dioxide
CH_4	Methane
H_2	Hydrogen
H_{2in}/CO_{2in}	Input H_2 : CO_2 ratio
H_{2conv}/CO_{2conv}	H_2 : CO_2 ratio of converted gas volume
MER	Methane evolution rate [Nm^3 CH_4 * m^3 pore space volume^{-1} * day^{-1}]
USC	Underground Sun Conversion (Project, 2017-2021)
USC-FlexStore	Underground Sun Conversion – Flexible Storage (Project of this report, 2020-2023)
USS	Underground Sun Storage (Project, 2013-2017)
USS2030	Underground Sun Storage 2030 (Project, 2021-2025)

3.6 References

Dopffel N., Jansen S., Gerritse J. (2021) Microbial side effects of underground hydrogen storage–Knowledge gaps, risks and opportunities for successful implementation. International Journal of Hydrogen Energy (46) 8594-8606. DOI:10.1016/j.ijhydene.2020.12.058

Fazeni-Fraisl K. et.al. (2021) “Geo-Methanation – Lifecycle Assessment” in Bauer, S. et.al. (2021) Underground Sun Conversion. Final Report. Available at: https://www.underground-sun-conversion.at/en/downloads/endbericht.html (Accessed: 02 May 2023)

Pichler M. (2021) „In Situ Fieldtest“ in Bauer, S. et.al. (2021) Underground Sun Conversion. Final Report. Available at: https://www.underground-sun-conversion.at/en/downloads/endbericht.html (Accessed: 02 May 2023)

Rice, D.D. (1992) Controls, Habitat, and Resource Potential of Ancient Bacterial Gas. Bacterial Gas Conference, Milan.

Rockmann R., Lubenau U. (2021) Untersuchungen zu Auswirkungen biochemischer Prozesse auf die Speicherung und Fließverhalten von Wasserstoff in Untergrundspeichern. Final project report. DBI. Available at: https://www.dvgw.de/medien/dvgw/forschung/berichte/g201816-sunconversion-abschlussbericht.pdf (Accessed: 02 May 2023)

Trautmann A. (2020) Wasserstoffversprödung von Werkstoffen bei der Erzeugung erneuerbarer Energien. Dissertation. Montan Universität Leoben, Lehrstuhl für Allgemeine und Analytische Chemie. Available at: https://pureadmin.unileoben.ac.at/ws/portalfiles/portal/8058465/AC16402019.pdf (Accessed: 02 May 2023)

3.7 Contact Details

RAG Austria AG

Schwarzenbergplatz 16, 1015 Wien, Austria

+43 664 3845255

benedikt.hasibar@rag-austria.at

www.rag-austria.at

Authors:

Benedikt Hasibar

Markus Pichler

4 Demand and Supply Model

Contents of this chapter have been published in the following peer-reviewed journal publication:

Rüdisüli, M., Mutschler, R., Teske, S.L., Sidler, D., van den Heuvel, D.B., Diamond, L.W., Orehounig, K., Eggimann, S., 2023. Potential of renewable surplus electricity for power-to-gas and geo-methanation in Switzerland. Int. J. Hydrogen Energy 48, 14527–14542. *https://doi.org/10.1016/j.ijhydene.2022.12.290*

4.1 Introduction

4.1.1 Motivation

To quantitatively investigate the techno-economic potential of geo-methanation at a national, regional, and local scale, an H_2 and CO_2 supply model is needed at an adequately high spatial and temporal resolution. The working principles of this model are described in the following chapter for the case of Switzerland, which may, however, readily be generalized for other countries and their energy systems (See the similar demand and supply model for Austria (AT) in chapter 4.5).

The demand and supply model is based on the existing Swiss energy system model of Rüdisüli et al. (2019) and the power-to-X model of Teske et al. (2019). These models are extended herein for the needs of geo-methanation in the context of the project “Underground Sun Conversion – Flexible Storage” (USC-FlexStore) and they are accompanied by additional energy system transition scenarios based on the latest national (Prognos, 2020) and international (ENTSOE, 2020a) energy system transition strategies.

4.1.2 Economic boundary conditions

Regarding potential sites for USC-FlexStore, there are generally two economically viable options (Teske et al., 2019): 1) close to CO_2 sources (e.g., cement plants, etc.) or 2) on the site of a power plant (e.g., hydropower plants, etc.). Proximity to CO_2 sources features the advantage that CO_2 does not have to be transported over long distances to USC-FlexStore sites, which would otherwise result in additional transportation and distribution costs. However, if there is not enough electricity generated at the CO_2 source, additional grid fees for the required electricity have to be paid, which will eventually increase the levelized costs of USC-FlexStore products. Therefore, sites at power plants (ideally with a nearby CO_2 source), are generally more economically viable. Municipal waste incineration plants (MWIP) feature both, sufficient on-site renewable electricity generation and separable CO_2. This is in accordance with regulations of the Federal Office for the Environment (FOEN), which claim that about 50% of their incinerated waste and thereof produced energy (heat and electricity) is renewable (Spoerri et al., 2010). They are therefore - along with run-of-river (RoR) power plants - the most promising site for USC-FlexStore (Gupta et al., 2022). RoR features, in particular, large amounts of renewable electricity generation at the same time when the largest amounts of surplus electricity from PV occur in summer. In other words, by using electricity from RoR for USC-FlexStore, an additional market to sell RoR electricity is established in times when electricity market prices are more and more on the decline due to a broad expansion of PV all over Europe. In these times, even negative electricity prices may occur (Götz et al., 2014). Without this additional market for RoR electricity, PV expansion may otherwise gradually displace hydropower from the market.

4.1.3 Geological boundary conditions

If geo-methanation is envisaged, besides economic boundary conditions, there are also geological boundary conditions that must be fulfilled. To this end, the GeoMol model (Baumberger and Allenbach, 2016) provided by the University of Bern (see chapter 5) is used. GeoMol is the geological 3D model of the Swiss Molasse Basin with information about which rocks can be found at which depth, large fracture

zones, etc. GeoMol also has a temperature component, that is, isotherms that determine the temperature increase with increasing depth. However, the area covered by these isotherms does not exactly correspond to the outline of the GeoMol model. Therefore, two outlines covered by the GeoMol model are used:

- A smaller (inner) one is the outline of the area covered by the isotherms, where data is available.
- The larger (outer) one is the outline of the “Top Bedrock” layer of the model.

As the principal outline in this work, outline 1) with the isotherms is used. As an extension, or if relevant, also outline 2) is used to quantify the additional potential for USC-FlexStore in geologically also interesting, yet not fully documented areas.

4.2 Materials, Methods

4.2.1 Scenarios

In this analysis, four scenarios of the Swiss Energy system are used to evaluate the potential of USC-FlexStore. While the “reference” scenario 1 features the current Swiss energy system as a benchmark, scenarios 2 - 4 represent a future Swiss energy system with low, medium, and high renewable energy and efficiency expansion. Renewable energy expansion is mainly achieved by the substitution of nuclear power by PV and wind, while increased efficiency is achieved by the widespread electrification of heat and mobility.

These scenarios do not represent particular years in the future, but they are rather snapshots of important intermediate states of the Swiss energy system transition. With the aid of the official transition pathway “ZERO Basis" of the Swiss Federal Office of Energy (SFOE) in their “Energy Perspective 2050+” (EP2050+) (Prognos, 2020), the scenarios can, however, roughly be allocated to the years 2020, 2030, 2040 and 2050.

To have greater variability with respect to different weather conditions, all scenarios are based on multiple historical weather years, namely, 2016, 2017, and 2018. This way, global warming can be considered as well since these weather years already contain characteristics of a future climate with mild and wet winters as well as hot and dry summers (Mutschler et al., 2021). Further climate change-related adjustments regarding energy demands (e.g., additional cooling) and supply (e.g., shifted hydropower) are not considered.

4.2.2 Basic modelling principles and assumptions

For USC-FlexStore, the availability of renewable surplus electricity is important (Teske et al., 2019). Momentary (hourly) electricity surpluses occur if the momentary electricity supply is larger than the momentary electricity demand (and vice versa for deficits). To this end, the Swiss electricity system is modelled based on hourly demand and supply profiles to determine the daily availability of net surplus electricity in all four scenarios. Net surplus electricity is the amount of surplus electricity that remains after ideal intraday load shifting has been implemented to avoid the curtailment of renewable (PV) electricity at noon. This is graphically illustrated in Figure 4-1, in which the dark green area is the electricity shifted to offset night deficits within the same day and the light green area is the remaining net surplus electricity that can eventually be used by additional consumers such as for USC-FlexStore. Ideal load shifting assumes that there are no round-trip losses. This allows for a variety of potential technical solutions for this purpose. Intraday ideal load shifting can, for instance, be achieved by short-term electricity storage (e.g., batteries) and/or demand-side management (e.g., charging BEV at noon instead of evening hours).

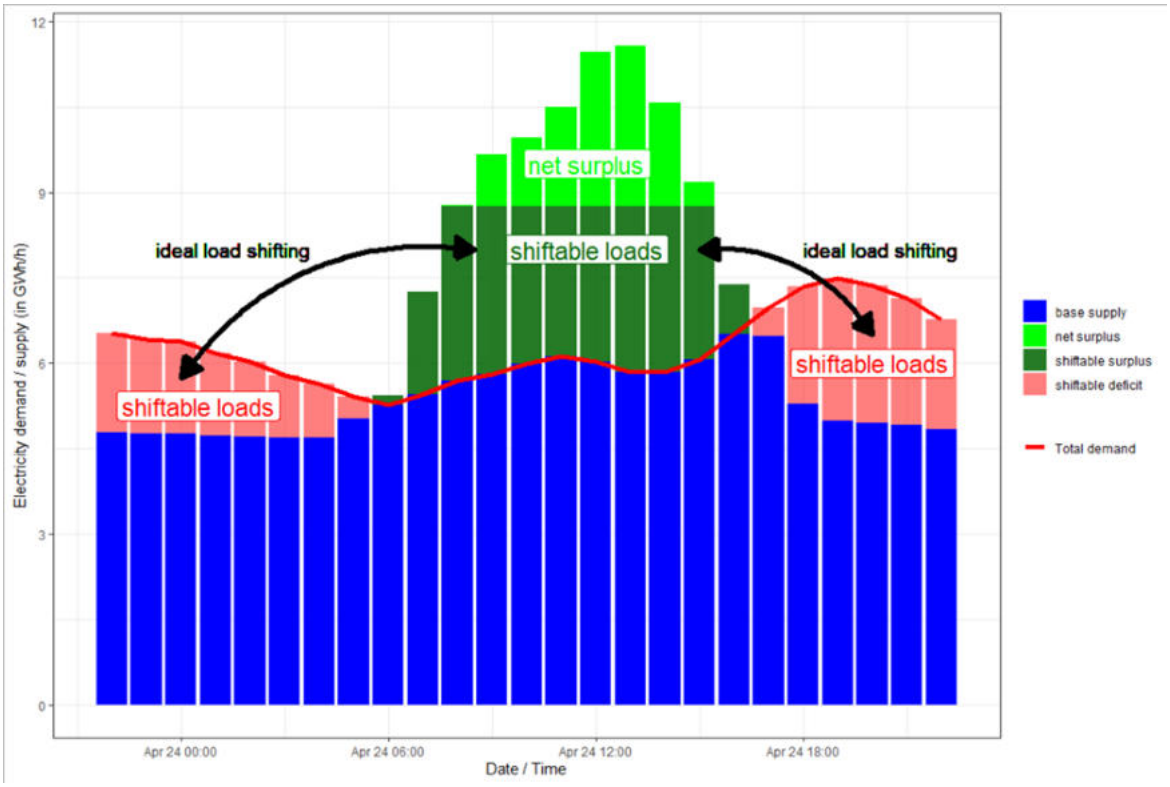

Figure 4-1: Schematic representation of the day/night balancing based on a section from 24 March 2016 in Scenario 3 (adapted from Teske et al. (2019).

In this respect, it is assumed that surplus generation at daytime (noon) and supply deficits during the rest of the day (night) are more likely to occur simultaneously in the future in many European countries due to similar PV expansion strategies (Lienhard, 2023). Therefore, it is assumed - in the sense of a worst-case scenario - that electricity exports are economically not viable due to these similar surplus situations in neighbouring countries and consequently low (at times even negative) prices on the electricity market (Götz et al., 2014).

Along with daily load shifting, flexible hydropower (storage and pumped hydro storage) is dispatched within five consecutive days based on the residual load as a proxy for the electricity market. Transmissive losses between different grid levels, etc. are not considered, instead, a “copper plate assumption” of the Swiss electricity grid is made.

In the next step, the amount of net surplus electricity available for USC-FlexStore at run-of-river (RoR) hydropower plants and municipal waste incineration plants (MWIP) - constrained by geological boundary conditions - are evaluated in a regionally aggregated as well as individual site-specific manner. With overall electrolysis (ELYSE) efficiency of 57% (Teske et al., 2019), the daily producible H_2 measured in the lower calorific value is calculated. Along with CO_2 from nearby industrial sources (cement plants, municipal waste incineration plants, and wastewater treatment plants), a daily feed of CO_2 and H_2 into the ground for USC-FlexStore is estimated. By default, this feed is non-stoichiometric due to a seasonal mismatch of CO_2 and H_2 supply. The tolerance of the geo-methanation process in the context of USC-FlexStore with respect to this non-stoichiometric feed of CO_2 and H_2 will be evaluated in separate work packages by means of a USC-FlexStore model (see chapter 2.2). As chapters 2 and 3 have outlined, the composition of the feed gases underlies restrictions. This model outlines the supply of CO_2 and H_2 respectively over time, which can be used to satisfy the mentioned conditions. Eventually, with the USC-FlexStore model, the CH_4 yield to meet a predefined gas demand is calculated.

A graphical overview of the model used in this study is shown in Figure 4-2. In the following chapters, the model is described in more detail.

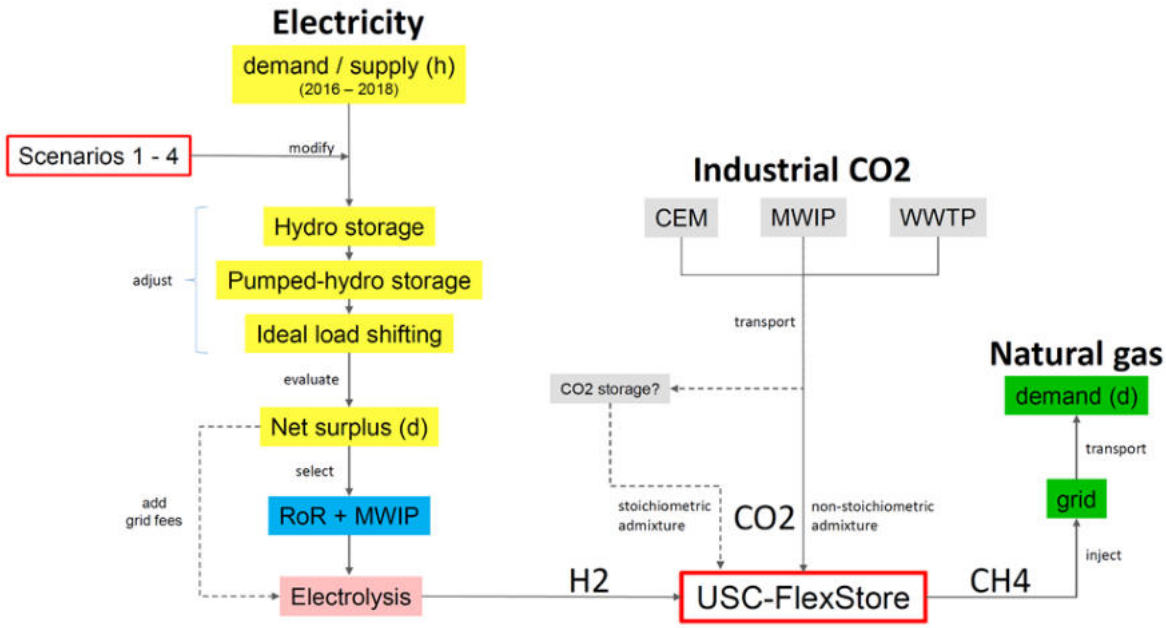

Figure 4-2: Schematic of the CO_2 and H_2 supply and demand model for USC-FlexStore.

4.2.3 Energy demand

4.2.3.1. Space heating and domestic hot water demand

The current annual Swiss space heating (SH) and domestic hot water (DHW) energy demand according to the Swiss national statistics on final energy consumption is about 72 TWh (weather-adjusted) and 12 TWh, respectively (BFE, 2019a). Both heat demands are still primarily covered by fossil natural gas and heating oil. In the future, there will be a substantial reduction of the SH demand by building retrofit and renewal. In contrast, for DHW no demand reduction is assumed. The evolution of this SH and DHW demand in the four scenarios is summarized in Table 4-1. All demands are in line with the scenario "ZERO BASIS" of "EP2050+" (Prognos, 2020).

Table 4-1: Main boundary conditions and assumptions on the evolution of the annual space heating (SH) and domestic hot water (DHW) demand (in TWh_th / year) in the four scenarios

Demand (in TWh_{th} / year)	**Scenario 1 (~2020)**	**Scenario 2 (~2030)**	**Scenario 3 (~2040)**	**Scenario 4 (~2050)**
Space heating (%reduction)	**72 (100%)**	**61** (-15%)	**54** (-25%)	**50** (-30%)
Domestic Hot Water (%reduction)	**12 (100%)**	**12** (-0%)	**12** (-0%)	**12** (-0%)

4.2.3.2. Gas demand

The current Swiss energy system (Scenario 1) has a total gas demand of about 34 TWh, which is mainly met by imported fossil natural gas (VSG, 2020). To achieve global decarbonization of the energy system, fossil natural gas should only be physically imported as a reserve, if the gas demand exceeds the availability of renewable gases such as biomethane (biogas) and SNG (including seasonal storage). This renewable gas can be produced as follows:

- **Biomethane**: Renewable biomethane (biogas) is produced uniformly and throughout the year both in CH and EU.
- **Synthetic Natural Gas:** Synthetic natural gas (SNG) is produced whenever there is renewable net surplus electricity by means of power-to-methane (including USC-FlexStore).

In the future energy system, a gas demand arises primarily from the following three energy sectors:

- **Industry**: In the industrial sector, several processes are hard to electrify and therefore still rely on gaseous (or liquid) fuels in the future. This is the case for high-temperature process heat, whose (gas) demand is assumed constant throughout the year.
- **Transport**: While short-distance and passenger cars mobility is assumed mostly electrified in the future, heavy-duty and long-distance transportation (trucks, buses, shunters, etc.) are still fueled by gaseous (and liquid) energy carriers such as H_2 and natural gas. Therefore, it is assumed that there is still a substantial and constant gas demand for this heavy-duty transportation.
- **Heat and Electricity**: Season-dependent gas demand for heating and electricity constitutes the remaining share of the future gas demand. It assumes that on a district-level, gas-fired combined heat and power (CHP) plants - depending on their role (guidance) in the energy system - will still provide (at least temporarily) electricity and heat, or vice versa. Due to a substantially larger need for this energy in winter, this gas demand follows a distinctive seasonal pattern with virtually no demand in July and its peak in January.

The evolution of this gas demand in the four scenarios distinguished by the energy sectors industry, transport, and others is summarized in Table 4-2. It is adapted from scenario “ZERO BASIS” of EP2050+ (Prognos, 2020). Figure 4-3, moreover, shows the monthly disaggregation of this gas demand by the different energy sectors. Based on the future annual gas demand per sector, the seasonal demand patterns are modelled according to normalized daily demand figures of gas customers. These daily figures are extrapolated from historical data of the Swiss gas market and given in a range of historical deviations for every day. The distribution patterns are furthermore influenced by the assumptions outlined above to consider the different influences of ambient temperatures and season per energy sector.

Table 4-2: Main boundary conditions and assumptions on the annual gas (Biomethane, SNG from USC-FlexStore and fossil natural gas) demand (in TWh_{th} / year) in the four scenarios.

Demand (in TWh_{th} / year)	**Scenario 1 (~2020)**	**Scenario 2 (~2030)**	**Scenario 3 (~2040)**	**Scenario 4 (~2050)**
Gas demand (%reduction)	**34 (100%)**	**29** (-15%)	**20** (-40%)	**14** (-60%)
Industry	11	10	7	6
Transport	0	1	2	3
Others	23	18	12	5

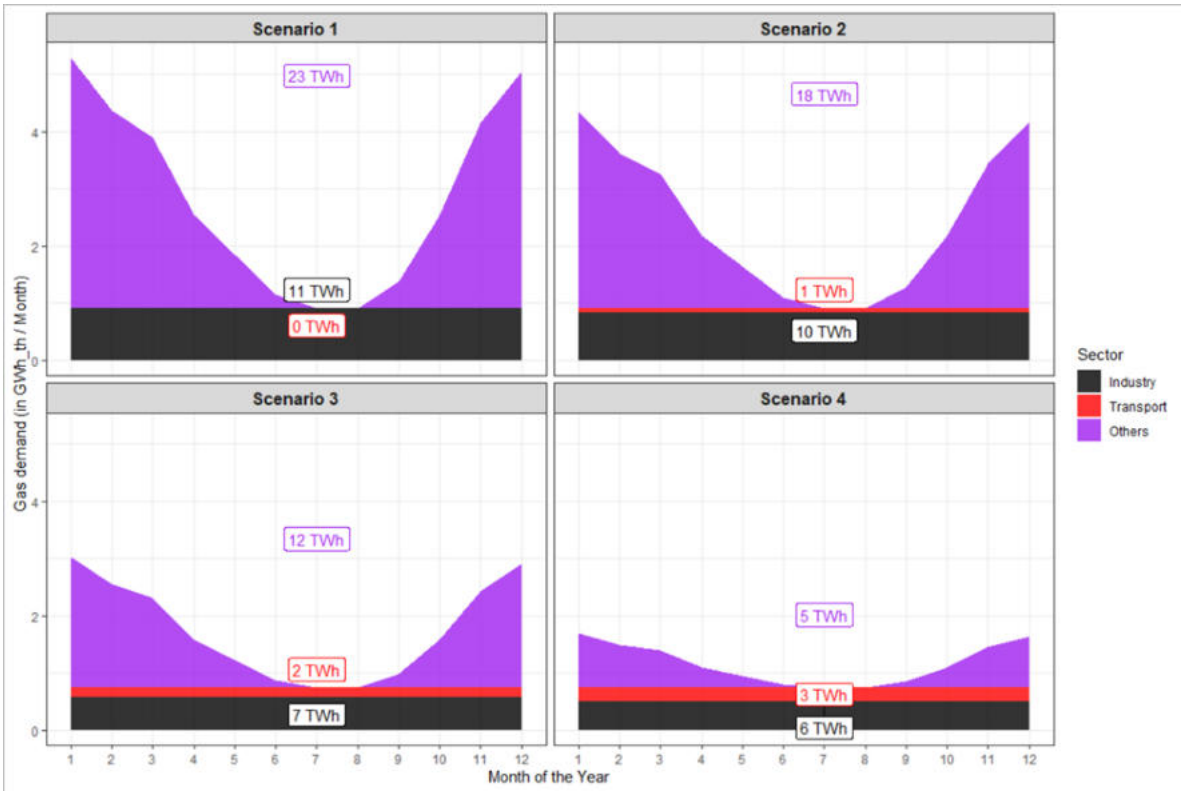

Figure 4-3: Monthly gas demand in the sectors industry, transport, and others in each scenario.

4.2.3.3. Electricity demand

Table 4-3 summarizes the main boundary conditions and assumptions on the annual electricity demand in the four scenarios. The total electricity demand increases from about 60 TWh in the reference Scenario 1 to about 67 TWh (+12%) in Scenario 4. In the following, the derivation of each part of this total electricity demand is described in more detail.

Table 4-3: Main boundary conditions and assumptions on the annual electricity demand (in TWh_{el} / year) in the four scenarios. The base electricity demand contains all current end-use electricity consumption (incl. 6% transmission losses), additional electricity demand from heat pumps, and e-Mobility are indicated in bold italic font. RET = Renewable Energy Technologies; EFF = Efficiency measures.

Demand (in TWh_{el} / year)	**Scenario 1 (~2020)**	**Scenario 2 (~2030)**	**Scenario 3 (~2040)**	**Scenario 4 (~2050)**
Base electricity demand (%reduction)	**60 (100%)**	**57** (-5%)	**54** (-10%)	**51** (-15%)
electric resistive heating SH	3.9 (100%)	1.9 (-2.0) (-50%)	0 (-3.9) (-100%)	0 (-3.9) (-100%)
Heat pumps SH *(+additional)*	*1.5* (***+0***) (10% SH)	5 (*1.5*+2.0***+1.5***) (33% SH)	7 (*1.5*+3.9***+1.6***) (50% SH)	10 (*1.5*+3.9***+4.6***) (75% SH)
electric resistive heating DHW	2.4 (100%)	0.7 (-1.7) (-80%)	0 (-2.4) (-100%)	0 (-2.4) (-100%)
Heat pumps DHW *(+additional)*	*0.3* (***+0***) (10% DWH)	2 (0.3+1.7***+0***) (40% DWH)	2.5 (*0.3*+2.4***+0***) (75% DHW)	2.5 (*0.3*+2.4***+0***) (75% DHW)
e-Mobility *(+additional)*	**-**	***+4***	***+8***	***+11***
Total electricity demand (%increase)	**60 (100%)**	**63** (+5%)	**64** (+7%)	**67** (+12%)

4.2.3.3.1. Base electricity demand and overall electricity savings

The annual base electricity demand is calculated from the 2016 - 2018 end-use electricity demand profiles at a 15-min time resolution of the Swiss TSO Swissgrid (Swissgrid, 2020). To be consistent with other datasets, these profiles are first aggregated to an hourly time resolution. The base electricity demand includes all end-use electricity consumption in the control block Switzerland (including a global 6% transmission and transformation losses).

The future development of this base electricity demand (without the additional electricity demand of the electrification of space heating and mobility) is based on the corresponding percentage reductions reported in EP2050+ (Prognos, 2020), which includes assumed population and economic growth. Base electricity demand reduction is mainly achieved by sufficiency and efficiency measures (e.g., for lighting, HVAC, etc.) as well as electrification of domestic hot water (DHW) and other processes (e.g., in

industry). For more details on the electrification of DHW, refer to chapter 4.2.3.3.4 “Heat pumps for Domestic Hot Water (DHW)”. The assumed percentage reductions in each future scenario 2 - 4 are linearly applied to the reference hourly electricity demand profiles of 2016 - 2018 (scenario 1). This way, daytime- and weather-dependent electricity demand variations such as for example for lighting are neglected.

4.2.3.3.2. E-mobility

The additional annual electricity demand of battery electric vehicles (BEV) for individual passenger car is taken from scenario “ZERO E” of EBP (2021). This scenario assumes net-zero greenhouse gas emissions in Switzerland in 2050 by completely replacing internal combustion engines vehicles (ICEV) by BEV. For reasons of efficiency and cost, electricity-based synthetic fuels (e.g., SNG) are not considered, while H_2 fuel cell electric vehicles (FCEV) only reach small market shares in passenger cars. The total electricity demand of BEV will be 11 TWh in 2050. Its derivation is based on detailed modelling of the Swiss new car market until 2050. To this end, for each year, a synthetic fleet of new cars of all drivetrains is created, with performance data, new sales prices as well as loyalty rates (brand loyalty, model segment loyalty, fuel type loyalty, and drivetrain loyalty by means of the “sim.car” microsimulation (De Haan et al., 2009; EBP, 2017). The simulated new vehicle sales are eventually incorporated into a cohort-based fleet and mileage model to enable a regional analysis of the new car market at the community level with the aid of "SynPop" (EBP, 2021), a synthetic population of Switzerland for spatial analysis of households and companies. For data on mobility behaviour, the national passenger transport model (NPVM) (ARE, 2016) and the micro-census on transport and mobility (MZMV) (BFS, 2020) are used.

The hourly recharging profiles of BEV are based on this MZMV. As in the MZMW, there are clear weekly patterns, yet no significant seasonal variations in people’s mobility, and seasonal variability is excluded by modelling 52 identical weekly recharging profiles. To derive these recharging profiles, the methodology of Pareschi et al. (2020) is adopted. They assume that all cars in the MZMV are BEV and create customizable recharging opportunities at the locations where the original car was stopping. They then check how many BEV would successfully complete multiple consecutive days of movements without running out of charge. All the recharging events of BEV are aggregated to form recharging profiles of a generic BEV fleet. In this respect, it is assumed all BEV are equipped with 60 kWh onboard batteries and charged at home with a standard 230 V socket at 2.3 kW. This allows the vast majority of BEV to be fully recharged overnight at home. The resulting recharging profiles are eventually aggregated by day of the week and linearly scaled to the annual electricity demand from above. Bi-direction charging (vehicles-to-grid) is not considered in this study. For more information on the derivation of these hourly recharging profiles, refer to Rüdisüli et al. (2022a).

4.2.3.3.3. Heat pumps for Space Heating (SH)

The percentage of heat pumps deployed to cover the annual SH demand in Table 4-1 is taken from Rüdisüli et al. (2019) as 75% in scenario 4 and then linearly adjusted in the other scenarios based on an assumed more progressive expansion of heat pumps compared to “EP2050+” (Prognos, 2020).

To obtain hourly electricity demand profiles for these heat pumps, the following procedure is applied:

- To have representative temperature data to estimate the hourly space heating and corresponding electricity demand of heat pumps, population-weighted hourly ambient air temperatures of MeteoSchweiz (2020) are used. For more details, refer to Rüdisüli et al. (2022b). From the hourly population-weighted temperatures, the daily mean temperature T_m(d) is calculated. The equivalent daily mean temperature T_m,eq(d) results as the weighted mean of that day and the three previous days according to the formula:

$$T\_m,eq(d) = 0.5 * T\_m(d) + 0.3 * T\_m(d^{-1}) + 0.15 * T\_m(d^{-2}) + 0.05 * T\_m(d^{-3}) \quad \textbf{Equation 4-1}$$

and a mathematical rounding down to whole degrees Celsius (e.g., -1.34 °C ⇒ -2 °C).

- For the hourly operation of heat pumps, standardized heat pump load profiles of SWM Infrastruktur GmbH (2021) are used at individual equivalent daily mean temperature steps of 1 °C (see Figure 4-4).

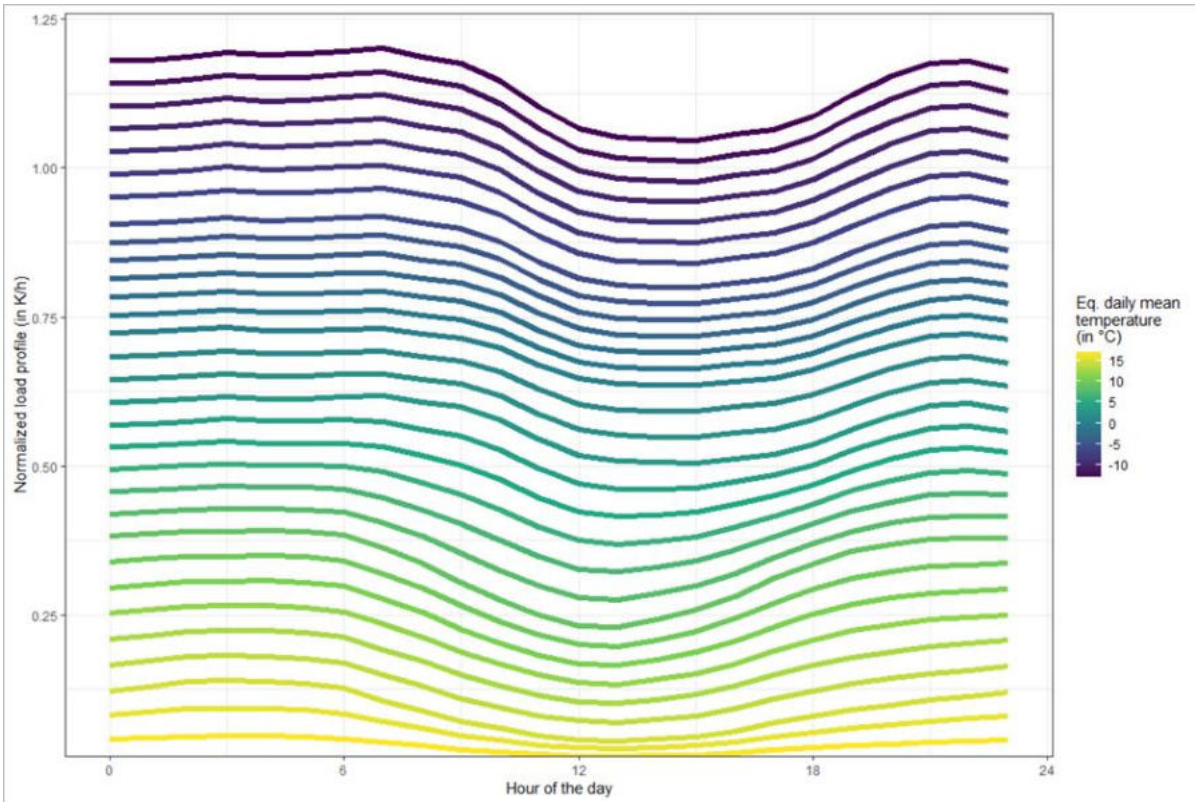

Figure 4-4: Standard load profiles for heat pumps (without mandatory interruption) of SWW infrastructure.

To only have their SH part without the DHW part, the “>= 18 °C” profile is subtracted from all other profiles. The reference temperature (T_ref) and the limiting constant (K) are set to T_ref = 18 °C and K = 0, respectively. The temperature index TMZ is calculated according to the following equation 4-2:

$$TMZ = \max(T_{ref} - T\text{-}m,eq(d); K) \quad \textbf{Equation 4-2}$$

- The annual SH demand covered by heat pumps in each scenario is based on the historical annual SH demand (BFE, 2019a) and the predefined SH demand reductions as well as heat pump deployment from Table 4-3. To account for already achieved SH demand reductions until 2019, the historical annual SH demands are first scaled by their corrected weather-adjusted SH demand, which shows that from 2010 to 2019 already an SH demand reduction of about 7% took place.
- The daily SH demand covered by heat pumps is then calculated by linearly scaling the corresponding annual SH demand covered by heat pumps by the daily TMZ relative to the annual sum of all TMZ.
- The hourly COP of state-of-the-art air-water heat pumps (ASHP) is calculated from corresponding hourly ambient air temperatures T_amb(h) and the quadratic regression proposed by Ruhnau et al. (2019):

$$COP(h) = 6.08 - 0.09 * Delta\_T(h) + 0.0005 * Delta\_T(h)^2 \quad \textbf{Equation 4-3}$$

where Delta_T is the hourly temperature difference between the heat source and heat sink defined as

$$Delta\_T(h) = T\_sink(h) - T\_source(h) \quad \textbf{Equation 4-4}$$

with the heat source as the ambient air temperature

$$T\_source(h) = T\_amb(h) \quad \textbf{Equation 4-5}$$

and the heat sink as the forward flow temperature of the heating system based on the heating curve

$$T\_sink(h) = 35\ [°C] - 0.75 * T\_amb(h) \quad \textbf{Equation 4-6}$$

which assumes 50% floor and 50% radiator heating.

In this study, only ASHP (no ground-source and water-source heat pumps) are considered, and only on-off modulating heat pumps are included. Eventually, the laboratory-based COP from (see equation 4-3) is scaled down by 14%, which is the average performance gap of real-world heat pumps in multi-family homes according to Roost et al. (2018). The resulting demand-weighted average COP is about 3.4.

- With the hourly COP from above and the hourly standardized load profiles of each day relative to the equivalent daily mean temperature, the daily heat supply by heat pumps is calculated. With this daily heat supply, the hourly load profiles are scaled such that their daily heat supply matches the daily SH demand from above. This way, the hourly electricity demand of heat pumps to cover their predefined share of the overall heat demand is calculated. To have a smooth transition at midnight, where two standard load profiles are joined, a Gaussian filter (Hamilton, 2015) with a window of 5 hours is run over the profile.
- As already in the base electricity demand a certain proportion comes from heat pumps and electric resistive heating (night storage and direct electric), this part, reported on an annual basis (BFE, 2019a), is linearly subtracted from the hourly electricity demand. To this end it is assumed that this present electricity demand for SH can concurrently be used by future heat pumps and only their additional electricity demand must be added to the base electricity demand profile. This assumption can be made since daily net surpluses relevant for USC-FlexStore are estimated on a daily basis (see chapter 4.2.2).

4.2.3.3.4. Heat pumps for Domestic Hot Water (DHW)

It is assumed that the current hourly electricity demand for DHW (mainly from resistive water boilers) can concurrently be used by future DHW heat pumps. This assumption can be justified - as with heat pumps for SH - by the fact that eventually daily demand and supply profiles are aggregated to obtain the resulting daily net surplus for USC-FlexStore.

4.2.4 Electricity supply

Table 4-4 summarizes the main boundary conditions and assumptions on the annual electricity supply in the four scenarios. The total electricity supply increases from about 61 TWh in the reference Scenario 1 to about 76 TWh (+25%) in Scenario 4. The annual and seasonal discrepancy between this electricity supply and the electricity demand from Table 4-3 can be used by USC-FlexStore to cover (at least partially) the remaining gas demand in Table 2. In the following, the derivation of each part of this electricity supply is described in more detail.

Table 4-4: Main boundary conditions and assumptions on the electricity supply in the four scenarios.

Supply (in TWh / year)	**Scenario 1 (~2020)**	**Scenario 2 (~2030)**	**Scenario 3 (~2040)**	**Scenario 4 (~2050)**
Nuclear	22 (all)	9 (Leibstadt)	- (none)	- (none)
PV	1.8	15	25	35
Wind	0.1	1	2	4
CCGT CH	-	-	-	-
Waste (inkl. CHP)	2	2	2	2
Run-of-River	16	16	16	16
Hydro storage	19	19	19	19
Total domestic electricity supply (%increase)	**61 (100%)**	**62** (+2%)	**64** (+5%)	**76** (+25%)

4.2.4.1. Nuclear

The annual generation of nuclear power in the four scenarios is based on the following phase-out assumption: In the reference scenario 1, all Swiss nuclear power plants (incl. Mühleberg, which was shut down on 20 December 2019) are still operational. In scenario 2, only the largest Swiss nuclear power plant Leibstadt (1.3 GW) is still in place, all other nuclear power plants have been shut down after their assumed 50 years of operation. In scenarios 3 and 4, all nuclear power plants are phased out. The hourly generation profile for 2016 - 2018 is taken from ENTSOE's transparency platform (TP) (ENTSOE, 2020b). While Leibstadt's generation profile shows the gross generation, all other nuclear power plants report their net generation. Hence, Leibstadt's profile is scaled down by a factor of 95%, which is the average difference between the net and gross nuclear generation derived from monthly statistics of Swissnuclear (2020). In scenario 2, a constant generation profile of Leibstadt with only a planned outage (annual revision) of 35 days between 2 June and 7 July is implemented, based on a preliminary analysis of the difference between the demand and all other inflexible generation technologies (PV, wind, RoR, waste and inflexible storage hydro).

4.2.4.2. Wind

The annual wind generation for scenarios 2 - 4 is adopted from EP2050+ (Prognos, 2020), while in the reference scenario 1, it corresponds to the historical values of 2016 – 2018 (BFE, 2020). The wind generation profile is generated from hourly capacity factors of current on-shore Swiss wind turbines and wind data recorded by MERRA-2 satellites. For further details on the derivation of these wind capacity factors, refer to the webpage “renewables.ninja” (Staffell and Pfenninger, 2016). Eventually, these capacity factors are linearly scaled to the annual wind generation in each scenario.

4.2.4.3. PV

The annual PV generation in the four scenarios is based on the substitution of nuclear power by PV as well as to cover the additional electricity demand from heat and mobility. In reference scenario 1, the annual PV generation corresponds to the historical values of 2016 - 2018 (BFE, 2020). In scenarios 2 and 3, the annual PV generation is equivalent to the phased-out nuclear power, while in scenario 4, it also covers the additional electricity from heat and mobility. Similarly, it also corresponds to the PV expansion envisaged in EP2050+ (Prognos, 2020) by 2050.

The hourly PV generation profile is estimated using an adapted method of Walch et al. (2020), which consists of three steps:

1. The physical potential is obtained from the incoming direct and global horizontal solar radiation and the surface reflectance (albedo) data from MeteoSchweiz (2020).
2. The actual radiation on the PV panels includes the roof tilt and orientation, as well as shading effects and sky visibility (see Walch et al. (2020) for details). For practical reasons and to maximize the used PV surface, it is assumed that panels are placed in adjacent and alternating, (approximately) east and west-facing rows at a lower tilt. This “EW” scenario hence models panels on flat roofs as alternating east and west-facing rows at 15° tilt, whereby all roofs with tilt angles below 10° are defined as flat.
3. The technical potential is obtained by multiplying the geographical potential with the PV system efficiency. It is assumed that all PV panels are monocrystalline panels with system efficiencies as reported in Walch et al. (2020).

These hourly PV generation profiles per roof are then aggregated to the national scale by selecting the roofs with the highest annual yield first. This way, a strategic PV expansion is implemented and the predefined annual generation in the four scenarios can be reached with the least number of roofs. For more details on this approach, refer to Walch et al. (2021).

4.2.4.4. Combined-Cycle Gas Turbines

In all scenarios, it is assumed that no new domestic combined cycle gas turbine (CCGT) power plants are built and used, as this would not comply with current CO_2 mitigation targets of Switzerland (“net-zero”). However, based on current political developments with respect to Switzerland’s integration in a future European electricity exchange market (Frontier Economics, 2021), the authors acknowledge that there may be a need for such domestic CCGT to offset winter electricity deficits in the future Swiss energy system.

4.2.4.5. Waste-to-Energy

Waste-to-Energy refers to electricity produced at the 30 municipal waste incineration plants (MWIP) in Switzerland. Their total annual electricity generation is derived from their CO_2 emissions (see chapter 4.2.5.1.2) and a uniform conversion factor of 0.52 GWh_{el} / t CO_2 to yield 2.1 TWh, which is in line with the official national statistics (BFE, 2020). Due to no assumed expansion of MWIP in Switzerland, this annual electricity generation remains constant in all scenarios. For the hourly generation, a constant (“must-run”) generation of 240 MW_{el} is assumed, irrespective of seasonally varying waste incineration schedules.

4.2.4.6. Hydropower

4.2.4.6.1. Run-of-River

According to the Swiss national hydropower statistics (BFE, 2017), there were 577 run-of-river (RoR) units with a power larger than 0.3 MW_{el} producing about 16 TWh of electricity (of which 2/3 in summer). This generation is assumed to remain constant in all scenarios. In other words, no additional RoR capacity is installed owing to a limited expansion potential (Prognos, 2020). Figure 4-5 shows all Swiss RoR hydropower plants with an installed capacity of more than 25 MW_{el} sorted in descending order including those RoR in the inner and outer geologically eligible perimeter (see chapter 4.1.3).

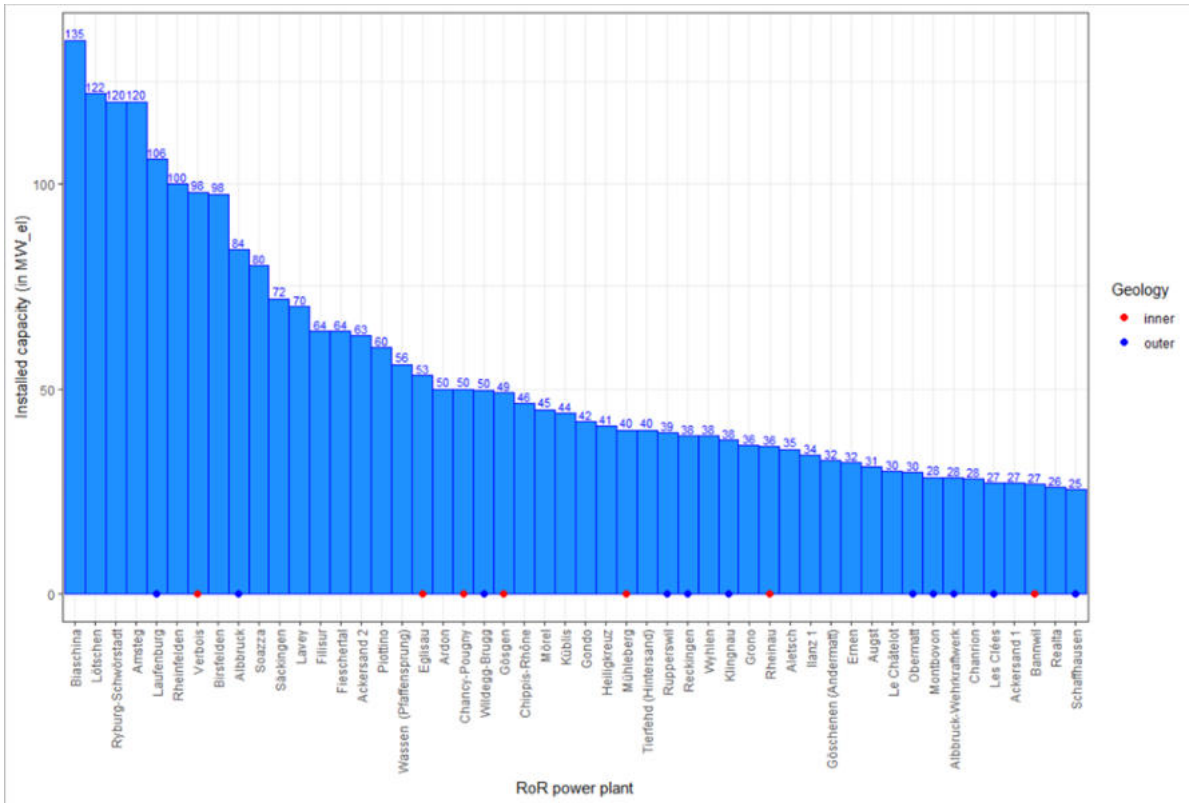

Figure 4-5: RoR hydropower plants (> 25 MW_{el}) in Switzerland. RoR power plants in the inner and outer geologically eligible perimeter are indicated with red and blue dots, respectively.

Hourly generation profiles are adopted using the method described in Dujardin et al. (2017). This method uses three principal sources of data:

- The monthly water runoff from the model PREVAH (Viviroli et al., 2009) with a 200 m resolution raster and the definition of the water catchment areas of BAFU (2021).
- The WASTA hydropower statistics (BFE, 2017), which gives the location and annual average generation for each RoR plant
- The monthly generation statistics of all RoR combined (BFE, 2019b)

With these sources, the following approach is employed to obtain the hourly electricity generation profile of each RoR power plant:

1. For each RoR power plant, given its location, the associated catchment area is computed by using H1 and H2 attributes in the small catchment definitions (this defines the cascading)
2. For each month, the corresponding PREVAH pixel values to obtain the monthly inflows that drain to each plant are aggregated
3. The annual generation from BFE (2017) and the inflow regime just above are used to obtain monthly generation values for each plant.
4. The monthly aggregated production values from BFE are used to correct them (as the WASTA database is not updated every year).
5. The monthly time series are then interpolated at a 1-h time resolution using Piecewise Cubic Hermite Interpolating Polynomial (PCHIP) followed by a 1-month-window moving average. This interpolation is done on the cumulative sum of the monthly electricity generation profile to guarantee that the monthly electricity generation is conserved. The hourly generation profile is then the time derivative of this interpolation.

Regarding international RoR power plants, mainly along the German border at the river Rhine, their capacity is fully assigned to Switzerland as it is assumed that due to similar surplus electricity situations in neighboring countries, USC-FlexStore at these international RoR sites may also use foreign net surplus electricity. The only exception is RoR Kembs, which is fully excluded from the analysis despite its 20% share for Switzerland, as it is fully located in France.

4.2.4.6.2. (Pumped) Hydro Storage

All the above-mentioned electricity generation technologies (nuclear, run-of-river, PV, wind, and waste) are inflexible in the dispatch of their electricity generation (must-run). In other words, they cannot shift their production to times with higher demand and thus higher prices on the electricity market - mostly due to physical, economic, and/or legal constraints. On the other hand, storage hydropower plants (HYD_DAM) are flexible in this respect as they can shift - within certain limits - their production to times of higher electricity demands and prices.

Therefore, the production of HYD_DAM is modelled individually for each year given the corresponding inflexible supply mix and electricity demand. As a proxy for electricity prices on the electricity market, the residual load is used (Dillig et al., 2016; Von Roon and Huber, 2010). The residual load is the momentary difference between the electricity demand and the inflexible electricity supply. It is positive for hours with deficits (i.e. demand larger than supply) and negative for hours with a surplus (i.e. supply larger than demand). Especially in summer, also HYD_DAM is partially forced to inflexibly produce electricity due to high natural inflows and limited storage capacities in their intermediate retention reservoirs. This inflexible share of HYD_DAM is heuristically modeled according to Beer (2018): First, the hourly HYD_DAM production profile is obtained by subtracting from the total Swiss electricity production profile (Swissgrid, 2018) all inflexible production at an hourly time scale. The remaining profile after this subtraction is roughly the hourly HYD_DAM production. Then, this HYD_DAM profile is linearly scaled to the annual HYD_DAM supply (BFE, 2019b). Next, a running minimum filter with a centered window of 7 days is applied to the profile, while assuming that this running minimum is the inflexible HYD_DAM production. This inflexible HYD_DAM production is then added to the other inflexible production profiles of all other technologies to calculate - along with the corresponding demand - the residual load for every hour in every year.

In a subsequent step, the remaining (i.e., flexible) hourly HYD_DAM production is summed for every consecutive time window of 5 days within a year. The number of 5 consecutive days is chosen heuristically such that only short-term production shifts within 5 days are allowed. HYD_DAM may theoretically also retain electricity for longer durations (e.g., seasonally), however, to be economically viable, they are filled in spring (and summer) from snowmelt and precipitation such that they are full in

autumn and can profitably produce electricity throughout winter. Consequently, they must stick to a seasonally inflexible generation schedule, which, however, is flexible within a couple of days. Therefore, in the model within these 5 consecutive days, HYD_DAM can shift its available electricity to the most profitable hours, i.e., the hours with the largest residual loads (deficits). To this end, the residual load profile is first made non-negative by shifting it such that the most negative value (i.e., the largest surpluses) becomes zero and consequently all other values are positive. In the next step, this shifted residual load is squared in order to give higher weights to hours with large deficits. Eventually, the shifted and squared residual load is normalized to 1 and the summed HYD_DAM production is linearly redistributed according to this normalized residual load, while not exceeding the maximum installed turbination power of 8.1 GW. These steps are iteratively repeated until all HYD_DAM production is adequately redistributed within these 5 consecutive days. With this heuristic approach, the annual production and seasonal storage scheme of HYD_DAM is intrinsically maintained, and the obtained profile has a smooth and realistic shape.

For pumped-hydro storage (PHS), in addition to flexible turbination, also flexible pumping is implemented within 5 consecutive days as an additional electricity demand. To this end, an updated residual load profile including the afore re-allocated HYD_DAM is calculated and inverted such that the hours with the largest surplus (e.g. lowest prices) are prioritized for pumping, and hours with the highest deficits (e.g. highest prices) are used for turbination such that a maximum price spread (arbitrage) can be exploited. As a boundary condition for PHS, pumping can only happen in surplus hours, while turbining can only happen in deficit hours. Moreover, the maximum pumping and turbination power of 3.7 GW must not be exceeded and the maximum storable electricity within these five consecutive days is a-priori determined as either the total Swiss PHS capacity of about 300 GWh (Piot, 2014) or the minimum of the summed surpluses and deficits within 5 consecutive days. Generally, a round-trip efficiency of 80% is assumed for PHS.

4.2.5 CO_2 supply

As a prerequisite for the conversion of H_2 to CH_4, CO_2 is needed. This CO_2 is separated and supplied in concentrated form from industrial CO_2 point sources. Due to their relatively straightforward CO_2 separation and market maturity, the only CO_2 sources considered in this study are cement (CEM), municipal waste incineration (MWIP), and wastewater treatment plants (WWTP). CO_2 emissions from the (petro-)chemical and metallurgical industries are not considered, as their CO_2 emissions, although of considerable quantitative relevance (BAFU, 2019; Swissmem, 2017), are typically strongly process-dependent and therefore hard to exploit. Direct Air Capture (DAC) of CO_2 from the atmosphere is, despite its infinite and location-independent potential (Gutknecht et al., 2018; Wurzbacher, 2017), neither considered due to economic constraints. Moreover, in Switzerland, there are about 150 raw biogas (biomethane) plants that emit about 140000 t of CO_2 per year, and they could therefore readily be used as CO_2 sources similar to WWTP (Meier et al., 2017). However, currently, only 15 of these biogas plants feed methane into the natural gas grid (Ruoss, 2014), although most of the plants are located near natural gas pipelines. Most of them use their produced methane in combined heat and power (CHP) plants for their own energy consumption and therefore they are not considered here for economic USC-FlexStore exploitation.

4.2.5.1. CO_2 sources

4.2.5.1.1. Cement plants (CEM)

Currently, there are 6 large cement plants (CEM) in Switzerland (Schweizer Zement, 2018), where CO_2 is emitted to the environment in the exhaust air stream. One-third of this CO_2 is of fossil origin and stems from the combustion process to supply heat to the rotary kiln, while the remaining two-third of CO_2 are geogenic and stem from the conversion of the clinker (CaCO3) to calcium oxide (CaO) (Volkart et al., 2013). The volumetric CO_2 content in the exhaust airflow is approximately 14% - 35% (Meier et al., 2017) and can be separated relatively easily and inexpensively during flue gas cleaning using amine scrubbing. The relevant CO_2 quantities are determined from the cement volumes published by the cement plants (Schweizer Zement, 2018) and an emission factor of 0.59 t CO_2 per tons of cement (Infras, 2000).

4.2.5.1.2. Municipal Waste Incineration Plants (MWIP)

The 30 municipal waste incineration plants (MWIP) in Switzerland (VBSA, 2019) emit CO_2 as a product of their combustion process. About 50% of this CO_2 stems from fossil sources (e.g., oil, coal, natural gas, etc.) (VBSA, 2016), while the other 50% is biogenic (food, wood, leather, etc.) and therefore CO_2 neutral. With a volumetric fraction of about 10% in the exhaust fume (Johnke, 2001; Reinhardt et al., 2008), CO_2 can be separated relatively easily and inexpensively as part of the flue gas cleaning process using amine scrubbing. To estimate CO_2 amounts from MWIP, the annual amount of combustible waste published by the MWIP on their websites (VBSA, 2019) is multiplied by an emission factor of 1.06 t CO_2 per tons of waste (BAFU, 2015).

4.2.5.1.3. Wastewater Treatment Plants (WWTP)

Wastewater treatment plants (WWTP) produce CO_2 in their anaerobic sludge digestion (fermentation), where CO_2 - together with CH_4 - is the main constituent of sewage gas (Gujer, 1999). The volumetric fraction of CO_2 in the sewage gas is about 33% and nearly 100% of biogenic origin. Nowadays, sewage gas is typically either already treated and fed into the natural gas grid, converted in on-site combined heat and power (CHP) plants for the WWTP's own electricity and heat requirements, or flared (Peyer et al., 2016). Unlike CEM and MWIP, using CO_2 from WWTP has the advantage that no additional CO_2 separation and gas upgrading units (gas cleaning and drying) are needed after anaerobic digestion (Witte et al., 2018b, 2018a). Instead, CO_2 can be used directly - along with the already contained CH_4 in the sewage gas - for USC-FlexStore.

According to BAFU (2017), in 2017, there were 759 WWTP with a dimensioning size of more than 200 population equivalents (pe) throughout Switzerland. For economic and operational reasons, only larger WWTP with pe > 10'000 are considered in this analysis, preferably if they are also located near RoR hydropower plants. Smaller-scale and special industrial WWTP, as well as WWTP without anaerobic sludge digestion, are not considered. The relevant CO_2 emission factors are obtained from the reported quantities of sewage gas and pe of all WWTP in the canton of St. Gallen (SG) (AFU, 2019). Assuming a volumetric CO_2 content in the sewage gas of 45% and a CO_2 density of 1.96 kg/Nm3, a median emission factor of 10.4 kg_CO_2 / (pe * year) is obtained. This emission factor is in line with the 10 kg_CO_2 / (pe * year) determined from measured amounts of sewage gas and corresponding pe in Holinger (2012).

4.2.5.2. CO_2 availability, requirements, and separation

Based on the emission factors from above, the annual potentials of CO_2 for USC-FlexStore are calculated. To this end, it is assumed that CO_2 is emitted constantly throughout the year. This assumption of constant CO_2 emissions is generally true for most CO_2 sources. However, it does not hold for WWTP in tourism areas with strong seasonal fluctuations for wastewater treated. In that case, this is even more disadvantageous for USC-FlexStore as the large quantities of CO_2 are produced in winter, while USC-FlexStore is generally done in summer when surplus electricity from PV is highest.

Under realistic conditions, only about 75% to 90% of the CO_2 in the exhaust fumes of CEM and MWIP can technically be separated by amine scrubbing (Meier et al., 2017). Contrarily, as above mentioned, with WWTP, CO_2 in the sewage gas can be used for USC-FlexStore without additional CO_2 separation and upgrading (Witte et al., 2018b). Therefore, a CO_2 separation efficiency for CEM and MWIP of 75% and of 100% for WWTP is assumed.

For stoichiometric conversion of H_2 and CO_2 to CH_4 according to Sabatier's reaction ($4\ H_2 + CO_2 = 1\ CH_4 + 2\ H_2O$), 5.5 g_$CO_2$ per g_H_2 (Teske et al., 2019) are needed. With a lower heating value (LHV) of 33.3 kWh / kg_H_2, 166 t CO_2 are needed per GWh_H_2, assuming a 57% efficient (Teske et al., 2019), 94.1 t CO_2 are needed per GWh of (surplus) electricity.

A summary of the individual-plant and cumulative CO_2 emissions (including the above-mentioned separation efficiencies) are displayed in Figure 4-6 per plant type. With these amounts of CO_2 and the stoichiometric conversion factor of 94.1 t CO_2 / GWh_{el}, more than 60 TWh of net surplus electricity would be needed for consuming all available CO_2. In this respect, CEM and MWIP alone account for more than 98% of the available industrial CO_2 for USC-FlexStore.

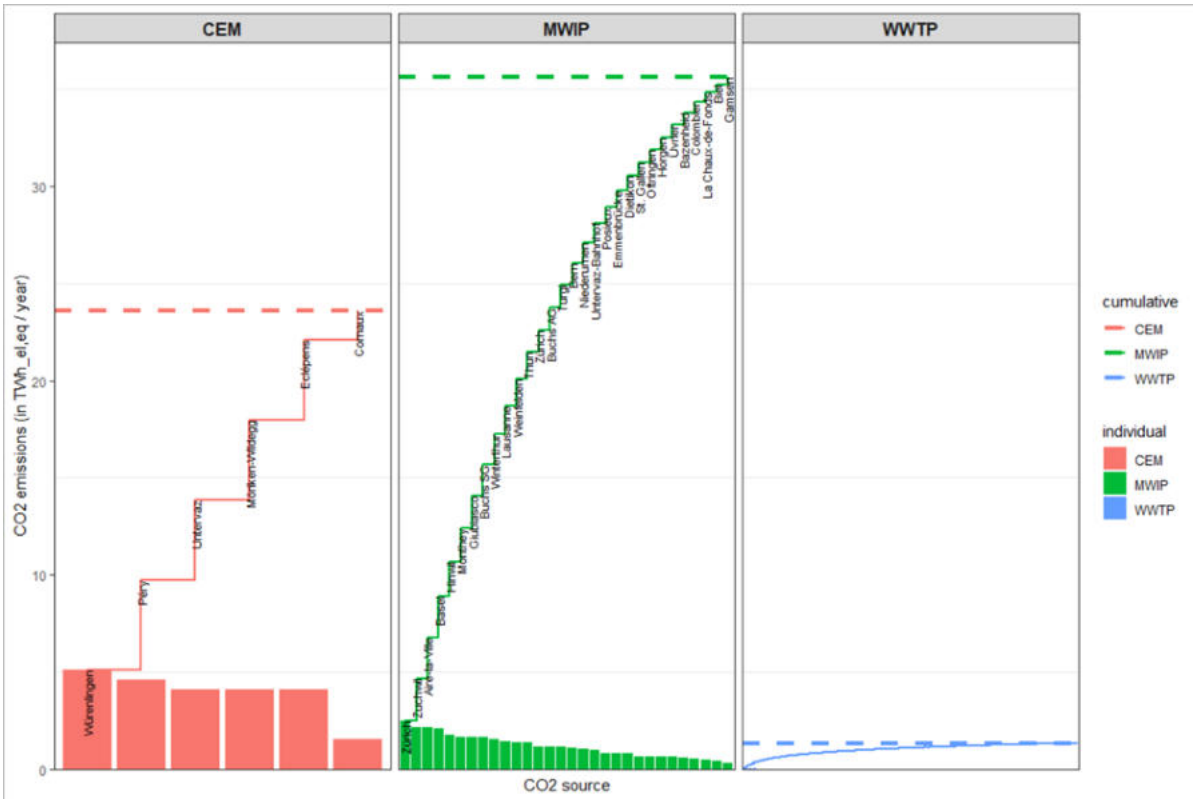

Figure 4-6: Individual and cumulative CO_2 emissions per type in TWh electricity equivalents (el,eq) per year, that is, for full conversion to CH_4 via USC-FlexStore with a conversion factor of 94.1 t CO_2 / GWh_{el},eq including a 75% separation efficiency for cement (CEM) and MWIP as well as 100% separation efficiency for WWTP.

4.2.5.3. CO_2 transportation

For USC-FlexStore at MWIP, no CO_2 transportation is needed, as the USC-FlexStore plant is immediately located on the premises of the CO_2 source. In turn, for USC-FlexStore at RoR, transportation of CO_2 (by truck or pipeline) is generally required. To find nearby CO_2 sources for each RoR, an underlying transportation problem must be solved. To this end, the R package `lpSolve` and its function `lp.transport` (Berkelaar, 2020) is employed. The "cost" of transportation for CO_2 from its source (i) to its sink (j) at the RoR is approximated by

$$Cost_{ij} = Distance_{ij} / \min(CO_2\_available_i, CO_2\_needed_j) \quad \textbf{Equation 4-7}$$

where $Distance_{ij}$ is the Euclidean distance (geographical or logistical boundary conditions are not considered) between two locations i and j, while $CO_2\_available_i$ is the total (annual) CO_2 available at source i and $CO_2\_needed_j$ is the annually needed CO_2 for full conversion of all available net surplus electricity to H_2 at RoR j based on a conversion factor of 94.1 t CO_2 / GWh_{el}. Besides the transportation distance, the employed cost function also accounts for CO_2 needed and available. This way, rather a small number of large CO_2 sources are used instead of several close-by yet smaller ones.

4.2.5.4. CO_2 storage

Owing to the assumed constant feed of CO_2 from industrial CO_2 sources, on-site CO_2 storage is required to achieve a tolerable deviation from stoichiometric CO_2 and intermittently produced H_2 injection into the ground for USC-FlexStore. Instead of CO_2 storage, also H_2 storage would be an option in this respect. However, due to technologically more challenging H_2 storage (Züttel et al., 2010) (in specific pressurized H_2 vessels), only CO_2 storage above ground is currently considered. This shall, however, further be elaborated based on the results from chapter 6, in which storage of the feed gases H_2 and CO_2 is investigated in full detail.

4.2.6 Natural gas grid

For the transport of natural gas (NG), there is a 19'300 km long NG grid in Switzerland, of which 2'300 km belong to the high pressure (5 - 85 bar, see Figure 4-7) and 17'000 km to the local low-pressure distribution grids (0.02 - 5 bar) (KSDL, 2021). For distances less than 500 km, it is assumed that natural gas can be transported in this grid with negligible losses and additional energy requirements. Although gas is preferably injected into the high-pressure NG grid at gate and customs stations, it is assumed that gas can be injected at any location without additional costs or efforts since costs for a possibly needed increase of pressure is highly dependent on the (typically unknown) reservoir pressure and subsequently the current operating pressure of the underground storage.

4.2.7 Project perimeters

Figure 4-7 shows a map of the potential USC-FlexStore sites (i.e. RoR, MWIP), CO_2 sources (i.e. CEM, MWIP, WWTP), and the high-pressure NG grid in Switzerland as well as the inner and outer geologically eligible perimeter for USC-FlexStore (see chapter 4.1.3).

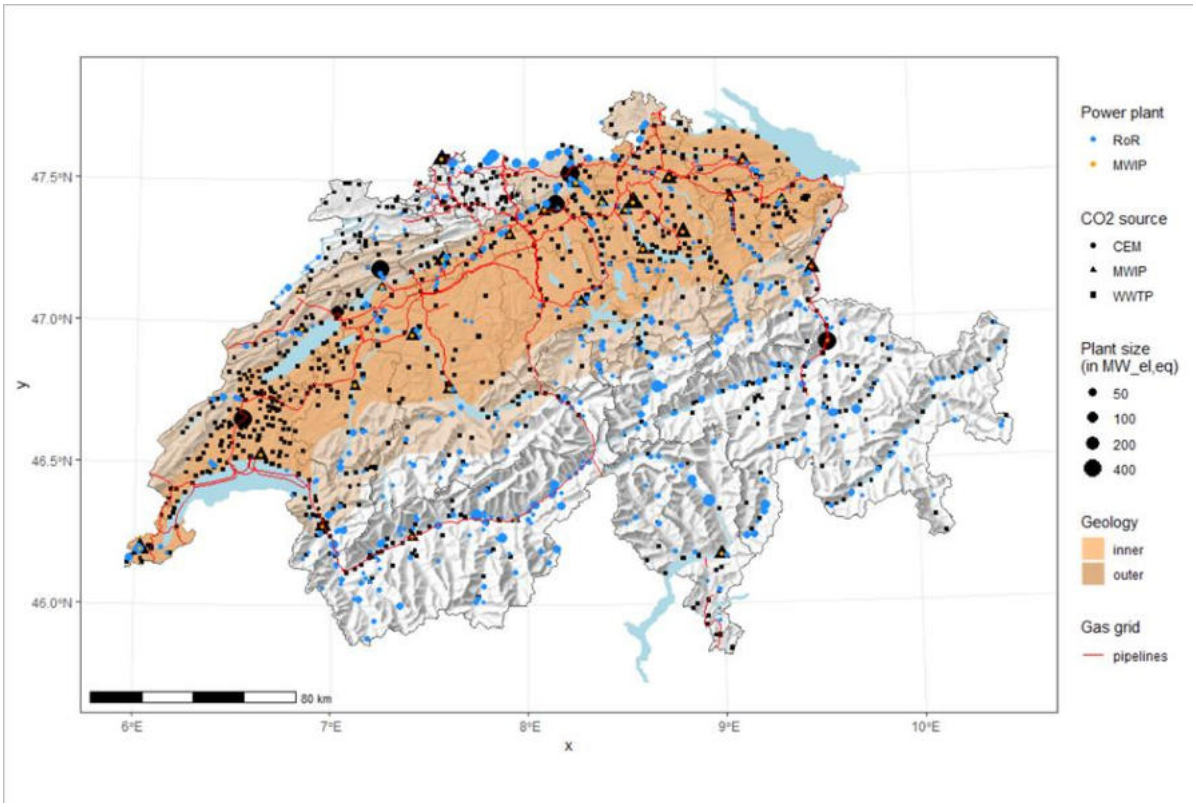

Figure 4-7: Map of all RoR hydropower plants (blue dots), CO_2 sources (CEM, MWIP, WWTP) as well as the high-pressure natural gas grid (red lines) in whole Switzerland as well as the geologically eligible inner and outer perimeter for USC-FlexStore.

4.3 Results and Discussion

4.3.1 National analysis

4.3.1.1. Electricity demand and supply

Figures 4-8a – 4-8c illustrate how flexible hydropower (PHS and storage) is dispatched in winter, spring and summer according to the heuristic approach presented in chapter 4.2.4.6.2 to meet the inelastic demand (incl. heat pumps and BEV) along with other domestic, yet inflexible, electricity supply technologies (PV, wind, RoR, conventional thermal (mainly MWIP), nuclear). In all seasons, typically, flexible hydro storage (Dam flex.) is gradually shifted away from noon hours, when PV is dominant - and prices therefore rather low - towards evening and night hours, when supply deficits increase due to additional BEV charging and phased-out nuclear supply - and therefore prices are high. With PHS, inexpensive surplus electricity at noon is pumped and shifted towards more profitable evening and night hours. In winter (see Figure 4-8a), typically, there is not enough surplus electricity to cover the night deficits, particularly, in scenarios 1 and 2, while in scenarios 3 and 4, due to the large PV expansion of 25 TWh and 35 TWh, respectively, in some days, even in winter, there is surplus electricity at noon that can be shifted by PHS. In the intermediate season, which is represented in Figure 4-8b, there is often enough surplus electricity at noon to completely fill the evening and night deficits, in particular in scenarios 2 - 4. However, due to physical limitations of PHS for example with respect to the installed pumping capacities of 2.7 GW, there are also deficits that cannot be offset by PHS although there would be enough surplus electricity available at noon. In summer (see Figure 4-8c), in all scenarios there is surplus electricity, almost throughout the day. This occurs as flexible hydro storage, although shifted away from noon hours, is still in excess. This situation, which would otherwise result in generally detrimental curtailment of renewable energy, can only be avoided by a different seasonal dispatch strategy of flexible hydropower or other means of seasonal storage such as USC-FlexStore.

a.

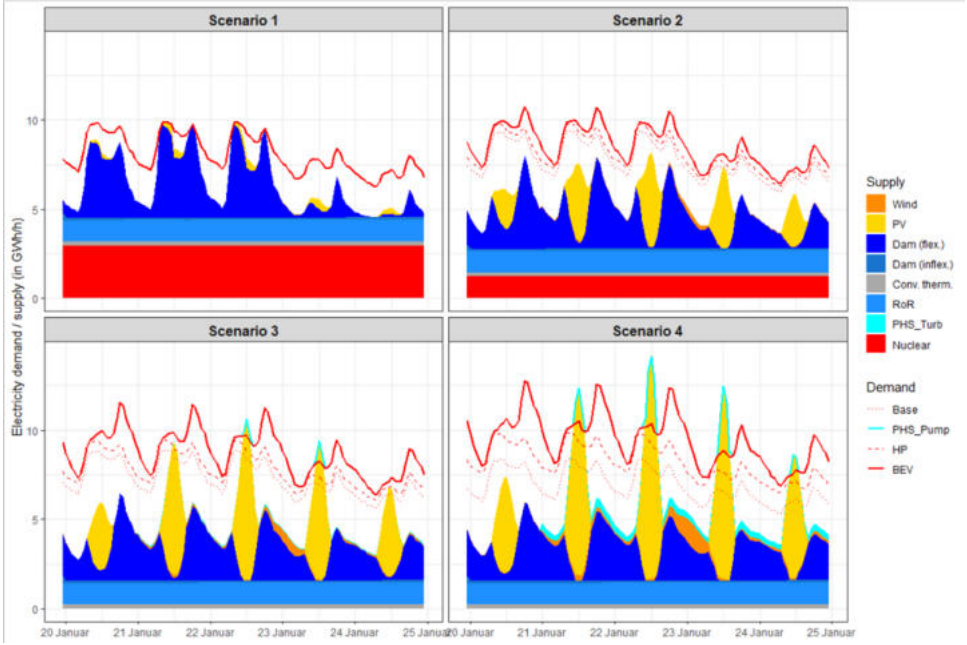

b.

c.

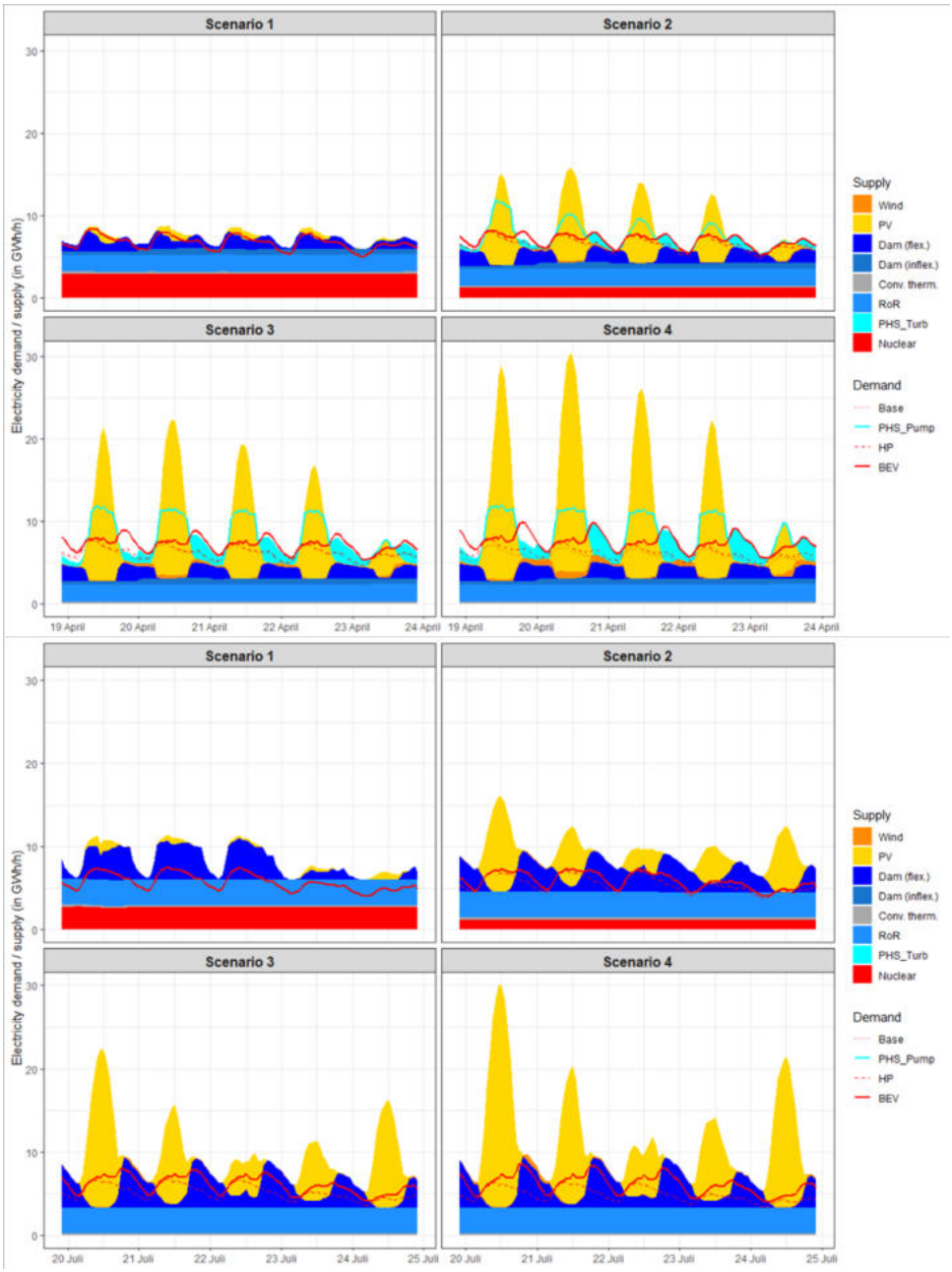

Figure 4-8: Dispatch of flexible hydropower (Dam and PHS) modeled to meet the inelastic electricity demand (red lines) along with other inflexible supply (wind, PV, RoR, conventional-thermal, nuclear) for an exemplary 5 consecutive days in all four scenarios in a) winter b) spring and c) summer.

4.3.1.2. Additional flexibility for ideal load shifting

Especially in the intermediate season (see Figure 4-8b), there are electricity surpluses at noon that cannot be shifted by PHS although there are corresponding deficits in the evening and at night due to physical limitations of PHS in terms of installed capacities, etc. This surplus can, however, be exploited by additional load shifting (i.e., additional flexibility in terms of additional storage capacities and/or demand-side management). What is left after this (ideal) load shifting, are net surpluses eligible for USC-FlexStore.

In Figure 4-9, the daily needed amount of flexibility (in GWh) with respect to an ideal (i.e., no losses) load shifting is displayed for all scenarios. While in Scenario 1 little additional flexibility is needed, it gradually increases to a daily maximum of about 53 GWh per day in Scenario 4. If all flexibility, including the one currently available from PHS, is counted, a maximum combined flexibility of 71 GWh per day is needed in Scenario 4. The current total PHS storage capacity of about 300 GWh (Piot, 2014) is, therefore, more than sufficient to effectively shift these domestic amounts of surplus electricity, while there is still enough PHS storage capacity to pump up low priced imported electricity and sell it later at higher prices (PHS arbitrage). In addition, the required 53 TWh of shiftable loads with Demand Side Management (DSM) are not excessively large to be found in a future energy system.

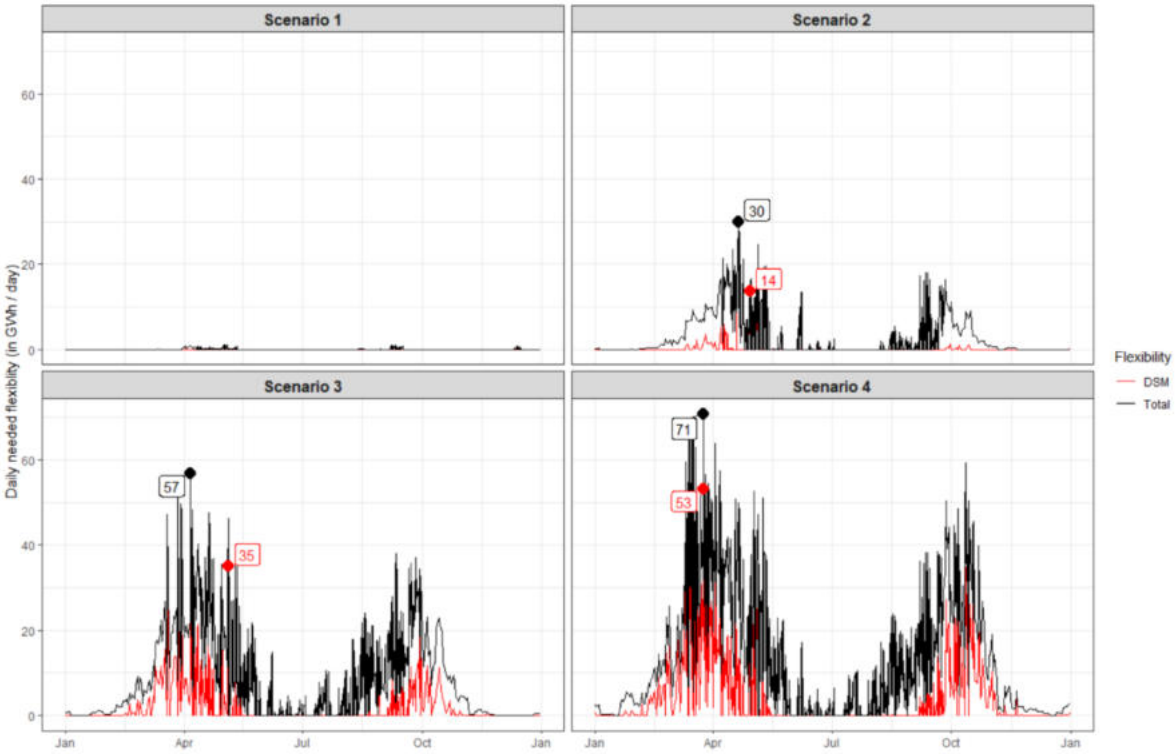

Figure 4-9: Needed daily flexibility (in GWh per day) to reach net surpluses.

In turn, the daily peak power demands (in one particular hour of the day) that need to be available for this ideal load shifting are more challenging. These daily peak power demands for DSM are displayed in Figure 4-10 for all scenarios. In Scenario 4, the maximum daily peak power demand is more than 25 GW, typically at noon when PV generation is maximal. Also in Scenario 3, a peak power demand of up to 17 GW is needed. In all these situations, the installed PHS pumping power of 3.7 GW is already exploited (i.e., subtracted). This illustrates that the requirements for ideal load shifting are high with respect to the needed power. Figure 4-10 also displays these daily peak power demands in descending order (from left to right as orange areas). The steep slope of this ordered representation shows that these peak power demands are needed only on a few days of the year and that curtailment (shaving) of these peaks (e.g., at 20 GW) would not result in an excessive spill of electricity. Nonetheless, the ideal load shifting assumed in this study to obtain the amounts of net surplus electricity eligible to USC-FlexStore may be rather optimistic.

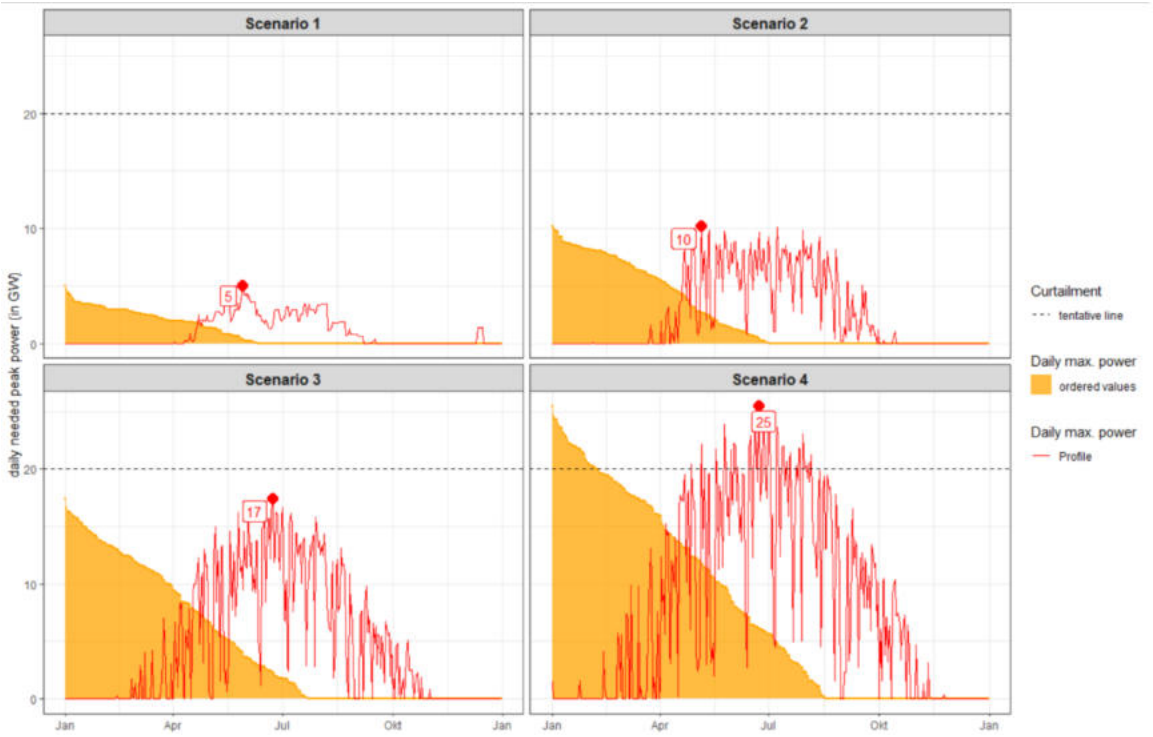

Figure 4-10: Needed daily flexibility (peak power in GW) to reach the reported net surpluses for USC-FlexStore.

4.3.1.3. Available net surplus electricity

The available amounts annually aggregated net surplus electricity for USC-FlexStore (after ideal load shifting) are displayed in Figure 4-11 for all scenarios in dark green. For comparison, also the corresponding net deficits (black), as well as the gross deficits (grey) and gross surplus (light green), are displayed. These annual net surpluses range between 4.9 TWh (in Scenario 1) to 17.3 TWh (in Scenario 4). As in this study, no exports are allowed, in reality, in particular in Scenario 1, the effectively usable net surplus for USC-FlexStore must be reduced by this potential export capacity, which, however, will gradually diminish in scenarios 2 - 4 due to similar surplus situations in neighboring countries (Lienhard, 2023). In all scenarios, the difference between net and gross surplus/deficits is comparatively small, hence by means of ideal load shifting only a relatively small amount of daily surpluses/deficits can be offset, while the largest shares of net surpluses/deficits feature a clearly seasonal pattern that can only be offset by seasonal mitigation such as seasonal storage including USC-FlexStore.

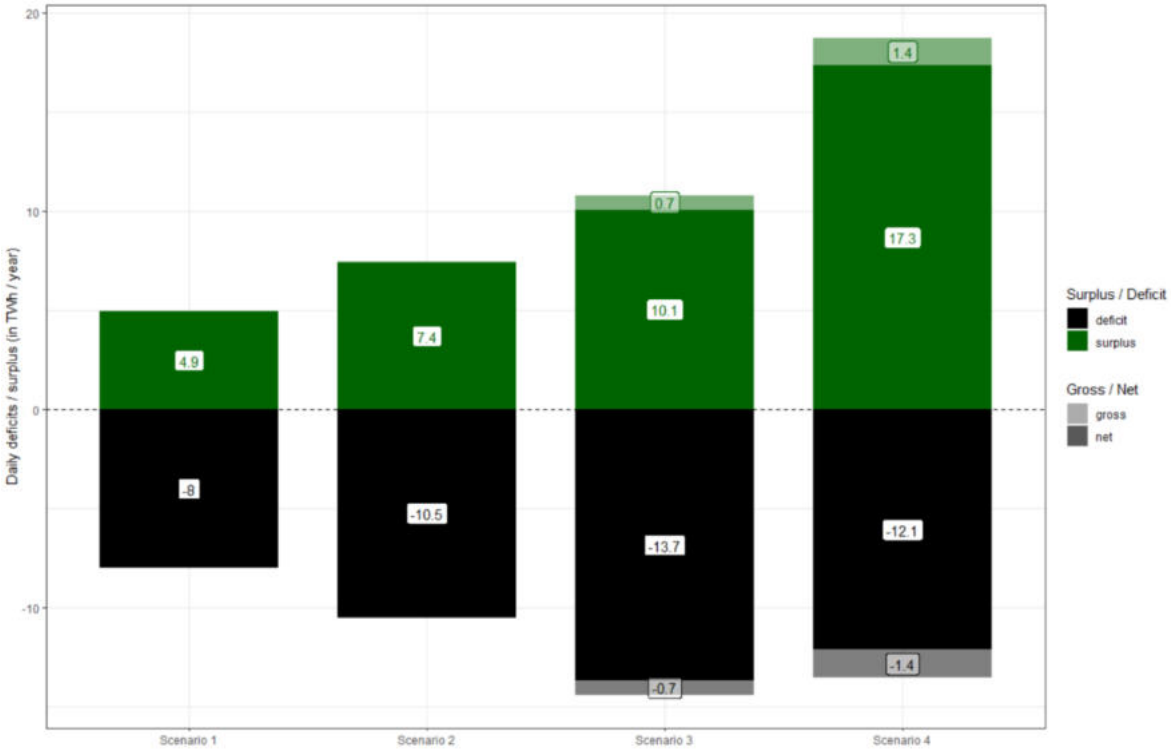

Figure 4-11: Annual net (dark green and black) and gross (light green and grey) surplus (positive values) and deficits (negative values) in each scenario.

4.3.1.4. Exploitable net surplus electricity

Figure 4-12 displays the total amount of net surplus electricity available in Switzerland (dark green) as well as the share simultaneously exploitable for USC-FlexStore at all MWIP (orange)), all RoR (blue), and both plant types combined (yellow) per scenario. While in scenarios 1 and 2 almost all net surplus of about 5 - 7 TWh can be exploited at MWIP and RoR power plants throughout Switzerland, this share decreases substantially in the two other scenarios such that in scenario 4 - with the highest degree of PV penetration and electrification - only about half of the available 17.3 TWh net surplus electricity can eventually be exploited simultaneously at these power plants without resorting to additional net surplus electricity from the grid at the expense of additionally incurred grid fees.

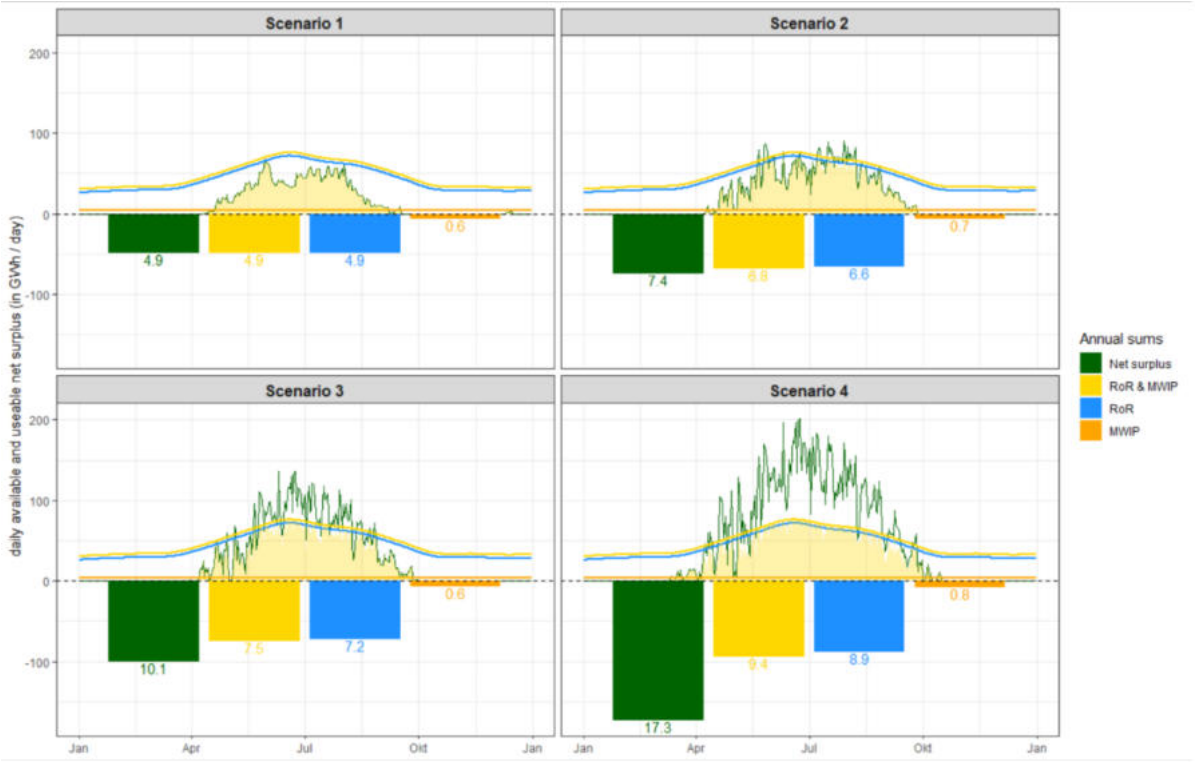

Figure 4-12: Daily (line) and annually (bars) available and exploitable net surplus electricity, respectively, at RoR and MWIP (and combined).

Figure 4-12 also shows that the largest amounts of net surplus electricity occur in summer when coincidentally RoR generation is highest, while it is constant throughout the year for MWIP. This is one reason why USC-FlexStore is presumably best situated at RoR (Gupta et al., 2022). Figure 4-13 shows for all RoR larger than 20 MW_{el} in Switzerland how much of their generated electricity can be used for USC-FlexStore and how much is still fed into the electricity grid in each season (half-year). RoR power plants within the outer and inner geology project perimeter are indicated by blue and red dots, respectively. Only a small portion of the summer generation, irrespective of the size of the RoR, is still fed to the grid, while in winter the situation is inverse and only a small portion is used for USC-FlexStore, as there is almost no net surplus electricity available in winter. Especially for large RoR power plants, their annual electricity generation eligible to USC-FlexStore may be more than 300 GWh per year (e.g. Ryburg-Schwörstadt)

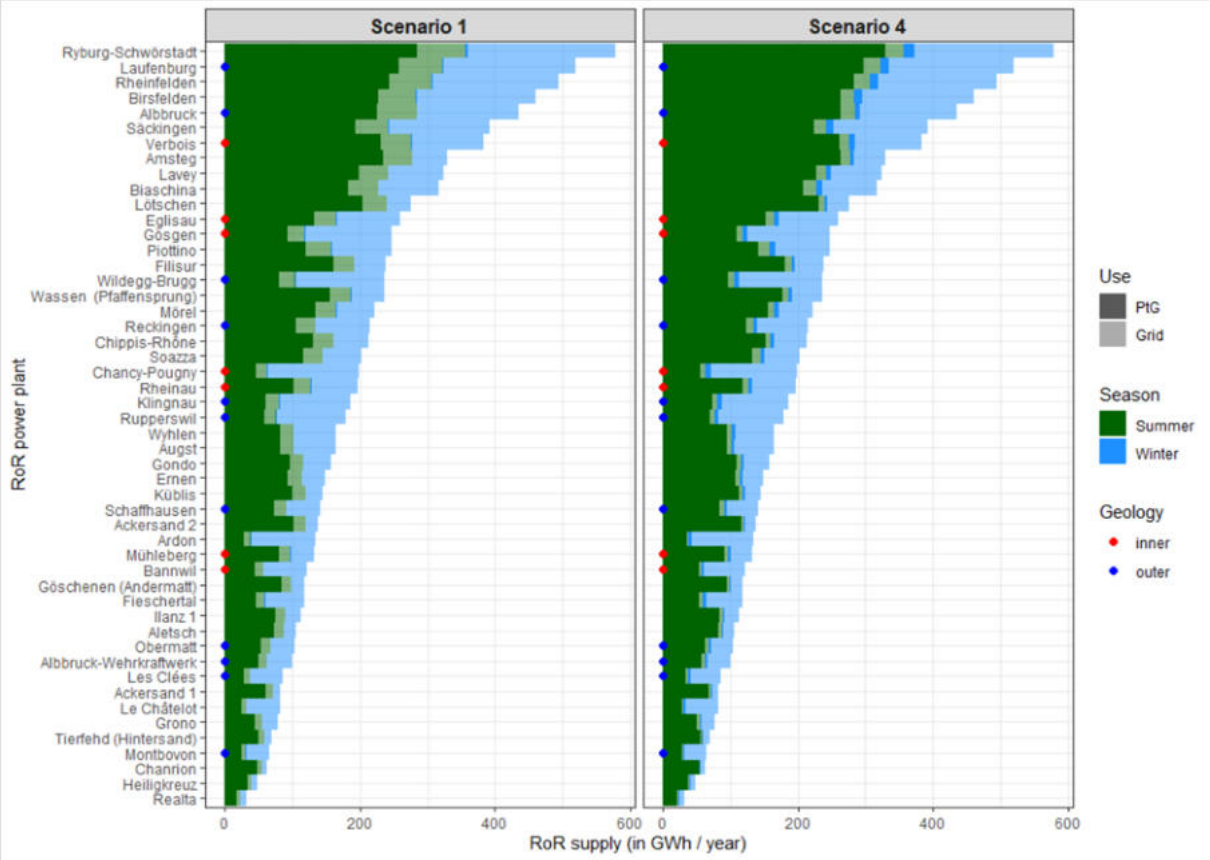

Figure 4-13: Use of generated electricity at RoR (> 25 MW_{el}) for USC-FlexStore or grid injection in the winter (blue colors) and summer (green colors) half-year for scenarios 1 and 4. RoR power plants in the inner and outer geological perimeter are indicated with red and blue dots, respectively.

4.3.1.5. Full load hours

The required total daily electrolysis power (in GW_{el}) to convert all daily exploitable net surplus electricity at RoR and MWIP is displayed in Figure 4-14 in descending order for all scenarios. Although the available daily net surplus electricity would allow for total installed electrolysis of up to 10 GW_{el} in Scenario 4, at RoR and MWIP combined only about 3 GW_{el} can be installed due to the above-mentioned gap between the available and the simultaneously exploitable net surplus at RoR and MWIP. The corresponding equivalent full load hours (eqFLH) are also displayed in Figure 4-14. While the eqFLH for MWIP is in the range of about 4000 h (slightly depending on the underlying year and scenario), for RoR, even though the electrolysis is run continuously over 24 h per day, the needed electrolysis power still decreases quite rapidly, leaving a large share of days in part-load operation, thus - depending on the underlying year and scenario - resulting in an eqFLH of only about 3000 h. Based on a business model of Teske et al. (2019) approximately 4000 h of eqFLH are - under current economic boundary conditions - required for economic operation of electrolysis. However, a more detailed techno-economic analysis regarding USC-FlexStore is needed (see chapter 6). Moreover, as the eqFLH of individual RoR sites may vary substantially from these national aggregates, they are provided in chapter 4.3.3.2.

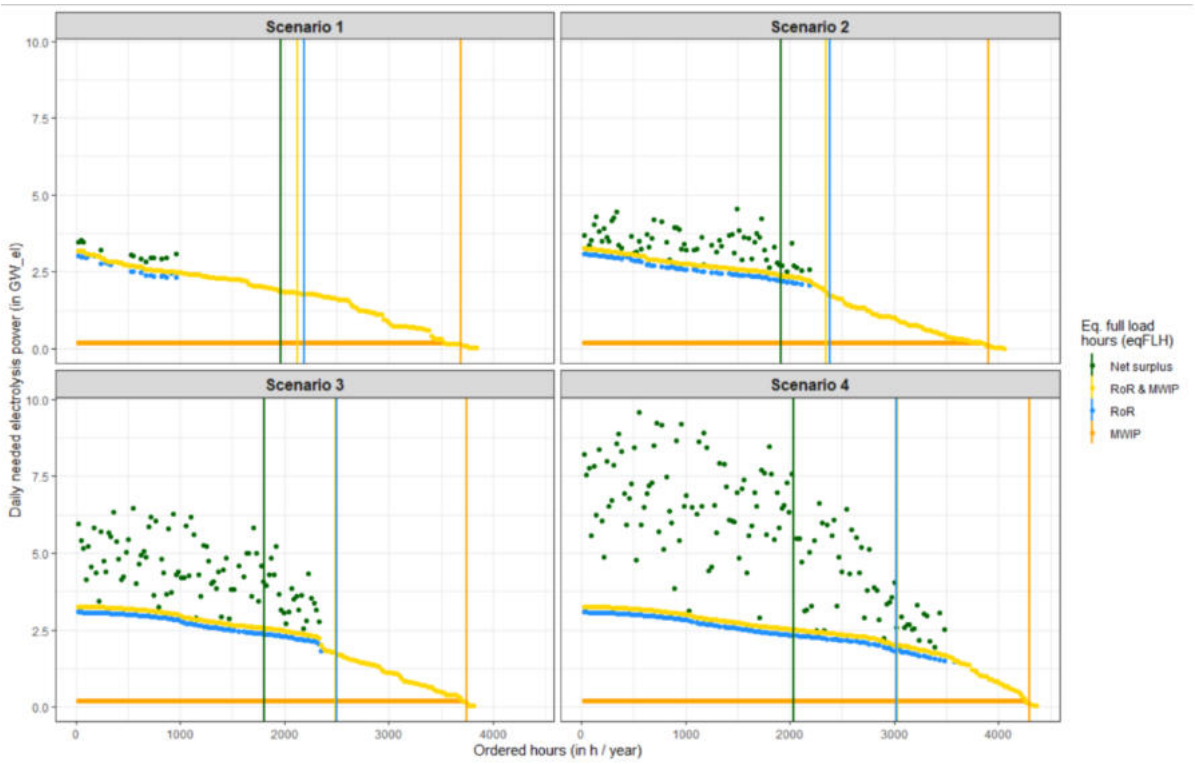

Figure 4-14: Ordered distribution of required electrolysis power (in GW_{el}) to convert all daily available net surplus electricity (green dots) at RoR and MWIP plants. Vertical lines indicate the corresponding equivalent full load hours (eqFLH).

4.3.2 Regional Analysis

4.3.2.1. Available and exploitable net surplus electricity

In Figures 4-15 and 4-16, the available net surplus electricity at the national scale and the exploitable net surplus electricity at RoR and MWIP sites in the inner and outer geology perimeter, respectively, are displayed for each scenario. Compared to the exploitable potential at the national scale with all RoR and MWIP included (see Figure 4-12), the geological boundary conditions result in a further reduction of the exploitable potential to a combined maximum of about 2.1 TWh and 4.2 TWh in the inner and outer perimeter, respectively, for scenario 4, compared to the corresponding national potential of about 10 TWh.

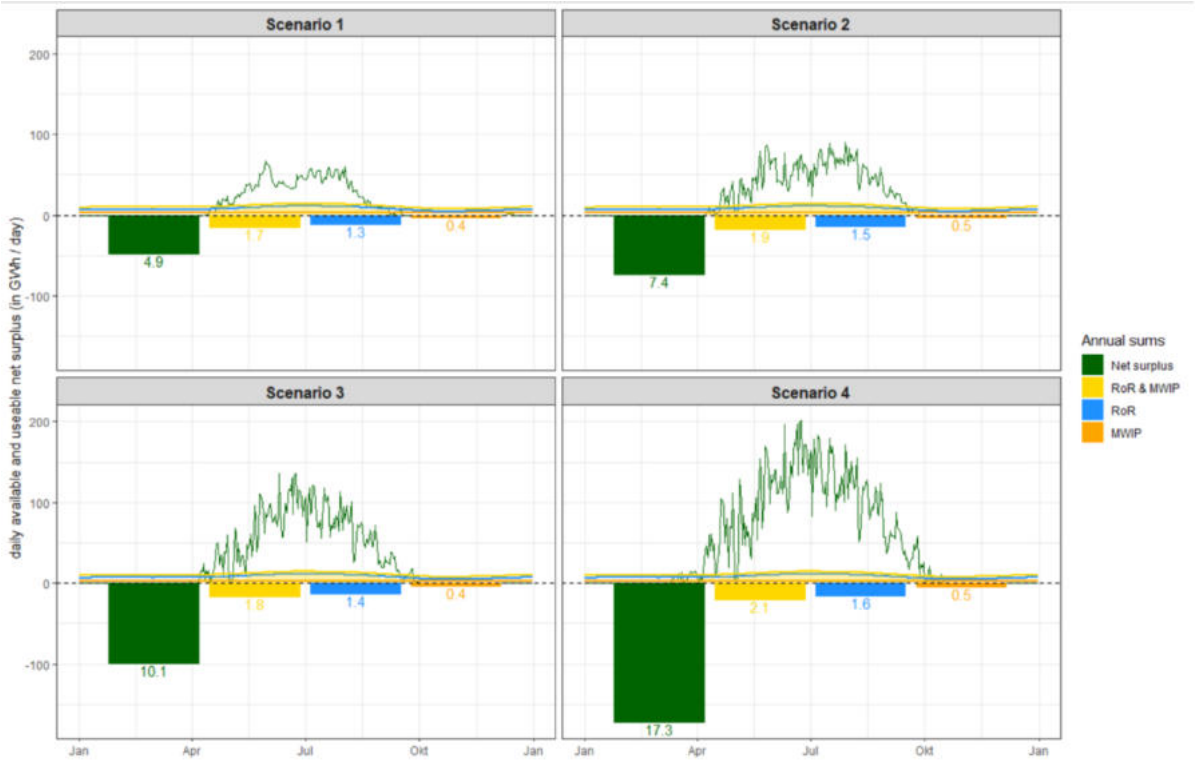

Figure 4-15: Total available net surplus electricity at national scale (dark green lines and bars) and simultaneously exploitable net surplus electricity at RoR (blue), MWIP (orange) and combined (yellow) in the inner geological perimeter according to Figure 4-7.

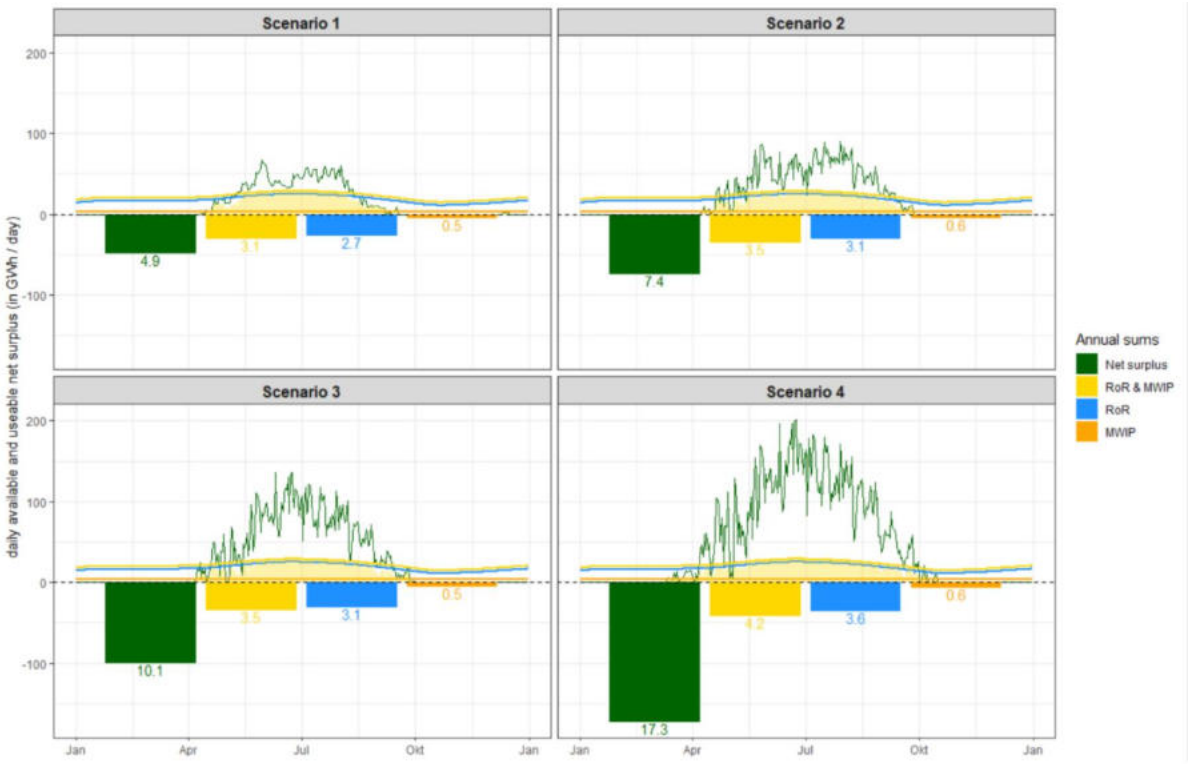

Figure 4-16: Total available net surplus electricity at national scale (dark green lines and bars) and simultaneously exploitable net surplus electricity at RoR (blue), MWIP (orange) and combined (yellow) in the outer geological perimeter according to Figure 4-7.

Figure 4-17 shows how this net surplus potential is used at individual RoR power plants in the inner (red dot) and outer (blue dot) geological perimeter for scenarios 1 and 4 divided by summer and winter half-year. If the inner perimeter is used, the RoR power plant with the largest potential is Verbois (GE) and Eglisau (ZH), whereas if the outer perimeter is used, it is Laufenburg (AG) and Albruck (AG). Irrespective of the geological perimeter, there is a small portion of RoR power plants that could use the brunt of the available net surplus electricity.

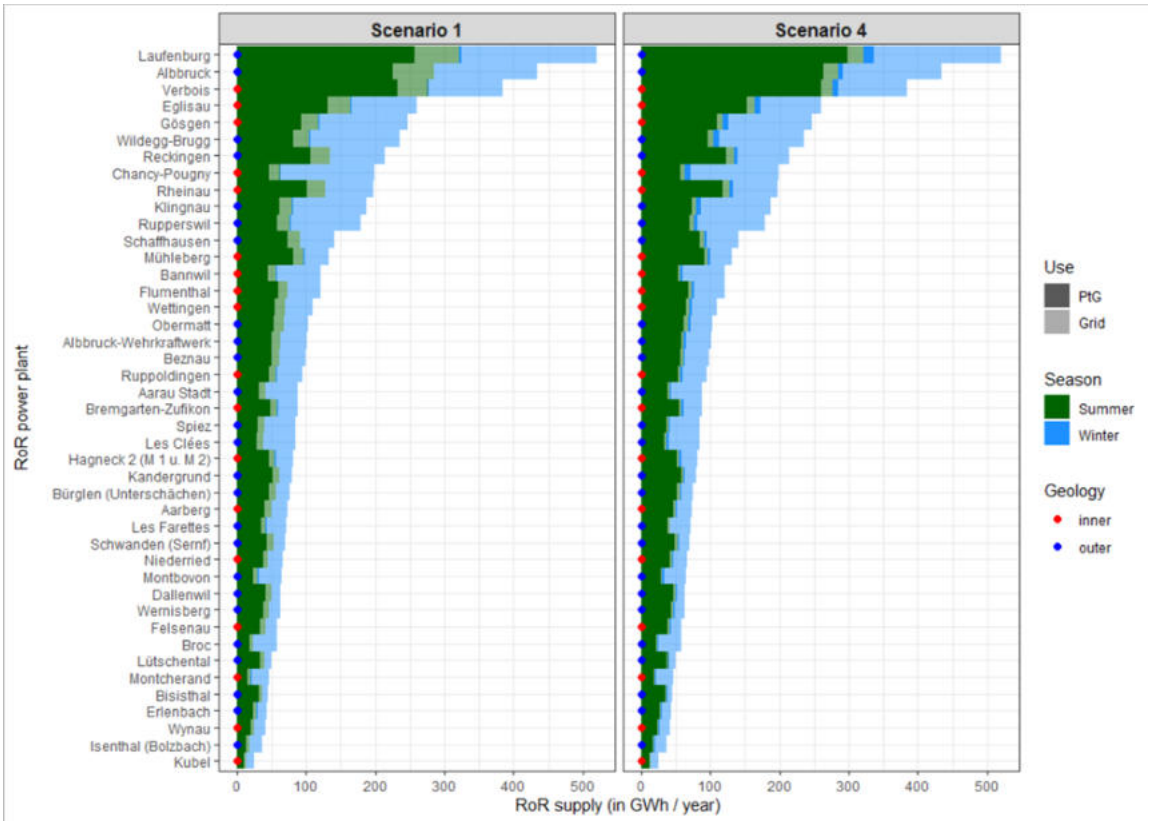

Figure 4-17: Use of generated electricity at RoR (> 10 MW_{el}) for USC-FlexStore or grid injections in the winter (blue colors) and summer (green colors) half year for scenarios 1 and 4. Only RoR power plants in the inner (red dot) and outer (blue dot) geological perimeter.

4.3.2.2. CO_2 sources

Figure 4-18 shows for scenario 4 the optimized transportation paths of industrial CO_2 to RoR power plants with USC-FlexStore infrastructure from the linear transportation problem described in chapter 4.2.5.3. Note that neither geographical nor logistical CO_2 transportation limitations are considered in the optimization.

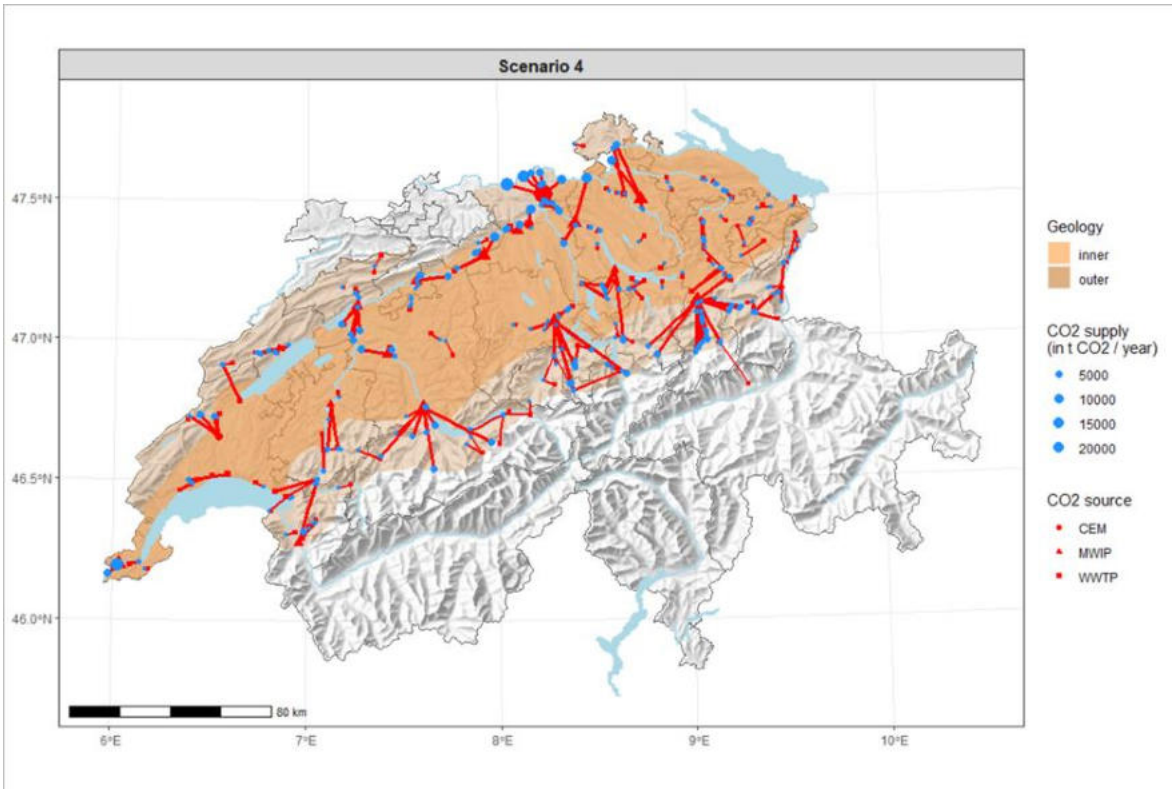

Figure 4-18: Linear connection of CO_2 sources and RoR power plants with USC-FlexStore.

In Figure 4-19, the set of connected CO_2 sources of the largest RoR power plants is displayed. Generally, to be cost-optimal, even these large RoR power plants feature only one dominant, mostly MWIP, source of CO_2 nearby. Only Felsenau has two CO_2 sources, namely one WWTP and one MWIP.

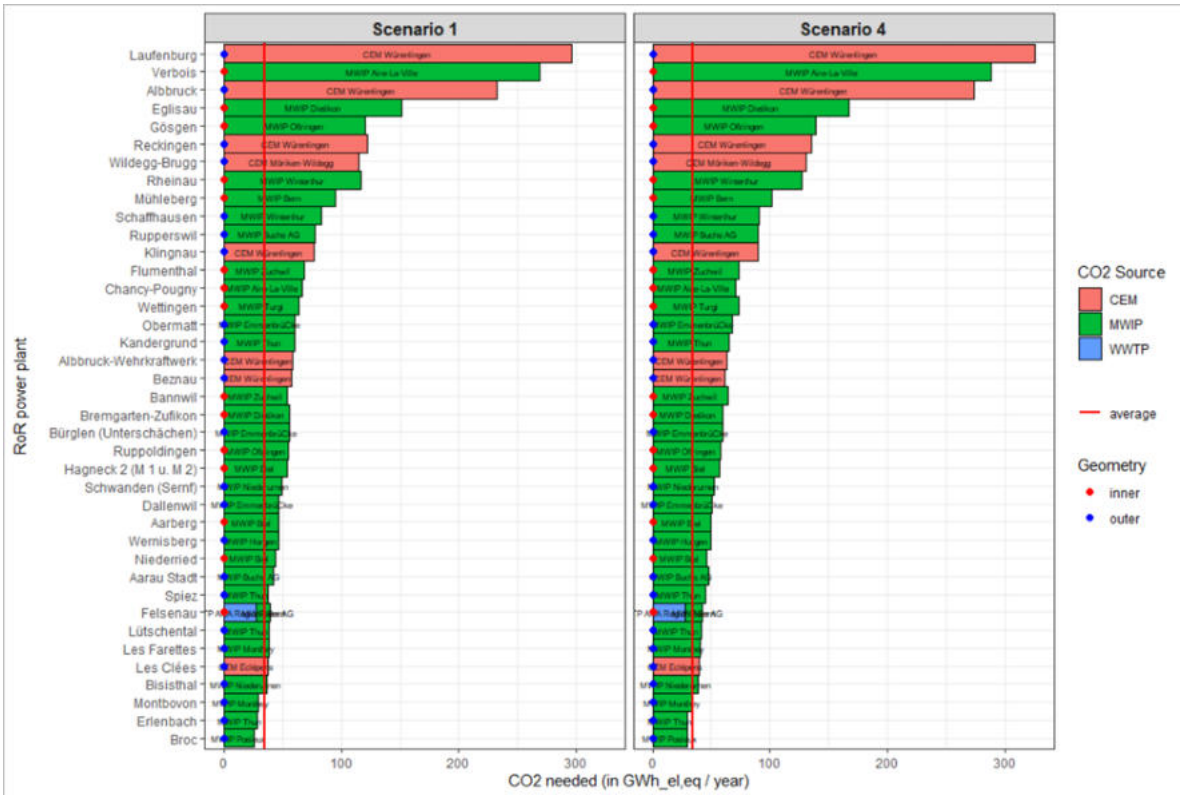

Figure 4-19: Connected industrial CO_2 sources of the largest RoR.

Figure 4-20, in turn, shows which CO_2 sources supply which RoR power plants (including their overall separable potential in transparent colors). To be cost-optimal, large CO_2 sources such as CEM generally have several RoR as recipients, and still, their overall separable potential is only partially exploited. Thus, industrial CO_2 in densely populated urban areas of the Swiss Central Plateau (Mittelland) is typically never a limiting factor for USC-FlexStore.

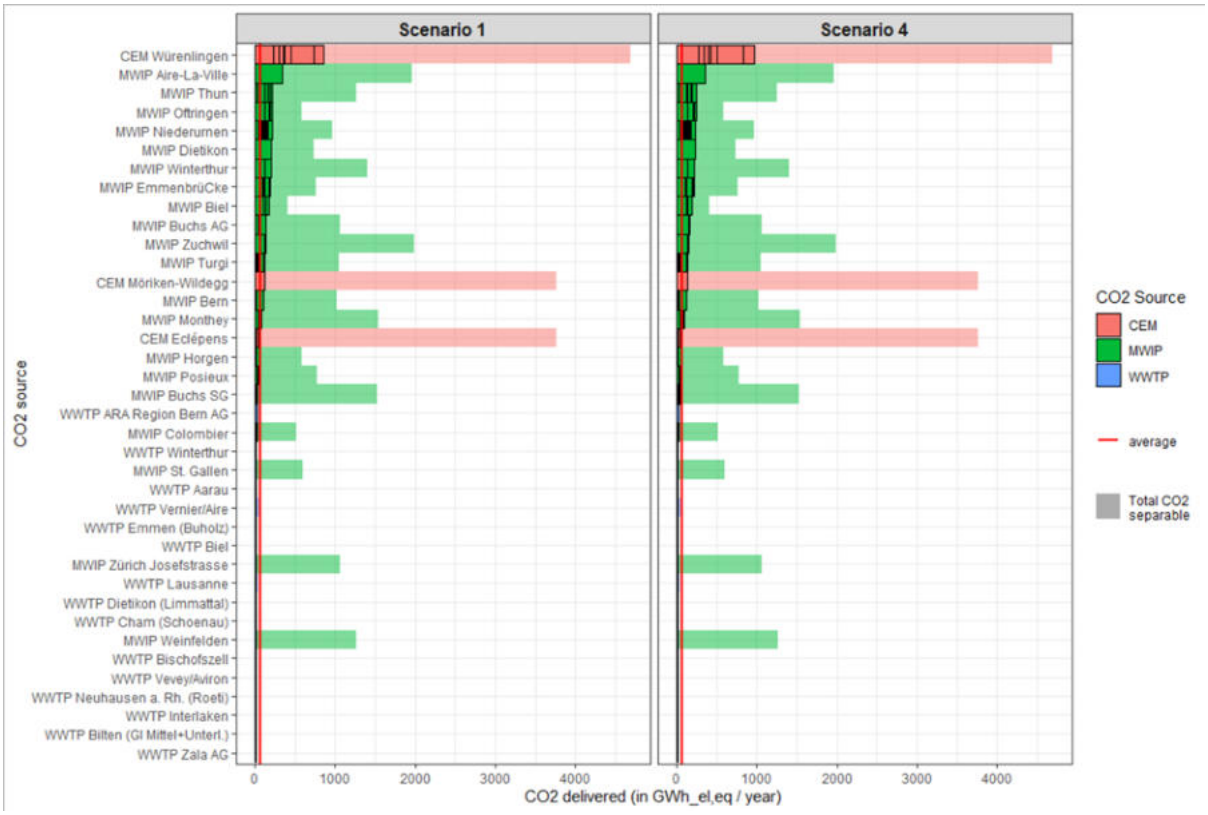

Figure 4-20: Exploitation of industrial CO_2 sources and their connected RoR.

Figure 4-21 shows the distribution of individual transportation distances between RoR and CO_2 sites as density plots. The median transportation distance is about 4 km. However, in this respect a clear distinction must be made between the different CO_2 sources: While WWTP are typically close to the RoR, the median transportation distance from CEM and MWIP is substantially longer. However, in that case, more CO_2 can be transported with a single connection, thus making this route still more cost-efficient despite the longer transportation distance.

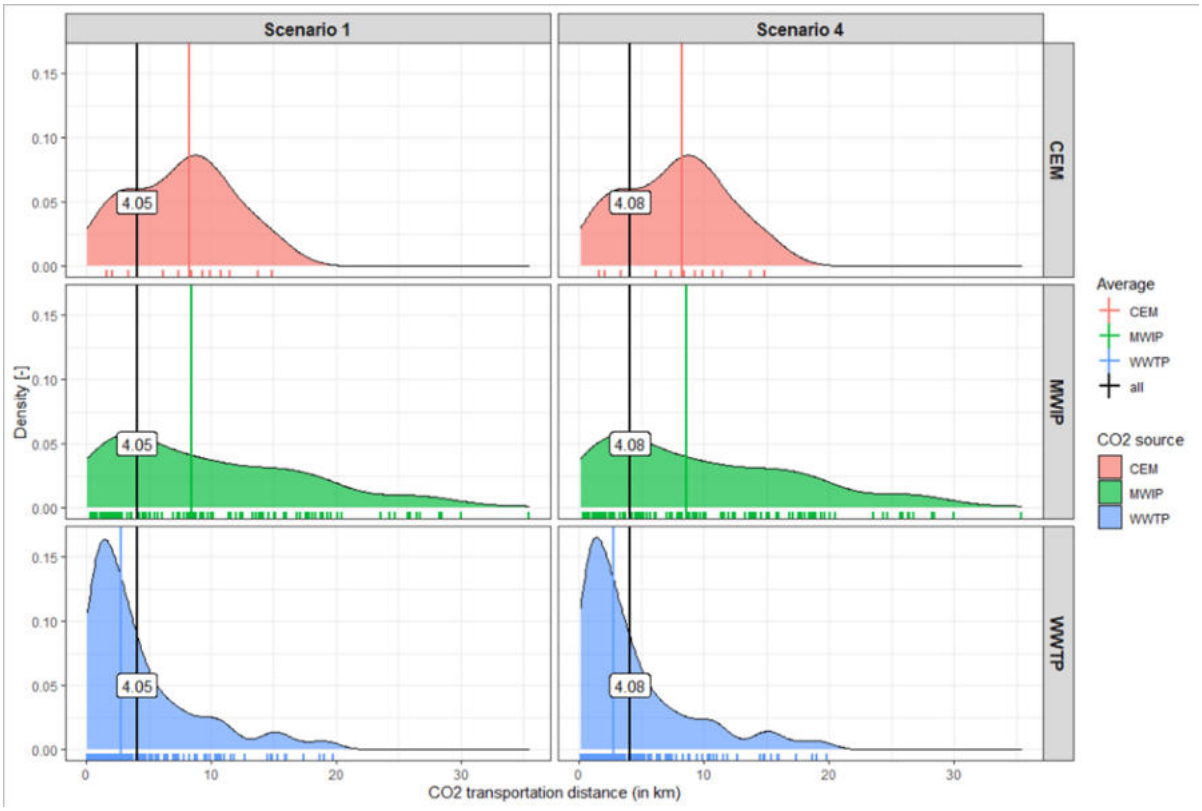

Figure 4-21: Distribution of the transportation distance of industrial CO_2 sources to RoR power plants in Scenarios 1 and 4 divided by CO_2 sources (including the median transportation distance).

Although CO_2 transportation distances are generally shorter than 10 km, there are some exceptions as shown in Figure 4-22 for RoR plants with CO_2 transportation distances longer than 15 km. There are RoR power plants with CO_2 sources almost 60 km away in total. Typically, these RoR are, however, small and located in mountainous (pre-alpine) regions, thus making them less suitable for USC-FlexStore.

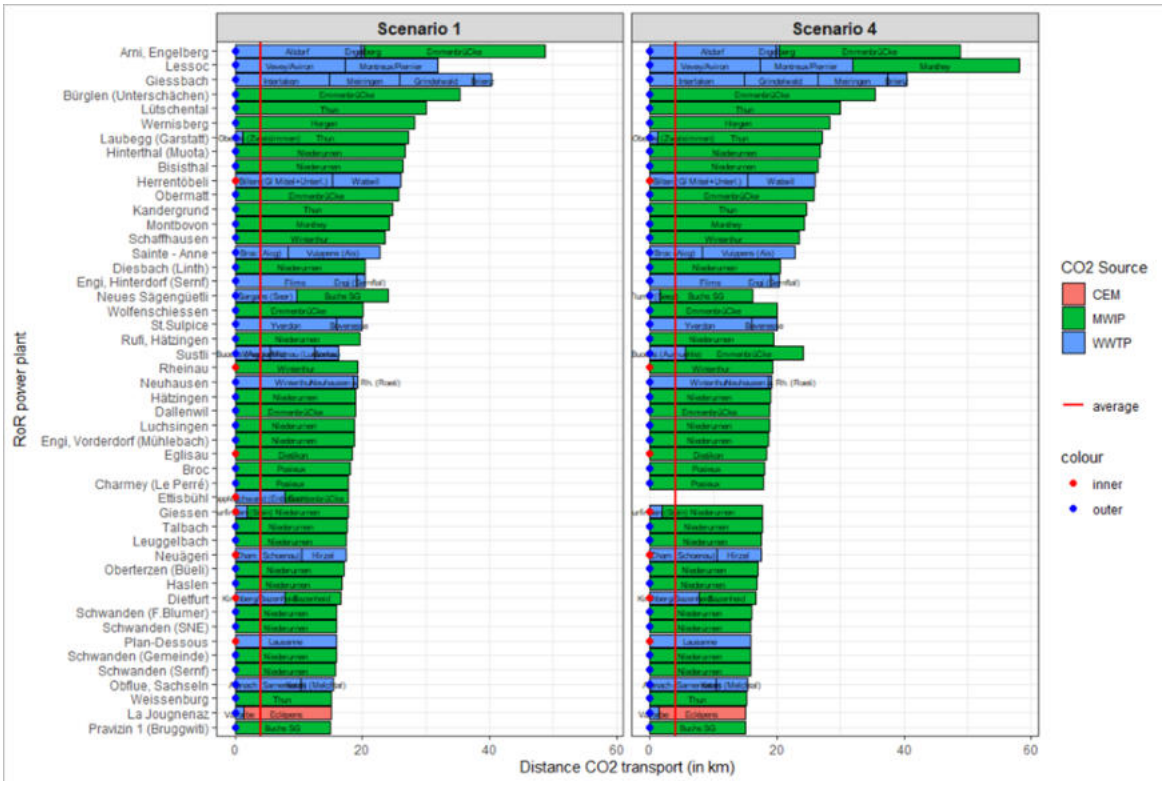

Figure 4-22: RoR power plants with aggregated CO_2 transportation distances of more than 15 km in scenario 1 and 4 divided by CO_2 sources.

4.3.2.3. Gas grid connection

In Figure 4-23, the Euclidean distance of RoR and MWIP to the next possible natural gas (NG) grid injection point is displayed. This may be either the high pressure or the local low-pressure gas grid. Some RoR and MWIP are even within these local low-pressure gas grids, thus favoring an immediate connection. As with CO_2 sources, distances to the NG grid are generally less than 5 km. Distances to the high-pressure grid are typically longer with a maximum of about 15 - 20 km (e.g. MWIP Niederurnen) for both RoR and MWIP.

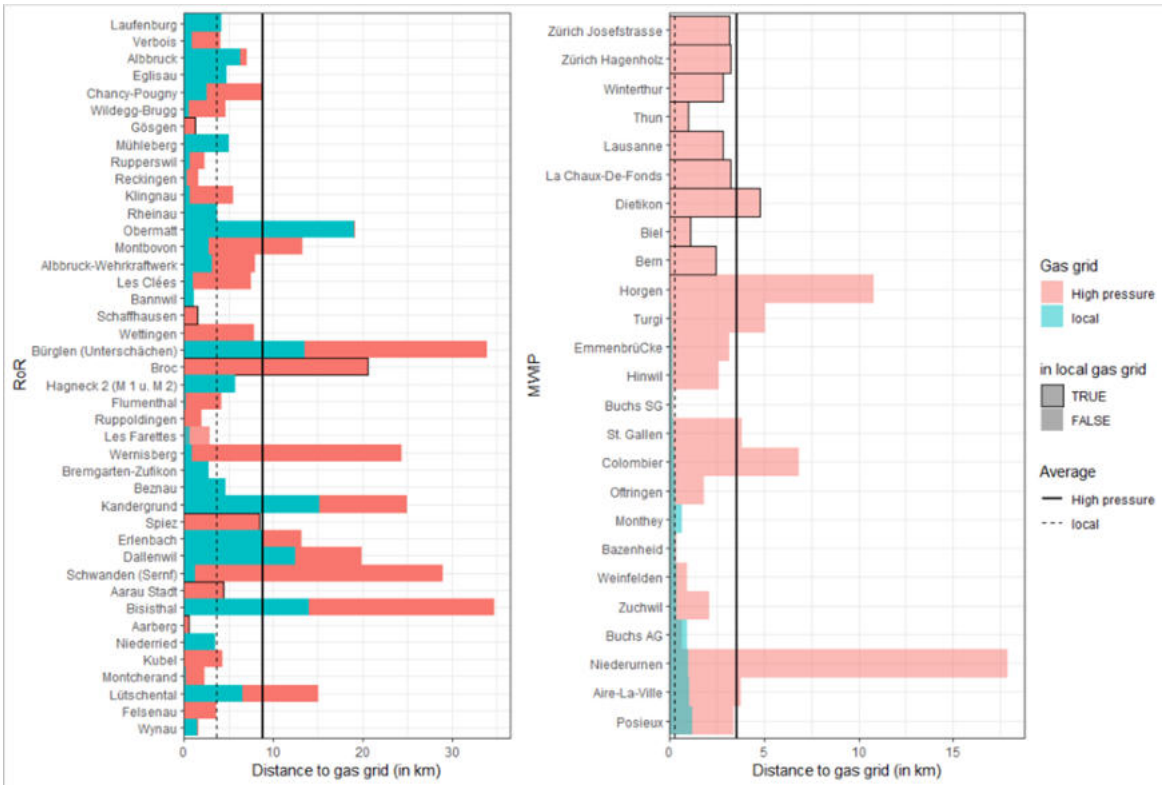

Figure 4-23: Distance to local low pressure or high-pressure natural gas (NG) grids for RoR (left) and MWIP (right) power plants. Power plants within the local low-pressure NG grid are in transparent colors.

4.3.3 Individual Sites (Local) Analysis

4.3.3.1. Stoichiometry

Figure 4-24 shows the stoichiometric ratio of H_2 production and (constant) CO_2 supply for all scenarios with the example of RoR Mühleberg. Similar stoichiometry profiles also result for other RoR power plants and can be found in Figure 4-25 represented as boxplots. In the summer half-year, there is over-stoichiometric H_2 production such that an ideal stoichiometry factor of one (i.e., 4 H_2 + 1 CO_2 = 1 CH_4 + 2 H_2O) is exceeded by a maximum factor of about 3. In other words, in summer typically about 3 times more H_2 is injected into USC-FlexStore than needed for ideal stoichiometric conversion. For some particular RoR (e.g., Chancy-Pougny), this stoichiometry exceedance even reaches values of up to 6. Contrarily, in winter, no H_2 is produced, thus CO_2 would be injected without any simultaneous H_2 as a reactant. To what extent, this non-stoichiometric injection of H_2 and CO_2 over the whole year is subject of chapters 2 and 3. As it has been demonstrated in chapter 3.3.4, over stoichiometric ratios of H2 within the feed gas or the storage, has high degrees of tolerance, while CO2 is restricted as chapter 2.4 has summarized.

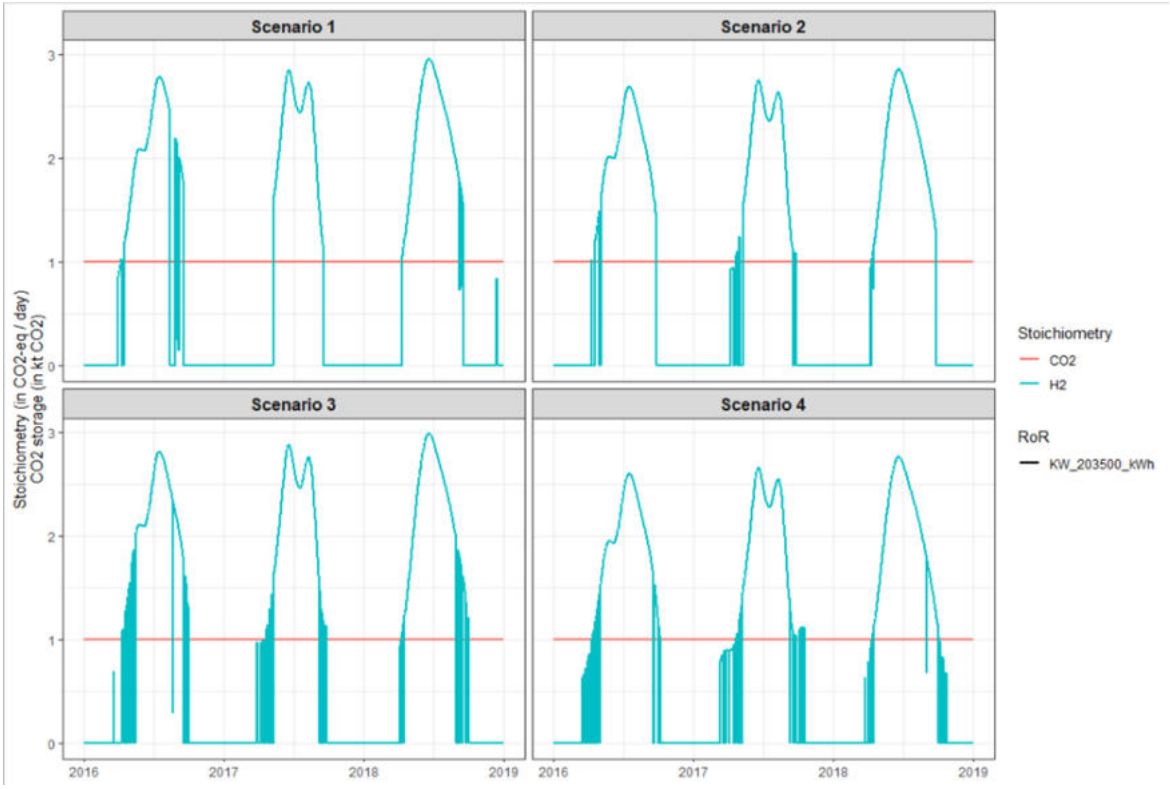

Figure 4-24: Daily stoichiometry of CO_2 and H_2 supply without intermittent CO_2 storage at RoR Mühleberg.

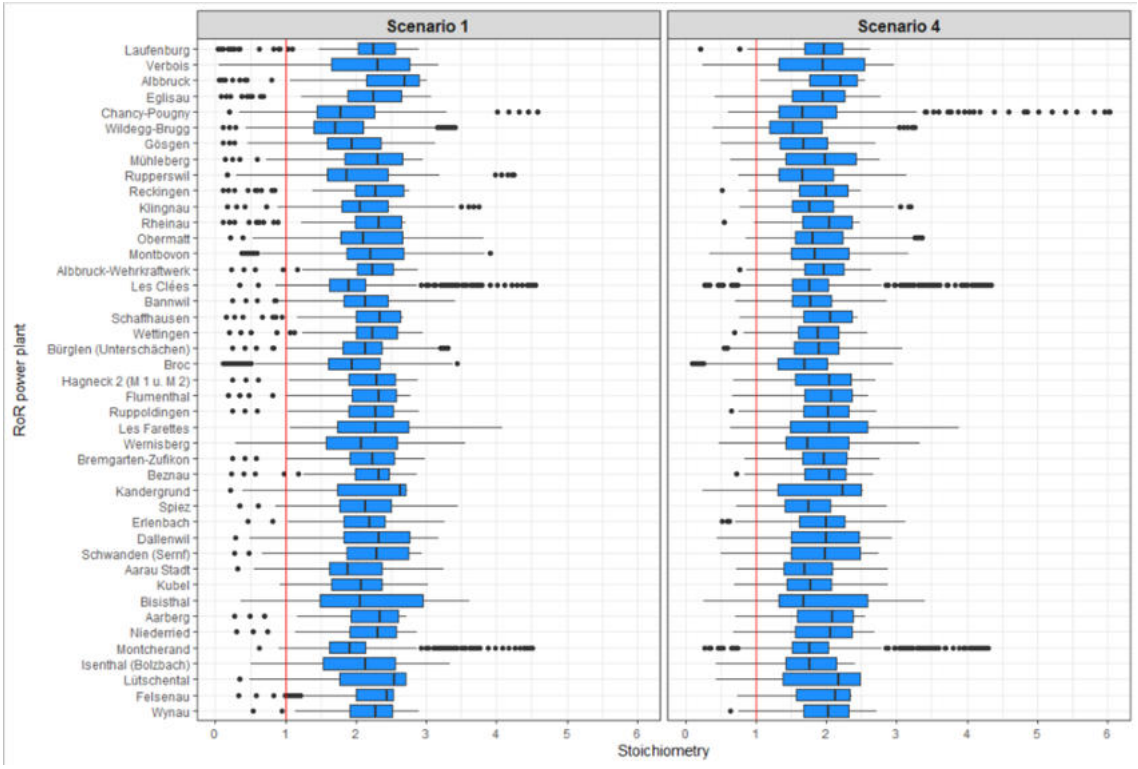

Figure 4-25: Boxplot of daily stoichiometry factors of CO_2 and H_2 injection at RoR power plants (> 10 MW_{el}) in the geologically eligible perimeter.

For stoichiometric injection of H_2 and CO_2 throughout the year, CO_2 needed to be stored in a CO_2 storage vessel (tank) and dosed according to the seasonal H_2 production. Figure 4-26 shows for all RoR power plants larger than 10 MW_{el} in the geologically eligible perimeter, the absolute and relative size of such required CO_2 storage for illustrative reasons. The relative size is the CO_2 storage proportional to the used net surplus electricity at the RoR power plants. This relative CO_2 storage size is constant throughout all RoR and decreases from about 60 to 50 t CO_2 storage per MWh of net surplus electricity used from scenarios 1 to 4, respectively. In absolute numbers, up to 15'400 t of CO_2 must be stored at RoR Laufenburg to achieve ideal stoichiometric CO_2 and H_2 injection for USC-FlexStore.

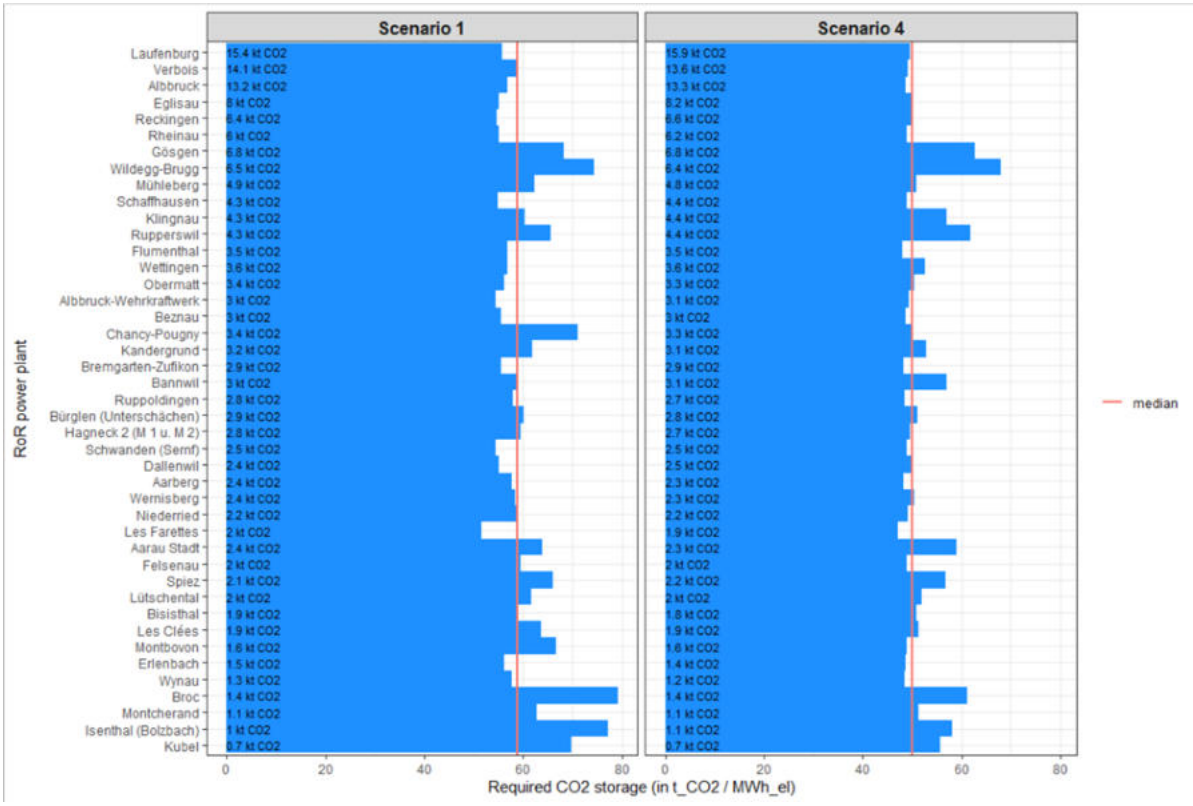

Figure 4-26: Required CO_2 Storage per used net surplus electricity (in t CO_2 storage per MWh net surplus electricity used) at RoR power plants (> 10 MW_{el}) in the geologically eligible perimeter.

4.3.3.2. Full load hours

While the equivalent full load hours (eqFLH) of all RoR power plants combined have already been shown in Figure 4-27, they are shown for the particular site of RoR Mühleberg in Figure 4-14 for all scenarios and distinguished between the underlying years 2016, 2017 and 2018. In that case, no other RoR power plants would use the net surplus electricity exploitable by RoR, and the eqFLH would - depending on the year - increase from about 2500 - 3000 hours in Scenario 1 to more than 3000 hours in Scenario 4. Whether this number of eqFLH is sufficient for the economic operation of USC-FlexStore at this particular site, is subject to subsequent techno-economic analysis (see chapter 6). Other eqFLH (in Scenario 4) can be found in Table 4-5.

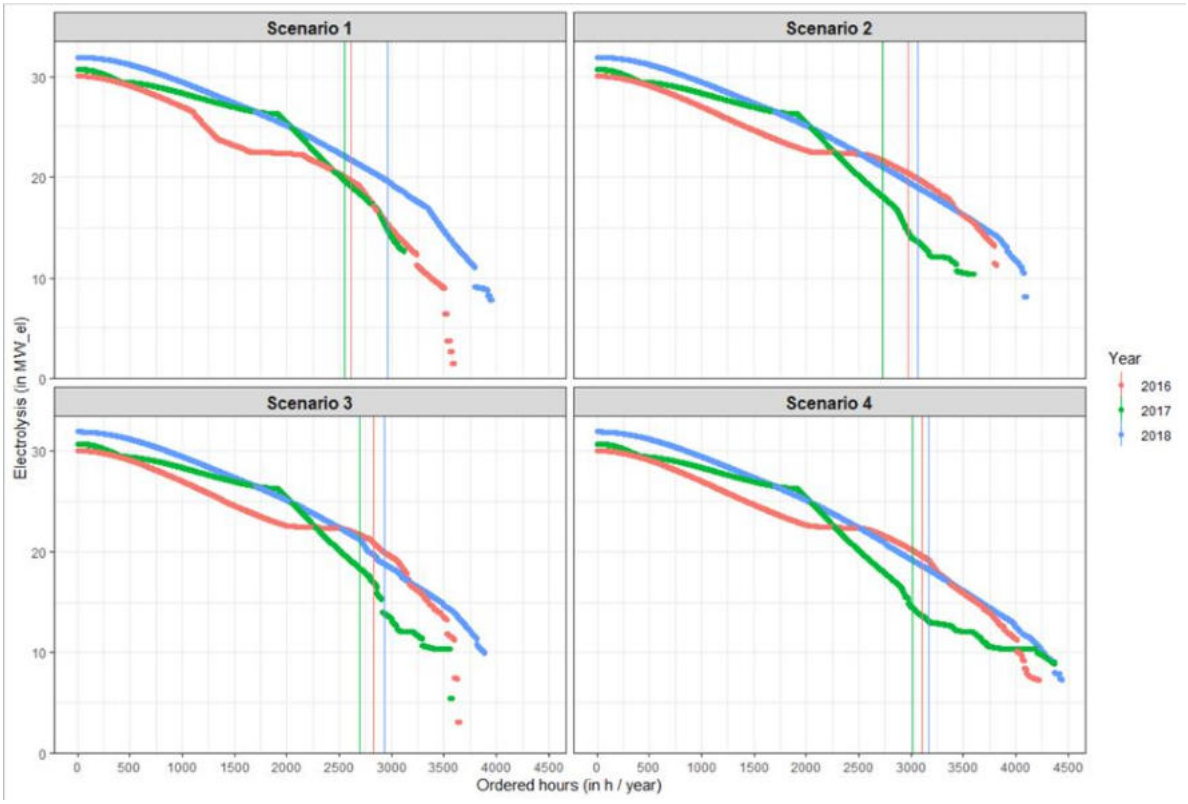

Figure 4-27: Hourly ELYSE power to convert all daily net surplus in each scenario for RoR Mühleberg

4.3.3.3. Top sites in Switzerland

The Top10 and Top5 sites for USC-FlexStore at RoR and MWIP based on their annual H_2 yield are listed in Table 4-5 along with their most relevant other characteristics. Of these Top10 RoR sites, five are in the inner and five in the outer geological perimeter, while only one Top5 MWIP site (i.e., Monthey) is not in the inner perimeter. The most promising RoR site in the outer perimeter is Laufenburg (AG), while in the inner perimeter it is Verbois (GE). If RoR and MWIP sites are combined, the most suitable MWIP site (Zürich Hagenholz) is only ranked 22 overall, thus in terms of annual H_2 yield, RoR sites are generally substantially more productive. This is corroborated by Gupta et al. (2022). However, further evaluation based on a full analysis, which also accounts for the other techno-economic characteristics including CO_2 transportation, equivalent full load hours, natural gas grid injection, etc. must be conducted (see in chapter 6).

Table 4-5: Summary of the top USC-FlexStore sites at RoR and MWIP power plants with their most relevant characteristics.

#	USC site			Net surplus Electricity						H2		CO2 source					Gas grid	
	Geology	Power Plant	Name	used	used	total gen.	total gen.	hours	eq. FLH	ELYSE	Yield	needed	#	Type	Name	Distance	HD	LP
				GWh / year	GWh / summer	GWh / year	GWh / summer	hours	h	MW_el	t H2 / year	t CO2 / year				km	km	km
1	outer	RoR	Laufenburg	320	313	519	323	4368	3427	95	5484	30162	1	CEM	Würenlingen	15	2.1	4.2
2	inner	RoR	Verbois	277	261	384	278	4368	2898	89	4733	26032	1	MWIP	Aire-La-Ville	0	4.2	0.9
3	outer	RoR	Albbruck	274	265	435	284	4224	3425	80	4683	25756	1	CEM	Würenlingen	11	7.0	6.1
4	inner	RoR	Eglisau	163	159	257	165	4368	3150	53	2792	15357	1	MWIP	Dietikon	18	3.1	4.8
5	outer	RoR	Reckingen	132	129	213	133	4368	3509	38	2259	12427	1	CEM	Würenlingen	9	1.6	0.3
6	inner	RoR	Rheinau	126	123	196	127	4368	3523	36	2164	11903	1	MWIP	Winterthur	19	2.8	3.8
7	inner	RoR	Gösgen	108	103	248	107	4368	3247	42	1853	10192	1	MWIP	Oftringen	9	1.2	0.0
8	outer	RoR	Wildegg-Brugg	94	91	237	95	4368	2567	45	1611	8863	1	CEM	Möriken-Wildegg	6	4.6	0.6
9	inner	RoR	Mühleberg	93	91	132	97	4368	3106	31	1598	8789	1	MWIP	Bern	10	3.6	5.0
10	outer	RoR	Schaffhausen	90	87	141	91	4368	3571	25	1548	8512	1	MWIP	Winterthur	24	1.5	0.0
22	inner	MWIP	Zürich Hagenholz	55	50	111	56	4368	4368	13	948	5212	1	MWIP	Zürich Hagenholz	0	3.2	0.0
28	inner	MWIP	Zuchwil	49	44	97	49	4368	4368	11	832	4575	1	MWIP	Zuchwil	0	2.1	0.4
30	inner	MWIP	Aire-La-Ville	48	44	96	48	4368	4368	11	818	4500	1	MWIP	Aire-La-Ville	0	3.8	1.1
35	inner	MWIP	Hinwil	40	37	81	40	4368	4368	9	689	3792	1	MWIP	Hinwil	0	2.6	0.1
39	outer	MWIP	Monthey	38	34	75	38	4368	4368	9	643	3539	1	MWIP	Monthey	0	0.3	0.7

4.4 Conclusions and Outlook

The main conclusions of this chapter are:

- Depending on the scenario, in the future Swiss energy system, there will be net surplus electricity between about 7 TWh (Scenario 2) and 17 TWh (Scenario 4), which is about 10% - 15% of the Swiss total annual end-use electricity demand.
- To reap these net surpluses, ideal load shifting with an additional maximum daily capacity of 50 GWh and a daily maximum peak power of 25 GW must be available, otherwise - due to additional losses and curtailment of surplus electricity - less net surplus electricity is available.
- At RoR power plants, between 6 TWh (Scenario 2) and 10 TWh (Scenario 4) of this nation-wide net surplus electricity can be exploited on-site for USC-FlexStore.
- If only RoR in the inner geologically eligible perimeter are used, only about 2 TWh of the total available net surplus electricity can be exploited.
- These exploitable amounts of net surplus electricity and thereof produced H_2 quantities define the current size of the underground storage for USC-FlexStore. Based on geological and microbiological boundary conditions the actual storage capacity must still be determined in further detail.
- Separable industrial CO_2 from cement plants (CEM), MWIP, and WWTP is abundantly available for an annual equivalent of more than 60 TWh net surplus electricity.
- Transportation distances of CO_2 to large RoR power plants are generally short (less than 5 km). However, in (pre-alpine) regions they may be larger (> 20 km).
- Injection points to the natural gas grid are typically also within short distance from large RoR power plants (< 5 km).
- The future gas demand (> 14 TWh_th) is still large enough to use all produced synthetic methane (SNG) from USC-FlexStore. Re-electfirifation of SNG in winter to cover the net electricity deficits between 10 TWh (Scenario 2) and 14 TWh (Scenario 3) is regarded as a measure of last resort, since demand for SNG in hard-to-decarbonize sectors remains sufficiently high and seems to be the more efficient use of energy. Even if exclusively used for re-electrifitcation, electricity deficits could not be closed in any Scenario by the generated geo-methane of a year.

4.5 Demand – Supply Model for Austria (AT)

4.5.1 Background

Based on the CH model to evaluate the potential for USC-FlexStore and geo-methanation a corresponding model for Austria (AT) is established. This model is primarily based on the evolution of the Austrian energy system from TYNDP 2022 (ENTSOE, 2022) report (scenario "Distributed Energy") to reach European-wide net-zero carbon emission targets by 2050. If data for TNYDP2022 is not in line with the latest national Austrian energy system transition policies, also other national sources are used such as "Energie- und Treibhausgas-Szenarien im Hinblick auf 2030 und 2050" (Umwelt Bundesamt, 2017) as well as Greiml et al. (2021, 2022).

The energy system model to evaluate the potential of USC-FlexStore in the Austrian context is based on the corresponding Swiss model. That is to say that all key assumptions from the Swiss model (see above) are - as consistently as possible - also applied to the Austrian model. These key assumptions are - amongst others:

Ideal load shifting within 24 hours to obtain net surplus electricity for USC-FlexStore (see chapter 4.2.2).

Dispatch of flexible hydropower within five consecutive days based on historical generation profiles / statistic and the residual load as proxy for prices on the electricity market (see chapter 4.2.4.6.2).

No export of electricity allowed due to assumed similar electricity surplus situation in neighbouring countries owing to similar weather conditions and renewables expansion (see chapter 4.2.2).

4.5.2 Methodology

4.5.2.1. Perimeter

As geologically suitable sites for USC-FlexStore, only the Austrian states of Niederösterrreich, Oberösterreich and Vienna are eligible, as in these states, there is already an exploitation of underground gas and oil reserves. In other words, these states have 1) a good record of geological surveys and 2) all the necessary infrastructure for underground gas storage. If grid fees for USC-FlexStore must be paid, as in the Swiss context, RoR power plant sites are selected. There are RoR power plants at the Danube, Inn, Enns and Traun River that are within the eligible perimeter. In particularly, the nine RoR at the Danube River are - due to their large installed capacities - very well suited. Morevoer, it must be noted that entire cascade of hydropower plants on the Enns River is operated in sunk surge operation, since the first hydropower plant in the cascade has a daily storage facility. Therefore, only the residual flow would be always available. The required CO_2 for the geo-methanation would be transported by pipelines to these RoR sites from nearby steel, cement and other (large) industries. With a grid fee exemption for USC-FlexStore, these industrial CO_2 sites would be selected as top sites for USC-FlexStore and (surplus) electricity would be taken from the grid. An overview of all these features and sites needed for USC-FlexStore is provided in the map of Figure 4-28.

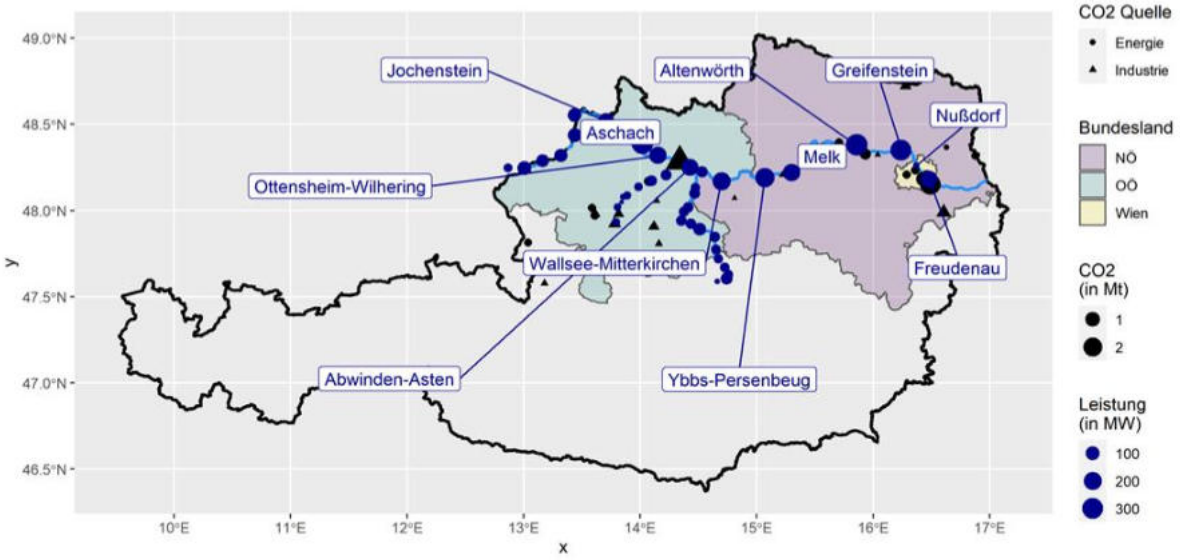

Figure 4-28: Overview of the Austrian perimeter eligible for USC-FlexStore with industrial CO_2 sources (including their annual CO_2 emissions) as well as run-of-river (RoR) hydropower plants (including their installed power) at the Danube, Inn, Enns and Traun River in the Austrian states of Niederösterrreich, Oberösterreich and Vienna.

4.5.2.2. Evolution of Electricity demand and supply

The evolution of the Austrian electricity demand and supply until 2050 to reach net-zero at a European-scale is derived both from TYNDNP 2022 report (ENTSOE, 2022) and the Austrian study "Energie- und Treibhausgas-Szenarien im Hinblick auf 2030 und 2050" (Umwelt Bundesamt, 2017) (scenario "Transition"). For TNYDP2022 data, the scenario "Distributed Energy" (DE) is used, which describes what it would take to reach 2030 EU climate goals and 2050 carbon neutrality by relying more on distributed sources (e.g., solar PV at residential level, etc.). It is important to note that DE is a top-down scenario, that is, a scenario built with little input from TSOs. In other words, the DE scenario serves as a guideline as to how the National energy and climate plans (NECP) could evolve over the next years to adjust to ever changing climate and policy targets on a European scale. Therefore, also the complementary national report "Energie- und Treibhausgas-Szenarien im Hinblick auf 2030 und 2050" is used. The corresponding years are 2030, 2040, and 2050, which is in line with the corresponding scenarios 2, 3 and 4 from the Swiss model. In scenario 1 (i.e., the reference scenario), values from 2015 (or 2020) are used (depending on the underlying sources in TYNDP 2022).

Based on "Energie- und Treibhausgas-Szenarien im Hinblick auf 2030 und 2050" (Umwelt Bundesamt, 2017) and TYNDP 2022 (ENTSOE, 2022), the annual end-use electricity demand (incl. 6% losses) in Austria increases from 56 TWh in scenario 1 to about 80 TWh in scenario 4 (see Figure 4-29). This increase is mainly due to a strong electrification of the transportation sector.

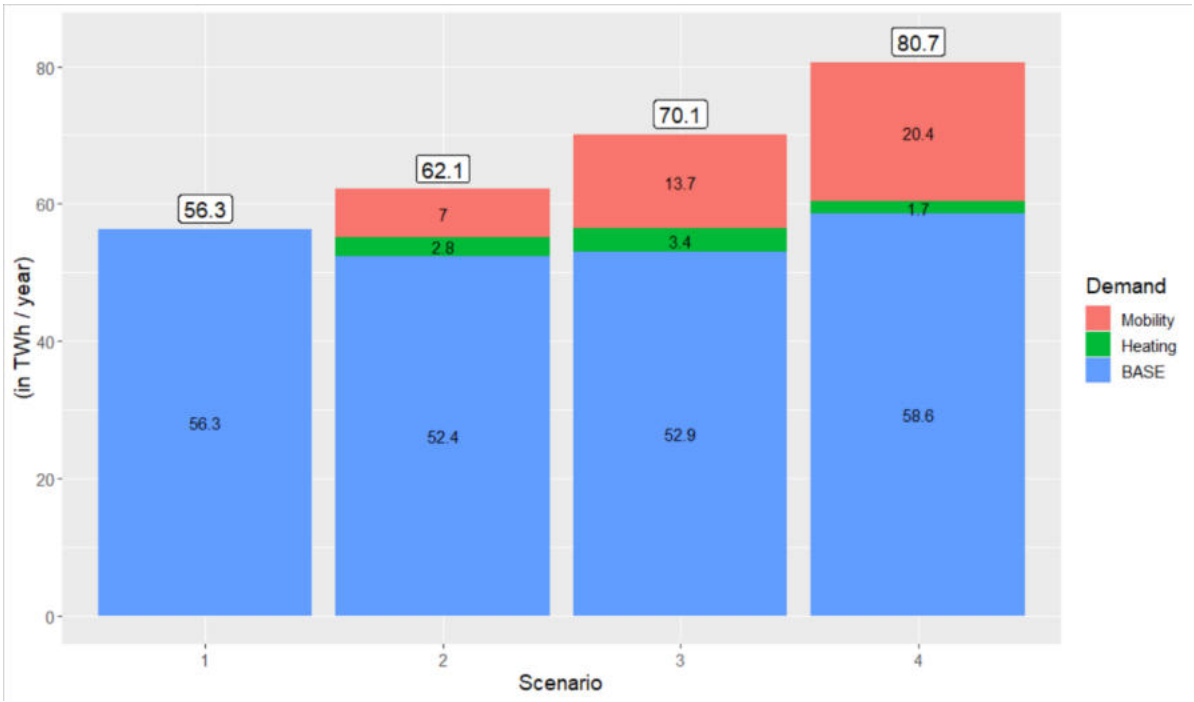

Figure 4-29: Evolution of the Austrian electricity demand from 2015 to a projected 2050 based on TYNDP 2022 (Distributed Energy) divided by sectors.

For the hourly base electricity demand (i.e., without additional electric passenger cars and heat pumps), the historical profiles of ENTSOE's transparency platform (TP) for the years 2016, 2017 and 2018 are used. On top of these profiles, the hourly electricity demand of the passenger cars and heat pumps for space heating and domestic hot water are added as in the Swiss model (see chapter 4.2.3.3).

The evolution of the installed electricity generation capacity in Austria is displayed in Figure 4-30. As can be seen, there is quite a substantial increase in wind and solar PV capacities with 12 and 27 GW by 2050, respectively. On the other hand, there is a phase-out of fossil (mainly) gas and oil power plants. Gas power plants with an installed total capacity of 1.2 GW remain in the system even in 2050 as back-up power plants to offset wind and solar shortages. These gas power plants can, however, also be fed by renewable gases. Installed hydropower capacities (including pumped storage) remain mainly unchanged. Hourly capacity factor profiles for PV and (onshore) wind are taken from ENTSOE's pan-European climate database in De Felice (2021).

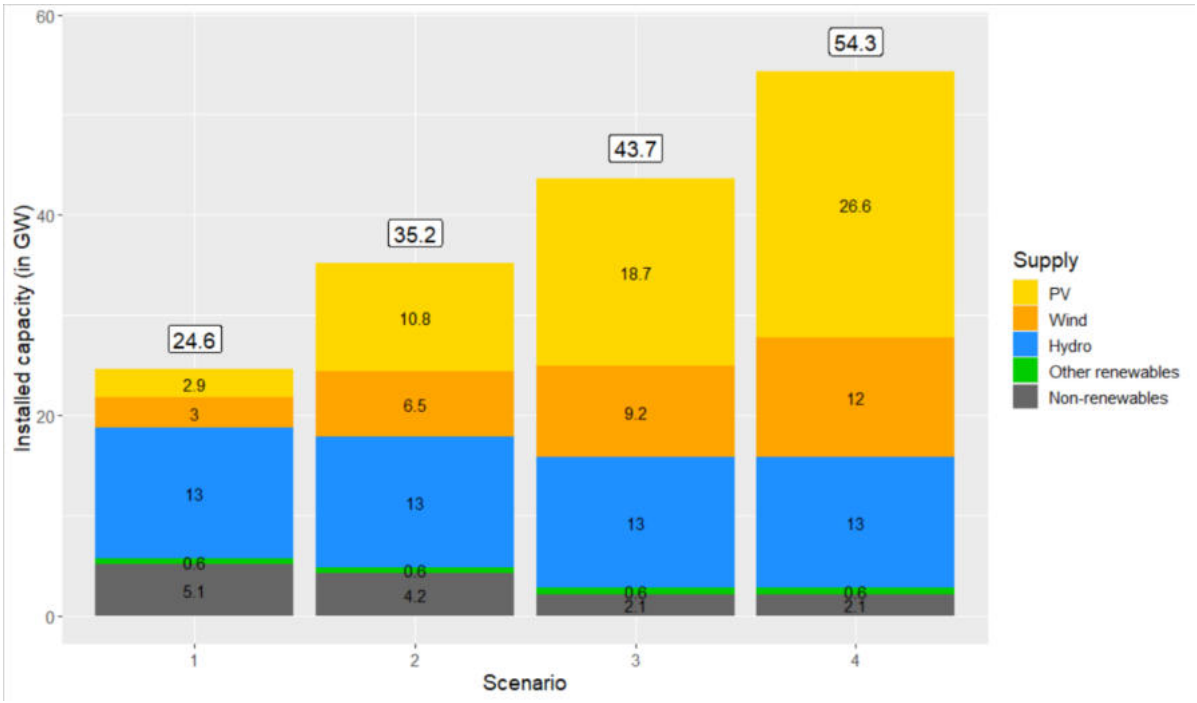

Figure 4-30: Evolution of the installed Austrian electricity generation capacities between today (Scenario 1) and 2050 (Scenario 4) based on ”TYNDP 2022“ (Distributed Energy) and "Energie- und Treibhausgas-Szenarien im Hinblick auf 2030 und 2050" (for PV and wind) divided by technologies.

In Figure 4-31, the evolution of the annual methane and hydrogen demand in Austria divided by different end-users is shown. There is a substantial increase in the hydrogen demand, mainly for heating and cooling as well as for transportation. In turn, there is a decrease in the annual methane demand, in particular for heating. Moreover, the remaining methane demand is mainly covered by domestic biomethane (not shown here). Still, even in 2050, there is a combined demand for hydrogen and methane of about 75 TWh, whereof a certain share could be covered by hydrogen and methane from USC-FlexStore.

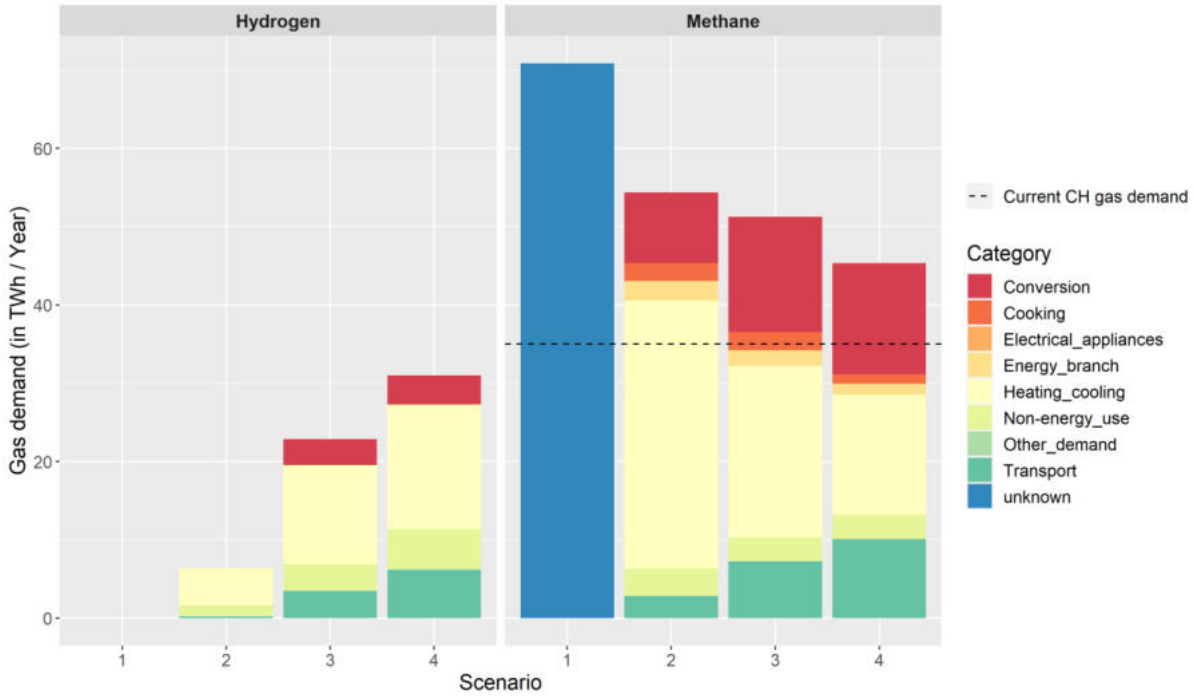

Figure 4-31: Evolution of the annual hydrogen and methane demand in Austrian divided by consumers (categories). For comparison also the current Swiss methane demand (VSG, 2022) is displayed (dashed line).

4.5.2.3. Industrial CO_2 sources

Available industrial CO_2 sources are obtained from the "European CO_2 inventory" (StatCube, 2022). Figure 4-32 displays these CO_2 sources individually and aggregated by the corresponding industrial line in the perimeter of Figure 4-28 for each scenario. Regarding CO_2 point sources, the idea is to estimate how CO_2 emissions from industry might evolve in the future, or whether some industrial sectors will emit minimum amounts that cannot be decarbonized due to the process (e.g., cement production via CaCO3 = CaO + CO_2) or if they come from an already high proportion of biogenic fuels (e.g., paper industry). Thus, CO_2 emissions are divided into fossil, biogenic and process-related emissions per industry. For example, the following is assumed: Paper & wood industry emit approx. 7.5 Mt CO_2 per year, of which 2 Mt CO_2 come from fossil sources. Therefore, it is assumed that at least 75% of the CO_2 emissions of the paper and wood industry would still be available in the future (i.e. scenario 4). Similarly, in the concrete and mining industry, the fossil share of CO_2 emissions is about 45%, while the rest is process-related and biogenic. From this we can derive a minimum amount of CO_2 available in the future for each site. As an example: LaFarge Perlmooser Mannersdorf emits 0.62 Mt CO_2. Depending on the type of decarbonization, there will still be at least 0.62 x 55% = 0.34 Mt CO_2 from biogenic and process-related sources in the future. Using this approach, we could estimate a future minimum CO_2 supply per site that

would be available at a minimum but could be higher depending on the specific implementation of decarbonization.

Two industry sectors are somewhat peculiar in this regard:

- **Refining & Petrochemicals:** since one can assume falling product demand, emissions should fall roughly proportionally. The development or minimum quantities are difficult to estimate.
- **Iron & Steel:** The high proportion of process-related CO_2 emissions would have to come from the blast furnace - this can be converted to electric arc furnaces (being implemented for individual blast furnaces in Austria) and thus achieve decarbonization of the process - the CO_2 quantity is therefore not available in the future.

Despite a clear reduction in industrial CO_2 emissions due to decarbonization, even in scenario 4, still about 10 Mt CO_2 are emitted per year, mainly from the steel plant "voestalpine Stahl GmbH" in Linz (Oberösterreich). With a conversion factor of 94 t CO_2 per GWh electricity (Teske, 2019), these 10 Mt CO_2 could be used with about 110 TWh of net surplus electricity to produce about 50 TWh of synthetic methane.

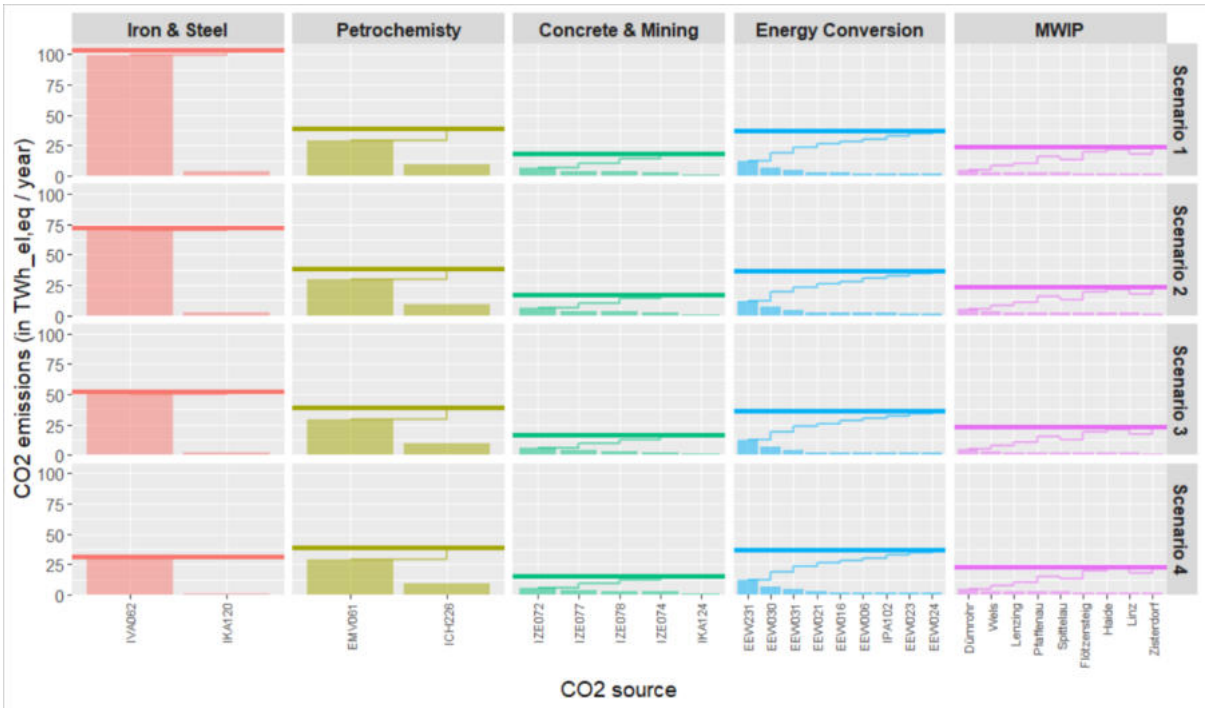

Figure 4-32: Austrian industrial CO_2 sources based on the "European CO_2 inventory" (including their annual CO_2 emissions per scenario) in the project perimeter in Figure 4-28.

4.5.3 Results

4.5.3.1. Monthly electricity demand and supply

Figure 4-33 displays the months electricity demand and supply divided by supply technologies and consumers as well as deficits and surpluses for each scenario. As can be seen, due to the large PV expansion, electricity surplus production in the summer half year increase substantially from scenario 1 to 4. Due to the coinciding large expansion of wind electricity winter deficits are not as prominent as in the Swiss case (with only a small wind expansion – due to social acceptance issues, etc.). This surplus generation of renewable electricity in the summer months can be used for USC-FlexStore. The available amounts of this net surplus energy are quantified in the next chapter.

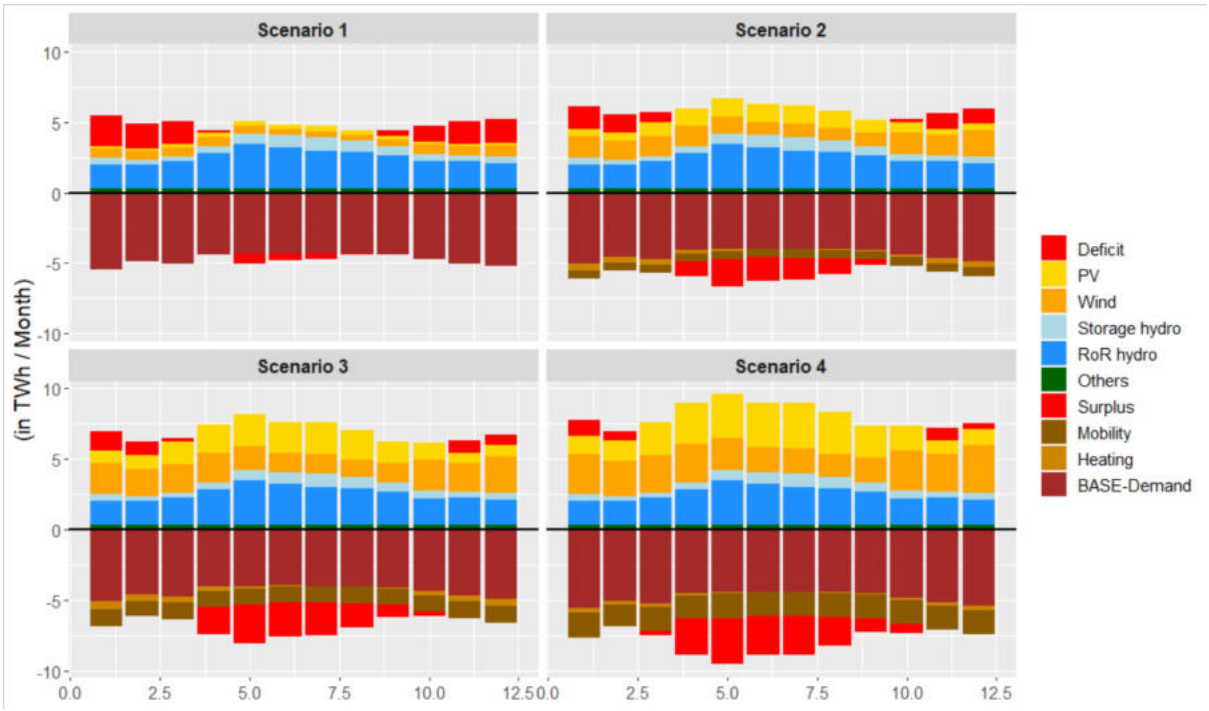

Figure 4-33: Monthly aggregated electricity demand and supply by generation technology and end-use consumers for each scenario. In red, monthly deficits (mainly in winter) and surpluses (mainly in summer) are displayed.

4.5.3.2. Net surplus electricity for USC-FlexStore

Based on the Austrian electricity demand and supply model, annual net and gross electricity surpluses and deficits are derived (see Figure 4-34). In the reference (scenario 1), there is a net electricity deficit of about 13 TWh, which is currently mainly covered by imports and the use of dispatchable (fossil) gas power plants. With the increased deployment of PV and wind in scenarios 2 to 4 (i.e., 2030 to 2050), a substantial amount of net surplus electricity (up to 15 TWh in Scenario 4) is generated, while net deficits reduce to about 7 TWh. The 15 TWh of net electricity surpluses are in a similar range as the about 20 TWh in Switzerland (see Figure 4-11). If economically viable, these up to 15 TWh of net surplus electricity can be used for USC-FlexStore.

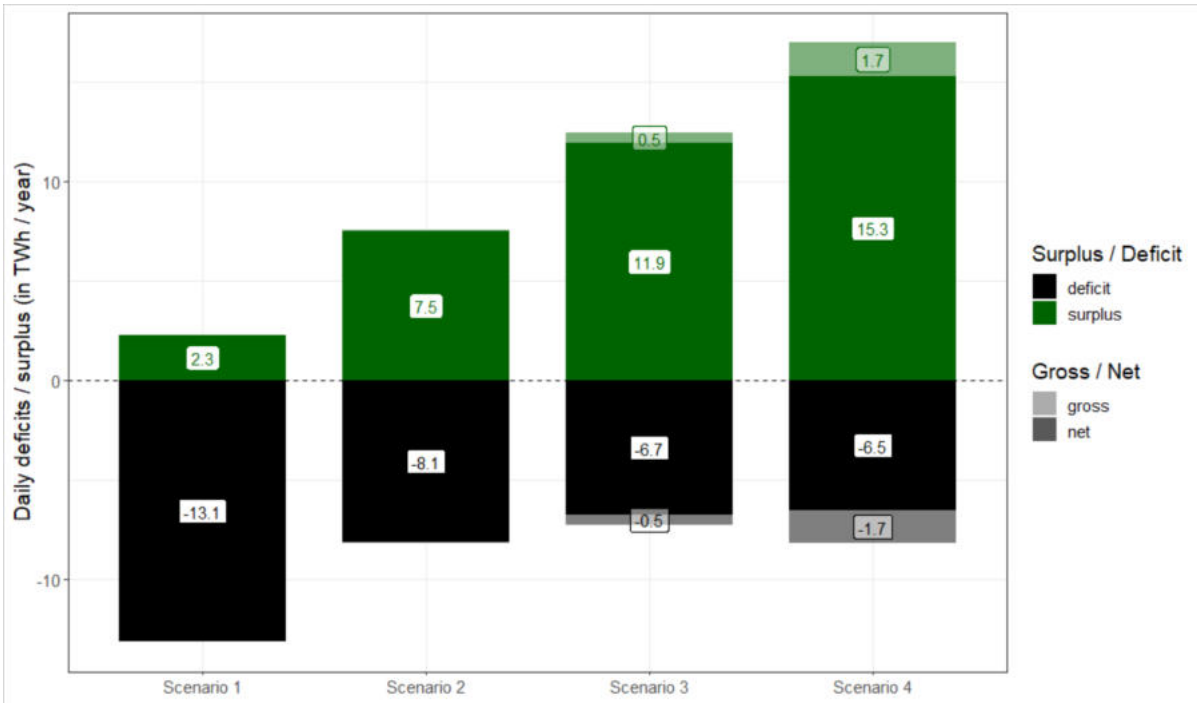

Figure 4-34: Annual gross and net electricity surpluses and deficits, respectively, derived from the Austrian electricity supply and demand model for the four scenarios.

If these 15 TWh net surplus electricity are used at RoR and municipal waste incineration (MWIP) plants, as in the Swiss context, about 13 TWh can be exploited. If, in turn, only the nine Danube River RoR hydropower plants in the project perimeter (see Figure 4-28) are considered, about 7.4 TWh net surplus electricity can be use in Scenario 4 (not shown in Figure 4-35). For scenarios 2 and 3 it would be 5.2 TWh and 6.5 TWh, respectively.

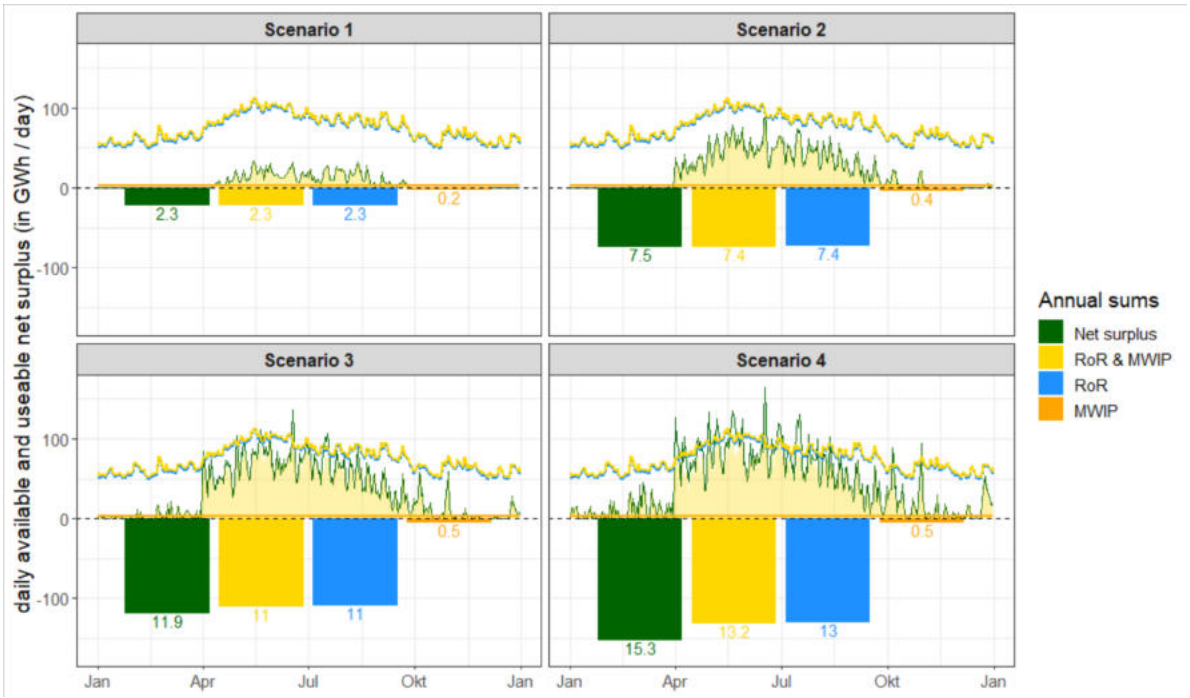

Figure 4-35: Daily (line) and annually (bars) available and exploitable net surplus electricity, respectively, at Austrian RoR and MWIP (and combined).

4.5.3.3. Top sites for USC-FlexStore

The Top sites for USC-FlexStore at RoR and MWIP in Austria (AT) based on their annual H_2 yield are listed in Table 4-6 along with their most relevant other characteristics. Of the top sites at RoR hydropower plants, all are at the Danube River within the project perimeter in Figure 4-28. The most promising RoR site is Altenwörth in Niederösterreich with an annual H_2 production of 18'145 t H_2. However, if also large nearby industrial CO_2 sources are needed, the RoR site in Abwinden-Asten just downstream of Linz (Oberösterreich) is of major interest. If MWIP sites are considered, due to their limited installed electricity generation capacity, they all yield an identical annual H_2 yield of 689 t H_2, thus all their electricity generation can be used for USC-FlexStore. In other words, due to the large installed electric capacity of the Danube River RoR sites, they are generally more suitable (i.e., productive than MWIP. This is in line with the Swiss case (see Chapter 4.3.3.3).

Table 4-6: Summary of the top USC-FlexStore sites at RoR and MWIP power plants in Austria (AT) with their most relevant characteristics.

#	USC site			Net surplus Electricity				H2	CO2 source
	Typ	Bundesland	Name	used	used	total gen.	total gen.	production	needed
				GWh / year	GWh / summer	GWh / year	GWh / summer	t H2 / year	t CO2 / year
1	RoR	Niederösterreich	Altenwörth	1060	891	1779	962	18145	99798
2	RoR	Niederösterreich	Greifenstein	916	772	1543	834	15679	86235
3	RoR	Oberösterreich	Aschach	866	745	1465	802	14818	81496
4	RoR	Niederösterreich	Ybbs-Persenbeug	747	611	1241	660	12778	70280
5	RoR	Niederösterreich	Wallsee-Mitterkirchen	736	584	1214	646	12591	69252
6	RoR	Niederösterreich	Melk	690	540	1155	604	11808	64945
7	RoR	Oberösterreich	Ottensheim-Wilhering	594	474	990	522	10168	55923
8	RoR	Wien	Freudenau	580	462	971	504	9924	54581
9	RoR	Oberösterreich	Abwinden-Asten	562	450	938	492	9612	52868
10	MWIP	Niederösterreich	Dürnrohr	40	34	666	333	678	3728
11	MWIP	Wien	Flötzersteig	40	34	266	133	678	3728
12	MWIP	Wien	Haide	40	34	266	133	678	3728
13	MWIP	Oberösterreich	Lenzing	40	34	333	167	678	3728
14	MWIP	Oberösterreich	Linz	40	34	266	133	678	3728
15	MWIP	Wien	Pfaffenau	40	34	333	167	678	3728
16	MWIP	wien	Spittelau	40	34	333	167	678	3728
17	MWIP	Niederösterreich	Wels	40	34	400	200	678	3728
18	MWIP	Niederösterreich	Zisterdorf	40	34	216	108	678	3728

4.5.4 Conclusions

Based on the model runs with above-described Austrian electricity demand and supply model, the following conclusions can be drawn with respect to the Austrian context:

- Due to the large expansion of solar PV electricity generation in summer there will be substantial amounts of renewable surplus electricity available in the future Austrian electricity that can be stored and shifted seasonally to cover electricity / energy deficits in winter. One promising option is USC-FlexStore.
- When electricity is subject to “grid fee”, the maximum available net surplus electricity for USC-FlexStore and geo-methanation is about 15 TWh.
- The nine Danube RoR power plants in Oberösterreich, Niederösterreich and Vienna are the most attractive locations for USC-FlexStore due to their…
    - … large capacity and large amount of surplus renewable electricity generation in summer
    - … nearby (industrial) CO_2 sources (mainly from steel industry)
    - … nearby large metropolitan areas with a high gas demand (Vienna, Linz, etc.)
    - … well recorded history and rich potential on depleted gas fields and hence known potential storage sites.

4.6 Abbreviations

3D	Three Dimensional
a	year(s)
ASHP	Air Source Heat Pump
AT	Austria / Austrian
BEV	Battery Electric Vehicle
$CaCO_3$	Calcium Carbonate
CaO	Calcium Oxide
CCGT	Combines Cycle Gas Turbine
CEM	Cement Production Site
CH	Switzerland / Swiss
CHP	Combined Heat and Power
CO_2	Carbon-Dioxide
DE	Distributed Energy
EU	European Union
DHW	Domestic Hot Water
DSM	Demand Side Management
ELYSE	Electrolysis
ENTSO-E	European association for the cooperation of Transmission System Operators for Electricity
eqFLH	Equivalent Full Load Hours
FCEV	Fuel Cell Electric Vehicle
FOEN	Federal Office for the Environment
GW_{el}	Gigawatt electric
H_2	Hydrogen
HYD-DAM	Storage Hydropower plant
ICEV	Internal Combustion Engine Vehicle
kWh	Kilowatt hours
M	Million
MW_{el}	Megawatt electric
MWIP	Municipal Waste Incineration Plant
MZMV	Micro-census on transport and mobility
NECP	National Energy and Climate Plans
NG	Natural Gas
NPVM	National passenger transport model
pn	Standardized pressure
pH	Acidity
PHS	Pumped Hydropoer Plant
PV	PhotoVoltaics
ROR	Run-of-Rivers-Powerplant
SFOE	Swiss Federal Office of Energy
SH	Space Heating
SNG	Synthetic Natural Gas
TP	Transparency Platform
TSO	Transmission System Operator
TWh	Terawatt hours
TYNDP	Ten-Year Network Development Plan
USC	Underground Sun Conversion
WP	Work Package
WWTP	Wastewater Treatment Plant

4.7 References

AFU, 2019. ARA Steckbriefe (Fact sheets WWTP).

ARE, 2016. Perspektiven des Schweizerischen Personen- und Güterverkehrs bis 2040 (Perspectives for Swiss passenger and freight traffic up to 2040).

BAFU, 2021. Wasser: Geodatenmodelle [WWW Document]. URL https://www.bafu.admin.ch/bafu/de/home/themen/wasser/zustand/karten/gedoatenmodelle.html (accessed 10.16.21).

BAFU, 2019. Schadstoffregister SwissPRTR (pollutant register SwissPRTR).

BAFU, 2017. Adressliste der Schweizer Kläranlagen mit Angaben zur Ausbaugrösse (Address list of the Swiss sewage treatment plants with information on the expansion size).

BAFU, 2015. Faktenblatt: CO2 Emissionsfaktoren des Treibhausgasinventars der Schweiz (Fact sheet: CO2 Emission factors of the greenhouse gas inventory of Switzerland).

Baumberger, R., Allenbach, R., 2016. 3D model of the Swiss Molasse Basin--A first step towards a national geological 3D model. Swiss Bull. Appl. Geol. https://doi.org/10.5169/seals-658183

Beer, M., 2018. Abschätzung des Potenzials der Schweizer Speicherseen zur Lastdeckung bei Importrestriktionen (Assessment of the potential of Swiss storage lakes to cover loads in the event of import restrictions). Zeitschrift für Energiewirtschaft 42, 1–12. https://doi.org/10.1007/s12398-018-0220-8

Berkelaar, M., 2020. Interface to “Lp_solve” v. 5.5 to Solve Linear/Integer Programs.

BFE, 2020. Schweizerische Statistik der erneuerbaren Energien (Swiss statistics on renewable energies) 2020.

BFE, 2019a. Analyse des schweizerischen Energieverbrauchs 2000-2018 -- Auswertung nach Verwendungszwecken (Analysis of Swiss energy consumption 2000-2018 - evaluation according to purpose). Bundesamt für Energie BFE (Swiss Federal Office of Energy (SFOE), Bern.

BFE, 2019b. Schweizerische Elektrizitätsstatistik (Swiss Electricity Statistics) 2019.

BFE, 2017. Statistik der Wasserkraftanlagen 2016 (Hydropower plants: statistics 2016).

BFS, 2020. Mikrozensus Mobilität und Verkehr (MZMV).

De Felice, Matteo. 2021. ENTSO-E Pan-European Climatic Database (PECD 2021.3) in Parquet format [Data set]. Zenodo. https://doi.org/10.5281/zenodo.5780185

De Haan, P., Müller, M., Peters, A., Hauser, A., Zurich, E., Volken, T., Bfe, E., Gysler, M., Pulfer, M., 2009. Lenkungsabgaben zur Senkung des CO2-Ausstosses beim Neuwagenkauf - Hintergrund, Mechanismen, Prognosen. Bundesamt für Energie BFE (Swiss Federal Office of Energy (SFOE), Bern.

Dillig, M., Jung, M., Karl, J., 2016. The impact of renewables on electricity prices in Germany - An estimation based on historic spot prices in the years 2011-2013. Renew. Sustain. Energy Rev. 57, 7–15. https://doi.org/10.1016/j.rser.2015.12.003

Dujardin, J., Kahl, A., Kruyt, B., Bartlett, S., Lehning, M., 2017. Interplay between photovoltaic, wind energy and storage hydropower in a fully renewable Switzerland. Energy 135, 513–525. https://doi.org/10.1016/j.energy.2017.06.092

EBP, 2021. Szenarien der Elektromobilität in der Schweiz (Electric mobility scenarios in Switzerland) – Update 2021. EBP.

EBP, 2017. Barometer Auto und Mobilität von morgen 2017 - Jährliche Erhebung zu Mobilität, Verkehrsmittelwahl und Autokauf in der Schweiz. EBP.

ENTSOE, 2020a. Planning the future grid - TYNDP [WWW Document]. URL https://tyndp.entsoe.eu/ (accessed 2.5.21).

ENTSOE, 2020b. Transparency Platform [WWW Document]. URL https://transparency.entsoe.eu/ (accessed 11.24.20).
ENTSOE, 2022. Ten-Year-Network-Development-Plan (TYNDP) 2022 – Scenario Report (Version April 2022). URL https://2022.entsos-tyndp-scenarios.eu/
Frontier Economics, 2021. Analyse Stromzusammenarbeit CH–EU - Schlussbericht. Frontier Economics.
Greiml, M., Fritz, F., Kienberger, T., 2021. Increasing installable photovoltaic power by implementing power-to-gas as electricity grid relief – A techno-economic assessment. Energy 235, 121307. https://doi.org/10.1016/j.energy.2021.121307
Greiml, M., Fritz, F., Steinegger, J., Schlömicher, T., Wolf Williams, N., Zaghi, N., Kienberger, T., 2022. Modelling and Simulation/Optimization of Austria's National Multi-Energy System with a High Degree of Spatial and Temporal Resolution. Energies 15, 3581. https://doi.org/10.3390/en15103581
Götz, P., Henkel, J., Lenck, T., Lenz, K., 2014. Negative Electricity Prices: Causes and Effects. Agora Energiewende, Berlin.
Gujer, W., 1999. Siedlungswasserwirtschaft. Springer.
Gupta, R., Rüdisüli, M., Patel, M.K., Parra, D., 2022. Smart USC-FlexStore deployment strategies informed by spatially explicit cost and value models. Appl. Energy 327, 120015. https://doi.org/10.1016/j.apenergy.2022.120015
Gutknecht, V., Snæbjörnsdóttir, S.Ó., Sigfússon, B., Aradóttir, E.S., Charles, L., 2018. Creating a carbon dioxide removal solution by combining rapid mineralization of CO2 with direct air capture. Energy Procedia 146, 129–134. https://doi.org/10.1016/j.egypro.2018.07.017
Hamilton, N., 2015. Functions Relating to the Smoothing of Numerical Data.
Holinger, 2012. Energieeffizienz und Energieproduktion auf ARA (Energy efficiency and energy production on ARA), Holinger AG im Auftrag des BAFU. Bundesamt für Umwelt BAFU (Federal Office for the Environment FOEN), Baden.
Infras, 2000. Emissionsfaktoren für stationäre Quellen (emission factors for stationary sources). Bundesamt für Umwelt BAFU (Federal Office for the Environment FOEN), Zürich.
Johnke, B., 2001. Emissions from Waste Incineration, in: Penman, J., Kruger, D., Galbally, I., Hiraishi, T., Nyenzy, B., Emmanul, S., Buendia, L., Hoppaus, R., Martinsen, T., Meijer, J., Miwa, K., Tanabe, K. (Eds.), Good Practice Guidance and Uncertainty Management in National Greenhouse Gas Inventories. Intergovernmental Panel on Climate Change (IPCC), Montreal, pp. 455–468.
KSDL, 2021. Schweizer Erdgasnetze | Koordinationsstelle Durchleitung [WWW Document]. 2021. URL https://www.ksdl-erdgas.ch/netzzugang/schweizer-erdgasnetze (accessed 10.16.21).
Lienhard, N., Mutschler, R., Leenders, L., Rüdisüli, M., 2023. Concurrent deficit and surplus situations in the future renewable Swiss and European electricity system. Energy Strateg. Rev. 46, 101036. https://doi.org/10.1016/j.esr.2022.101036
Meier, B., Ruoss, F., Friedl, M., 2017. Investigation of Carbon Flows in Switzerland with the Special Consideration of Carbon Dioxide as a Feedstock for Sustainable Energy Carriers. Energy Technol. 5, 864–876. https://doi.org/10.1002/ente.201600554
MeteoSchweiz, 2020. IDAweb - Data portal for teaching and research - MeteoSwiss [WWW Document]. URL https://www.meteoswiss.admin.ch/home/services-and-publications/beratung-und-service/datenportal-fuer-lehre-und-forschung.html (accessed 11.24.20).

Mutschler, R., Rüdisüli, M., Heer, P., Eggimann, S., 2021. Benchmarking cooling and heating energy demands considering climate change, population growth and cooling device uptake. Appl. Energy 288, 116636. https://doi.org/10.1016/j.apenergy.2021.116636
Pareschi, G., Küng, L., Georges, G., Boulouchos, K., 2020. Are travel surveys a good basis for EV models? Validation of simulated charging profiles against empirical data. Appl. Energy 275, 115318. https://doi.org/10.1016/j.apenergy.2020.115318
Peyer, T., Nijsen, R., Heller, T., Reuter, M., 2016. Kläranlagen - Ideal für Power-to-Gas. Aqua Gas 7/8, 42–46.
Piot, M., 2014. Bedeutung der Speicher-und Pumpspeicherkraftwerke für die Energiestrategie 2050 der Schweiz (Significance of storage and pumped storage power plants for Switzerland's 2050 energy strategy). Wasser Energ. Luft 4, 259–265.
Prognos, 2020. Energieperspektiven 2050+ (Kurzbericht). Bundesamt für Energie BFE (Swiss Federal Office of Energy SFOE), Bern.
Reinhardt, T., Richers, U., Suchomel, H., 2008. Hazardous waste incineration in context with carbon dioxide. Waste Manag. Res. 26, 88–95. https://doi.org/10.1177/0734242X07082339
Roost, M., Ménard, M., Lehmann, M., Ott, W., Sitzmann, B., 2018. WP-GAP: Performance Gap bei Mehrfamilienhäusern mit Wärmepumpe – die Rolle der Betreiber. Bundesamt für Energie BFE (Swiss Federal Office of Energy (SFOE), Bern.
Rüdisüli, M., Bach, C., Bauer, C., Beloin-Saint-Pierre, D., Elber, U., Georges, G., Limpach, R., Pareschi, G., Kannan, R., Teske, S.L., 2022a. Prospective life-cycle assessment of greenhouse gas emissions of electricity-based mobility options. Appl. Energy 306, 118065. https://doi.org/10.1016/j.apenergy.2021.118065
Rüdisüli, M., Romano, E., Eggimann, S., Patel, M.K., 2022b. Decarbonization strategies for Switzerland considering embedded greenhouse gas emissions in electricity imports. Energy Policy 162, 112794. https://doi.org/10.1016/j.enpol.2022.112794
Rüdisüli, M., Teske, S.L., Elber, U., 2019. Impacts of an Increased Substitution of Fossil Energy Carriers with Electricity-Based Technologies on the Swiss Electricity System. Energies 12, 2399. https://doi.org/10.3390/en12122399
Ruhnau, O., Bannik, S., Otten, S., Praktiknjo, A., Robinius, M., 2019. Direct or indirect electrification? A review of heat generation and road transport decarbonisation scenarios for Germany 2050. Energy 166, 989–999. https://doi.org/10.1016/j.energy.2018.10.114
Ruoss, F., 2014. Quellen erneuerbaren Kohlendioxids in der Schweiz. HSR (OST), Rapperswil.
Schweizer Zement, 2018. Berichterstattung cemsuisse.
Spoerri, A., Lang, D.J., Staeubli, B., Scholz, R.W., 2010. Technological change in Swiss thermal waste treatment: An expert-based socio-technical analysis. Waste Manag. 30, 1382–1394. https://doi.org/10.1016/j.wasman.2010.02.008
Staffell, I., Pfenninger, S., 2016. Using bias-corrected reanalysis to simulate current and future wind power output. Energy 114, 1224–1239. https://doi.org/10.1016/J.ENERGY.2016.08.068
StatCube, Statistische Datenbank von STATISTIK AUSTRIA, https://www.eea.europa.eu/data-and-maps/data/data-viewers/greenhouse-gases-viewer
Swissgrid, 2020. Aggregierte Energiedaten aus dem Regelblock Schweiz (Aggregated energy data from the Swiss control block) [WWW Document]. URL https://www.swissgrid.ch/de/home/customers/topics/energy-data-ch.html (accessed 11.24.20).

Swissgrid, 2018. Aggregated energy data of the control block Switzerland [WWW Document]. URL https://www.swissgrid.ch/de/home/operation/grid-data/generation.html
Swissmem, 2017. Energie- und CO2-Statistik.
Swissnuclear, 2020. Energieproduktion der Kernkraftwerke - swissnuclear [WWW Document]. URL https://www.swissnuclear.ch/de/energieproduktion-der-kernkraftwerke-_content---1--1014.html (accessed 11.24.20).
SWM, 2021. Lastprofil Wärmepumpe [WWW Document]. URL https://www.swm-infrastruktur.de/strom/netzzugang/bedingungen/waermepumpe (accessed 10.16.21).
Teske, S.L., Rüdisüli, M., Schildhauer, T.J., Bach, C., 2019. Potentialanalyse Power-to-Gas in der Schweiz (Potential analysis of power-to-gas in Switzerland). Empa, Dübendorf. https://doi.org/https://doi.org/10.5281/zenodo.2649817
VBSA, 2019. Kehricht-Verwertungs-Anlagen (KVA).
VBSA, 2016. Monitoring-Bericht zur CO2-Branchenvereinbarung für das Jahr 2015 (Monitoring report on the 2015 CO2 interbranch agreement). Bundesamt für Umwelt BAFU (Federal Office for the Environment FOEN) / Bundesamt für Energie BFE (Swiss Federal Office of Energy SFOE), Bern.
Umwelt Bundesamt, 2017, Energie- und Treibhausgas-Szenarien im Hinblick auf 2030 und 2050", Synthese Bericht, im Auftrag des BMLFUW https://www.umweltbundesamt.at/fileadmin/site/publikationen/rep0628.pdf
Viviroli, D., Zappa, M., Gurtz, J., Weingartner, R., 2009. An introduction to the hydrological modelling system PREVAH and its pre- and post-processing-tools. Environ. Model. Softw. 24, 1209–1222. https://doi.org/10.1016/j.envsoft.2009.04.001
Volkart, K., Bauer, C., Boulet, C., 2013. Life cycle assessment of carbon capture and storage in power generation and industry in Europe. Int. J. Greenh. Gas Control 16, 91–106. https://doi.org/10.1016/J.IJGGC.2013.03.003
Von Roon, S., Huber, M., 2010. Modeling Spot Market Pricing with the Residual Load. Enerday - 5th Conference on Energy Economics and Technology, 16.04.2010, Dresden, Munich.
VSG, 2020. Erdgas und Biogas in der Schweiz - Jahresstatistik des VSG. gaz energie.
Walch, A., Castello, R., Mohajeri, N., Scartezzini, J.-L., 2020. Big data mining for the estimation of hourly rooftop photovoltaic potential and its uncertainty. Appl. Energy 262, 114404. https://doi.org/10.1016/j.apenergy.2019.114404
Walch, A., Rüdisüli, M., Castello, R., Scartezzini, J.-L., 2021. Quantification of existing rooftop PV hourly generation capacity and validation against measurement data. J. Phys. Conf. Ser. 2042, 012011. https://doi.org/10.1088/1742-6596/2042/1/012011
Witte, J., Kunz, A., Biollaz, S.M.A., Schildhauer, T.J., 2018a. Direct catalytic methanation of biogas – Part II: Techno-economic process assessment and feasibility reflections. Energy Convers. Manag. 178, 26–43. https://doi.org/10.1016/J.ENCONMAN.2018.09.079
Witte, J., Settino, J., Biollaz, S.M.A., Schildhauer, T.J., 2018b. Direct catalytic methanation of biogas – Part I: New insights into biomethane production using rate-based modelling and detailed process analysis. Energy Convers. Manag. 171, 750–768. https://doi.org/10.1016/J.ENCONMAN.2018.05.056
Wurzbacher, J., 2017. Capturing CO2 from air, in: J., L., C., B. (Eds.), Internationaler Motorenkongress. Springer Vieweg, Wiesbaden, pp. 499–511. https://doi.org/10.1007/978-3-658-17109-4_32
Züttel, A., Remhof, A., Borgschulte, A., Friedrichs, O., 2010. Hydrogen: the future energy carrier. Philos. Trans. R. Soc. A Math. Phys. Eng. Sci. 368, 3329–3342. https://doi.org/10.1098/rsta.2010.0113

4.8 Contact Details

Company
Empa - Swiss Federal Laboratories for Materials Science and Technology
Überlandstrasse 129
CH – 8600 Dübendorf
+41 58 765 11 11
https://www.empa.ch/web/empa/contact-form
www.empa.ch

Authors:
Martin Rüdisüli
Robin Mutschler

5 Geological potential of the Swiss Molasse Basin

5.1 Introduction

An indispensable prerequisite for commercial application of geo-methanation in Switzerland is a demonstration that suitable geological formations are present in the subsurface. Switzerland has no known natural or artificially engineered gas storage reservoirs in geological formations at relevant depths for geo-methanation. Thus, there is no direct experience to draw on in evaluating the local geological suitability and volumetric potential for this technology. In view of this and of the constraints of the current research project, a literature study has been carried out to assess the theoretical suitability of the Swiss subsurface for geo-methanation. The following steps were followed in conducting this study:

(1) Define geological criteria required for successful geo-methanation based on properties of potential reservoir formations, their porewater and their likelihood of being capable of retaining injected gas at the selected site.

(2A) Compile relevant information (stratigraphy, lithologies, hydrogeology and structures) for geological units in the only promising geological region in Switzerland, the Swiss Molasse Basin.

(2B) Assess each unit based on the criteria defined in step 1. Rank units based on a combination of their apparent suitability for geo-methanation and the degree of certainty to which their key properties are known.

(2C) Using a publicly accessible 3D geological model of the Swiss Molasse Basin (*GeoMol*), delimit areas where the formations occur within the correct depth–temperature interval for geo-methanation, including the presence of potential gas trap structures. Produce maps showing the locations of suitable formations as a basis for planning of exploration campaigns.

(3) Outline future steps required to establish definitive feasibility of geo-methanation by testing promising traps for their gas injectivity and retentivity, including the expected duration and costs of an exploration campaign.

(4) Discuss potential conflicts of use between geo-methanation and other subsurface technologies in the SMB.

These steps were successfully carried out and the results are presented in this Chapter. Only a short summary of step 2 is included herein. The full compilation of geological data and its assessment as well as more detailed information on how the delimited maps shown in Chapter 5.4 were constructed, are given in the extended project report, which is available from the authors on request.

In addition to the topics in the steps outlined above, the present study also assessed the permitting process for deep drilling projects in Switzerland, and the perspective of exploration companies on public acceptance of such drilling projects. A brief summary of findings on the latter topic, which were obtained by a number of expert interviews with industry geologists, is given in Chapter 6.3.3. A separate, more detailed report, which will eventually be published as an independent report by the SFOE, is in progress. Once complete, it will be available via the SFOE *Artemis* platform.

5.2 Criteria for geological formations suitable for geo-methanation

5.2.1 Reservoir criteria

5.2.1.1. Geometry: Volume, thickness, and depth

The storage volume is a crucial parameter for successful geo-methanation in Switzerland as it defines how much gas can be stored in one site. In this report we refer to gas volumes in their expanded state at the Standard Pressure and Temperature used by the natural gas industry, namely 15.6 °C and 1 atmosphere (101.325 kPa), abbreviated herein as STP.

Regardless of the reservoir geology, considerations of economic viability set minimum requirements on potential storage volumes for the USC technology. Estimates of the hypothetical storage volume required for feasible implementation of geo-methanation at specific sites have been estimated in chapter 6.3.5, table 6-9. These estimates are based on the amount of locally produced excess electricity, on requirements for successful electrolysis to produce H_2, on the range of probable feed-gas ratios between CO_2, H_2 and CH_4, and on the ratio of "process gas" (the theoretical portion of gas that can be generated in the reservoir and produced by geo-methanation) to "cushion gas" (the portion of gas required to maintain pressure and preclude invasion of formation water in the reservoir).

As positive indicators we defined the range from the smallest hypothetical storage volume calculated (4.5 Mio. m^3_{STP}; Model A, MWIP Zuchwil) to the largest one calculated for a single site (400 Mio. m^3_{STP}, Case 2, RoR Verbois; table 6-9). Larger storage volumes are possible from a technical point of view, e.g., the large-scale natural gas storage site at Puchkirchen (Austria) operated by RAG contains around 860 Mio. m^3_{STP} of natural gas. However, larger volumes in the Swiss context would require transporting H_2 and CO_2 from distant locations to the storage site or running the electrolysis with electricity form the national grid, both of which would significantly increase costs.

Table 5-1: List of geological criteria for geo-methanation implementation, as used to guide the present study. Each of these criteria is described in detail in Chapter 5.2.

	Criteria	Positive indicators	Cautionary indicators
RESERVOIR	Storage vol.	4.5–400 Mio. m^3_{STP}	< 4.5 Mio. m^3_{STP}
	Thickness	> 5 m	< 3 m
	Depth	> 600 m and in desired T-range	< 600 m or outside desired T-range
	Temperature	35 to 70 °C	< 36 or > 70 °C
	Mineralogy	No chlorides	Presence of KCl, high amount of NaCl
	Porosity	> 20 vol.%	< 10 vol.%
	Permeability	50 to 3000 mD	< 50 or > 3000 mD
IN-SITU PORE WATER	pH	6 to 9	< 6 or > 9
	Salinity	30 to 150 g/L, > 3 g/L K^+	< 30 g/L or > 150 g/L, > 10 g/L K^+
RETENTION	Aquifer type	Porous rock matrix	Fracture or karst
	Caprock/seal	Present & tight; directly above reservoir	Fractured; other formations between reservoir and seal
	Trap struct.	Stratigraphic or anticlinal traps	Fault traps

When determining the aquifer volume, a crucial factor is the thickness of the formation. The experience by RAG suggests that, from a purely technical standpoint, the geo-methanation-technology can be implemented even if the reservoir is only 1 m thick (e.g., Speicher Lehen). While such a thin reservoir is sufficient for a test site, thicker units, preferentially > 5 m, are desired to achieve economically viable volumes of gas. In order to increase the area of contact between the injection wellbore and the formation, a section of the well can be drilled parallel to the lateral extent of the reservoir formation (e.g., horizontally), as is done routinely throughout the world in commercial gas fields. This was done at the large-scale natural gas storage site Puchkirchen, where the reservoir is only 14 m thick. Thus, each well has a nearly 1 km long horizontal section completed with pre-perforated liners to increase the area of contact and reduce the number of wells required for economic operation of the site.

Both porosity of the formation and the density of the gas mixture depend on the depth of the storage formation. As the injected gases are much more mobile than formation water, a minimum depth of 600 m below surface is defined to ensure that the gases can be retained adequately, provided that the reservoir is capped by a suitable sealing formation. This 600 m depth is based on empirical observations of successful gas storage projects, including the Puchkirchen site. The maximum depth value for geo-methanation is not defined by gas-retention considerations, but instead by the depth where the reservoir temperature exceeds that at which methanogens can flourish (see below).

5.2.1.2. Temperature and pressure

Temperatures generally increase with depth into the Earth. Therefore, the in-situ temperature of any given reservoir formation is closely linked to its depth. Temperature has a marked effect on the activity of microbes. Based on microbial experiments done as part of the investigations at the Lehen site, an optimal temperature window of 45 ± 15 °C was identified for methanogenesis. However, it is likely that successful microbial methanogenesis is also possible at temperatures up to 90 °C, as extremophile methanogens are known to exist in the subsurface. The understanding of these microbes and the conditions under which they thrive are currently poorly constrained. For the present initial appraisal of the potential of the SMB for geo-methanation we thus only considered the temperature interval 30 to 60 °C, for which ample experimental data is available from BOKU (Chapter 2.2).

Fluid pressure, whether of the injected gas or the existing formation fluid, also depends on the depth of the reservoir. However, no positive or cautionary indicators are listed in Table 5-2. This is because the quantitative and qualitative effects of pressure variations on microbes are still unknown. Long-term tests at the Lehen site conducted during 2021 suggest that a reduction in pressure inside the formation had an invigorating effect on the microbial consortium. At present it is unclear if the increase in microbial activity was directly caused by the pressure variations or by the movement of formation water into and out of the reservoir rock and wells in response to the pressure fluctuations. From a purely economic standpoint, drilling to greater depths is costly and high in-situ pressures require more energy for compression and injection of the gases.

5.2.1.3. Microbiology

The mineralogy of the reservoir primarily affects the composition of the formation water and is in turn affected by changes in water composition due to dissolution of the injected gases. The first aspect is of concern in reservoirs capped by or containing evaporite rocks. The sulphate minerals (e.g., anhydrite $CaSO_4$ and gypsum $CaSO_4 \cdot 2H_2O$) and halide minerals (e.g., halite NaCl, sylvite KCl) present in such evaporites have high aqueous solubilities and result in an in-situ porewater that is unfavourable to microbial activity. The second aspect is that injection of CO_2 typically acidifies the porewater with which it comes into contact. Any calcite or other carbonate minerals in the reservoir may therefore undergo slight degrees of dissolution, which may enhance permeability. As the amount of carbonate dissolution is small, it is unlikely to cause mechanical instabilities in the reservoir rock.

5.2.1.4. Porosity

Knowledge of the connected (gas-accessible) porosity of a formation is crucial to calculate its storage capacity. However, the value of the porosity provides little information on how easy it is to inject or extract fluids from the formation. Therefore, positive and cautionary indicators for permeability were defined as well. The experience of RAG shows that permeabilities of as little as 50 mD are sufficient for injection of gas into a reservoir. They also found that values of over 3000 mD were disadvantageous, especially in siliciclastic reservoirs, as the high injection/extraction rates led to mechanical erosion and disaggregation of the reservoir rock near the wellbore.

5.2.2 In-situ porewater criteria

While the reservoir is filled with gas in a geo-methanation scenario, there will always be a residual amount of original formation water present (termed the irreducible water saturation). This residual water is essential to the success of the geo-methanation technology, because all the microbial processes take place in this water film and thus its composition has a marked effect on microbial activity. A key factor is the pH of the water. Microbes are relatively sensitive to acidic or alkaline pH and only thrive under more or less neutral conditions (pH = 6 to 9). They are also sensitive to certain ions in solution. Investigations at Lehen showed that microbial activity stopped once the well was flushed with a KCl solution such that a concentration of potassium of 10 g/L was reached. Apparently, the inhibiting effect is due to the high concentration of the potassium ion itself, rather than to the increase in salinity, as potassium renders membrane transport into the microbe cells less effective. The toxicity of potassium for certain methanogens was investigated by Chen and Cheng (2007). They found that at concentrations > 3 g/L potassium, the efficiency of methanogenesis significantly decreased.

Besides the potassium concentration, overall salinity has an effect on microbial activity as well. Previous studies have reported an upper limit of 150 g/L for bio-methanation (Strobel et al., 2020). The cautionary limit of < 30 /L was chosen as this concentration is the limit between a brackish and a saline groundwater. Saline groundwaters are otherwise preferred for geo-methanation as they have no potentially conflicting uses as drinking or process water.

5.2.3 Permeability and retention criteria

The gas mixture that forms during geo-methanation operations (consisting of H_2, CO_2 and CH_4) is extremely buoyant and has low viscosity. These properties render the gas highly mobile in the subsurface. However, successful geo-methanation requires the gas mixture to remain at or close to the injection well in order to facilitate maximum extraction of the newly formed methane. The reservoir thus needs to consist of a porous rock matrix for gas storage, rather than a network of fractures and/or karst features. While the latter often show the desired high permeabilities, they are highly heterogeneous and show a large contrast in transport properties between the rock matrix and the fractures. Gas injected into such an aquifer will be transported nearly exclusively along the fractures, resulting in a highly erratic shape of the storage plume. This causes issues in retention and recovery of the product methane.

To ensure storage periods of several months and to trap the cushion gas over decades, the reservoir requires a caprock. This acts as a seal to prevent advective escape of the gases towards the surface. Such a caprock must not only be mechanically intact (i.e., unfractured) but also impermeable to gases (CO_2, CH_4 and H_2). It also needs to be directly above/surrounding the reservoir in question in order to ensure that the injected gases and produced methane remain at or near the injection site. For relatively flat lying or continuously dipping formations, hydrodynamic trap structures are needed to prevent the gases from migrating laterally away from the injection and production wells as this can occur even under small hydraulic gradients and in only slightly inclined strata. Stratigraphic and anticlinal traps (Figure 5-1) are preferred. Fault traps are also suitable if the faults are impermeable (e.g., due to clay fillings) and the offset places the reservoir formation against a sealing rock formation (Figure 5-1). However, many faults are highly permeable (e.g., little to no fillings). Even if the presence of a fault can be deduced, e.g., from seismic surveys, its permeability can normally only be determined by hydraulic testing from nearby wells.

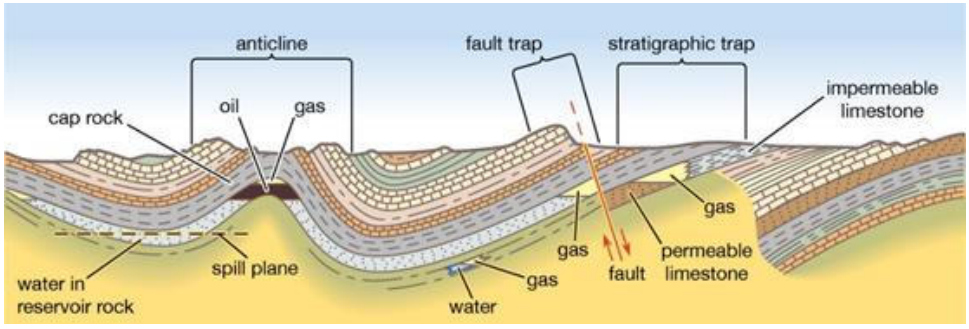

Figure 5-1: Types of gas traps. For geo-methanation, anticlinal or stratigraphic traps are preferred (Encyclopædia Britannica® Online).

5.3 Geological background

5.3.1 Geology of the Swiss Molasse Basin (SMB)

The oldest rocks in Switzerland belong to the crystalline basement. Within the basement, small pull-apart basins filled with Late Palaeozoic sediments (304 to 252 Ma old) can be found. Together, they are covered by sediments deposited during the Mesozoic era (Triassic to Cretaceous periods). In the Triassic (252 to 201 Ma ago), sandstones, dolomites and evaporites were deposited under fluviatile to shallow marine and sabkha-type conditions. During the Jurassic (201 to 145 Ma ago) and Cretaceous (145 to 65 Ma ago), the area we know as Switzerland today was covered by a sea with water depth (and thus depositional conditions) changing over time. The resulting deposits are therefore a relatively heterogeneous succession of carbonates, shales and claystones and are often laterally variable due to syn-sedimentary tectonic activity. Overall, the thickness of the Mesozoic sediments ranges from 200 to 1000 m (Figure 5-2).

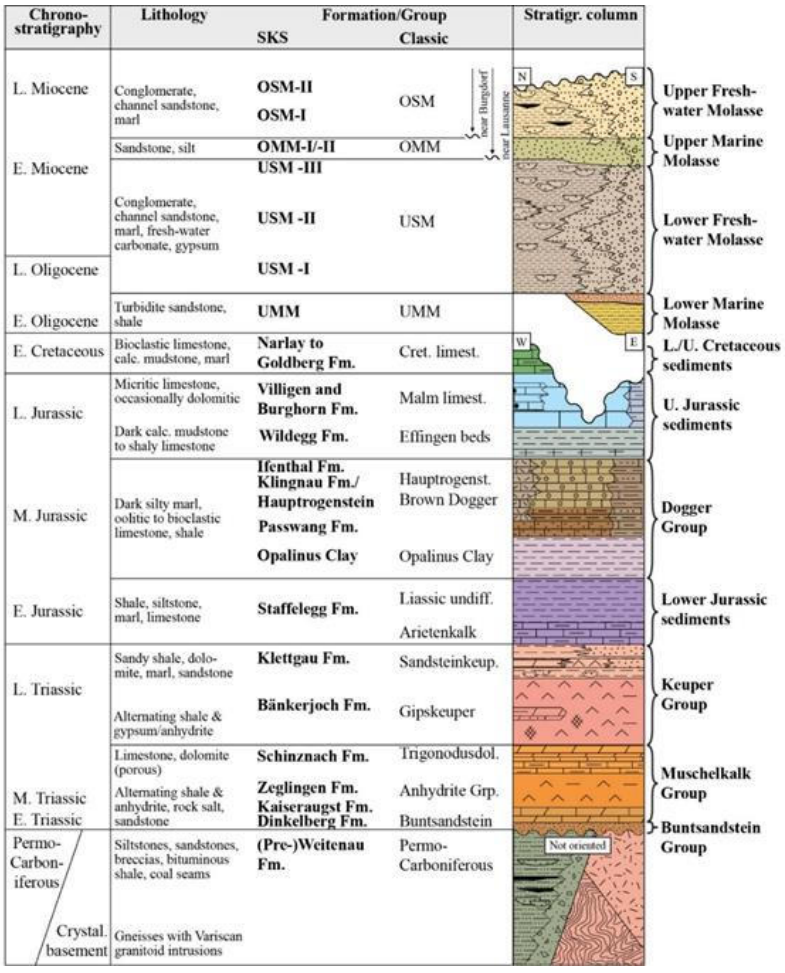

Figure 5-2: Simplified lithostratigraphy of the SMB. Formation names and colours are given according to the recommendations of the Swiss Committee for Stratigraphy (SKS; names in bold type). Names used in older literature are listed in column labelled "Classic". Both nomenclatures are heavily based on the formations occurring in northern Switzerland (Jordan & Deplazes, 2019) and might not be representative across the entire SMB.

Sedimentation was largely interrupted when the Alpine orogeny started during the Upper Cretaceous (ca. 40 Ma ago). The continental collision led to an overall uplift of the area and the erosion of the Lower Cretaceous and/or Upper Jurassic sediments. The weight of the growing mountain chain bent the European plate downwards, creating the North Alpine Foreland Basin (NAFB) along the northern edge of the Alps between Savoy (France) in the west and Linz (Austria) in the east. To the north, a gentle bulge where the Jura Mountains would start forming at a later stage developed. The part of the NAFB located within modern day Switzerland is the Swiss Molasse Basin (SMB; Figure 5-3), which underlies the relatively flat midlands (also known as the Swiss Plateau) between the Alps and the Jura Mountains. The SMB is roughly 300 km long from west to east. In the Geneva area, it is only 30 km wide (Geneva Basin). Towards the east, the width increases and in the area of Lake Constance, the SMB is about 80 km wide.

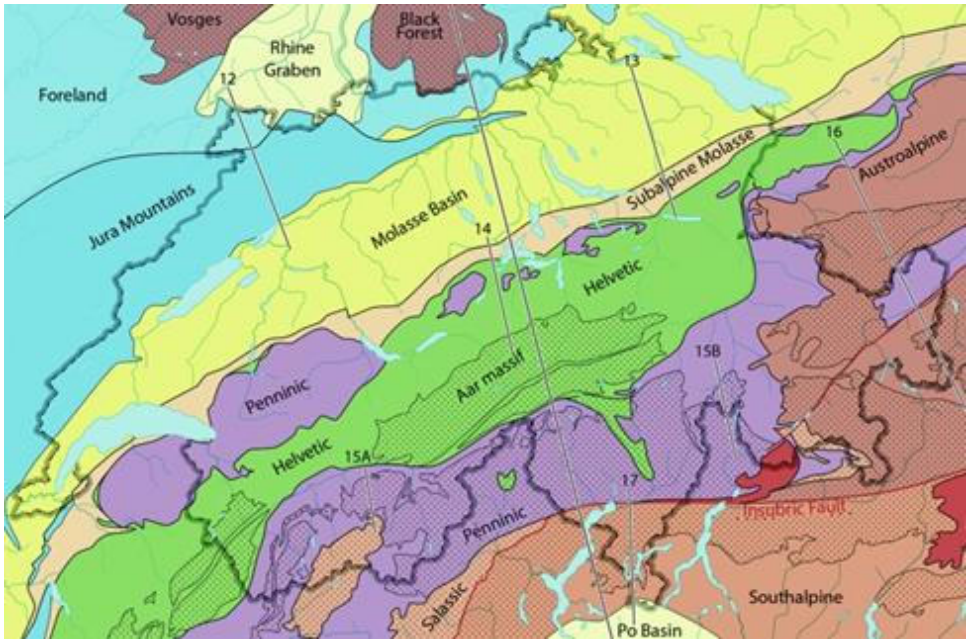

Figure 5-3: Tectonic map of Switzerland and the surrounding areas (modified after Pfiffner, 2021) showing the Jura Mountains (light blue), Swiss Molasse Basin (SMB; yellow) including the Subalpine Molasse (light orange) along the Alpine front and the different zones of the Alps in purple, green and shades of red. Only the area of the SMB will be assessed for its suitability for geo-methanation in this study.

In this basin, clastic sediments (primarily sandstones, mudstones and conglomerates) were deposited in two megacycles, each recording the transition from a transgressive (marine) to a regressive stage (terrestrial, freshwater). The overall thickness ranges from a few hundred meters in the NE of Switzerland to around 5500 m in the SE. The Molasse deposits at the southern margin of the SMB (approx. 5–20 km from the Alpine front) are folded and thrusted and are referred to as the Subalpine Molasse. The more distal Molasse sediments are flat-lying and denoted as the Plateau Molasse (Kuhlemann & Kempf, 2002). They have seen relatively little deformation.

Underneath these Molasse deposits, the Mesozoic strata are present, dipping towards the SW at around 3-4° (Figure 5-4). They were compacted during burial but remained relatively unaffected by deformation or metamorphic overprint. Only along the southern edge of the Jura Mountains they are folded and faulted (Subjurassic Zone), and there are important corridors of major and locally active strike-slip faults (e.g., near Fribourg) that cross the basin in N–S trends and often crosscut the Tertiary and some or all

of the Mesozoic sediments. However, between these deformed zones, large volumes of the sedimentary rocks appear to be intact and hence potentially of interest for gas storage.

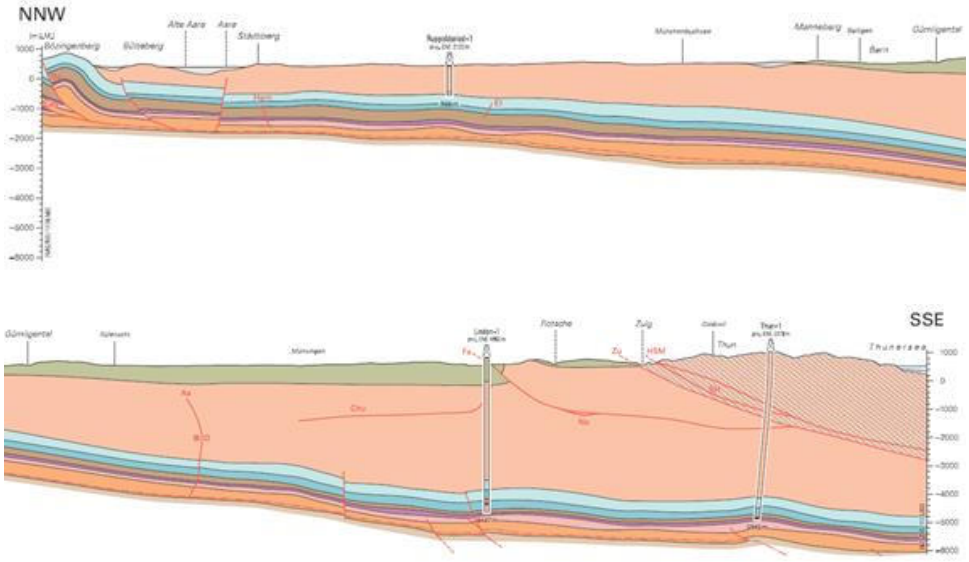

Figure 5-4: Cross-section from the southern margin of the Jura Mountains (NNW; Bözingerberg) to the Alpine front (SSE, Lake Thun), across the entire SMB along the Biel/Bienne-Bern-Thun line. The Mesozoic strata are shown in orange/pink (Triassic), purple (Lower Jurassic), brown (Middle Jurassic) and blue (Upper Jurassic). They are folded and faulted in the Jura Mountains but relatively undisturbed across the SMB. Above the Mesozoic strata are the Lower Freshwater Molasse (peach color) and the Upper Marine Molasse (olive green color). Both increase in thickness from north to south towards the Alpine front. The Molasse sediments are faulted in the subjurassic and subalpine zones.

The situation is very different for the Mesozoic sediments making up the Jura Mountains (Figure 5-3 and 5-4). From 10 to 3 Ma, the main stage of the Folded Jura Mountain formation was taking place. During this time, the Upper Triassic to Jurassic/Cretaceous sediments were sheared off the older underlying rocks along the ductile evaporitic deposits of Middle to Upper Triassic age (= décollement horizons) and bent into large-scale folds. This led to the formations becoming dissected by faults and fracture networks. These structures cut across formation boundaries, and hence reduce the volumes and retentivity of any potential reservoirs for gas storage. We therefore excluded the Jura Mountains in this first appraisal for the geological potential of the Swiss subsurface for geo-methanation.

The rocks making up the Alps today (Figure 5-3) have seen even more substantial deformation. In addition, many of the formations have been buried to great depths during the Alpine orogeny and their texture and mineralogy has been modified by metamorphism. This resulted in rocks with very low matrix porosities and permeabilities and abundant faulting and fracturing. Some of these fracture networks are known to permit water flow over many kilometers and even to ~10 km depth (Diamond et al., 2018). The rocks of the Alpine domain are thus unsuitable for the injection, extraction or storage of fluids, and are excluded from further discussion.

In view of these regional-scale geological features, our study focuses exclusively on the SMB. This region represents a large potential target area, and it underlies the most intensely populated and

industrialized area of Switzerland, a coincidence that favors commercial implementation of geo-methanation schemes.

5.3.2 Knowledge of the subsurface in the SMB

Exploration for oil and gas has been underway at fluctuating levels of activity since 1912. Between the mid-1950s and 2010, some 32 deep (> 500 m) exploration wells were drilled and more than 8'500 km of seismic lines were shot across the SMB (Figure 5-5; Lahusen, 1992; Leu, 2012). However, only a small gas field (74 Mio. m^3) was found and exploited in Entlebuch (Vollmayr and Wendt, 1987). Many unproductive wells nevertheless showed hydrocarbon shows at different geological levels, e.g., oil shows in the Staffelegg and Klettgau Formations (primarily in central and eastern Switzerland) and gas shows in the USM, throughout the Jurassic strata and in the Muschelkalk Group (Leu, 2012). These shows are of great interest as they identify formations potentially acting as reservoirs. The lack of commercial production means that the acquired well data are the main asset of the investors, and so access to the majority of the data is still restricted. Some of the available subsurface data from petroleum exploration, primarily thickness, porosity and permeability values, have been compiled as part of a first appraisal of the SMB for CO_2 sequestration in deep saline aquifers (Chevalier et al., 2010).

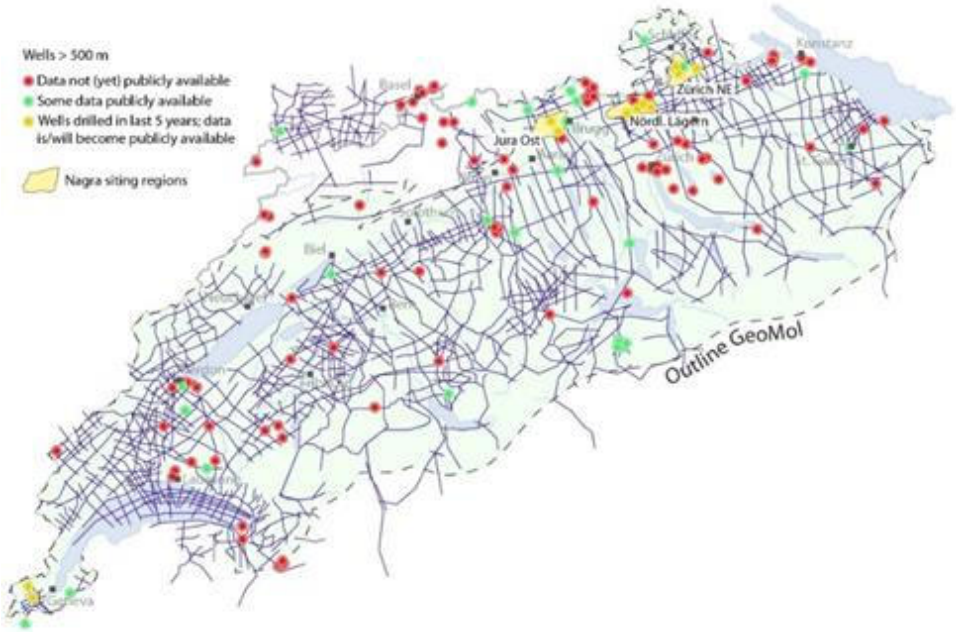

Figure 5-5: Map of all the seismic lines shot and wells drilled to > 500 m depth before 2017 within the Swiss Molasse Basin and the adjacent Jura Mountains. Wells drilled since 2017 are marked in yellow. Red well markers indicate that the data obtained are not publicly available, while green markers indicate wells where at least some data are publicly available via the federal geoportal (map.geo.admin.ch).

Besides oil and gas exploration, the subsurface of the SMB has primarily been investigated as part of the search for a deep geological repository for radioactive waste by the National Cooperative for the Disposal of Radioactive Waste (Nagra). The first extensive exploration program was conducted in the 1980s and consisted of extensive seismics and 6 deep wells in Northern Switzerland (eastern end of the Tabular Jura to the Zürich Unterland). The exploration was later extended east into Canton Schaffhausen and Zürcher Weinland with more seismics and an additional deep well as the focus shifted from the crystalline basement as a potential host formation to the Opalinus Clay. In the last few years,

Nagra has conducted extensive exploration in and around the three siting regions (from east to west): Zürich Nordost, Nördlich Lägern and Jura Ost (yellow in Figure 5-5). This included 2D and 3D seismic surveys and the drilling of eight new deep wells (TBO wells) in 2020/21. For each well, the entire Mesozoic section was cored and data on mineralogy, structures and hydrogeology were collected. Where the data was available at the time the present study was compiled, it was included. In addition to the data collected from deep wells, Nagra also compiled detailed information from shallower wells, tunnels as well as outcrops in the Tabular and easternmost Folded Jura. Together this leads to a detailed understanding of the different lithologies, their lateral and vertical distribution as well as their mineralogical and chemical composition and petrophysical properties in Northern Switzerland. The most up to date compilation of this information is given in Jordan & Deplazes (2019).

In the last decade, the subsurface has also received renewed attention in relation to the transition from fossil to renewable and green energies (e.g., geothermal, thermal energy and gas storage, CCS). Several new deep wells have been drilled for a range of projects (mostly geothermal). The most extensive geothermal exploration campaign is ongoing in the Canton of Geneva. This exploration campaign focuses on the suitability of the entire geology of the Geneva Basin (Quaternary to Palaeozoic deposits) for the production of geothermal energy and/or seasonal storage of thermal energy. The exploration campaign involved 2D as well as extensive 3D seismics (results expected 2023/24), the drilling of two new deep wells (2018 and 2019) with additional, deeper wells currently being planned (2024/2025). The results from the exploration campaign will become publicly available in the near future as they are funded by the Federal Office of Energy. However, the time and format of publication, is currently unknown.

Based on all of these exploration campaigns and projects, Chevalier et al. (2010) defined three classes of exploration maturity within the SMB (Figure 5-6): Largely unexplored areas (red) with very little information available, areas with moderate density of well and seismic data (yellow) and the best explored areas with comparatively abundant information in the NE of the SMB, the central part between Fribourg and Olten, and the Lausanne–Yverdon area. The currently ongoing exploration campaigns are shown in grey (Figure 5-6). In the well explored areas, the geology (i.e., which lithologies are present and the depth intervals they occur at are well constrained due to seismics. In addition, these areas contain most of the wells drilled for exploration (petroleum, nuclear waste disposal and geothermal) and where data is, at least partially, publicly available. These areas are thus the most favorable regions for future projects as the higher degree of understanding of the subsurface reduces the exploration risk.

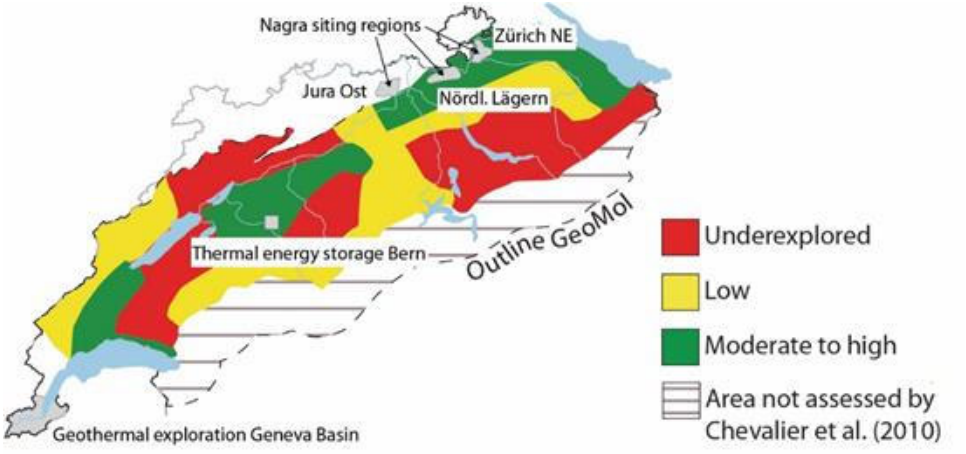

Figure 5-6: Exploration maturity of the Swiss Molasse Basin with the ongoing exploration campaigns indicated in grey (modified after Chevalier et al., 2010).

5.3.3 Geological Model of the SMB (GeoMol)

Despite the incomplete exploration of the SMB, a 3D geological model has been developed over the last 10+ years (Allenbach et al., 2017). The model contains 12 stratigraphic horizons (Table 5-2), covering the entire lithostratigraphy shown in Figure 5-2. The area of the SMB within which GeoMol is defined, is shown in Figure 5-7 (orange line). For the purpose of the present USC-FlexStore project we refer to this as “outer geological perimeter”, e.g., where geological information is available in 3D.

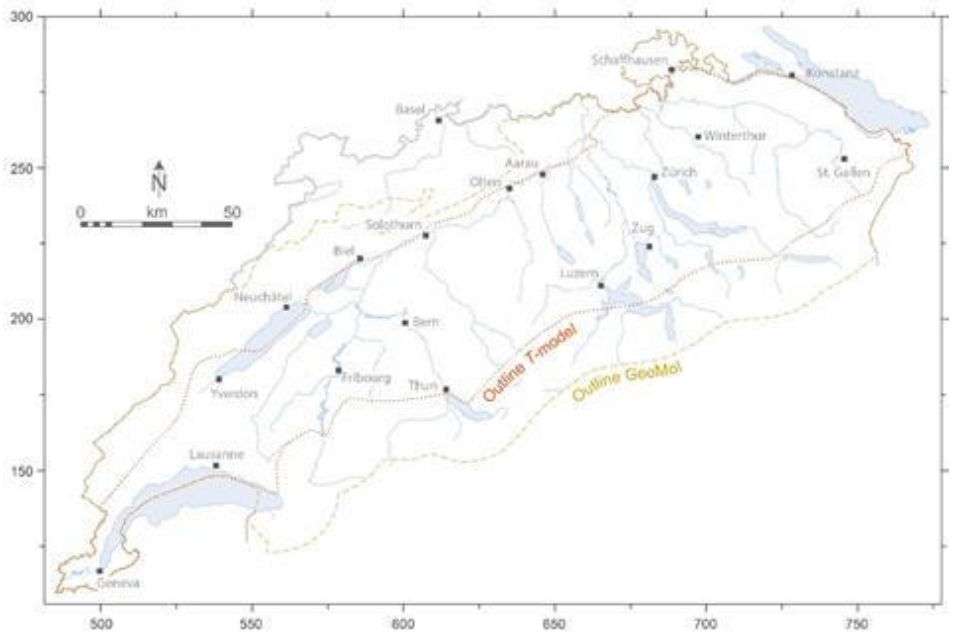

Figure 5-7: Areas in which the 3D geological model GeoMol (“outer geological perimeter”; in yellow) and the temperature model (“inner geological perimeter”; in red) are defined.

Due to the uncertainties of the underlying data and the large distances over which data has to be interpolated, GeoMol does not represent an accurate depiction of the geology of the SMB. For example, most of the geological horizons included in GeoMol consist of more than one formation and often formations with good (= aquifer) and bad reservoir properties (= seals) are contained within a single horizon (Table 5-2). In addition, in some horizons lateral transitions between formations exist (e.g., Hauptrogenstein to Brown Dogger within the Dogger horizon). These are also not considered in GeoMol. In order to subdivide these horizons and determine the distribution of individual formations of interest, additional studies were taken into considerations (see Chapter 5.3 for details).

GeoMol also contains a valuable temperature model which represents the interpolation of temperature measurements based on purely conductive heat transport. The data are available as a 3D model as well as various 2D horizons. Among the latter are several isotherms, two of which were used in this study (Chapter 5.3.4). The area within which the temperature model is defined is shown in Figure 5-7 (red perimeter). For the USC-FlexStore project we refer to this as the “inner geological perimeter”. It is equal to the area in which the occurrence of potential aquifer formations in the correct depth-temperature interval for geo-methanation was delimited (Chapter 5.3.4)

Besides the different geological horizons and the temperature model, GeoMol also includes around 500 faults (normal, reverse and strike-slip). Many of the faults included are relatively small-scale (a few km) and only represented by a single plane. However, other fault zones extend over 20 to 30 km and consist of a complex geometry including different branches (e.g., flower structures) and were simplified for modelling purposes. No synclines/anticlines are included in GeoMol as of yet. However, some structures are included in the maps of the final report of the GeoMol project (Allenbach et al., 2017).

Unfortunately, GeoMol does not contain any information on the properties of the geological formations such as mineralogy or porosity and permeability. This information is only available from analysis of samples from or close to the surface and samples/measurements from deep wells. The data are often highly variable, and so far, nobody has attempted to interpolate the properties between different boreholes and include them in the model. For this study, we primarily relied on the compilation done by Chevalier et al. (2010).

5.3.4 Delimitation of geological units based in criteria for successful geo-methanation

Each potential sealed aquifer evaluated in Table 5-2 corresponds to a 3D rock body in the subsurface. A primary aim of this study is to delimit the geographical extent of these bodies and quantitatively estimate their depths and thicknesses. The locations of any major faults that transect the bodies must also be identified. Fold axis traces shown by Allenbach et al. (2017) were assumed to be relevant for all formations above the Triassic décollement horizons. Digital delimitation of the target bodies was carried out on a copy of the GeoMol 3D dataset, made available by Swisstopo.

Table 5-2: Stratigraphic units and corresponding layers between horizons modelled in GeoMol. As the layers generally represent entire stratigraphic groups comprising several formations, they often contain one or several aquifers and seals in the same unit.

Stratigraphic unit	Layer	Top horizon	Bottom horizon	Geological formations contained in layer (aquifer/aquitard/neither)
Upper Freshwater Mol.	OSM	TFels	TOMM	OSM (sandstones, conglomerates, mudstones)
Upper Marine Mol.	OMM	TOMM/TFels	TUSM	OMM
Lower Freshwater Mol.	USM	TUSM/TFels	BKän	USM (sandstones, conglomerates, mudstones)
E./L. Cretaceous sedim.	Kreide	BKän	TUMa	Goldberg to Narlay Fm
U. Jurassic sediments	Ob. Malm	TUMa/BKän	TLMa	10+ formations, among them the Etiollets Fm
	Unt. Malm	TLMa	TDo	Wildegg Fm., Bärschwil Fm.
M. Jurassic Dogger Group	Dogger	TDo	TLi	10+ formations, among them the Ifenthal Fm., Hauptrogenstein and Klingnau Fm.

Stratigraphic unit	Layer	Top horizon	Bottom horizon	Geological formations contained in layer (aquifer/aquitard/neither)
L. Jurassic deposits	Lias	TLi	TKeu	Staffelegg Fm. (Beggingen Mb. and 10 others)
U. Triassic Keuper Grp	Keuper	TKeu	TMus	Klettgau Fm. (Ergolz/Gansingen/Berlingen/Seebi /Gruhalden/Belchen Mb.), Bänkerjoch Fm.
M. Triassic Muschelkalk Grp	Muschel-kalk	TMus	BMes	Schinznach Fm. (Stamberg Mb. and 4 others), Zeglingen Fm., Kaiseraugst Fm.
L. to M.Triassic Buntsandstein Grp	Combined with Muschelkalk			Dinkelberg Fm.
Permo-Carboniferous sediments	Permokarb.trog	BMes	BPK	Weitenau Fm., Pre-Weitenau Fm. (sandstones, conglomerates, mudstones)
Crystalline basement		B/Mes/BPK	n/a	No formations differentiated

[1]Where overlying Molasse units have been eroded.

[2]Where Lower Cretaceous limestones have been eroded in the eastern SMB.

A digital model of the rock body representing each of the horizons was extracted from GeoMol based on the following criteria: (a) must lie deeper than 600 m below the surface and (b) lie between the 30 °C and 60 °C isotherms (Figure 5-8, light brown polygons). A tailored workflow was developed for this study using a query tool in MoveTM software (Petex, v.2019.1). Steps in this process are shown in (Figure 5-8). The resulting delimited bodies and any cross-cutting faults in GeoMol were exported as ZMAP files with a 200 m grid resolution, then imported into a geographic information system software package (ESRI's ArcGis, v.10.8) for further mathematical manipulations. The distances between the upper and lower bounding surfaces of each body were calculated with the 3D Analyst tool 'Raster math' (Figure 5-8d), permitting integration of the enclosed rock volume, and yielding vertical thickness maps of each body at 200 m spatial resolution. The map views for each horizon from GeoMol represent the starting point to further constrain the areas of interest to geo-methanation. As shown in Table 5-2, GeoMol only contains the main geological units of the SMB and not each formation/member. Therefore, the maps obtained do not show the true extent of the aquifer but a larger area, often including the seal and/or a second or even third aquifer. To display only the formations of interest, the maps were delimited further based on published data on thickness and/or lateral transitions between formations and/or members.

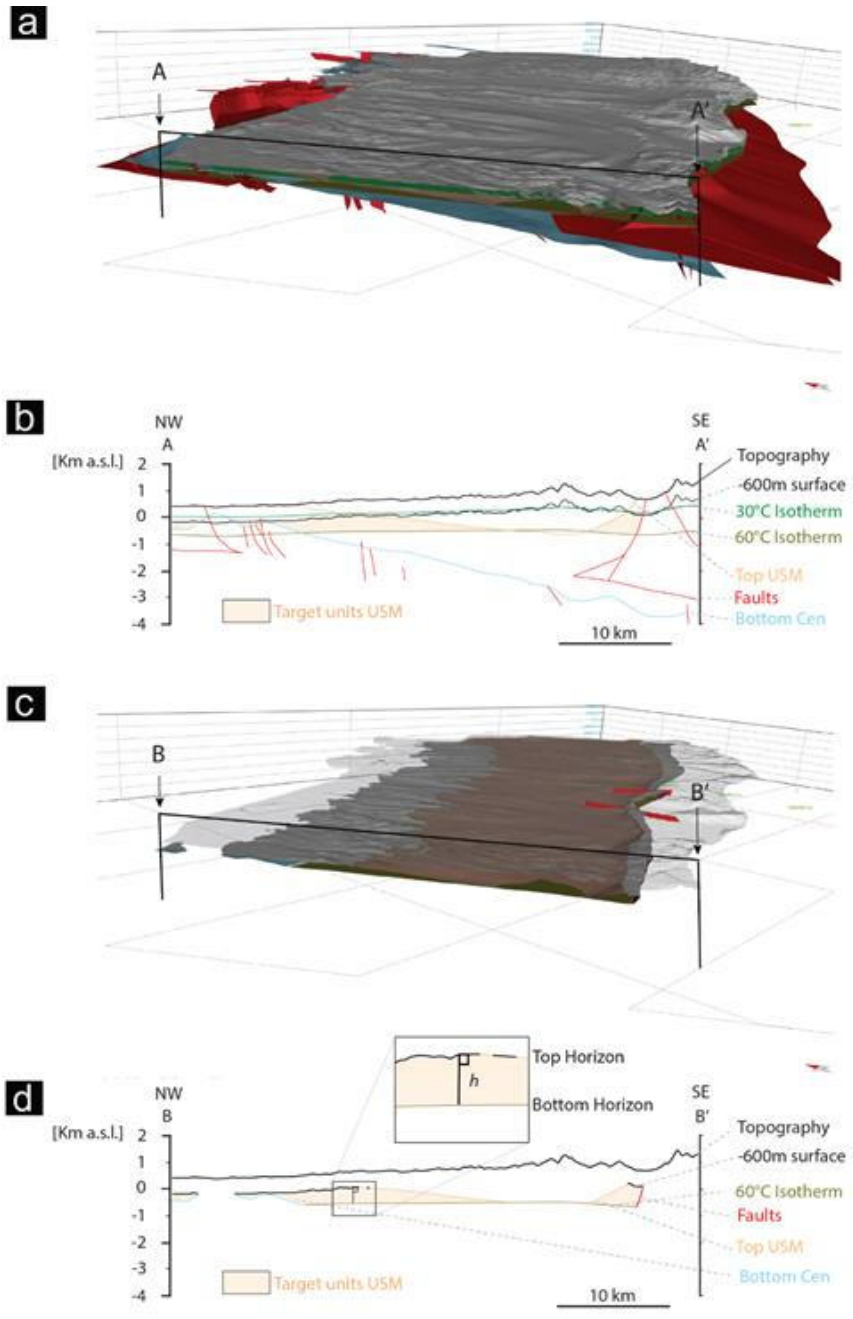

Figure 5-8: (a) 3D view towards the West showing the land-surface topography in grey (DEM) and the underlying modelled geological units of the Molasse basin. The surfaces dividing geological units have been clipped along the trace of the A–A' cross-section, visible in the front of the diagram. (b) A–A' cross-section view of the horizons. Highlighted by the light brown polygon is the target area that satisfies the required conditions of depth >600 m and 30 °C ≤ T ≤ 60 °C. (c) 3D clipped view towards the West showing the modelled surfaces of the target bodies, including subvertical fault planes (red). The position of cross-section B–B' is visible in the front of the diagram. (d) B–B' cross-section view of the target horizons forming a Top Horizon and a Bottom Horizon of the target area; h represents the vertical distance between the two horizons.

5.4 Characterization and ranking of potential target formations

In 2010, Chevalier et al. compiled data on all geological units in the Swiss Molasse Basin and assessed their suitability as a reservoir or seal for CO_2 sequestration in the depth interval between 800 and 2500 m. In the stratigraphic column (Figure 5-9), units are colored according to their reservoir properties: Aquifers are blue, indicating that porosity and permeability are sufficient to allow for the injection/extraction of a fluid. Seals are orange and are characterized by petrophysical properties which do not allow for any substantial movement of fluid. Units in white show properties between an aquifer and a seal and are not considered further. For this study, we have re-assessed all aquifer formations identified by Chevalier et al. based on the criteria for geo-methanation described in Chapter 5.2.:

Rank 1 – Potentially suitable lithology for geo-methanation with trap structures locally present/likely.

Rank 2 – Potentially suitable lithology for geo-methanation but poorly constrained, limited distribution or uncertain regarding gas retention properties (seal/traps).

Rank 3 – Potentially suitable lithology for geo-methanation but very poorly constrained and not very abundant, implying a high exploration risk.

Rank 4 – Unsuitable for geo-methanation due to fractured/karstified nature.

Formations assigned rank 4 are the fracture- and/or karst-hosted reservoirs of the pre-Triassic crystalline basement as well as the massive limestones of Upper Jurassic (“Malm”; excluding the Etiollets Formation in the Geneva Basin, Chapter 5.3.7) and Lower Cretaceous age (Table 5-3). These formations will not be discussed further in this study. The remaining formations are all porous reservoirs hosted by clastic sediments (primarily sandstones) or various carbonates.

For formations of rank 1 to 3, we delimit geographical areas within the SMB where (1) the formations occur in the critical target temperature–depth interval for geo-methanation and (2) where the members or sub-units showing aquifer properties are most likely present and sealed. This is based on the geological and temperature model in GeoMol and information from literature characterizing individual formations in detail. More detail is available in the full report for work package 4 which is available upon request from the authors.

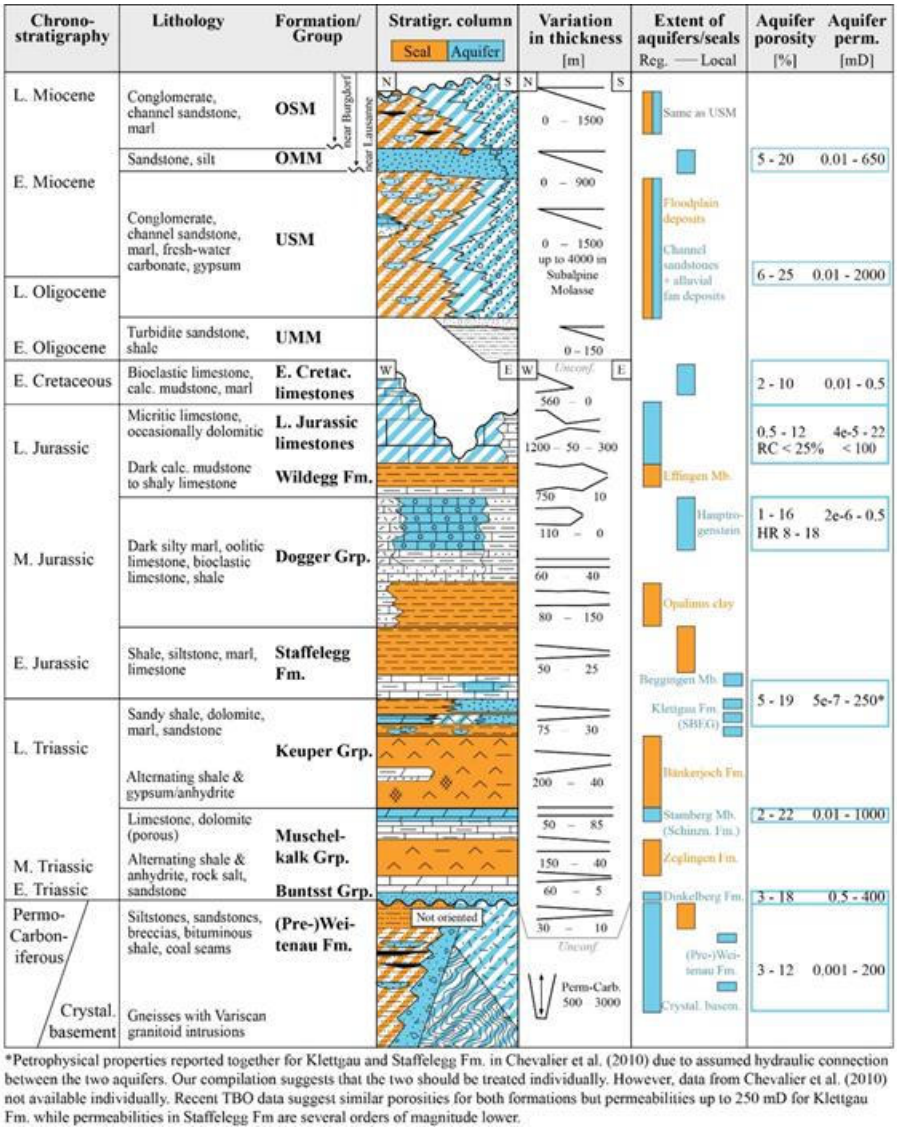

*Petrophysical properties reported together for Klettgau and Staffelegg Fm. in Chevalier et al. (2010) due to assumed hydraulic connection between the two aquifers. Our compilation suggests that the two should be treated individually. However, data from Chevalier et al. (2010) not available individually. Recent TBO data suggest similar porosities for both formations but permeabilities up to 250 mD for Klettgau Fm. while permeabilities in Staffelegg Fm are several orders of magnitude lower.

Figure 5-9: Stratigraphic column of the Swiss Molasse Basin (SMB) modified after Chevalier et al. (2010). The first four columns show the age, encountered lithologies and their basin-wide distribution and stratigraphic names based on the valid definition and nomenclature of the Swiss Committee for Stratigraphy (SKS). Column 5 shows the basin-wide variations in thickness. Column 6 identifies regional- to local-scale aquifers (blue) and impermeable seals (= caprocks; orange). Ranges of aquifer porosities and permeabilities measured are shown in column 7 and 8.

5.4.1 Pre-Weitenau Formation

Several SW–NE trending Permo-Carboniferous troughs have been postulated across the SMB (McCann et al., 2006). So far only one of these troughs, the North Swiss Permo-Carboniferous Basin (NSPB), has been confirmed by drilling. The NSPB is filled by up to 3000 m of Carboniferous fluviatile deposits (Pre-Weitenau Formation), followed by 150 to 300 m of Permian alluvial fan deposits and fine-grained playa sediments (Weitenau Formation). Unfortunately, very little petrophysical data are available for the Palaeozoic sediments and therefore it is difficult to assess the reservoir properties of the lithologies in question. However, the depositional environment of the Pre-Weitenau channel sandstones is similar to that of the sandstones of the Klettgau Formation (Chapter 5.3.4), USM (Chapter 5.3.8) and OSM (5.3.10). All of these channel sandstones are surrounded by relatively impermeable floodplain deposits and represent composite, at least partially internally sealed reservoirs.

Although these small-scale reservoirs can be assumed to be present, the Pre-Weitenau Formation is assigned rank 3 due to the poor knowledge of their extent and specific properties. The Carboniferous fluviatile sequence occurs within the target depth–temperature interval for geo-methanation along the northern edge of the SMB, from Brugg and across the Zürich Unterland. The deposits lie at depths of 1150 to nearly 1400 m below surface and are up to 400 m thick (Figure 5-10).

Gases injected into the Pre-Weitenau Formation are likely to be retained by stratigraphic trapping within channel sandstones embedded in impermeable floodplain deposits. Several faults cut across the delimited area but their permeabilities, and hence their influence on gas retention, are unknown. No anticlines are present in the Pre-Weitenau Formation as it is located beneath the décollement horizon of the Jura Mountains (Sommaruga et al., 2017).

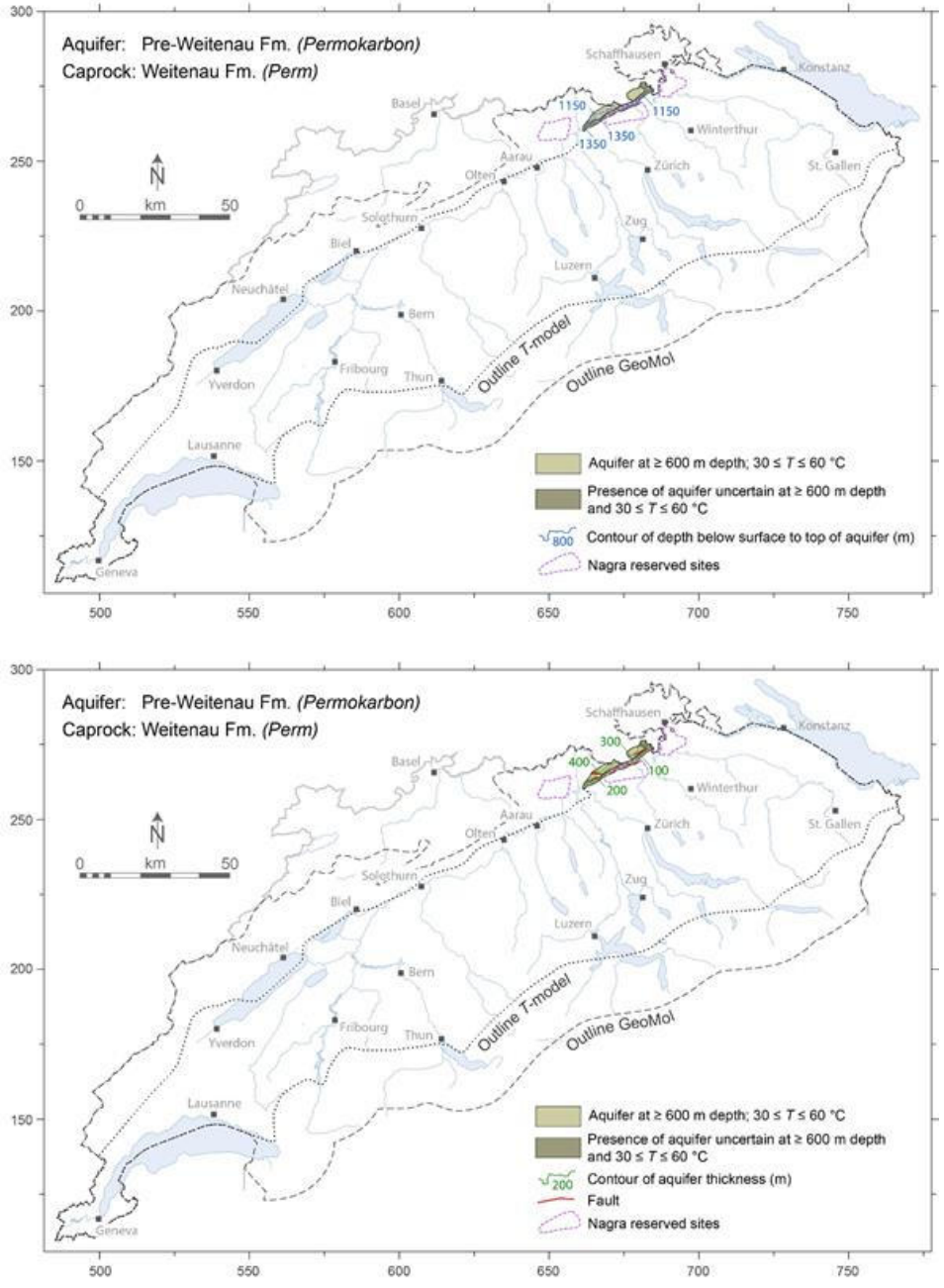

Figure 5-10: Delimited Pre-Weitenau Formation. Top map: depth below surface to top of aquifer. Bottom map: vertical thickness of the formation and locations of known faults. The three Nagra siting regions are assumed to be off limits for geo-methanation projects.

5.4.2 Dinkelberg Formation

The Dinkelberg Formation consists of a quartz-rich sandstone with variable degrees of cementation by quartz and clay minerals. This results in variable porosities between 3 and 18 vol.% with an average around 10 vol.%, while permeabilities vary from 0.5 to 400 mD with an average of around 200 mD. Thus, the Dinkelberg Formation represents a good porous-matrix aquifer of regional extent (Chevalier et al., 2010; Jordan, 2016). Overall, the Dinkelberg Formation is assigned to rank 1 with respect to its potential suitability for geo-methanation due to its regional extent and thickness, comparatively low degree of internal heterogeneity and suitable petrophysical properties. It occurs in the target depth–temperature interval for geo-methanation along the northern edge of the SMB, primarily across the regions of Zürich Unterland and Zürich Weinland. The deposits lie at depths of 800 to 1400 m below surface and they are up to 30 m thick (Figure 5-11):

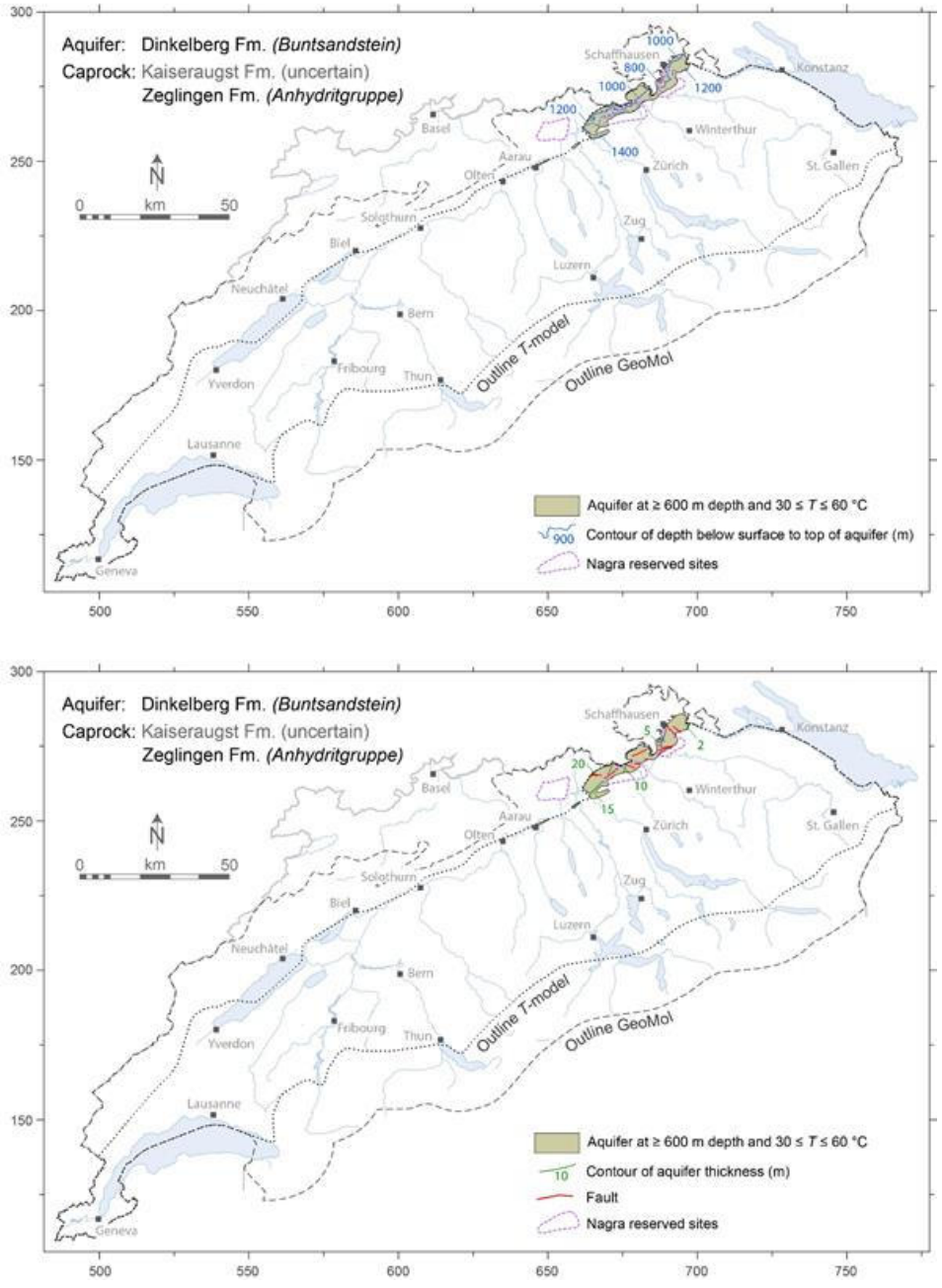

Figure 5-11: Delimited Dinkelberg Formation. Top map: depth below surface to top of aquifer. Bottom map: vertical thickness of the aquifer and locations of known faults. Isopachs are modified after Chevalier et al. (2010). The three Nagra siting regions are assumed to be likely off limits for geo-methanation projects.

The biggest uncertainty in assessing the suitability of the Dinkelberg Formation is how well the reservoir is sealed. The Dinkelberg Formation is overlain by the Kaiseraugst Formation, an up to 60 m thick heterogeneous succession of dolomites, limestones and marls, which is unlikely to act as a good seal. In the Lake Constance area, the basal sandstone of the Kaiseraugst Formation is even hydraulically linked to the Buntsandstein aquifer (Chevalier et al., 2010). In addition, the generally gentle dip of the formation towards the south would result in northward migration of any injected gases. Trap structures are thus needed to create a laterally closed and well-sealed reservoir. As the Dinkelberg Formation is

located beneath the basal décollement horizon of the Jura Mountains, no anticlinal traps are expected. However, several faults crosscutting the Dinkelberg Formation have been identified (Figure 5-11). Where their offsets juxtapose the Buntsandstein directly against the evaporites of the younger Zeglingen Formation (which has excellent sealing capacities), they may have created fault-bounded traps (c.f. Figure 5-21).

5.4.3 Schinznach Formation – Stamberg Member

The Schinznach Formation consists predominantly of tight limestones that accumulated on a shallow marine carbonate platform (Pietsch et al., 2016; Adams and Diamond, 2019). Early diagenetic dolomitization has affected two horizons, the youngest being the anhydrite-bearing Stamberg Member, which hosts the Muschelkalk aquifer. In the northeast of the SMB its rock-matrix porosities are 20 vol.% and permeabilities are up to 1000 mD. Here burial compaction is minimal and the primary reservoir properties have been enhanced by Neogene dissolution of anhydrite and by slightly karstified fracture sets that flank major faults (Aschwanden et al., 2019a). In this area, the Stamberg Member constitutes a promising (sub)regional gas-storage reservoir. Further south in the basin, burial compaction has reduced the matrix porosity and permeability of the dolomites to low values, with permeabilities < 60 mD (Aschwanden et al., 2019a). Faults in this southern realm may still provide fracture porosity and permeability, but whether these zones are adequately sealed or not for gas storage is unknown.

Due to its regional extent and thickness, comparatively low degree of internal heterogeneity and suitable reservoir properties along the north-eastern margin of the SMB), the Muschelkalk aquifer is assigned rank 1 with respect to its potential suitability for geo-methanation. The Stamberg Member occurs in the correct depth-temperature interval for geo-methanation along the Jura Mountains from Oensingen in the west to Baden and then across the regions of Zürich Unterland and Zürich Weinland. There it lies at depths of 800 to 1200 m below surface and is around 30 m thick (Figure 5-12).

The Stamberg Member is sealed by the evaporites of the Late Triassic Bänkerjoch Formation. However, all Mesozoic formations are gently dipping towards the south, resulting in northwards migration of the injected gases through the reservoir formation. To create a laterally constrained reservoir, trap structures are thus needed. Faults and anticlines are present across the entire area of interest. Where faults are bordered by folds in the maps, the faults are mostly thrusts and the folds are mostly the accompanying ramp anticlines. In the eastern sector the indicated faults are steep strike-slip structures flanked by subvertical fracture networks.

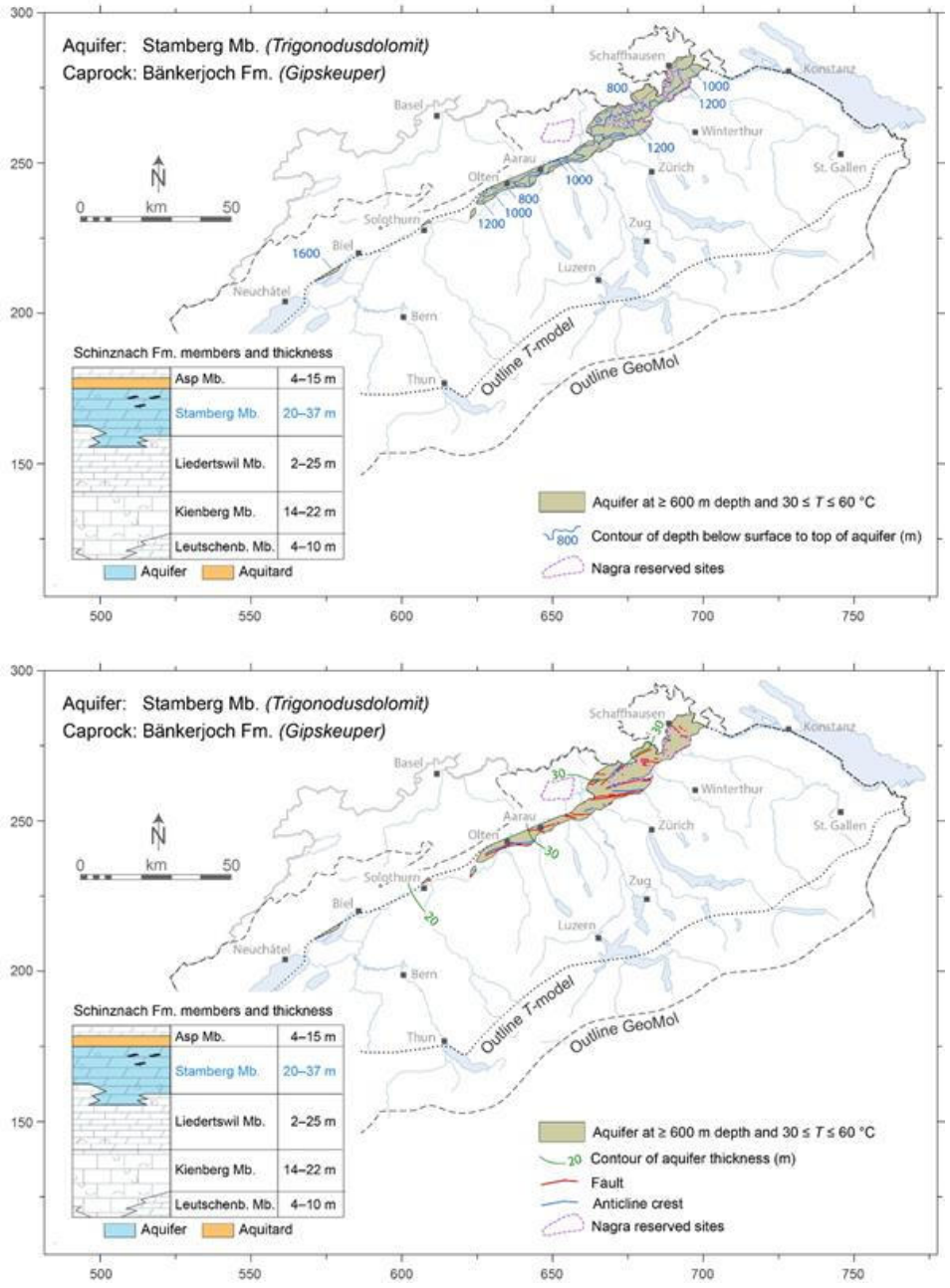

Figure 5-12: Delimited Schinznach Formation – Stamberg Member. Top map: depth below surface to top of aquifer. Bottom map: stratigraphic thickness of the Member and locations of known faults and anticline crests. Isopachs are modified after Adams et al. (2019). The three Nagra siting regions are assumed to be likely off limits for geo-methanation projects.

5.4.4 Klettgau Formation – SBEG Members

The Klettgau Formation was deposited in a flat basin with alternating continental (fluviatile and playa to sabkha environments) and shallow marine conditions. The formation consists of six members (inserts Figure 5-13), four of which likely show aquifer properties ("SBEG" Members). The sandstones of the Seebi and Berlingen members occur exclusively in the eastern portion of the SMB. The Gansingen Member is present only in north-western Switzerland. In contrast, the Ergolz Member is present across the entire area where the Klettgau Formation is defined (SMB east of Solothurn). No petrophysical data are available for the individual members but averaged porosities and permeabilities for the entire formation are up to 19 vol.% and 250 mD respectively (Chevalier et al., 2010, Nagra, 2022b). In addition, a large number of groundwater analyses are available from widespread sites (Waber et al., 2014), suggesting that the SBEG Members of the Klettgau Formation act as aquifers at the (sub)regional scale.

Based on the high degree of internal heterogeneity of the formation, its lack of member-specific petrophysical data, its considerable volume and its likely abundance of trapping structures (see below), the SBEG-Members of the Klettgau Formation are assigned rank 2 with respect to their potential suitability for geo-methanation. The Klettgau Formation occurs in the correct depth-temperature interval for geo-methanation along the Jura Mountains from Wangen a. A. in the west to Baden and then across the regions of Zürich Unterland and Zürich Weinland to the border with Germany near Etzwilen. The Ergolz Member is present across the entire area of interest, while the Gansingen Member is missing in the north-easternmost area. The coeval Berlingen Member occurs only in the Lake Constance area and thus lies outside the desired depth–temperature range. The Seebi Member is restricted to the north-eastern corner of the area of interest (Figure 5-13). Overall, the Klettgau Formation lies at depths of 800 to 1200 m below surface. The sandstones of the Ergolz Member are 3 to 16 m or more thick, the Gansingen Member 2 to 7 m and the Seebi Member 3 to 24 m thick.

The SBEG Members are likely sealed above by various mudstones. The Ergolz sandstones are overlain by the Ergolz mudstones, whereas the Seebi, Berlingen and Gansingen Members are sealed by the mudstones of the Gruhalden Member (cf. insets in Figure 5-13). However, locally there appears to be hydraulic connections between the Klettgau Formation and the overlying Staffelegg Formation (Chevalier et al., 2010), implying that sealing is not guaranteed everywhere.

All Mesozoic formations are gently dipping towards the south, resulting in northwards migration of the injected gases through the reservoir formation. Trap structures are thus needed to create a laterally closed and well-sealed reservoir. Where the Berlingen, Gansingen and Ergolz Members are present, stratigraphic trapping is likely due to the lateral changes in facies (inserts in Figure 5-13). Folds are only present in the Zürich Unterland and further west. Most of them overlap with faults, suggesting that the faults are mostly thrusts and the folds the accompanying ramp anticlines (Figure 5-13). Faults not associated with anticlines are known, suggesting that fault traps are a possibility, especially where the offset along a fault places a reservoir member next to a sealing member (within the Klettgau Fm., the overlying Staffelegg Fm, or the underlying Bänkerjoch evaporites).

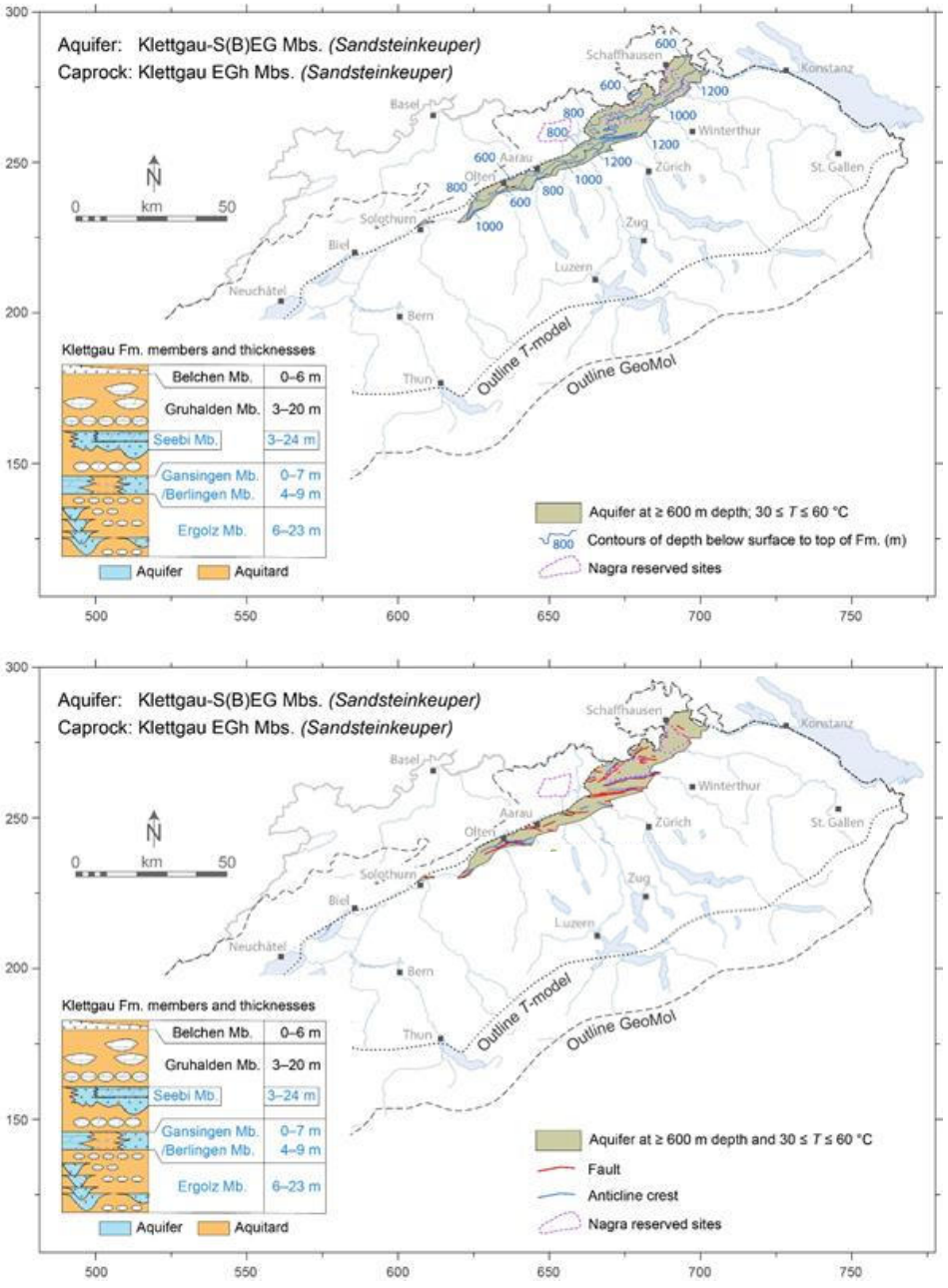

Figure 5-13; Delimited Klettgau Formation – SBEG Members. Top map: depth below surface to top of formation. Bottom map: locations of known anticline crests and faults within the delimited area. See inset diagram for ranges of stratigraphic thicknesses of the members. The three Nagra siting regions are assumed to be likely off-limits for geo-methanation projects.

5.4.5 Staffelegg Formation – Beggingen Member

The Staffelegg Formation is only defined in Northern Switzerland, between the River Doubs/Mount Weissenstein in the west and the Randen Hills in the east. It was deposited in a shallow marine basin with strong terrestrial input, resulting in a highly heterogeneous, siltstone-marl-dominated sedimentary succession with some intercalated limestones and sandstones (Reisdorf et al., 2011). Further east, marls were deposited in deeper basins while in the west, marls and limestones were deposited. Out of all these deposits, only the Beggingen Member, an arenitic limestone at the base of the Staffelegg Formation was identified as a potential aquifer. It shows porosities up to 15 vol.% and permeabilities of 100 mD (Chevalier et al., 2010). However, only a small number of groundwater samples from the Beggingen Member have been analyzed (Waber et al., 2014), suggesting that the lithology shows reservoir properties only locally.

Based on the high degree of internal heterogeneity, poor reservoir properties and limited thickness (< 6 m), the Beggingen Member has been assigned rank 3 with respect to its potential suitability for geo-methanation. The lithology occurs in the correct depth/temperature interval for geo-methanation along the Jura Mountains from Wangen a. A. in the west to Baden and then across the regions of Zürich Unterland and Zürich Weinland to the border with Germany near Etzwilen (Figure 5-14). In some areas, the Beggingen Member is likely sealed by the mudstone-rich layers of the younger Staffelegg Formation. However, the lateral discontinuity of most members and the overall highly heterogeneous nature of the formation makes its hydraulic properties unpredictable and thus rather unreliable as a regional-scale seal. At the same time, the heterogeneity of the formation likely resulted in the formation of stratigraphic traps. Folds are only present in the Zürich Unterland and further west. Most of them overlap with faults, suggesting that the faults are mostly thrusts and the folds the accompanying ramp anticlines (Figure 5-14). Additional steep faults are also present, possibly serving as hydraulic barriers to fluid flow and hence acting as gas traps, especially where the offset along a fault places a reservoir member next to a sealing member (within the Staffelegg Fm., the overlying Opalinus Clay or the older Bänkerjoch evaporites).

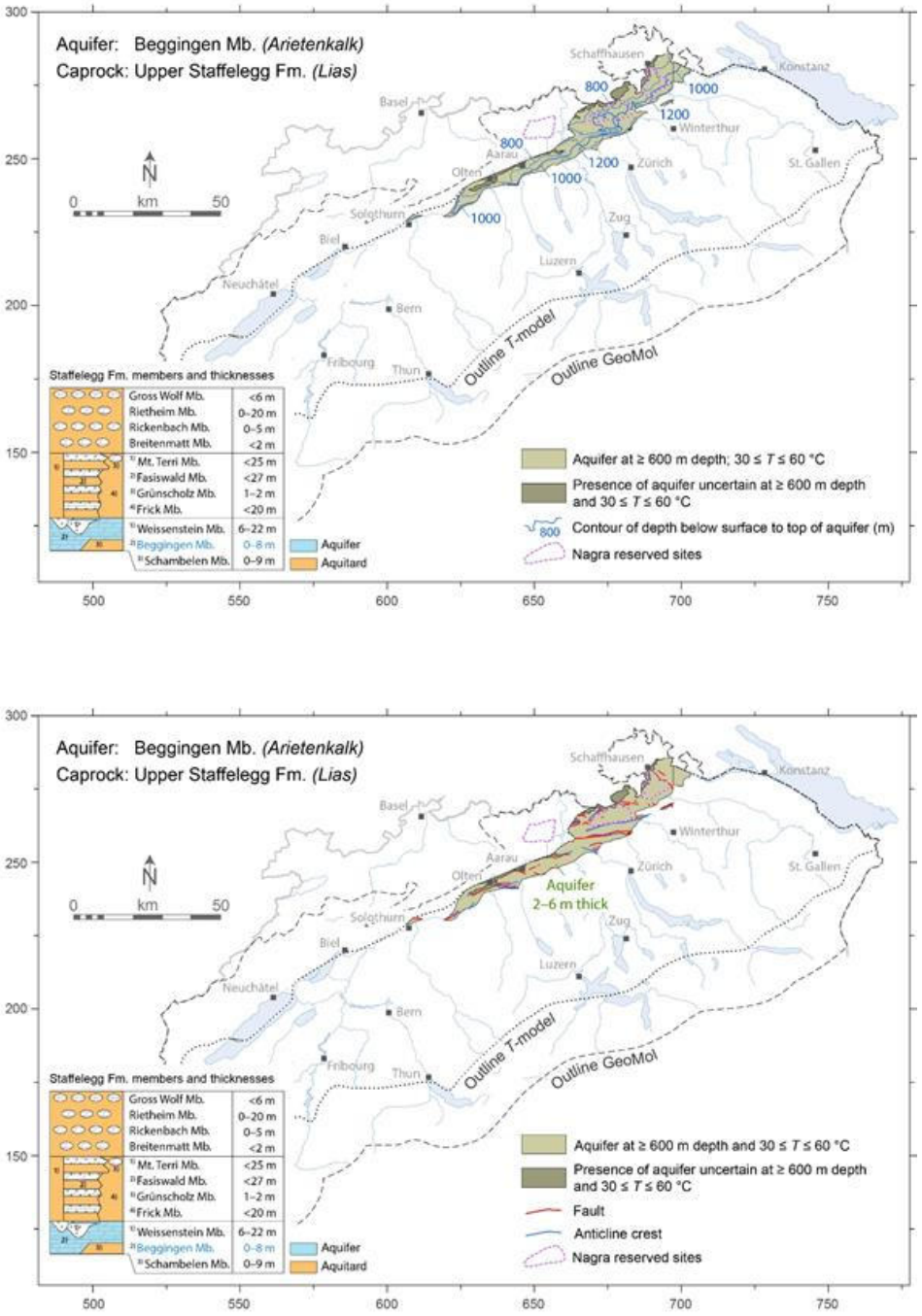

Figure 5-14: Delimited Staffelegg Formation – Beggingen Member. Top map: depth below surface to top of formation. Bottom map: stratigraphic thickness of Beggingen Member with locations of known faults and anticline crests. The three Nagra siting regions are assumed to be likely off limits for geo-methanation projects.

5.4.6 Hauptrogenstein

The Hauptrogenstein is an up to 150 m thick oolite, occurring only in the central to western SMB, between Brugg and Echallens. It was deposited as a shoal on a shallow carbonate platform, surrounded by mudstone-rich fore- and backshoal deposits to the east and west, respectively. It is exploited as a main aquifer in the Jura Mountains (e.g. Neuchatel and La-Chaux-de-Fonds) but reservoir properties are less certain in the SMB where porosities of at most 18 vol.% and permeabilities of only 0.5 mD have been measured (Chevalier et al., 2010; Nagra, 2022a; Nagra 2022b).

The Hauptrogenstein was assigned rank 2 due to its thickness, lateral extension and the likelihood for stratigraphic, anticlinal and fault traps. However, the lack of petrophysical data across the SMB introduces uncertainty in its properties. The formation occurs in the correct depth-temperature interval for geo-methanation along the Jura Mountains from the River Reuss in the east to the area of Orbe in the west (Figure 5-15), at a depth of 600 to 1600 m. Between Egerkingen and Mägenwil, the top of the Hauptrogenstein is shallower than 600 m and/or the 30 °C temperature limit. In the eastern part of this area, the Hauptrogenstein might even lie outside the correct depth-temperature interval completely. The thickness of the Hauptrogenstein ranges from 30 to 150 m, being thickest in the centre of the area of interest (Figure 5-15).

The overlying Ifenthal Formation is relatively impermeable but also highly heterogeneous. Its suitability as a regional-scale seal is therefore uncertain and would need to be investigated in detail. In the east where the Hauptrogenstein transitions to the Klingnau Formation, some of the limestones might be locally sealed by marls of similar age due to interfingering (i.e., they form stratigraphic traps). A large number of long anticlines are present in the area of interest, at least some of which are ramp anticlines riding on low-angle thrusts. Steep faults are also present, with potential to form structural traps, especially between Biel/Bienne and Neuchâtel as well as west of Yverdon-les-Bains.

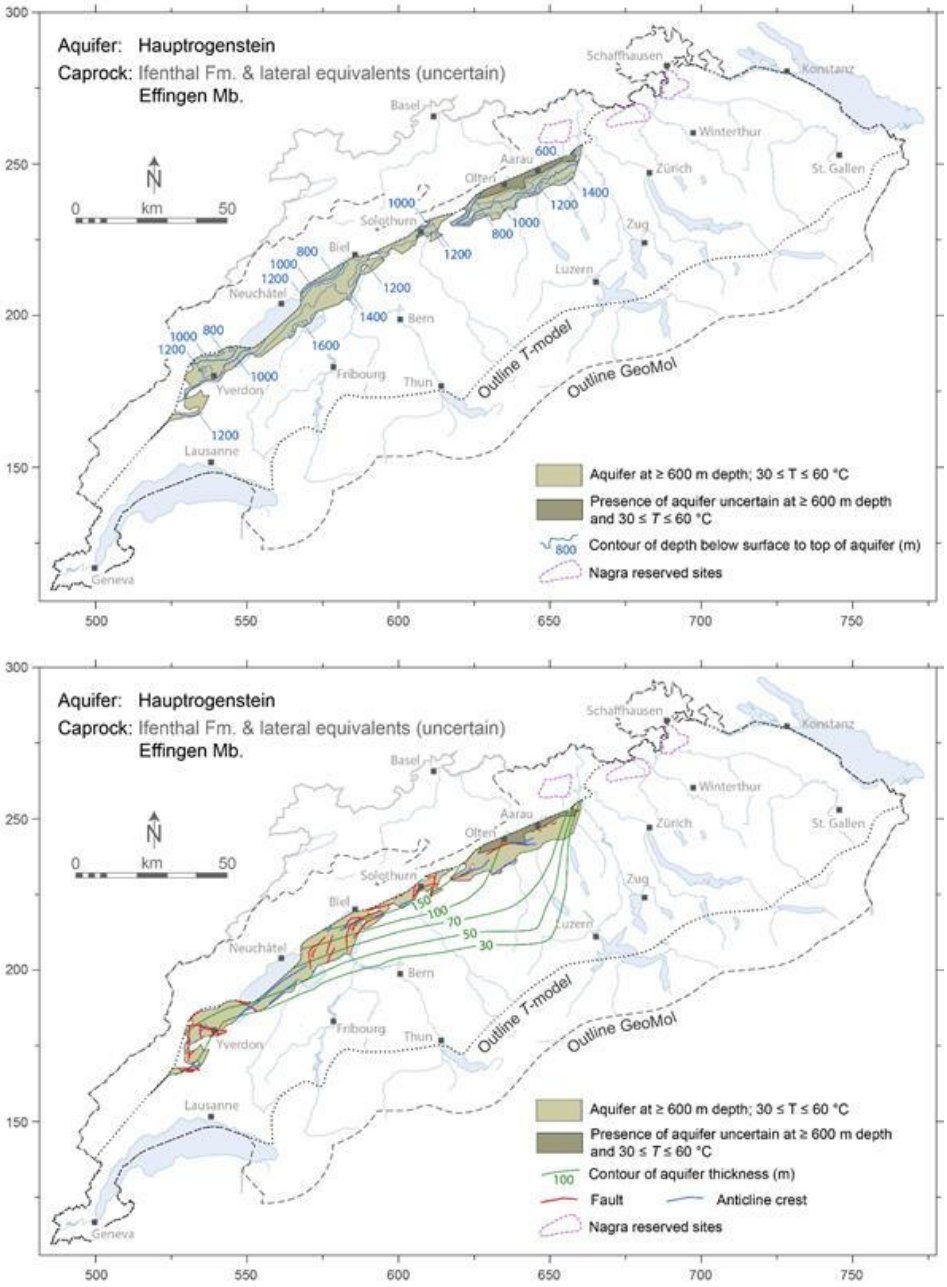

Figure 5-15: Delimited Hauptrogenstein. Top map: depth below surface to top of formation. Bottom map: stratigraphic thickness of formation and locations of known faults and anticline crests. Isopachs are modified after Chevalier et al. (2010). The three Nagra siting regions are assumed to be likely off limits for geo-methanation projects.

5.4.7 Etiollets Formation

The Etiollets Formation is the only porous aquifer within the Late Jurassic sequence. It was deposited on a shallow carbonate platform as patch reefs which formed on local highs. Within the SMB, its occurrence is restricted to the Geneva Basin, southwest of Gland. The Etiollets Formation shows porosities between 1 to 25 vol.% and permeabilities up to 100 mD (Rusillon, 2016).

Although the above reservoir properties are encouraging, the lateral extent and thickness of the patch reefs is unclear, as is question whether the reefs are sealed above (see below). Accordingly, the formation was assigned rank 3. The Etiollets Formation occurs in the correct depth–temperature interval for geo-methanation across the Geneva Basin (except for the Jussy area) and up to St. Cergue – Gland VD at depths of 750 to 1550 m. The variations in thickness of the entire formation are substantial, ranging from 80 to 350 m over a few kilometers (Figure 5-16).

No anticlines are present in the delimited area but there are a number of steep, large-scale faults, some of which cut to the north-west and to the west of the City of Geneva. If these steep faults are impermeable, then this structural situation could lead to fault compartments that could trap injected gas.

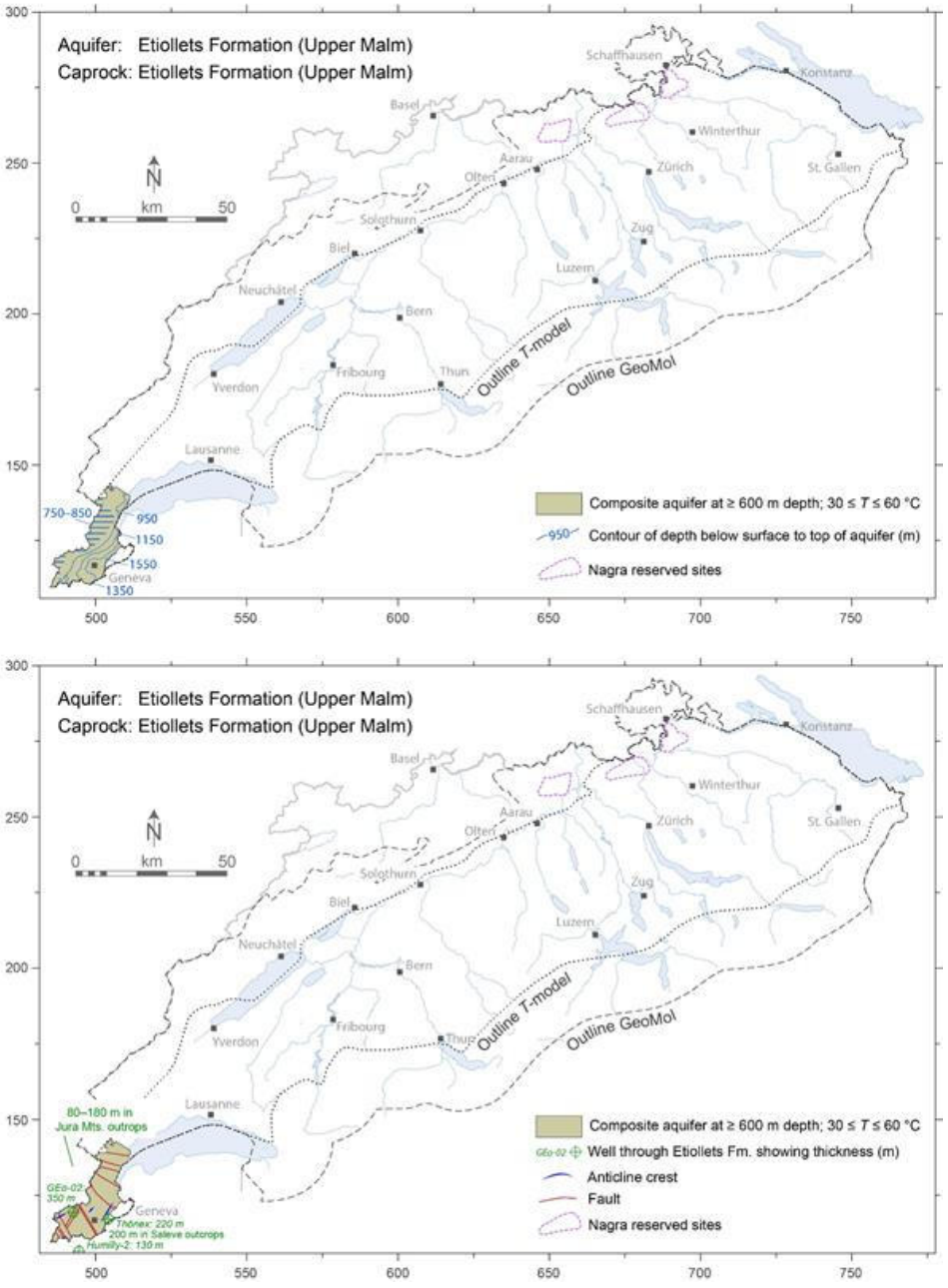

Figure 5-16: Delimited Etiollets Formation. Top map: depth below surface to top of formation. Bottom map: stratigraphic thickness of formation and locations of known faults and anticline crests. Thickness information is derived from Jenny et al. (1995) and the newly drilled GEo-02 well (pers. comm. SIG). The three Nagra siting regions are assumed to be likely off limits for geo-methanation projects.

5.4.8 Lower Freshwater Molasse (USM)

The Lower Freshwater Molasse (USM) consists of fluviatile deposits comprising three main lithotypes: a) conglomerates, b) sandstones and c) silt- and mudstones. The conglomerates, which represent alluvial fan deposits, are present along the Alpine front relatively close to their source rocks (i.e., in the proximal realm of the basin; Platt & Keller, 1992). Their diagenetic history suggests that they retain elevated porosity and permeability, but no quantitative subsurface data are available. However, the conglomerate fans are not capped by impermeable seals, as they are directly overlain by more conglomerates from the later stages of Molasse deposition (OMM and OSM). The USM conglomerate fans are therefore not considered as potential reservoirs for geo-methanation and are excluded from Figure 5-17.

In the more distal areas of the basin, sequences of alternating sandstones and mudstones were deposited by meandering rivers. The sandstones represent channel fillings while the fine-grained sediments represent the associated overbank deposits. The channel sandstones form individual (2 – 8 m thick) or amalgamated beds of up to 50 m thick with average porosities of nearly 20 vol.% and permeabilities of up to 500 mD. The fine-grained floodplain deposits show porosities of < 10 vol.% and permeabilities around 1 mD. The USM can therefore be assumed to contain numerous small reservoirs where the channel sandstones are embedded in sealing floodplain deposits (i.e., they form a composite aquifer). Depending on the age of the USM, the volumetric ratio between sand- and mudstones differs. While the older USM deposits are more marl-rich, the younger USM deposits contain abundant sandstones. The two age units are not differentiated in Figure 5-17.

The USM is assigned rank 2 due to its regional extent and thickness and its nature as a composite, at least partially internally sealed aquifer. The formation sits within the target depth–temperature interval for geo-methanation across almost the entire SMB. Due to its great thickness, the USM reaches the surface in western and north-eastern Switzerland but in central and eastern Switzerland its top lies at 800 to 1400 m below surface. Where the USM lies at shallower levels (800 m and less) it is often 600 m or more thick, whereas in the deeper parts of the target depth–temperature interval it is between 200 and 400 m thick (Figure 5-17).

As described above, the USM simultaneously represents a potential reservoir and a potential seal in the same unit. The intercalation of sand- and mudstones results in a plethora of potential stratigraphic traps across the entire USM. This means that any exploration well is likely to encounter at least some sandstone layers with adequate reservoir properties. However, lateral variations in lithologies and petrophysical properties are common and not well constrained. Therefore, the suitability and size of each small reservoir as well as the integrity of each corresponding seal has to be assessed individually.

Due to the abundance of stratigraphic traps, anticlines and faults are of lesser importance for gas retention in the USM. There are nevertheless several anticlines present in the area of interest, predominantly in central to western Switzerland (Figure 5-17). They run (sub)parallel to the folds of the Jura Mountains. The faults show three sets of orientations: N-S, NW-SE or subparallel to the axis of the SMB.

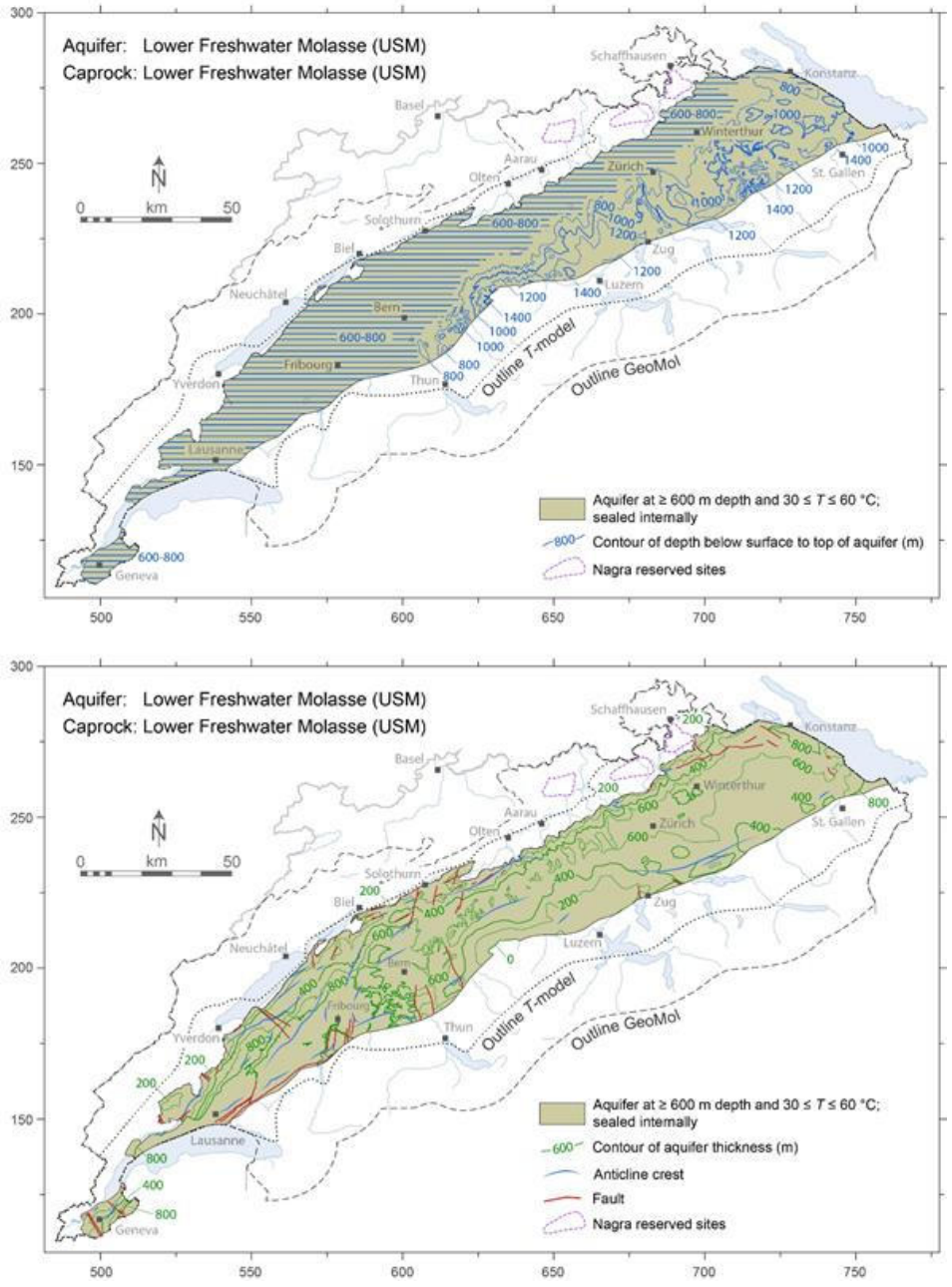

Figure 5-17: Delimited Lower Freshwater Molasse (USM). Top map: depth below surface to top of USM. Bottom map: vertical thickness and locations of known faults and anticline crests. The three Nagra siting regions are assumed to be likely off limits for geo-methanation projects.

5.4.9 Upper Marine Molasse (OMM)

The Upper Marine Molasse (OMM) consists of shallow marine deposits comprising three main lithotypes: a) conglomerates, b) sandstones, which are often amalgamated and which dominate the older OMM deposits, and c) silt- and mudstones, which alternate with the sandstones in the younger OMM. Analogous to the USM, the conglomerates are not considered as potential reservoirs owing to their lack of obvious seals. The sandstones of the OMM on the other hand are considered a good local- to regional-scale aquifer with porosities of 5 to 20 vol.% and permeabilities of up to 650 mD.

The OMM is laterally extensive and up to 900 m thick. Although the reservoir characteristics are promising where measurements are available, data are completely lacking across large areas of the SMB. The extent to which the OMM sandstones are hydraulically sealed above is unclear and the presence of gas traps is uncertain (see below). The OMM is thus assigned rank 2. The formation sits within the target depth–temperature interval for geo-methanation south-east of Bern, across Central Switzerland and all the way to Lake Constance in the east (Figure 5-18). The top lies at < 600 m depth across most of the area of interest. Only in eastern Switzerland is the top of the OMM within the required depth–temperature interval. The thickness of OMM deposits in the area of interest ranges from 200 to over 800 m.

The OMM sandstones are partly sealed internally by mudstone intercalations and also by the mudstone-rich terrestrial deposits of the overlying OSM (Chapter 5.4.10). However, in both cases, lateral variations in lithologies and petrophysical properties are common and not well constrained. The quality of the OMM seal thus has to be evaluated at a local scale.

Stratigraphic traps are less abundant than for the USM. Steep faults are limited to the area south-west of Bern as well as close to Lake Constance. Several small anticlines can be found across the area of interest as well as a very long, open anticline stretching from the Entlebuch area across Central Switzerland to the River Thur.

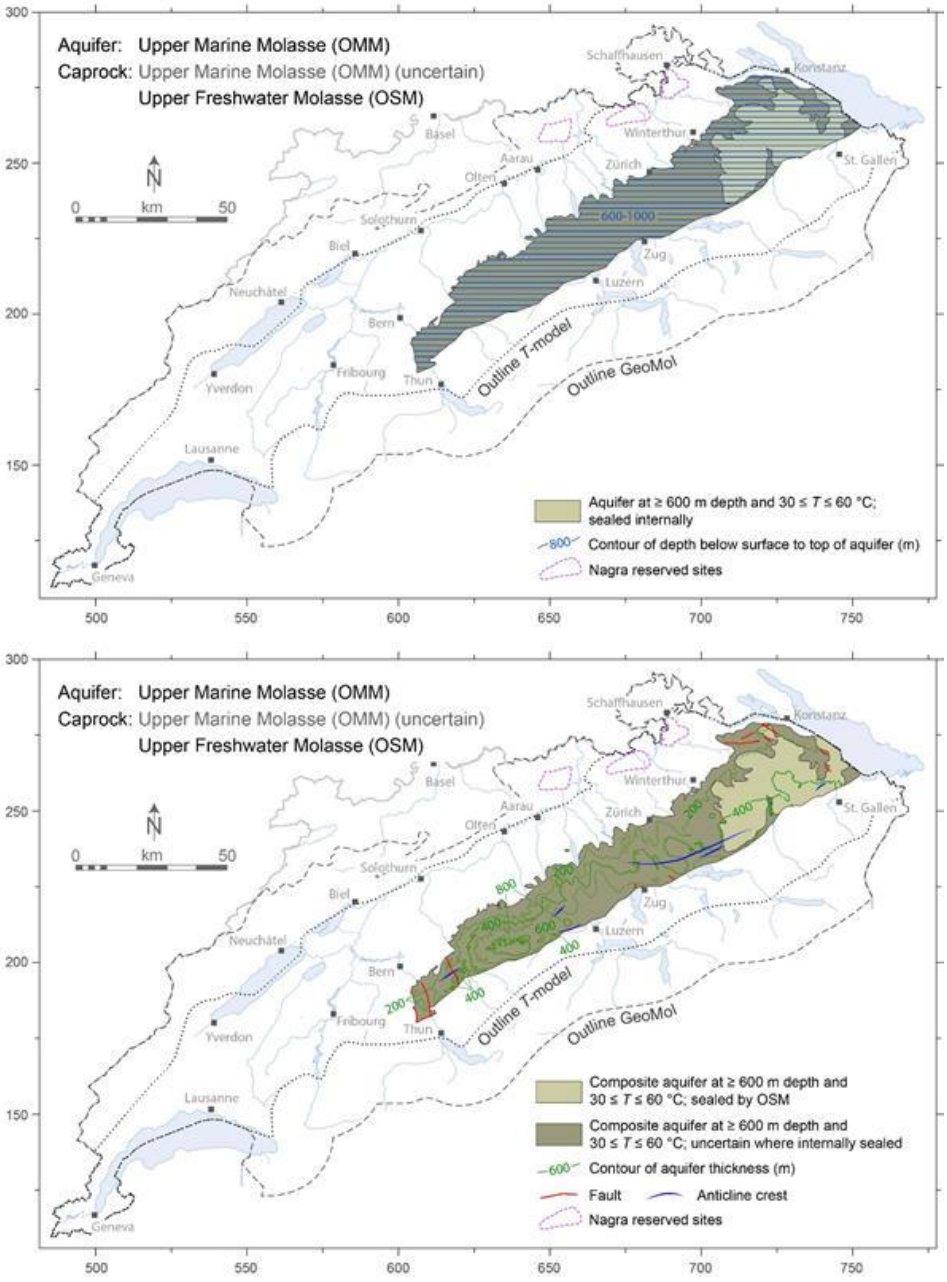

Figure 5-18: Delimited Upper Marine Molasse (OMM). Top map: depth below surface to top of OMM. Bottom map: vertical thickness and locations of known faults and anticline crests. The three Nagra siting regions are assumed to be likely off limits for geo-methanation projects.

5.4.10 Upper Freshwater Molasse (OSM)

The Upper Freshwater Molasse (OSM) consists of fluviatile deposits comprising three main lithotypes: a) conglomerates, b) sandstones and c) silt- and mudstones. Analogously to the USM and OMM, the conglomerates appear unsealed above and are therefore not considered as potential reservoirs. Compared to the USM, the OSM is often more mudstone-rich and sandstones are less abundant (only about 10 vol.%; Gander, 2004). Unfortunately, few petrophysical data are available for the OSM. Gander (2004) estimates the porosity of OSM sandstones to be in the range of 5 to 10 vol.% and reports permeability values between 0.01 and (rarely) 100 mD.

Overall, the OSM is very similar to the USM but it contains fewer sandstones, which raises exploration risks. In addition, the OSM is not capped by a distinct sealing unit and instead its potential reservoir properties rely on it being internally sealed by its own mudstone layers, thus forming a composite aquifer. However, lateral variations in lithologies and petrophysical properties are common and not well constrained, thus local-scale tests must be performed to prove its reservoir character. Based on these features, the OSM is assigned rank 2. The OSM sits within the target depth–temperature interval for geo-methanation in a small area between St. Gallen, Konstanz and Lake Constance and lies between 600 and 800 m below surface, with thicknesses between 50 to 150 m (Figure 5-19). Besides the expected stratigraphic traps, there are only two small faults and a lone anticline north of St. Gallen.

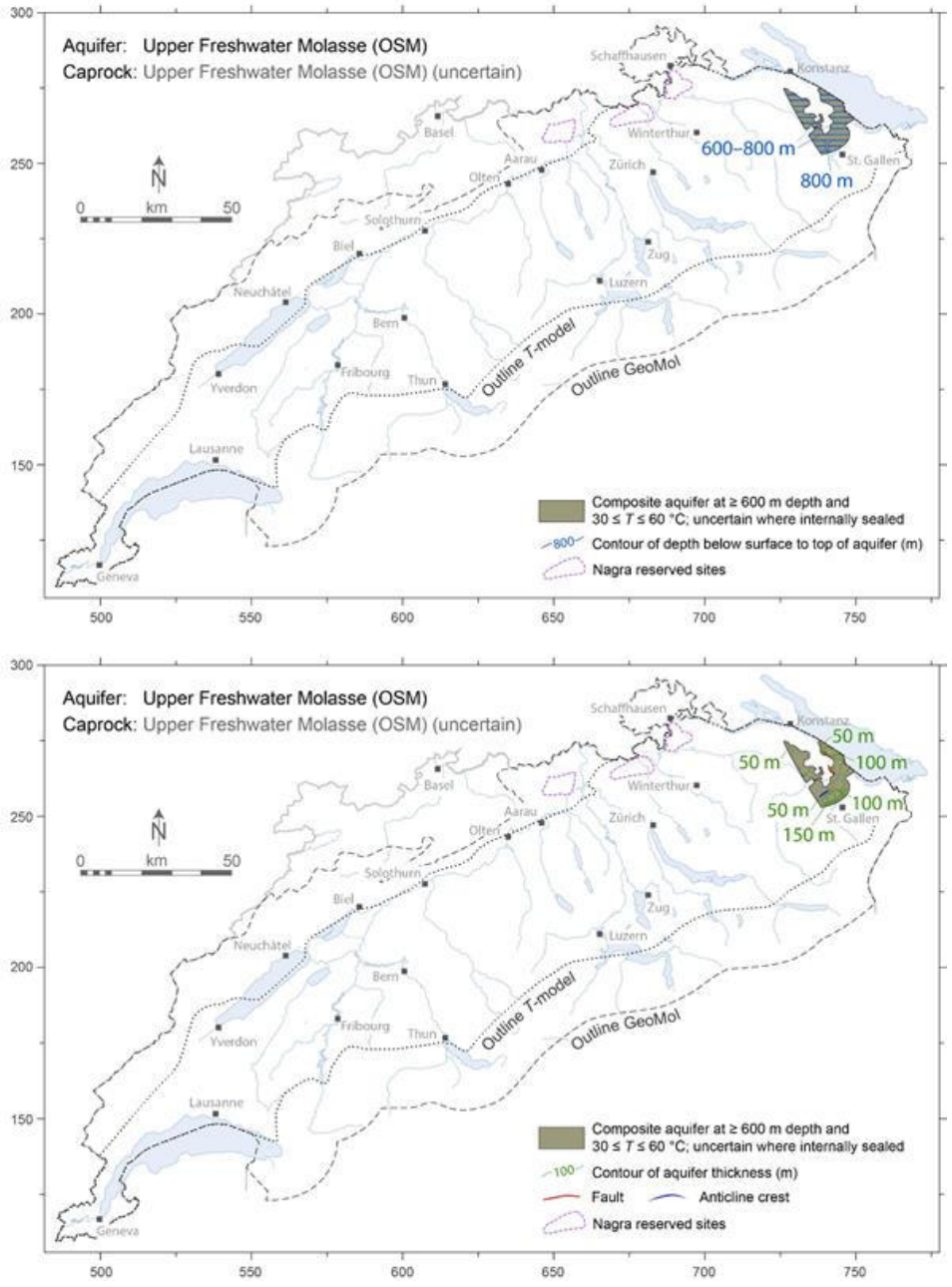

Figure 5-19: Delimited Upper Freshwater Molasse (OSM). Top map: depth below surface to top of OSM. Bottom map: vertical thickness and locations of known faults and anticline crests. The three Nagra siting regions are assumed to be likely off limits for geo-methanation projects.

5.4.11 Uncertainties and significance of delimited aquifers

The maps presented in this Chapter are based heavily on data incorporated in the GeoMol geological model (geological horizons) and the associated *T*-model (isotherms). Both of these models have inherent uncertainties related to their geological input data and the processing thereof, to the inter- and extrapolation of 3D information across the entire model extent, and to the linking of the individual model sections (Allenbach et al., 2017).

Within the large-scale units defined by GeoMol, the possible distribution of aquifers and seals –as shown in the maps in this Chapter– is based on our interpretations of the literature on the subsurface geology of the SMB. Here, many points of interpretation are uncertain. A primary uncertainty is the quantification of petrophysical properties (rock-matrix porosity and permeability, fracture porosity at formation scale, and permeability derived from borehole hydraulic tests). Information on these properties is patchy throughout the delimited reservoirs of interest, and the available information is not currently integrated into GeoMol. Our generalized classifications of certain lithoacies as aquifers and seals may therefore not be reliable across the entire delimited areas, especially as over 100 years of hydrocarbon exploration, the overall reservoir quality in the SMB has been found to be relatively poor (Leu, 2012). Porosity and permeability values encountered are generally lower than expected due to overcompaction of the sediments related to the late uplift and erosion and a complex diagenetic overprint leading to increased cementation of pores. The poor reservoir qualities and generally small volumes of porous formations enclosed by trap structures, limits the size of potential reservoirs.
Additional uncertainties are related to the locations of major faults and anticlines in the delimited reservoirs. The positions of the structures indicated in the maps in Chapter 5.4, have been taken directly from GeoMol. It is very likely however, that many more minor faults exist in reality. Irrespective of whether a fault is included in GeoMol or not, very little information on the properties of the fault are likely available.

While the position of faults can be deduced, e.g., from seismic surveys, its permeability can normally only be determined by hydraulic testing from nearby wells which is not commonly done or at least reported. Whether the number of anticlines included in GeoMol is complete or not, is unclear. Overall, anticlines represent larger structures than individual faults and are thus harder to miss. They have also been prime targets during the hydrocarbon exploration in Switzerland and are therefore comparatively well-studied. Leu (2012) suggests that many of these anticlines are breached and this is why no hydrocarbon resources are present in the SMB. The breached traps are the result of a combination of relatively thin sealing formations and recent compressive tectonic deformation related to the formation of the Jura Mountains. Unfortunately, the author gives no information on the abundance and distribution of breached traps across the SMB.

Despite the above uncertainties, we are confident that the maps provided in this Chapter serve as useful first-order guides to the SMB in two respects. First, the areas *not* classified as "sealed aquifers" can be understood as regions where gas storage and geo-methanation are *unlikely to be feasible*, based on the current state of geological knowledge. Second, the areas delimited as "sealed aquifers" (olive shades in the maps) can be understood as regions where gas storage and geo-methanation *may well be feasible*, once more detailed subsurface information becomes available. Thus, these delimited areas in the maps should not be taken to indicate *definitive feasibility.* Steps necessary to establish definitive feasibility are discussed in the following chapter.

5.4.12 Suitability map for geo-methanation in the SMB

The potential quality of sealed aquifers deduced in this study (as expressed by their ranking in Table 5-3) can be used as a primary guide in exploring for geo-methanation sites. In addition, the chances of exploration success are enhanced where more than one sealed aquifer is present in the sedimentary stack beneath the same geographical site. At such sites a single well may permit several aquifers to be tested for their suitability for geo-methanation, thereby lowering costs as well as risks. Finally, the presence of structural traps for gas can be used as a third criterion in exploration.

As a practical aid in exploration and in planning the use of the subsurface, a map has been constructed summarising the geographical distribution of the above three criteria throughout the SMB, coloured according to a suitability scale (Figure 5-20). The map considers only the sealed aquifers judged to be potentially suitable, i.e., those ranked 1, 2 or 3 in Table 5.3.

Examination of the number of these aquifers in the sedimentary stack at each geographical location defines 23 distinct areas: 8 with one aquifer in the subsurface, 6 with two, 3 with three, 4 with four, and 2 with five stacked aquifers. Each of these areas is assigned a numerical score corresponding to the sum of stacked aquifers, each weighted by its quality ranking. The range of the scores is then represented by a colour scale spanning from yellow-green (lower suitability) to intense green (higher suitability). The presence of anticline crests in the subsurface is denoted by blue lines in the map (taken from Figure 2-4 in Allenbach et al., 2017). Unfortunately, the locations of fault-bounded structural traps versus leaky faults could not be evaluated with the available information (see discussion in Chapter 5.5), and so none are shown in Figure 5-20. All known faults in each reservoir unit are shown in the preceding maps in this chapter.

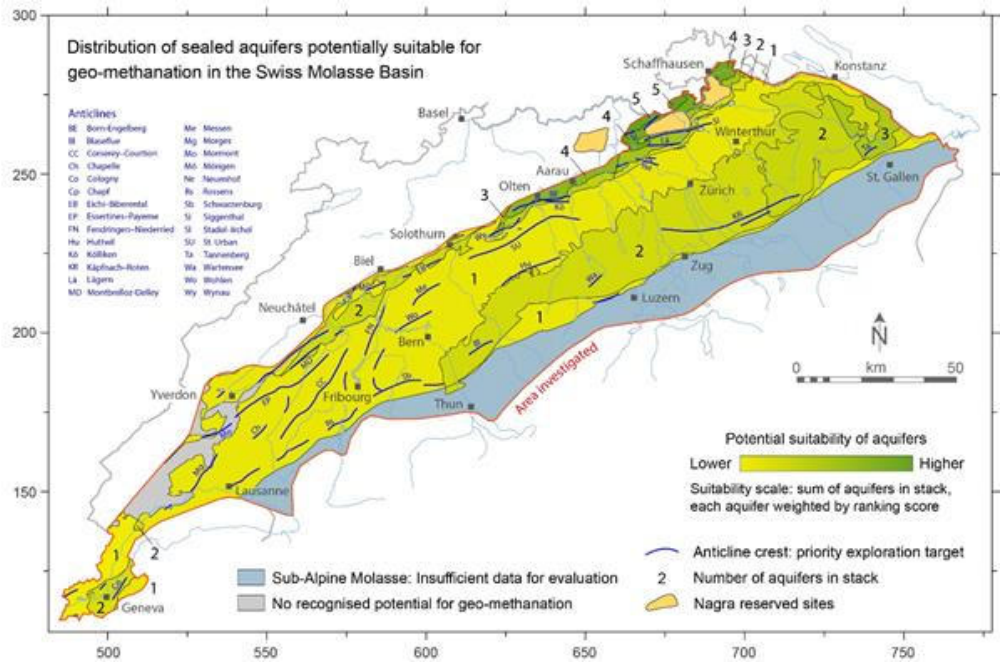

Figure 5-20: Map showing relative suitability of areas in the Swiss Molasse Basin for geological gas storage under conditions required for USC-FlexStore geo-methanation (greater than 600 m deep, temperature 30–60 °C). Shades of green denote the sum of sealed aquifer formations locally present in the sedimentary stack, each aquifer being weighted by the reciprocal of its quality ranking (1, 2 or 3; Table 5-3). Blue lines show locations of the crests of known elongated dome structures (anticlines) in the sub-surface, which may serve as gas traps. Areas distant from blue lines may or may not contain other un-known anticlines. Faults (not shown in this map) may also create gas traps, but less commonly than anticlines. All known faults are shown in the maps of individual reservoir units (maps in this chapter).

Table 5-3: Criteria (positive indicators) and SMB geological units screened for geo-methanation implementation. A "y" (for "yes") indicates that the criterion is fulfilled; "(y)" indicates that the criterion is barely fulfilled or highly uncertain; and "n" (for "no") indicates that it is not fulfilled. The units are ranked from 1 to 4, where 1 denotes "potentially suitable for geo-methanation" and 4 denotes "likely unsuitable for geo-methanation".

	Crystalline basement	(Pre-)Weitenau Fm.	Dinkelberg Fm.	Schinzn. Fm. (Stamb.Mb.)	Klettgau Fm. (SBEG Mbs.)	Staffelegg Fm. (Beg. Mb.)	Hauptrogenstein	Up. Jur./Lower Cret. Limest.	Up. Jur, Etiollets Fm.	Lower Freshwater Molasse	Upper Marine Molasse5	Upper Freshwater Molasse
Rank	4	3	1	1	2	3	2	4	3	2	2	2
Extent & heterogeneity of aquif.[1]	reg (h)	loc (h)	reg (l)	reg (l)	loc (h)	reg (h)	reg (l)	reg (h)	loc (h)	loc (h)	reg (l)	loc (h)
Thickness: > 5 m	y	y	y	y	y	(y)	y	y	?	(y)	y	(y)
Porosity[2]: > 20 vol.%	n	?	n	y	n	n	n	n	y	n	(y)	?
Porosity[3]: > 10 vol.%	n	?	y	y	y	y	y	n	y	y	y	?
Permeability: 50 to 3000 mD	y	?	y	y	y	y	?	n	n	y	y	?
Aquifer type: Porous matrix	n	y	y	(y)	y	y	y	n	(y)	y	y	y
Caprock: Present & tight	(y)	y	(y)	y	y	(y)	(y)	(y)	(y)	(y)	(y)	(y)
Trap structures[4]	f	s	f	a/f	a/f/s	a/f	a/f/s	a/f	s	a/f/s	a/f/s	a/f/s

[1]reg. = regional extent; loc. = local extent; h = highly heterogeneous with respect to lithological distribution and/or distribution of water-conducting features; l = low degree of heterogeneity with respect to lithological distribution and/or distribution of water-conducting features. All formations are heterogeneous when it comes to the distribution of petrophysical properties (porosity and permeability) as evidenced by the spread of the values in Figure 5-9.

[2]Positive indicator for porosity given in Table 5-1.

[3]Cautionary indicator for porosity given in Table 5-1.

[4] a = anticlinal traps possible, f = fault traps possible, s = structural trapping (due to different lithotypes present in the same formation/member). For the purpose of creating the combined map of potential reservoirs for geo-methanation (Figure 5-20), the areas where the OMM is likely sealed by the overlying OSM (light olive area in Figure 5-20) was ranked as 1.5 while the remaining OMM was ranked as 2.

5.5 Establishing feasibility of geo-methanation in the SMB

Chapter 5.4 has shown that the SMB includes numerous formations that may meet the criteria for geo-methanation, and that in places these formations are folded or offset by faults that may have created traps suitable for gas storage. A demonstration of the definitive feasibility of geo-methanation at one or more specific sites requires going beyond the coarse spatial resolution of the present study and conducting a dedicated exploration campaign at the kilometre scale. This Chapter outlines the main features required of target gas traps and it describes typical exploration aims and steps.

Any such campaign will require considerable investments of time and capital. However, owing to the currently incomplete knowledge of the deep SMB, there is no guarantee that these investments will result in a successful discovery. To estimate the stake at risk and to aid initial planning of an exploration campaign, this Chapter also provides a brief overview of typical exploration costs and a time schedule.

5.5.1 Properties of gas traps at km-scale

The various gas species (CH_4, H_2 and CO_2) involved in geo-methanation spontaneously form a single gas phase that has much lower density and viscosity than the immiscible saline porewater in the reservoir formation. These properties of the gas phase render it highly buoyant and mobile in any sealed aquifer that has a monoclinal dip (Chapter 5.3). Since all the identified sealed aquifers in the SMB dip slightly to the SE, gas-trap structures (anticlinal, stratigraphic, fault-bounded or combinations thereof) will be essential to retain the gas phase in a well-defined pocket during the short- to medium-term storage periods (months to years) envisaged for geo-methanation.

Numerous anticlines and faults are indicated inside the delimited "sealed aquifers" in the maps in Chapter 5.3, but only in Northern Switzerland is the resolution of subsurface knowledge sufficient to define the geometry of the traps clearly. This is the area where Nagra has performed 3D seismic surveys calibrated by several deep wells (the "Nagra reserved sites" outlined in the maps in 5.3 are only a part of the total Nagra investigation area).

An example geological cross-section in the Nagra investigation area is shown in Figure 5-20, where a ramp anticline above a low-angle thrust may possibly provide gas traps in the sealed Schinznach, Klettgau and Staffelegg Formations as well as the Hauptrogenstein (although at this locality the folded Hauptrogenstein lies shallower than the 600 m depth limit for geo-methanation). The cross-section also suggests that fault-bounded traps might be present in the Dinkelberg Formation, where the faults may be sealed by the overlying Zeglingen evaporites (note that, in this particular cross-section, the temperature of the Dinkelberg sandstones is higher than the 60 °C maximum for geo-methanation, and so the Figure 5-21 serves only to illustrate the trapping principle for that formation). While cross-sections with these geometries are promising, they do not show if the potential traps are closed in the 3rd dimension outside the 2D plane of the diagram. Ramp anticlines can be expected to decrease in amplitude in both directions along the strike of their crests, forming elongate domes. Purely fault-bounded traps need at least two intersecting faults to form a hydraulic barrier on the up-dip side of the reservoir. In the Nagra investigation area the information required to verify closure of potential anticlinal and fault-bounded traps is available in the 3D seismic interpretation. Comparable information is unfortunately not available elsewhere in the relevant portion of the SMB, although in Canton Geneva the interpretation of a large 3D survey is currently underway.

Whereas some promising trap structures are present in the mapped reservoirs (Figure 5-20), it is not known if they could actually retain injected gas. To our knowledge, no borehole hydraulic tests have ever been performed in the area of interest to test promising traps for their gas retentivity. Furthermore, despite the long history of oil and gas exploration in the SMB (Chapter 5.3.2), no natural gas-bearing reservoirs have been discovered so far within the depth–temperature interval pertinent to geo-

methanation. Thus, there is no proof from nature that the potential traps are gas-tight over long periods. Some authors have argued that the anticlines have leaked the gas that they once contained (Leu, 2012). Others suggest that the anticlines and thrusts had not yet formed during the period when burial conditions were conducive to gas generation within the known SMB source rocks (e.g., Mazurek et al., 2006) and thus gas reservoirs never formed.

5.5.2 Exploration steps

Installation of a geo-methanation site at a depth of 600–1900 m in the SMB requires a gas exploration company to select one or more sites. Geological criteria are paramount, but also non-geological criteria need to be considered, such as ease of permitting and proximity to sources of CO_2 feed gas and to electricity for hydrolytic production of H_2, as described in Chapters 4 and 6.

As far as the subsurface is concerned, an industrial exploration campaign has three aims: (1) find a suitable closed gas-trap structure composed of a porous and permeable saline aquifer rock sealed by an impermeable caprock; (2) if, as expected for the SMB, the structure contains no natural gas cap, then create an artificial gas cushion within the apex of the trap by injecting methane; and (3) demonstrate the technical feasibility, long-term gas retentivity, and environmental safety of the site. Initial steps deal with planning, obtaining exploration permits, possibly establishing a joint venture, and conducting an information and risk dialogue with the public and with local authorities. Further typical steps are outlined the following.

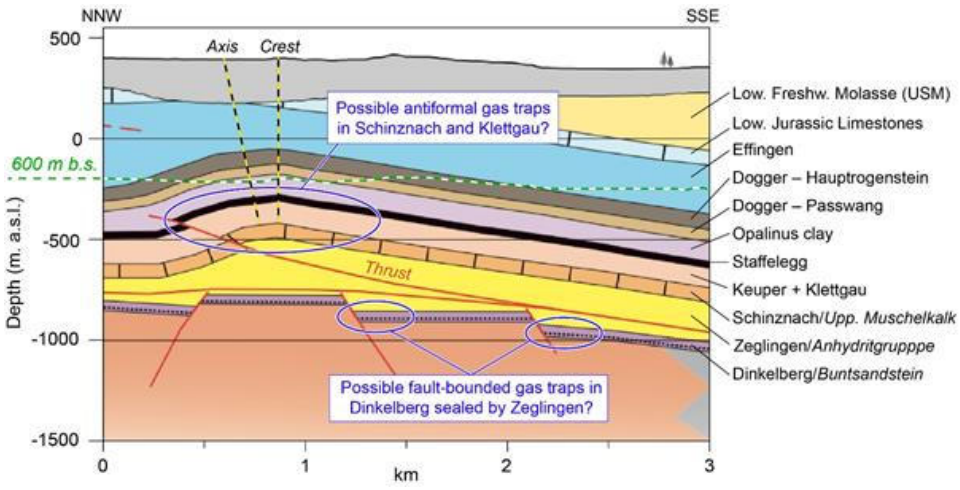

Figure 5-21: An example cross-section of potential gas traps 15 km ENE from Aarau, where Nagra has conducted detailed 3D seismic imaging, coring of deep wells and geological interpretation. The labelled low-angle thrust carries a ramp anticline (Chestenberg) that folds four potential sealed-reservoir units: Schinznach–Stamberg, Klettgau–SEG, Staffelegg–Beggingen and Hauptrogenstein (here the latter is shallower than 600 m depth limit for geo-methanation). The axis and crest of the fold are projected onto the surface, illustrating their relative locations if viewed in a map. Below the thrust, steep normal faults may conceivably create traps in the Dinkelberg Fm. No information is available as to whether these potential traps are closed in the third dimension outside the 2D plane of the diagram, and whether they are tight or leaky for gas. Note vertical exaggeration of scale. Diagram modified after Nagra (2008; Beilage 5.2-14).

5.5.2.1. Site selection

Based on the present report, on the literature containing km-scale structural analyses, and on any more recent geological data, one or more target gas-trap structures should be selected. These may be traps that have already been explored to some extent. A 3D seismic survey of the priority trap is performed to define its structure and dimensions at high spatial resolution (Figure 5-22). An existing survey of the relevant land area may perhaps be procured. For example, in the Nagra investigation areas, seismic imaging of the subsurface is sufficient to plan well sites. Otherwise, a new dedicated survey must be conducted over an area of ≥ 10 x 10 km^2. Such surveys normally deploy vibrator-trucks on existing roads and set out large arrays of portable geophones. The results allow favorable drilling sites to be identified.

5.5.2.2. Site characterisation and baseline modelling

Prior to drilling, an environmental impact study is conducted, including a survey of flora and fauna in local (sub)surface ecosystems. Monitoring using gas detectors is employed to ensure that gas injected into the target trap does not leak into and contaminate any overlying aquifers, or migrate to the surface where it could influence the biosphere, create hazards of explosion and of suffocation of wildlife and humans, and contribute to global atmospheric warming. Gas monitoring is started prior to drilling to establish the natural baseline of gas contents and emissions from rock outcrops, soils, surface water bodies and shallow aquifers at the site. This monitoring is continued during drilling, including on the well pad, and for several years after gas injection has commenced. A seismic monitoring array is also installed to record the baseline activity prior to perturbing the subsurface fluid pressure by injecting gas.

The drill pad is installed and the main well is drilled, completed for gas injection, and preferably rock cores are extracted over the depth interval of the planned gas cap. Analyses of the core combined with downhole geophysical logging allow calibration of a seismic-based 3D geological model of the gas-trap structure. Sampling of formation fluids allows characterization of the natural microbial consortia and evaluation of their suitability for geo-methanation. Downhole gas injection tests are performed to confirm that gas can be introduced into the aquifer at the desired rates without causing unwanted formation damage or felt seismicity. Observation wells are drilled at strategic points identified in the refined structural model, in order to test fluid pressure fluctuations. Information from all possible sources is integrated in a 3D numerical reservoir model, and this is used to simulate gas injection and extraction scenarios, including consequences of the attendant pressure fluctuations and fluid–rock chemical reactions.

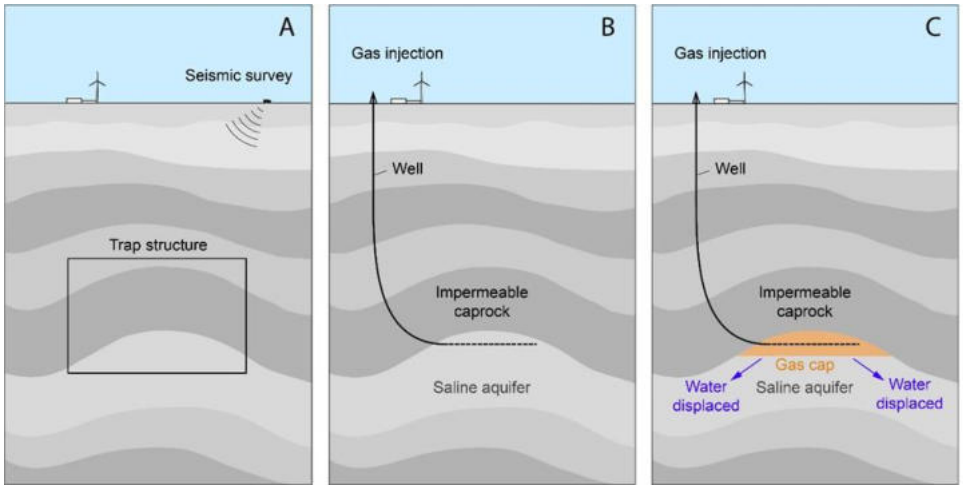

Figure 5-22: Illustration of exploration for a geo-methanation site and creation of a gas cap. (A) Trap structure (an anti-clinal fold in this example) is identified in a 3D seismic survey. (B) A well is drilled to demonstrate that the trap contains a porous and permeable saline aquifer sealed by an impermeable caprock, and to test for the presence of natural gas in the trap. (C) In the absence of a natural gas accumulation (as expected in the Swiss Molasse Basin), methane is injected into the trap, displacing the formation water from the pores in the aquifer rock and thereby creating an artificial gas cap.

5.5.3 Creation of an artificial gas cap and medium term monitoring

No pristine or exhausted gas caps are known in the SMB at the appropriate depth–temperature conditions for geo-methanation (Chapter 5.3.2). If new exploration fails to find gas in the trap targeted for geo-methanation (Figure 5-22) then a sizeable gas cap (≥ 4.5 million m^3_{STP}) will have to be created in the apex of the trap structure to provide a cushion in which the CO_2 and H_2 reactants can be injected. In principle, use of Swiss-produced biomethane (biogas) for this purpose may favour acceptance of the geo-methanation technology by the public and facilitate certification of the gas yield as "green methane". In practice, the costs and supply limitations of local biomethane may preclude this opportunity.

The creation of an artificial gas cap entails displacing the existing formation water from the aquifer within the trap by injecting overpressured methane (Figure 5-22). An important issue to address in the planning, testing and monitoring phases of the exploration campaign is the fate of this displaced formation water. If the total connected pore volume of the aquifer is very large (e.g., of sub-regional scale), then the pressure anomaly caused by water displacement can dissipate radially from the injection point without hydrofracturing the aquifer or its caprock. If the target gas trap is relatively small and bounded by faults, then the displaced porewater may force an escape through the faults, potentially inducing seismicity if the faults are naturally close to their critical failure-stress state. Poor management of injection rates and fluid pressure may also induce hydrofracturing of the aquifer and its caprock. To facilitate successful pressure management, the injection well is normally fitted with fibre-optic detectors to monitor temperature and pore fluid pressure at various depths. One way to manage fluid pressure in the aquifer at high gas injection rates is to simultaneously extract formation water through a separate well. In this case the environmentally sustainable disposal of the saline water needs to be planned in advance and its execution monitored.

Methane can be procured and slowly injected into the trap while continuously monitoring fluid pressure, seismicity and environmentally relevant gas emissions. Injection and monitoring over a period of 6 years is proposed to ensure that the cushion gas can be safely contained and managed in the trap structure. Geo-methanation tests can proceed concurrently by injecting CO_2 and H_2 and sampling their concentration through all wells.

Favourable performance of the site can then allow sustained commercial geo-methanation to begin, possibly with drilling of additional wells to achieve the desired production rate and storage volume.

5.5.4 Typical time schedule for an exploration and gas injection campaign

Figure 5-23 shows a typical schedule for the steps prior to sustained commercial geo-methanation. At least six additional months would be necessary at the outset to plan the project from scratch. If the first selected site is found to be inadequate for gas storage, then the same exploration steps could be repeated at other prospective sites.

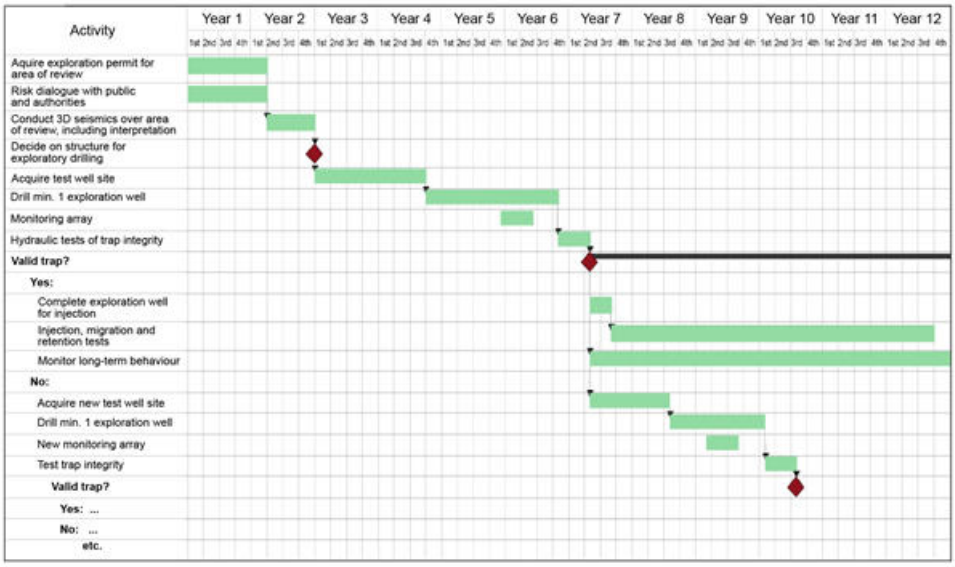

Figure 5-23: Time-schedule of typical operations to explore for a geo-methanation site and create a gas cap in a favourable trap structure. Modified after Häring et al. (2013).

5.5.5 Typical costs for an exploration and gas injection campaign

An example of typical costs for an exploration campaign and creation of a gas cap is given in Table 5-4. Included are one main exploration well to be used for both injection and extraction, and two narrow-bore observation wells to be sited on the margins of the planned gas trap.

Table 5-4: Typical costs to plan and explore for a geo-methanation site, to create a gas trap containing 4.5 million m^3_{STP} and to monitor its integrity over a 6-year period. Included are one injection/extraction well and two narrow-bore observation wells, all drilled to depths of 2000 m. Based on information provided by Dr. Werner Leu (Geoform Geological Consulting and Studies Ltd., Vevey, Switzerland).

Phase	Activity	Cost (kCHF)	Cumulated Cost (kCHF)
Project set-up	Define project organization	20	20
Site selection	Global site selection	60	80
	Data evaluation	105	185
	Storage assessment	60	245
	Apply site selection criteria	100	345
	Define a joint venture	15	360
Permit and risk dialogue	Permit and communication	140	500
	3D seismic exploration	2 255	2 755
	Baseline monitoring	445	3 200
	Numerical modelling 1	130	3 330
Installation well site	Site acquisition & drilling permits	290	3 620
	Drilling/completion operations	23 350	26 970
	Numerical modelling 2	100	27 070
Injection of gas	Acquire & transport gas	2 000	29 070
	Initial injection & monitoring	1 800	30 870
Medium term (6 years) monitoring	Monitoring after injection	5 500	36 370
	Well site maintenance	2 600	38 970
	Numerical modelling 3	200	39 170
		Grand total	**39 170**

5.6 Possible conflicts of use of the subsurface in the SMB

The geological subsurface of the Swiss Molasse Basin is being used or is planned to be used for a variety of engineering and resource-related purposes. Some of these uses are well-established and widely implemented while others are relatively new and, like geo-methanation, are at the exploration stage. Nevertheless, the geological conditions (e.g., lithologies, depth intervals, structures) required for the various technologies are sufficiently well known to assess their potential for conflicts of use with future geo-methanation projects.

As part of our geological screening of the Swiss Molasse Basin, we established a catalogue of criteria which need to be fulfilled to successfully implement geo-methanation (Chapter 5.2). One of the main criteria is that the temperature of the formations in questions must lie between 30 and 60 °C, so that microbial methanogenesis can take place. In addition, a minimum depth of 600 m was defined to ensure retention of gases. Based on the variable geothermal gradients throughout the basin, the depth range in which geo-methanation is feasible varies according to geographic location and to the availability of suitable reservoirs. The potential reservoirs occur in a stack, therefore some of them are present at only 600 – 800 m depth (corresponding to either the minimum depth or to the depth of the 30 °C isotherm), whereas others are as deep as 1400 – 1600 m (corresponding to the depth of the 60 °C isotherm). We also established that only well-sealed reservoirs within closed trap structures are likely to be suitable for geo-methanation.

Conflicts of use primarily arise when two subsurface applications target the same potential reservoir and/or seal in the same depth range. Other conflicts may arise from the risk of leakage of injected fluids (via faults or poorly completed wells) into overlying formations that have other uses. In the following chapter we thus list the target geology and depth range for a number of subsurface utilisations. This compilation only broadly assesses the subsurface technologies that are more or less likely to be in conflict with a potential geo-methanation site. It does not replace a more detailed assessment of site-specific conflicts of use during a future selection process. At present we see no conflict of use whereby one subsurface technology could be compromised by seismicity induced by another subsurface technology. Of course, the risks and hazards posed by induced seismicity are relevant for surface installations and for the population at large and must be evaluated for each project, but this is beyond the scope of the present study.

5.6.1 Infrastructure

Infrastructure or engineering projects are only of concern for a potential geo-methanation reservoir, if they reach to depths of ≥ 600 m. This is likely to be the case only in the Alps, where, due to the extreme relief, tunnels and pipelines may be installed at depths of more than 1 km (e.g., Gotthard Base Tunnel). However, the Alpine geological domain is not suitable for geo-methanation due to the abundance of fractures and poor reservoir properties of most formations (Chapter 5.3.1). Therefore, no conflict of use between geo-methanation and underground infrastructure projects is expected at the reservoir level. Existing underground infrastructure has to be considered during planning and developing of a site for geo-methanation, similarly to other construction sites.

5.6.2 Potable groundwater

Potable groundwater in Switzerland is derived from unconsolidated Quaternary aquifers are at a depth < 50 m. Thus, no conflict of use is likely between geo-methanation, and these currently exploited shallow groundwaters. However, some mineral waters with commercially relevant salinities of less than 2.5 g/L are known rarely at depths of up to 1000 m (Waber et al., 2015). In karst regions (e.g., along the foot of the Jura mountain chain), potable groundwater may upwell from 200–300 m depth (Waber et al., 2015). It is therefore advisable to carefully evaluate each specific geo-methanation site for any potential conflict. Moreover, in the distant future, deeper aquifers might be targeted to ensure the potable water supply, although these tend to be more saline. In order to maintain the quality of these deep potable groundwater reserves, current concepts for geo-methanation consider only formations containing groundwaters with salinities > 30 g/L (Table 5-1).

5.6.3 Mineral resources

A number of different resources have historically been and are currently exploited in the Swiss Molasse Basin:

- Sandstone: used as building stones
- Clay: raw material for the brick industry
- Gypsum: raw material for building materials
- Salt: raw material for the chemical industry, water treatment, road and table salt

The sandstones potentially have reservoir characteristics while the clays and evaporites could act as seals. However, for economic reasons, building stone, clay and gypsum are all exclusively quarried in open pits at the surface. These rocks also occur within the depth interval of interest for geo-methanation but while there are reserves at or near the surface which can be exploited (in Switzerland or abroad), there is no interest in exploiting deeper reserves of these commodities of low commercial value.

Salt is produced by dissolution mining along the northernmost edge of the SMB near Basel. This type of production is currently profitable down to about 450 m. There are further reserves at greater depth, including the depth interval of interest for geo-methanation. However, large quantities of salt are present at shallower depth in the Jura Mountains. It is therefore unlikely that the salt formations at depths > 600 m, which can be excellent seals for potential geo-methanation reservoirs, are compromised.

In addition to the above mineable commodities, ore deposits (e.g., Cu, Zn, Pb and U) are known to occur in many sedimentary basins worldwide. However, the geological history and small size of the SMB are not thought to have been conducive to the formation of such ores. So far, there are no geological, geophysical or geochemical indications that such deposits could exist in the subsurface of the SMB, and the geological history and small size of the SMB are considered to be unfavorable for the formation of such ores. Accordingly, no exploration for deep ore deposits has ever taken place in the SMB. In the unlikely case of discoveries large enough to warrant mining at depths greater than 600 m, a conflict of interest would arise with respect to geo-methanation.

5.6.4 Hydrocarbons and coal

5.6.4.1. Oil and natural gas

Exploration for conventional hydrocarbons in the Swiss Molasse Basin has been ongoing for around 110 years. However, only one semi-commercial gas field (Entlebuch) has been discovered despite abundant oil and gas shows in wells and at the surface (Leu, 2012).

Nearly all formations with reservoir characteristics in the subsurface of the SMB have shown traces of hydrocarbons in one or more wells. This indicates that any of the identified potential reservoirs for geo-methanation might contain some oil or gas, especially since trap structures (anticlines and to a lesser degree fault-bounded traps) are the primary exploration target for geo-methanation. However, based on the long history of failed hydrocarbon exploration in Switzerland, it is unlikely that any encountered hydrocarbons would have commercial value. A conflict of use is therefore not expected. However, the presence of hydrocarbons can present a substantial risk for drilling operations and should always be considered during planning.

In the last 15 years, several formations have been investigated for their potential as unconventional reservoirs, i.e., for shale gas or coal bed methane (CBM). Potential shale gas formations include the Carboniferous terrigenous sediments (Pre-Weitenau Formation) and Early Jurassic marine shales ("Toarcian shales" in the western SMB, the Rietheim Member of the Staffelegg Formation in Northern Switzerland; Leu & Gautschi, 2014). Palaeozoic troughs are present or are assumed to be present beneath the Mesozoic sediments in a large part of the SBM. Similarly, the marine shales can be found across the entire SMB. A potential reservoir for geo-methanation would thus likely be in an area where potential shale gas resources are present. There is a clear conflict of interest between the two technologies: both Carboniferous and Early Jurassic shales act as caprocks for potential reservoir formations for geo-methanation (channel sandstones of the Pre-Weitenau Formation and Beggingen Member of the Staffelegg Formation, respectively). While geo-methanation relies on these two caprocks being intact, shale gas production relies on fracturing them. However, due to the large lateral extent of shale gas formations and the small volume required for a geo-methanation reservoir, a conflict of interest could be avoided by proper coordination.

The possible presence of CBM is limited to the coal seams of the Carboniferous sediments of the Palaeozoic troughs. So far, such coal seams have only been confirmed by drilling in the Weiach area. However, based on the organic geochemistry of hydrocarbon shows, carbonaceous sediments are inferred to be present in the Geneva basin (Do Couto et al., 2021) and in the St. Gallen area (Omodeo-Salé et al., 2020). Due to the small volume of coal that has been found or can be assumed to be present, the potential of CBM in Switzerland is limited and commercial production is not envisaged. Despite geo-methanation potentially targeting the same formations or overlying formations, a conflict of interest is therefore not envisaged.

5.6.4.2. Coal

Evidence for the presence of coal seams in the SMB is summarized in the above paragraph on CBM. As is the case for CBM exploitation, the likely small volumes of coal present, their great depths and render profitable mining unlikely, even if the environmental concerns of burning coal could be mitigated by CO_2 sequestration. Therefore, no conflict of use between coal and geo-methanation in the Pre-Weitenau Formation or any overlying formations is envisioned.

5.6.5 Geothermal energy

5.6.5.1. Shallow geothermal: Ground source heat pumps (GSHP)

Shallow geothermal energy is widely exploited in the SMB in conjunction with heat pumps for space heating. In 2021, over 110,000 GSHP had been installed in Switzerland and by 2050 this number is expected to reach 250,000 installations. Boreholes for GSHP are typically only 120 to 150 m deep. Thus, there is currently no conflict of use between geo-methanation, but this could change in the future if deeper wells begin to be used for GSHP, as they could potentially breach the seal formation of a geo-methanation reservoir.

In a few cases, much deeper wells (500 to over 2700 m) have been used for GSHP applications. However, these are mostly instances where a failed deep well (e.g., a dry hydrothermal well) has been retroactively fitted as a GSHP. Nevertheless, in the future these deeper GSHP might become more common and then a conflict of use between such systems and geo-methanation could arise at specific sites.

5.6.5.2. Medium-depth geothermal: Hydrothermal energy

Medium depth geothermal in Switzerland makes use of naturally occurring warm/hot groundwaters at depths of 500 to around 4500 m (Geothermie Schweiz, 2022). Thus, they cover the entire depth range suitable for geo-methanation. They also target the same lithologies as they too rely on formations with good fluid-reservoir characteristics. However, for a commercially viable hydrothermal system, production rates of several tens of liters of groundwater per second have to be reached. In the SMB this is mostly achieved in reservoir formations where, in addition to matrix porosity and permeability, additional flow paths have been created by faults, fractures and karst features. Fractured reservoirs are likely unsuitable for geo-methanation as fractures often propagate across the overlying seal as well, creating paths for gas to escape. Therefore, conflicts of use between geo-methanation and medium-depth geothermal are foreseeable only in very porous and permeable formations.

Most of the thermal water occurrences in the SMB are concentrated in the eastern part of the Canton of Aargau (Schinznach, Baden, Zurzach). The thermal waters are linked to major, steeply-dipping faults surrounding the Permo-Carboniferous troughs (McCann et al., 2006). These structures permit warm basement fluids to rise rapidly from depths of several hundreds of meters. However, where such normal faults related to Palaeozoic troughs are impermeable, they may bound gas traps in the Dinkelberg Formation and possibly younger formations as well (e.g., Figure 5-20). Thus, rather than causing a conflict of use, water-conducting fault zones help to exclude areas that are unsuitable for geo-methanation and hence they delineate areas that are uninteresting for exploration.

5.6.5.3. Deep geothermal: Enhanced geothermal systems

Deep geothermal systems in the SMB target largely intact crystalline basement at depths of over 4.5 km. This is substantially deeper than the depth range of interest to geo-methanation. However, the wells of a potential EGS system would penetrate all Tertiary and Mesozoic strata. This could lead to a conflict of interest, if an area suitable for EGS underlies an area suitable for geo-methanation, as the integrity of the caprock would be endangered. Due to the relatively small size of potential geo-methanation reservoirs, the large vertical distance between the two reservoir depths and the fact that inclined wells may be envisaged for EGS, conflict of use should be avoidable with good project coordination.

5.6.6 Seasonal storage

5.6.6.1. Aquifer thermal energy storage (ATES)

ATES projects may target a variety of depth ranges, depending on the temperature of the injected water. For low temperature ATES (< 40 °C) the target depths are often only a few tens of metres while high-temperature ATES more commonly targets depths of 130 to 500 m. This is shallower than the minimum depth required for geo-methanation. A potential geo-methanation well could thus penetrate the reservoir and seal of an ATES reservoir. As water is less mobile, this is less critical than the piercing of a caprock of a reservoir containing gases. Careful completion of the geo-methanation well may be sufficient to circumvent a conflict. Similarly to geo-methanation, an ATES system does not take up huge volumes and it may thus be possible to avoid such a spatial interference.

Reservoirs at depths of over 1200 m have also been used successfully for HT-ATES outside of Switzerland, showing that the technology is in principle feasible in the depth interval needed for geo-methanation. The two technologies could therefore target the same potential reservoirs, but HT-ATES typically does not require a fluid trap structure. In areas where trap structures are proven or likely, priority should thus be given to geo-methanation (and other gas storage applications). Where the integrity of the seal is not sufficient, ATES might be a valuable alternative to make use of an area originally targeted for geo-methanation. Applying both technologies close to each other in the same reservoir may pose a conflict due to fluctuations in far-field pressure of the formation water induced by pressure control measures (injection and/or extraction of fluid).

5.6.6.2. Seasonal storage of natural gas or hydrogen

The suitable depth interval for seasonal gas storage is generally between 600 and 3000 m. This overlaps with the depth interval in which geo-methanation is possible. Outside Switzerland, exhausted natural gas reservoirs are favored sites for seasonal gas storage. However, Switzerland has no known gas reservoirs, whether exploited or not, that could be re-purposed for gas storage. Injection into sealed porous aquifers containing trap structures would be an alternative. These plays are identical to those targeted for geo-methanation, thus a direct conflict of use seems assured. However, the two technologies could make use of the same reservoirs alternately, e.g., by storing the gas that is most profitable in any given year or season.

5.6.7 CO_2-sequestration

According to Chevalier et al. (2010), the suitable depth interval for CO_2-sequestration in the SMB is 800 to 2500 m. This largely overlaps with the depth interval in which geo-methanation is possible. The two technologies also target the same sealed reservoir formations and trap structures. A conflict of use between the technologies is therefore likely, especially as the volume of sealed reservoirs with suitable petrophysical properties in the SMB is likely limited. Whether or not to fill this limited space permanently with CO_2 or use it for seasonal storage purposes (geo-methanation but also seasonal storage of CH_4 and H_2) is a political question.

The only difference between the two technologies is the reservoir volume targeted. In order to make a significant impact on CO_2 emissions, a permanent sequestration reservoir for CO_2 needs to have a large volume (i.e., be laterally extensive and > 20 m thick; Chadwick et al., 2008). Geo-methanation, on the other hand, is a storage approach whereby the gases are injected and extracted into the same reservoir volume cyclically, requiring a much smaller overall volume. Some small sealed reservoir areas might therefore be suitable for geo-methanation while unsuitable for CO_2 sequestration. This is especially likely in reservoirs consisting of laterally constrained porous bodies within a low-porosity formation (e.g., OSM, USM, Klettgau Formation and Pre-Weitenau Formation).

5.6.8 Radioactive waste disposal

The final geological repository for nuclear waste in Switzerland will be hosted in the Opalinus Clay in Northern Switzerland at a depth of 400 – 1000 m (Nagra, 2022c). While the Opalinus Clay is an aquitard and therefore is of no interest as a geo-methanation reservoir, the aquitards above and below are potentially suitable for geo-methanation. The primary concern for a nuclear waste repository, however, is long-term isolation of the waste and therefore deep drilling projects are unlikely to be approved in the vicinity of the repository to ensure this. A conflict of use of the subsurface between radioactive waste disposal and geo-methanation is therefore likely.

In Switzerland, three potential siting regions for a final repository have been investigated in detail. These are (from west to east) Jura Ost, Nördlich Lägern and Zürich Nordost as marked in all maps in Chapter 5.4). In September 2022, Nördlich Lägern was identified as the region where conditions are ideal for the safe construction and operation of a final repository. While the Nuclear Energy Law dictates that a safe distance between the (potential) repository volume and any projects targeting the deep subsurface needs to be maintained, quantitative limits on this distance are not stipulated. It is therefore not yet possible to assess whether the entire region of Nördlich Lägern will have to be excluded for geo-methanation or only parts of it. Similarly, it is currently unclear whether or not the two remaining potential siting regions will be kept as reserve sites or if deep projects (e.g., geo-methanation) could perhaps be authorized in the near future. As the region of Northern Switzerland represents the best-studied area within the SMB (i.e., with the lowest geological risk) it is the prime target for the exploration for geo-methanation. In addition, it is the area where most Mesozoic formations fall within the required depth-temperature range for geo-methanation, increasing the number of potential reservoirs for geo-methanation.

5.6.9 Possible conflict of use vs. chance for joint exploration?

Several underground technologies may in principle target the same sealed reservoir formations and the same depth range of interest for geo-methanation. However, most of those require conditions slightly different (highlighted in **bold** below) to those required for geo-methanation:

- Natural gas: well-sealed reservoirs with traps **where economically significant amounts of gas have accumulated**. As a gas cushion is required for geo-methanation**,** such traps could perhaps be used for geo-methanation after part of the natural gas has been exploited or even during gas exploitation.
- Oil: well-sealed reservoirs with traps **where economically significant amounts of oil have accumulated**. Such traps could perhaps be used for geo-methanation once exploitation has depleted most of the oil.
- Medium depth geothermal energy: reservoirs with **high enough transmissivity (often fractured reservoirs) to allow for a substantial fluid production rate**.
- Seasonal storage – ATES: sealed reservoirs. **Traps are preferred but not crucial if the natural flow of groundwater is slow.**
- Seasonal storage – Natural gas or hydrogen: well-sealed reservoirs with traps, **regardless of their temperature**.
- CO_2-sequestration: well-sealed reservoirs with large volume traps.

The criteria listed in bold cannot be assessed by indirect geophysical methods from the surface. Instead, they require the drilling of wells from which petrophysical data can be collected (from wireline logs and sampling of core material) as well as hydraulic testing (e.g., pump or injection tests). Thus, a shift from focusing on the potential conflict of interest between the different technologies to joint exploration by parties with different application aims might be advisable. By doing that, the most suitable use of an encountered reservoir body could be decided on after its detailed characterization. This could minimize exploration risk and maximize success rates of underground projects.

Several of the listed technologies are (in principle) feasible at depths greater than the maximum depth envisaged for geo-methanation in the SMB (1400 to 1600 m). However, a detailed investigation of the Muschelkalk aquifer (Stamberg Member of the Schinznach Formation) showed that the reservoir properties become unfavourable at depths > 1500 m due to compaction and secondary dolomite cementation (Aschwanden et al., 2019a). As the geological formations above and below have been subjected to the same burial history, it can be assumed that, at least for the older Mesozoic units, the petrophysical properties are equally unfavorable at these depths. Therefore, more exploration projects would likely be targeting the depth interval between ca. 500 and 1500 m, making coordination between potentially conflicting projects more vital.

An additional issue which renders conflicts of use more likely and coordination between projects more important is the degree of exploration maturity (i.e., knowledge of the subsurface) in different regions within the SMB (Figure 5-6). Overall, exploration maturity is relatively low, imparting a high risk of failure or underperformance to new projects. In order to avoid this, areas which have been studied in greater detail represent more interesting potential targets. In the SMB these areas are primarily in NE Switzerland, which for several decades has been explored for a deep repository for nuclear waste and the Geneva Basin, which has seen extensive geothermal exploration in recent years. In these areas, the geometries and, to a degree, reservoir properties of different formations are better constrained than

in the rest of the SMB. This strongly reduces the exploration risk for new projects, irrespective of the technology. Northern Switzerland is also the only area where, due to the gentle SE-dip and relatively weak burial compaction of the pre-Tertiary strata, the Mesozoic and Palaeozoic sediments are sufficiently shallow and porous for geo-methanation and for many of the other geo-resource technologies. On the other hand, possible conflicts of use in NE Switzerland are exacerbated by the presence of three potential siting regions for a nuclear waste repository, the occurrences of the highest heat flow and largest abundance of thermal waters in the basin, as well as the only explored Palaeozoic trough (with potential for fluid reservoirs and coal resources).

5.7 Outlook

Our understanding of the composition and the properties of the subsurface of the SMB are based on a relatively small amount of data which are unevenly distributed (heavy focus on Northern Switzerland and the Mesozoic formations over the Tertiary ones). This results in a relatively high exploration risk, especially outside the well-studied areas. Within the well-studied areas, potential conflicts over the utilization of the subsurface might arise (Chapter 5.6). The best solution to solve these issues would be an SMB-wide exploration campaign as recently proposed in Swiss Federal Parliamentary Motion 20.4063, to increase the data on the subsurface of the SMB and generally reduce the exploration risk. However, the costs and sheer size of such an undertaking are prohibitive. An alternative is to define a number of smaller areas of interest, which are then explored in detail rather than conducting a basin-wide exploration program. These areas would ideally fill in blanks on the exploration map of Switzerland (Figure 5-6) and cover both the Mesozoic and Tertiary units. Another approach would be to re-evaluate and re-compile all existing subsurface data, regardless of the original motivation for their acquisition, to create a basis for all kinds of underground technologies. To be effective this would require obtaining rights to make private data (e.g., old wells and seismic data) publicly available for compilation.

A further option are detailed studies on individual formations and their aquifers, such as the work on the Muschelkalk Group by Aschwanden et al. (2019a, b), Adams and Diamond (2019) and Adams et al. (2019), or the rock-typing approach by Rusillon (2016) for the reef complexes in the GGB. These studies do not necessarily have a specific technological application in mind but focus on understanding the geological history of a single formation. Such studies should include assessment of depositional facies, diagenetic and burial history as well as the evaluation of petrophysical properties to allow for better inter- and extrapolation across the SMB. Studies evaluating the different formations of the Molasse deposits are especially crucial. These units make up large volumes of the sedimentary filling of the SMB but are very poorly studied. They also show geometries which appear well suited to seasonal storage of both gases and fluids (e.g., hot water).

Another area of research which can be done largely using existing data is defining structures (faults, folds) in more detail. Structures had to be simplified in order to be incorporated into GeoMol. However, understanding their real complexity is crucial in assessing their potential to act as traps. Thus, a re-evaluation focusing on the genesis of families of structures in the areas of interest to this study would be beneficial to further exploration for geo-methanation but also for other storage applications in the subsurface (e.g., seasonal gas or hot water storage, CO_2 sequestration; Chapter 5.6.9).

5.7.1 Open question: Geo-methanation up to 90 °C?

For this study, we adopted a temperature range of 30 to 60 °C as a limiting condition for geo-methanation, based on the experience at the Lehen site in Austria and the related laboratory experiments performed by BOKU (see chapter 2). However, geo-methanation at higher temperatures (i.e., up to 100 °C) is known to occur commonly in nature. Recent results from BOKU suggest that temperatures above 60 °C might even be advantageous for USC-type geo-methanation. At these temperatures, microbially mediated acetogenesis (whereby CO_2 and H_2 are converted to acetate, CH_3COOH, instead of methane) seems to be inhibited and thus methane production is increased (see chapter 2.1.3).

In theory, it would be possible to re-map the distribution of all potential reservoir formations using an upper temperature limit of 90°C (isotherm already included in T-model of GeoMol). This would substantially increase the delimited areas for all formations towards the south and west of the SMB. However, there are a few reasons why this might not be beneficial.

The first is that the exploration maturity of the SMB is in general relatively low (Chapter 5.3.2). The best explored areas, where the reliability of geological information is highest and the exploration risk lowest, are in the northern (to north eastern) SMB (Figure 5-6). This is the reason why many of the interesting formations have been stratigraphically studied and formally defined only in this area, while no formal definition exists further afield. Therefore, expanding the screening to temperatures up to 90 °C would increase the area where geo-methanation is theoretically possible but would also strongly increase the geological uncertainties and thus increase exploration risk, especially in the southern SMB where the number of wells is low (Figure 5-5).

Increasing the temperature would not only increase the geographical area where geo-methanation is possible but also the depth range at which the formations are of potential interest. The disadvantage brought by increasing depth is that formations generally become tighter, i.e., lose porosity and permeability due to increased burial. A well-studied example is the Stamberg Member of the Schinznach Formation (Chapter 5.3.3). In Riehen (BL), the formation is transmissive enough to allow for the production of nearly 20 L/s of geothermal water from 1500 m depth. Similarly, at Schlattingen (TG), 6 L/s are produced from 1200 m depth. At Triemli (ZH), the same formation showed negligible transmissivity at a depth of 2700 m. As most of the formations are already closer to the cautionary porosity value than the positive value (Table 5-3), increasing the depth would likely render more formations and/or areas unsuitable for geo-methanation based on the petrophysical properties. Together with the increased geological risk, the high uncertainties with respect to petrophysical properties make these deeper zones high risk targets for future exploration. In addition, drilling to and operation at greater depths is costlier. This would need to be taken into account as part of the economic viability scoping calculations.

5.8 Summary and conclusions

In order to evaluate the geological units in Switzerland for their suitability for the USC-FlexStore technology, this report first defines geological criteria required for successful geo-methanation. The criteria (presented in Chapter 5.2) are based on the experience of project partner RAG at the pilot site in Lehen (Austria; Chapter 4), on information from project partner BOKU (Chapter 2) regarding activity of methanogenic microbes, and on best-practice principles from the literature on geological storage of CO_2. The resulting set of criteria for reservoir formations suitable for gas storage concern properties governing its gas storage capacity (thickness, volume, depth range, rock matrix porosities), gas injectibility and production (rock-matrix permeability and fracture distribution) and microbial activity (temperature interval, ranges of pH and salinity of groundwater). Equally important are criteria that govern gas retention in the subsurface such as minimum reservoir depth, presence of an impermeable caprock sealing the reservoir formation and of trap structures such as anticlines, changes in depositional environment resulting in intercalated reservoir rocks (= stratigraphic trapping) and seals or impermeable faults.

In view of these criteria, our consideration of the geology of Switzerland and of the availability of information on its subsurface led us to discard the following regions from study: the Folded Jura Mountains, the Tabular Jura Mountains, the Sub-Alpine Molasse and the Alpine realm. Thus, the present study deals exclusively with the remaining geological realm known as the Swiss Molasse Basin (SMB). This coincides geographically with the Swiss Plateau, where the majority of the Swiss population lives and works.

In Chapter 5.3 the geology of the SMB and the past and present exploration campaigns of the subsurface are described. Overall, the SMB consists of a sequence of sedimentary rocks of Palaeozoic, Mesozoic and Cenozoic age atop the crystalline basement. The SMB has been explored for hydrocarbons mostly since the second half of the 20th century, for sites suitable for disposal of radioactive waste since the 1980s, and more recently for geothermal energy, thermal energy storage and geological sequestration of CO_2. Despite this activity, the exploration maturity of the SMB is generally low and highly heterogeneous. Besides a geographical bias of information density towards northern Switzerland, there is also a clear bias towards the Mesozoic sediments rather than the Palaeozoic or Tertiary ones. A key information source for the present study is the GeoMol digital model of the anatomy of the SMB, which defines the three-dimensional (3D) disposition of horizons separating major geological units (mostly at the stratigraphic Group level). This model, constructed and made available by the Swiss Federal Office of Topography (Swisstopo), includes major faults and fold axes, and is linked to a 3D temperature model of most of the SMB.

Chapter 5.4 presents a compilation of all relevant information on the geological units within the Swiss Molasse Basin from published literature. This includes data on the lithology, geographical distribution, thickness and petrophysical properties (porosity and permeability). In addition, we attempted to assess how homogeneous or heterogeneous all of these characteristics are within a unit, both laterally and vertically as well as the state of knowledge. Based on this and the geological criteria for geo-methanation in Chapter 5.2, we assigned ranked each of the identified reservoir formations. A ranking scale of 1 to 4 was applied, where 1 denotes "potentially suitable for geo-methanation" and 4 denotes "likely unsuitable for geo-methanation". This step led to exclusion of two fracture- and karst-based aquifers, as these do not permit containment of gas within a predictable zone over the required time periods. The remaining units were ranked as follows:

1 Sandstones of the Triassic Dinkelberg Formation
1 Dolomites of the Triassic Schinznach Formation – Stamberg Member

2 Sandstones and dolomites of the Triassic Klettgau Formation – SBEG Members
2 Oolitic limestones of the Jurassic Hauptrogenstein,
2 Channel sandstones of the Oligocene/Miocene Lower Freshwater Molasse (USM)
2 Beach sandstones of the Miocene Upper Marine Molasse (OMM)
2 River-channel sandstones of the Miocene Upper Freshwater Molasse (OSM)

3 Sandstones of the Carboniferous Pre-Weitenau Formation
3 Limestones of the Jurassic Staffelegg Formation – Beggingen Member
3 Limestones of the Etiollets Formation

For each of the units ranked 1 to 3, we derived maps showing where the formations occur within the required depth–temperature interval according to the 3D geological and temperature models. Most of the Mesozoic units fall within the target range only along the foot of the Jura Mountains and/or in Northern Switzerland. The Tertiary strata fall within the desired depth–temperature interval away from the Subjurassic Zone to the south and across the central SMB. In addition, for each unit, the depth to the formation, the thickness of the formation and any fractures and folds affecting the unit were mapped. These maps show three key results: (1) Areas *not* classified as "sealed aquifers". These should be understood as regions where gas storage and geo-methanation are *unlikely to be feasible*, based on the current state of geological knowledge. (2) Areas delimited as "sealed aquifers". These should be understood as regions where gas storage and geo-methanation *may well be feasible*, once more detailed (km-scale) subsurface information becomes available, particularly regarding gas traps. (3) Sites within the delimited reservoirs where anticlines are known to exist. These are favored traps for gas storage but their closure and gas retentivity are unknown and cannot be deduced from the literature. Exploration costs and risks are lowered by drilling in areas where several potential reservoir units are present in the subsurface, stacked one upon the other. Based on this principle, the color-coded map in Figure 5-24 (a repeat of Figure 5.20) shows the most suitable areas for geo-methanation exploration in the SMB. The color scale reflects the number of potentially suitable sealed aquifers in the subsurface, each aquifer weighted by its quality ranking. Priority exploration targets are defined where the most suitable areas (darker greens) coincide with the known presence of anticlines (blue lines).

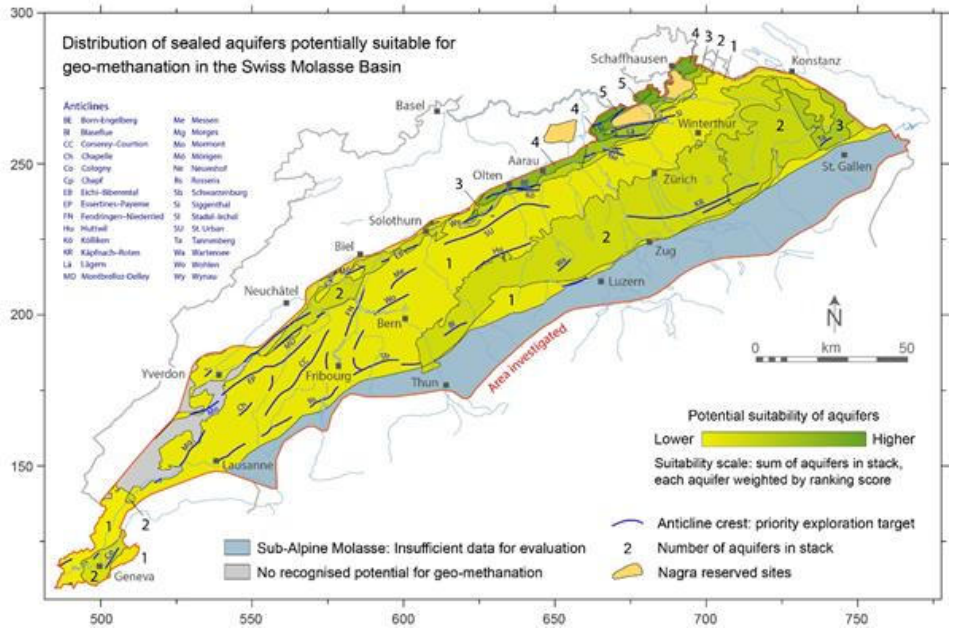

Figure 5-24: Map showing relative suitability of areas in the Swiss Molasse Basin for geological gas storage under conditions required for geo-methanation (greater than 600 m deep, temperature 30–60 °C). Shades of denote the sum of sealed aquifer formations locally present in the sedimentary stack, each weighted by its quality ranking. Future wells drilled through several aquifers have higher likelihood of finding suitable reservoirs. Gas trap structures are essential for successful geo-methanation: blue lines show locations of known elongated dome structures (anticlines) that may serve as traps and are therefore priority exploration targets. Areas distant from blue lines may or may not contain anticlines. Faults may also create gas traps but less commonly than anticlines - see maps in Chapter 5.4 for fault locations.

Chapter 5.5 outlines the future steps required to establish *definitive feasibility* of geo-methanation in the SMB. This will entail new exploration campaigns focusing at the km-scale on one or more of the potential gas traps shown in our maps. These campaigns should conduct seismic surveys (preferably in 3D), drilling of new wells including their coring and logging, and hydraulic testing of the traps. This will prove whether gas can be injected, extracted and retained in the traps according to the technical requirements of commercially viable geo-methanation sites. The chances of discovering a natural gas cap in the SMB are low and therefore an artificial gas cap will likely need to be created to serve as a pressure cushion. This would require injection of ≥ 4.5 million m^3_{STP} into the trap. Such a campaign targeted at a first potential trap structure is estimated to take approximately 12 years to complete and would cost approximately CHF 39 million (*indicative estimate*). If the first campaign fails to demonstrate a suitable geo-methanation site, then each further exploration attempt could entail similar investments of costs and time. There are numerous options to reduce costs and time, including entering joint ventures, procuring existing geophysical surveys, re-evaluating previously explored structures, and drilling into structures that enclose more than one prospective sealed aquifer. However, even after several attempts, there is no guarantee that the investments would yield in a successful geo-methanation site.

Chapter 5.6 discusses potential conflicts of use of the subsurface in the SMB. Several of the underground technologies discussed may in principle target the same sealed reservoir formations and the same depth range of interest for geo-methanation. However, most of those require conditions slightly different to those required for geo-methanation, e.g., high transmissivities for hydrothermal systems, presence of oil/gas for hydrocarbon exploitation. These conditions, however, cannot be assessed by indirect geophysical methods from the surface. Instead, they require the drilling of wells to assess in-situ conditions. A shift from focusing on the potential conflict of interest and trying to avoid it to joint exploration by parties with different application aims could minimize exploration risk and maximize success rates of underground projects.

In a final outlook, Chapter 5.8 addresses other topics arising from our study. (1) Further exploration is encouraged in the structurally complex Sub-Alpine Molasse. Unfortunately, its internal makeup is not well defined, and it is not included in the GeoMol model. However, a comparison with Austria is suggestive. The tectonic setting of the large natural gas reservoirs discovered and exploited in Salzburg is comparable to that of the Sub-Alpine Molasse in Switzerland. The Tabular Jura Mountains also warrants detailed consideration. (2) Suggestions are provided for additional scientific and exploration studies that could be undertaken to support implementation of gas storage and geo-methanation in the SMB in general. (3) Methanogenic microorganisms are known to flourish at temperatures at least up to 90 °C in some environments, opening the possibility that geo-methanation could be implemented at greater depths in the SMB than considered in the present study. However, the literature shows that porosity and permeability in the SMB units decrease rapidly with depth of burial, implying that little will be gained by the costlier enterprise of drilling deeper.

5.9 Abbreviations

ATES	Aquifer Thermal Energy Storage
BL	Swiss Canton of Basel-Landschaft
$CaSO_4$	Calcium Sulphate
CCS	Carbon Capture and Storage
CO_2	Carbon-Dioxide
Fm.	Formation
H_2	Hydrogen
H_2O	Water
HT	High Temperature
KCl	Potassium Chloride
Ma	Million years
mD	Millidarcy
MWIP	Municipal Waste Incineration Plant
NaCl	Sodium Chloride
OMM	Upper Marine Molasse (Obere Meeres Molasse)
OSM	Upper Freshwater Molasse (Obere Süsswasser Molasse)
pH	Acidity
SMB	Swiss Molasse Basin
TBO	Deep Well (TiefenBOhrung)
TG	Swiss Canton of Thurgau
T-range	Temperature Range
UMM	Lower Marine Molasse (Untere Meeres Molasse)
USM	Lower Freshwater Molasse (Untere Süsswasser Molasse)
ZH	Swiss Canton of Zürich

5.10 References

Adams, A. and Diamond, L.W. (2019) Facies and depositional environments of the Upper Muschelkalk (Schinznach Formation, Middle Triassic) in northern Switzerland. Swiss Journal of Geosciences, 112, 357–381.

Adams, A., Diamond, L. W., & Aschwanden, L. (2019). Dolomitization by hypersaline reflux into dense groundwaters as revealed by vertical trends in strontium and oxygen isotopes: Upper Muschelkalk, Switzerland. Sedimentology, 66(1), 362-390.

Allenbach, R., Baumberger, R., Kurmann, E., Michael, C. S. & Reynolds, L. (2017) GeoMol: Geologisches 3D-Modell des Schweizer Molassebeckens – Schlussbericht. Bundesamt für Landestopographie swisstopo, Bern, p. 128.

Aschwanden, L., Diamond, L. W., & Adams, A. (2019a). Effects of progressive burial on matrix porosity and permeability of dolostones in the foreland basin of the Alpine Orogen, Switzerland. Marine and petroleum geology, 100, 148-164.

Aschwanden, L., Diamond, L. W., Mazurek, M. & Davis, D. W. (2019b) Creation of Secondary Porosity in Dolostones by Upwelling Basement Water in the Foreland of the Alpine Orogen. Geofluids 2019, 1-23.

Chadwick, A., Arts, R., Bernstone, C., May, F., Thibeau, S., & Zweigel, P. (2008). Best practice for the storage of CO2 in saline aquifers-observations and guidelines from the SACS and CO2STORE projects (Vol. 14). British Geological Survey.

Chen, Y. and Cheng, J. J. (2007). Effect of potassium inhibition on the thermophilic anaerobic digestion of swine waste. Water environment research, 79(6), 667-674.

Chevalier, G., Diamond, L.W. and Leu, W. (2010) Potential for deep geological sequestration of CO 2 in Switzerland: a first appraisal. Swiss Journal of Geosciences 103, 427-455.

Diamond, L. W., Wanner, C., & Waber, H. N. (2018). Penetration depth of meteoric water in orogenic geothermal systems. Geology, 46(12), 1063-1066.

Do Couto, D., Garel, S., Moscariello, A., Bou Daher, S., Littke, R., & Weniger, P. (2021). Origins of hydrocarbons in the Geneva Basin: insights from oil, gas and source rock organic geochemistry. Swiss Journal of Geosciences, 114(1), 1-28.

Gander, P. (2004). Geologie und Hydrogeologie der Oberen Süsswassermolasse – Dokumentation des aktuellen Kenntnisstandes. Nagra Arbeitsbericht NAB 04-04, Nagra, Wettingen, p. 70.

Häring M. O., Leu W., Zappone A. and Diamond L. W. (2013) Road map to a CO2 injection test in Switzerland. In Mazzotti et al., Roadmap for a Carbon Dioxide Capture and Storage pilot project in Switzerland. Report for BFE contract SI/500827-01 prepared for Swiss Federal Offices for Energy and Environment, 21 pp.

IEA-GHG. (2009). Development of storage coefficients for CO2 storage in deep saline formations (118 pp). Technical study report 2009/13. Stoke Orchard (UK): IEA Greenhouse Gas R&D Programme.

Jenny, J., Burri, J.P., Muralt, R., Pugin, A., Schegg, R., Ungemach, P., Vuataz, F.D. & Wernli, R. (1995). Le forage géothermique de Thônex (Canton de Genève): Aspects stratigraphiques, tectoniques, diagénétiques, géophysiques et hydrogéologiques. Eclogae Geologicae Helvetiae, 88(2), 365-396.

Jordan, P. (2016). Reorganisation of the Triassic stratigraphic nomenclature of northern Switzerland: overview and the new Dinkelberg, Kaiseraugst and Zeglingen formations. Swiss Journal of Geosciences, 109(2), 241-255.

Jordan, P. and Deplazes, G. (2019). Lithostratigraphy of Consolidated Rocks expected in the Jura Ost, Nördlich Lägern and Zürich Nordost Regions. Nagra Arbeitsbericht NAB 19-14, Nagra, Wettingen, p. 188.

Kuhlemann, J., & Kempf, O. (2002). Post-Eocene evolution of the North Alpine Foreland Basin and its response to Alpine tectonics. Sedimentary Geology, 152(1–2), 45–78.

Lahusen, P. H. (1992). Hydrocarbon exploration in the Swiss Molasse Basin. Eclogae Geologicae Helvetiae 85, 707–714.

Leu, W. (2012). Swiss oil/gas exploration and lessons learnt. Swiss Bulletin für angewandte Geologie 17(1), 49–59.

Leu, W., & Gautschi, A. (2014). The shale gas potential of the Opalinus Clay and Posidonia Shale in Switzerland-A first assessment. Swiss Bulletin für Angewandte Geologie, 19(2), 95-107.

Mazurek, M., Hurford, A. J., & Leu, W. (2006). Unravelling the multi-stage burial history of the Swiss Molasse Basin: Integration of apatite fission track, vitrinite reflectance and biomarker isomerisation analysis. Basin Research, 18, 27–50.

McCann, T., Pascal, C., Timmerman, M. J., Krzywiec, P., López-Gómez, J., Wetzel, L., ... & Lamarche, J. (2006). Post-Variscan (end Carboniferous-Early Permian) basin evolution in western and central Europe. Geological Society, London, Memoirs, 32(1), 355-388.

Nagra (2022c) Der Standort für das Tiefenlager – Der Vorschlag der Nagra. Bericht (68 pp.), Nagra, Wettingen.

Omodeo-Salé, S., Eruteya, O. E., Cassola, T., Baniasad, A., & Moscariello, A. (2020). A basin thermal modelling approach to mitigate geothermal energy exploration risks: The St. Gallen case study (eastern Switzerland). Geothermics, 87, 101876.

Pietsch, J. S., Wetzel, A., & Jordan, P. (2016). A new lithostratigraphic scheme for the Schinznach Formation (upper part of the Muschelkalk Group of northern Switzerland). Swiss Journal of Geosciences, 109(2), 285-307.

Pfiffner O.A. (2021) The Geology of Switzerland. In: Reynard E. (eds) Landscapes and Landforms of Switzerland. World Geomorphological Landscapes. Springer, Cham.

Platt, N. H., & Keller, B. (1992). Distal alluvial deposits in a foreland basin setting—the Lower Freshwater Miocene), Switzerland: sedimentology, architecture and palaeosols. Sedimentology, 39(4), 545-565.

Reisdorf, A. G., Wetzel, A., Schlatter, R., & Jordan, P. (2011). The Staffelegg Formation: a new stratigraphic scheme for the Early Jurassic of northern Switzerland. Swiss Journal of Geosciences, 104(1), 97-146.

Rusillon, E. (2017). Characterisation and rock typing of deep geothermal reservoirs in the Greater Geneva Basin (Switzerland & France). Doctoral dissertation, University of Geneva.

Sommaruga, A., Mosar, J., Schori, M., & Gruber, M. (2017). The role of the Triassic evaporites underneath the North Alpine Foreland. In Permo-Triassic Salt Provinces of Europe, North Africa and the Atlantic Margins (pp. 447-466). Elsevier.

Strobel, G., Hagemann, B., Huppertz, T. M., & Ganzer, L. (2020). Underground bio-methanation: Concept and potential. Renewable and Sustainable Energy Reviews, 123, 109747.

Vollmayr, T., & Wendt, A. (1987). Die Erdgasbohrung Entlebuch 1, ein Tiefenaufschluss am Alpennordrand. Bulletin der Vereinigung schweizerischer Petroleum-Geologen und-Ingenieure, 53(125), 67-79.

Waber, H.N., Heidinger, M., Lorenz, G. and Traber, D. (2014). Hydrochemie und Isotopenhydrogeologie von Tiefengrundwässern in der Nordschweiz und im angrenzenden Süddeutschland. Nagra Arbeitsbericht NAB 13-63, Nagra, Wettingen, p. 267.

Waber, N., Bissig, P., Huggenberger, P., Meylan, B., Milnes, E., Schürch, M., and Walter, U. (2015). Tiefengrundwasser. Aqua & Gas 4, 32–41.

5.11 Contact details

Institute of Geological Sciences, University of Bern
Dr. Daniela B. van den Heuvel
Baltzerstrasse 1+3
3012 Bern
Switzerland

+41 31 684 87 61
daniela.vandenheuvel@geo.unibe.ch
www.geo.unibe.ch/

Prof. Larryn W. Diamond

Ferdinando Musso Piantelli

Philippos Garefalakis

6 Operational and Economic considerations

6.1 Introduction

The content of this chapter is the investigation of techno-economic aspects of an installation on a single reservoir and generalization for Switzerland and development of a working use case as marketable service.

The tasks are:

1. Assessment, design and dimensioning of a single installation (OST)
2. Requirements for locations including options for changes in grid tariffs (OST)
3. Legal and economic constraints and boundary conditions (OST)
4. Scenarios for the buildup of storage capacities and potential in Switzerland, including socio-ecological and economic consideration based on literature research (OST)
5. Use cases for need-owners as a product and sector coupling service (OST)
6. Requirements to have gas recognized as renewable (OST, Energie 360°, RAG)

The aim is to analyze different scenarios for possible use cases. This includes the development of different plant concepts, the presentation of possible use cases as well as the cost analysis of the different concepts and their sensitivities. In particular, the major influencing factors are to be highlighted.

The basis for the content is formed by the results from the previous chapters and additional studies. The aim is to define what a geo-methanation plant in Switzerland would look like, what plant elements it could contain, what scale of plant is realistic and what costs are associated with it. In addition, the legal framework is briefly explained, and social acceptance is considered.

6.2 Materials, Methods

The basis for the operational and economic considerations is formed by the results from the previous chapters and additional studies. The aim is to show how geo-methanation could be realised in Switzerland.

The first step is to determine the framework conditions for a possible plant. This includes a literature study on the legal framework and social acceptance. The geological and process-specific framework conditions are based on results from the University of Bern and Boku Vienna. The site evaluation in Switzerland is based on results from Empa and the University of Bern.

In collaboration with RAG and Energie 360°, an evaluation was made of what a geo-methanation plant in Switzerland could look like. For this purpose, various plant concepts were developed, examined for their advantages and disadvantages, and the most suitable three concepts were selected for further evaluation.

Based on these three concepts, the techno-economic study could be carried out using the net present value (NPV) model. It is based on a NPV model that was developed in the EU project Store&Go[1]. The model calculates the power-to-gas production costs of hydrogen and methane and the NPV to produce the two gases in a power-to-gas plant. The calculation of the NPV results from the difference of the present value of cash inflows and outflows.

The present value of cash inflows is calculated as the sum of the gas revenue and the salvage value of the equipment, while «gas» can stand for methane, oxygen or hydrogen. The present value of cash

[1] For more information on the Store&Go project. https://www.storeandgo.info/

outflows consists of the sum of the investment and replacement costs, the operational costs as well as the feedstock costs for water, CO_2 and electricity. This model allows the assessment of the different service lives of various plant elements. This is particularly relevant for geo-methanation, as once an underground storage facility is developed, it can be used for an extensive period. Depreciation over the years is calculated using a discount rate.

The calculation of different plant concepts and sizes enables a comparison of the three concepts and their cost sensitivity. The overall results are discussed in connection with findings from the site assessment and the techno-economic study. In the economic analysis, the lifetime of the plant corresponds to the considered period. During this period the depreciation and operation of the plant is incorporated. The NPV is evaluated for this period and if positive, the operation is profitable.

The most cost-influential input parameters have been identified and are listed below in Table 6-1. The plant size is defined by size of the electrolyser. With the electrolyser's dependency on electricity and water, its size varies. The individual components of the plant are laid out accordingly, matching the size of the given electrolyser. Being the core of the operation, the size of the plant is always given in the size of the electrolyser. Please note, that all energy contents for gas are shown in the upper heating value. While in chapter 4 the lower heating value has more relevance due to its actual impact on the energy system, withing this chapter the upper heating value is of more relevance, since this value is generally accepted as standard for manufacturers, markets and need-owner. There is no discrepancy though, as comparable hydrogen production rates are given either in m^3 or in t.

Table 6-1: Important operating parameters when modelling the techno-economic parameters of a geo-methanation plant.

Parameter	Input data	Reference / Comment
Plant size (electrical input of electrolysis)	10-1'000 MW	Depending on user input.
Operating hours electrolysis	3000 h/a	Full load hours in the years 2016 to 2018 in scenario 4 (according to Figure 4-27, chapter 4.3.3.2)
Operating hours CO_2 source	8760 h/a	Constant addition of CO_2
Operating hours gas production	8760 h/a	Year-round gas production with distribution according to Energie 360° data
Lifetime of the plant	30 years	Assumption
Length methane pipeline	1 km	Assumption
Length hydrogen pipeline	1 km	Assumption
Discount rate	6%	Assumption

To calculate the production cost of the hydrogen, the price for electricity is an important parameter. The price depends on the yearly operating hours. The two extremes would be either to operate the plan only when cheap power is available or the whole year around, no matter the price of electricity. Since cheap electricity is only available at peak times of power production, the plant would choose to operate when there is excess electricity available. An uninterrupted operation would result in higher costs for electricity. Thus, there is an optimum of the operational hours to be found, depending on the availability of cheap electricity. The prices for electricity depending on operating hours is displayed in Table 6-2.

Table 6-2: Electricity prices depending on operating hours per year. Source: (Graf et al. 2021)

Full load hours per year	**1000**	**2000**	**3000**	**4000**	**5000**	**6000**	**7000**	**8000**
% of the year	11%	23%	34%	46%	57%	68%	80%	91%
Mean electricity price 2020 (€/MWh)	0.70	3.20	6.40	9.90	13.90	18.30	23.20	28.80
Mean electricity price 2030 (€/MWh)	2.50	7.70	13.90	20.60	28.00	36.00	44.80	54.60
Mean electricity price 2050 (€/MWh)	2.60	8.70	16.20	24.50	33.60	43.50	54.40	66.70

Based on these assumptions for the electricity costs, the economic efficiency calculation is carried out, using the figures for the year 2030. Next to electricity, additional feedstocks are needed. Their costs are described in Table 6-3.

Table 6-3: Costs of feedstock for a geo-methanation plant.

Feedstock§	**Input data**	**Reference / Comment**
Water	0.002 €/kg	SVGW: 2 CHF/m^3 drinking water[1]
Carbon dioxide	50 €/ t_{CO2}	Source: (Graf et al. 2021)[2], range: 5-350 €/t; assumption: at a pressure of 30 bar(a)
Cushion gas	0.3 €/m^3	Internal information (further information: chapter 6.3.5 Plant sizes)

[1] See http://trinkwasser.svgw.ch/index.php?id=762

[2] See "Heiz- und Brennwerte - OST"

The potential income from geo-methanation comes from the sale of the products. The three revenue generating products are listed in Table 6-4.

Table 6-4: Assumptions about the revenue from the sale of the products.

Product	**Input data**	**Reference / Comment**
Methane	1.54 €/m^3	Assumption biogas according to internal information: 14 Ct./kWh with 11.03 kWh/m^3 methane (volume-specific calorific value, gas volume at standard conditions (0 °C, 101 325 Pa))
Hydrogen	3.00 €/kg	Assumption
Revenue: Oxygen	50.0 €/t	Source: (Graf et al. 2021)

6.3 Results and Discussion

The groundwork for the results of the techno-economic study is laid by the previous chapters and additional studies.

6.3.1 Legal and economic framework conditions for a geo-methanation plant.

To be able to define one or more sites that would be suitable for geo-methanation, legal, geological, technical and economic considerations are necessary. The siting requirements are strongly dependent on the following three factors:

1) the geological findings by the University of Berne (see chapter 5),
2) the availability of gas and electrical infrastructure and
3) due to tariffs for the electricity grid; the local energy generation potential as determined by Empa (see chapter 4).

The framework conditions are also laid down by the legal foundations. Some important elements are presented below.

6.3.1.1. Legal and economic constraints

This chapter provides an overview of legal and economic constraints and boundary conditions including forecasts of future energy prices. According to a dispatch on the Federal Act on a Secure Electricity Supply with Renewable Energies, the Federal Council proposes to open up the electricity market to all customers (BFE, 2019). Since 2009, large consumers (from 100 000 kWh per year) have been able to choose their supplier themselves, which could also be possible for households and small businesses in the future.

Additionally, the opening of the electricity market also serves to strengthen decentralised electricity production. Today, the electricity market is mainly centralised. In the dispatch it states that the complete opening of the electricity market strengthens decentralised renewable electricity production. End consumers and consumers who produce electricity themselves (prosumers), producers and electricity suppliers are given economically important freedoms, thus better integrating renewable electricity in the market. To protect small end consumers such as households from price abuse, the provision of basic supply will be continued. In this, an electricity product is offered consisting exclusively of domestic renewable energy. Due to the partial or full opening of energy markets, energy prices for electricity will reflect national and European availability better and therefore be much more linked to supply and demand than today (Figure 6-1) (IEA, 2020).

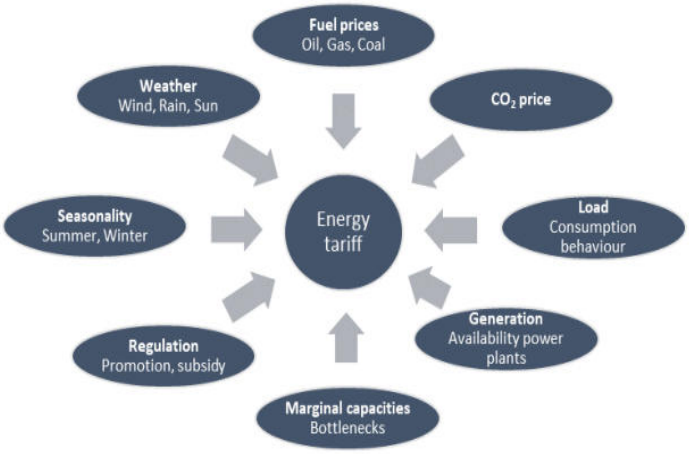

Figure 6-1: Factors influencing the pricing of electrical energy. Based on (VSE, 2020)

6.3.1.2. The energy tariff

The energy tariff is the price for the electrical energy supplied. Prices within Switzerland vary between network operators, sometimes considerably. Since 2009, large consumers with a consumption of more than 100,000 kWh/year can freely choose their electricity supplier and negotiate the electricity price on an individual basis. However, large consumers can also decide to forego participating at the free market - and purchase electricity at regulated prices from the local grid operator. Just like consumers with a consumption of less than 100,000 kWh/year, they remain so-called fixed customers. For fixed customers, the energy tariff is based on the production costs - and on long-term purchase contracts of the distribution grid operator (cf. Art. 4 StromVV).

In addition to the market price, several surcharges are added to the energy tariff for end customers, consisting of:

- Risk surcharges for balancing energy,
- risk surcharges for volume changes,
- system services (SDL),
- grid costs and
- concession fees.

6.3.1.3. Fees for the cost-covering feed-in remuneration (KEV) for the promotion of renewable energies

From 2018, a new system applies to support the production of renewable energies. New features include a modified feed-in tariff with obligations for direct marketing, investment contributions and a market premium for large-scale hydropower. To support this, a grid surcharge of 2.3 cents/kWh is levied on all end consumers on a solidarity basis. The maximum amount of the surcharge is determined within the legal framework by the Federal Council. (ElCom, 2021)

6.3.1.4. The price for grid usage (VSE, 2020)

The costs for the construction, operation and maintenance of the electricity grids are passed on to the end consumers through the grid usage tariffs. The tariff structure is precisely defined by the StromVG (Stromversorgungsgesetz; Electricity Supply Act) and StromVV (Stromversorgungsverordnung; Electricity Supply Ordinance). As a rule, there is a basic tariff that is supposed to cover the fixed costs such as metering and billing. A large part must be charged based on the energy consumed (energy tariff) due to the legal requirements. Swissgrid's system services include balancing power or compensation for power plants that are "black-start capable" (i.e., they can start without power after a blackout). These services not only prevent blackouts, but they also guarantee constant voltage and frequency. About one third of the grid costs are the capital costs (i.e., depreciation) of the installed infrastructure, especially lines, substations and transformer stations.

6.3.1.5. The levies (ElCom, n.d.)

Every year, the Federal Council determines the amount of the levy for the promotion of renewable energies, such as KEV/EVS, EIV, investment contributions and market premiums. The amount is equal throughout Switzerland. With the Energy Strategy 2050, this grid surcharge was increased to 2.3 cents/kWh. In addition, there are communal and cantonal levies and fees. These can be, for example, concession fees or local political energy levies. While in some communes there are no such levies, in others they amount to up to 7 cents per kWh.

6.3.1.6. Regionalization of grid tariffs

Prices within Switzerland vary between grid operators, sometimes considerably. The reasons for this are manyfold (ElCom):

- Different grid costs exist due to topographical conditions of the supply area, different consumption patterns of end consumers or efficiency differences of the grid operators.
- Differences in the energy tariff result from a differentiated ecological product mix, or from a different share of own production. Grid operators with advantageously negotiated procurement contracts in energy purchasing can offer energy more cheaply than companies with a high share of expensive own production. In addition, there are considerable differences in the distribution margins of the grid operators.

For some grid operators, taxes and levies to the public authorities play a significant role, which vary greatly throughout Switzerland.

6.3.1.7. Electricity Spot market prices

The spot market prices for electricity are expected to rise in future. It is expected to increase to 65 €/MWh in 2030 and 80 €/MWh in 2050 (median value from examined studies) (Böhm et al., 2018; Zauner et al., 2019). In the following diagram the trends of spot market prices are shown over the year. Figure 6-2 shows spot market prices in 2030 and higher volatility in the form of significantly larger fluctuations in spot market prices in 2050 compared to the 2017 reference data.

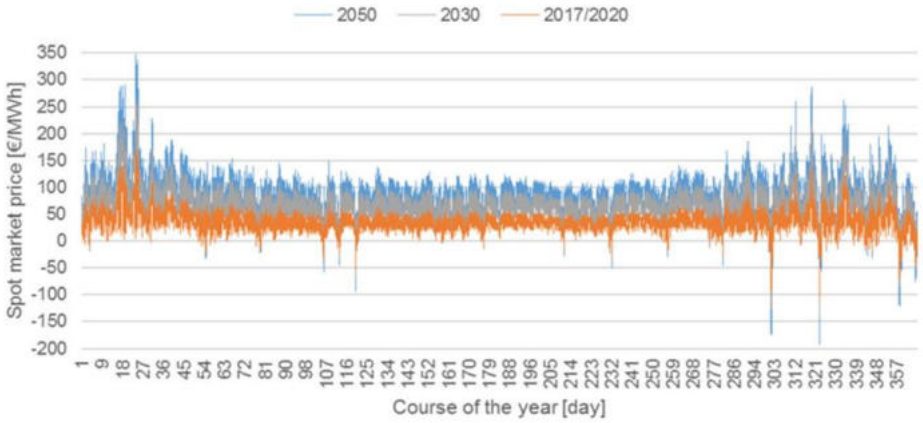

Figure 6-2: Spot market prices for 2017 and forecasts for 2020, 2030 and 2050. Source: (Zauner et al., 2019)

6.3.1.8. Composition of gas prices

The price of natural gas for the end customer is defined by the price during procurement and grid usage fees. Within the grid usage charge, the price for infrastructure and supply logistics are covered. Additional taxes and levies will be added on top. For example, a mineral oil tax is levied on all fossil fuels. In the case of fuels for heating, a CO_2 tax is also paid. A mineral oil tax plus a mineral oil surcharge is payable on all fossil fuels for vehicles.

The price of natural gas varies greatly throughout Switzerland. The different billing systems of the gas supply companies make it difficult to compare them with each other. There are different categories, such as household, heating or dual fuel. These are often subdivided into different purchase quantity categories. The basic charges for the service of providing gas or also the performance prices between gas suppliers vary greatly.

In the IEA World Energy Outlook 2020 (IEA, 2020) different price scenarios for the development of fossil gas are evaluated. According to the stated policies, the gas prices are expected to trend back to the

prices in 2010. They assume a price for natural gas of around 21.0 CHF/ MWh in 2025, 23.5 CHF/ MWh in 2030 and 26.1 CHF/ MWh in 2040 (in comparison to 21.0 CHF/ MWh in 2019 and 27.3 CHF/ MWh in 2010).

However, due to political events in 2021, the situation is likely to have changed. This shows the exposure of the energy market to geopolitical events.

6.3.1.9. Swiss Law affecting Power-to-X systems

In (Kober et al., 2019), M. Schreiber and S. Heselhaus analysed the regulatory framework of Power-to-X in Switzerland. There the following legal provisions are discussed:

- legal provisions of Power-to-X systems in general;
- legal provisions that only affect P2X-installations which feed electricity back into the public grid;
- legal provisions that affect the direct sale of gas produced in Power-to-Gas plants, as opposed to the use of gas to produce heat or electricity;
- and legal provisions that affect the use of liquid or gaseous fuels produced in P2Xfacilities.

Some relevant points from this publication for this project are listed below (table 6-5).

Table 6-5: Legal provisions that affect Power-to-X systems, the power-to-x market as well as the use of e-fuels. Source: (Kober et al., 2019), complemented in the case of any new legislation, e.g., on grid fees.

Environmental law	Large-scale P2X-installations may require an Environmental Impact Assessment (EIA) according to the EIA-Regulation (SR 814.011). This would be the case if the installation occupies more than 5'000 m^2 of space or if it produces more than 1'000 t of chemical products annually, section 70.5 of the annex to the EIA-Regulation. The same would be true for P2X-installations that store more than 50'000 m^3 of gas or more than 5'000 m3 of liquids, section 22.3 annex to the EIA-Regulation. An EIA-requirement would also exist if the installation includes a gas power plant with a capacity of more than 50 MW_{th}, section 21.2 lit. a annex to the EIA-Regulation.
Safety regulations	Potentially dangerous chemicals such as hydrogen and methane need to adhere to the Classification, Labelling, Packaging (CLP)-requirements under the Chemicals Ordinance (ChemO, SR 813.11), which incorporates the European Union CLP requirements into Swiss law. Both hydrogen and methane require the warning labels H220 and H280, the prevention directions P210, the response directions P377 and P381 as well as the storage direction P403; see annex 2 section 1 ChemO, annex VI Tab. 3.1 EU CLP-Regulation 1272/2008. Both substances also require the safety data sheet according to Art. 5 subsection 1, annex 2 section 3.1 ChemO, Art. 31 EU REACH-Regulation 1907/2006. In addition, methane is registered under REACH (no. 01-2119474442-39). In addition, all pressurized appliances must adhere to the requirements of the Pressurized Appliance Ordinance (Druckgeräteverordnung, SR 930.114). Finally, certain installations that may pose an extraordinary danger in the case of a major accident are subject to specific safety requirements, which are stipulated in the Major Accidents Ordinance (MAO, SR 814.012). Under the MAO, the operators of these installations must implement specific procedures to prevent damage in the case of a major accident. These especially include the

	measures according to Art. 3, annex 2.1-2.5 MAO. The MAO also includes the right of the enforcement agency to control the measures and the corresponding reports by the operator and, where necessary, order additional measures (see, for example, Art. 6-8b MAO).
Grid tariffs	The characteristic of an electricity consumer as a “Final Consumer” has potentially severe financial implications. Final Consumers must pay the grid tariffs according to Art. 14 subsection 2 Electricity Supply Act (ESA, SR 734.7). These include the grid surcharge that is used to finance, inter alia, the subsidies for renewable energy producers, if the distribution grid operators – as is commonly the case – pass them on to the Final Consumers under Art. 35 subsection 1 Energy Act (EnA, SR 730.0). The term “Final Consumer” is defined in Art. 4 subsection 1 lit. b ESA as consumers that buy electricity for their own consumption. The law explicitly exempts two categories of consumers from the term “Final Consumer”, namely the consumption of electricity for the operation of a power plant and the electricity used to power pumps in pumped storage hydropower plants.
Power-to-methane as biogas	Gas from Power-to-methane-facilities could potentially be regarded as “biogas”. This could be the case where Power-to-Gas-installations use electricity from renewable energy plants. However, the Energy Act does not define the term “biogas”, and in other acts, the legislator uses substitutes such as “biogenous gas” or “biogenous fuels”. It is therefore unclear what exactly falls under the term biogas. First, it would be possible to define “biogas” identically to the term “biogenous gas” under Art. 2 lit. c Energy Promotion Ordinance (EnFV, SR 730.03). This term only applies to gas from photosynthesis, so it does not cover hydrogen or methane produced in Power-to-Gas-plants. Second, one could define “biogas” in accordance with the term “biogenous fuels” used in Art. 2 subsection 3 lit. d Mineral Oil Tax Act (MinOTA, SR 641.61). Under such an approach, gas from Power-to-Gas-installations may qualify as biogas if certain ecological criteria are met (see the following section on the Mineral Oil Tax Act for details). Third, it could be argued that the term “biogas” should be defined independently from terms used in other statutes. In this case, it would be unclear whether gas from Power-to-Gas-installations could be considered “biogas”.
Mineral Oil Tax	When used as fuel, hydrogen and synthetic methane from power-to-methane are exempt from the Mineral Oil Tax if the energy used stems from renewable sources and certain ecological criteria are met. When used as a combustible, hydrogen and synthetic methane do not fall under the Mineral Oil Tax.

6.3.1.10. Product gas quality and gas grid injection

Produced gas needs to meet certain quality levels assessed based on the Wobbe Index before it can be injected into the grid. The Wobbe Index is an indicator of the interchangeability of fuel gases, e.g. when the Wobbe Index for synthetic natural gas (SNG) is similar as for natural gas, then they are interchangeable. If the produced gas reaches the required range, no additional product gas purification is necessary, and the product gas can be injected into the gas grid. The product gas is gas after the methanation reactor up to and including the product gas purification. The product gas is cooled, and water is separated from the non-condensable gases.

The specifications with which a renewable gas must comply in order to be allowed to be injected into the gas grid to an unlimited extent are provided in the table below.

Table 6-4: Technical specifications on the required gas composition for the injection of gas into the network for Austria, Germany and Switzerland. Sources: [1] ÖVGW regulation „G B210 Gasbeschaffenheit"; [2] DVGW Worksheets G260 and G262 for H-Gas; [3] SVGW Worksheets G13 and G18; [4] This is the advised maximum level. System operators are allowed to apply lower levels depending on local circumstances.

Component	Unit	Austria	Germany	Switzerland
Wobbe Index	MJ/Nm^3	47,70 – 56,92	46.1 – 56.5	47.88 – 56.52
Gross calorific value	MJ/Nm^3	35,54 – 47,63	30.2 – 47.2	38.16 – 47.16
Relative density	-	0,555 – 0,7	0.55 – 0.75	0.5 – 0.7
Methane	mole-%	-	≤95	≥96
Oxygen	mole-%	≤1	≤3	≤3
Carbon dioxide	mole-%	≤4	≤5	≤5
Carbon monoxide	mole-%			≤3
Hydrogen	mole-%	≤10	≤10()	≤2
Hydrogen sulphide	mg/Nm^3	≤5	≤5	≤5
Sulphur from mercaptans	mg/Nm^3	≤6	≤6	≤5
Total sulphur	mg/Nm^3	≤30	≤30 Avg/y	
Dew point (hydrocarbons from 0.1 - 7 MPa)	°C	-2	-2	

The product gas purification step is the conditioning of the product gas. The output of the purification is called synthetic natural gas (SNG). The quality of the SNG should reach the specification of the gas grid operator for injection.

The possibility to inject SNG into the gas grid and the resulting effort (technical and economical) depend mainly on three parameters:

- The capacity of the gas grid
- The operating pressure of the gas grid
- The required gas quality of the gas grid

These parameters depend strongly on the structure of the gas grid. The maximum operating pressure of the gas grid determines the dimensions of the compressor of the feed-in plant. The typical level of maximum operating pressure is about 80 – 100 bar for the transportation system on a national level. On a regional transportation level, a wide range between 16 bar and 70 bar can be found. The distribution

grids are operated mainly in low (25 mbar) or medium pressure (up to 1 bar), sometimes with a feeder system at 4 – 16 bar for regional distribution.

The requirements regarding gas quality define the necessary grade of gas processing. They are based on national and European regulations. Examples are the German DVGW G 260 (A) “Gasbeschaffenheit (gas properties)”, the European EASEE Gas CBP 2005-001/02 “Harmonisation, of Gas Qualities” and the Swiss SVGW “Richtlinien für die Gasbeschaffenheit” G13 and G18 (Meier et al., 2017a). Those documents rule the permissible range for relevant gas parameters like Wobbe Index, caloric value, and density. Partially the maximum shares of hydrogen, carbon dioxide, oxygen and sulphur are defined.

6.4 Public acceptance of Power-to-X projects and CCU

In recent years different renewable energy projects experienced public resistance resulting in major impediments of their deployment and further development (Azarova et al. 2019). Investigating the social acceptance of new technologies has therefore become an important measure to enhance the success rate of the planned project. Utilizing saline aquifers as an underground methane synthesis reactor and storage facility is a first of its kind project and hence to the knowledge of the authors no investigation of the social acceptance of this technology is existent at present. Therefore, literature was searched and reviewed in the following on the related topics, social acceptance of power-to-gas (PtG), hydrogen, carbon capture and storage (CCS) as well as carbon capture and utilization (CCU).

6.4.1 Public acceptance of Power-to-Gas and Power-to-X

Azarova et al. were the first to take a closer look at the acceptance of power-to-gas technology in local communities in Switzerland, Italy, Germany and Austria. The survey was constructed as a choice experiment with 2000 participants. The main finding which resulted is that power-to-gas will probably not be confronted with major social acceptance problems as did other storage types like for example pump-hydro (Azarova et al. 2019). König et al. analyzed the social acceptance of power-to-gas in the region of Baden-Württemberg through interviews with experts and focus groups with a total of 36 people. Regarding acceptance of new PtG infrastructure the focus lies on the source of power for the electrolysis as well as the source of CO_2 for the methanation. A good communication between the stakeholders and the local community is key for attaining the community's support (König et al. 2018).

In the USC-FlexStore project facility for hydrogen production and transportation underground is planned. Therefore, a positive public perception of hydrogen is important. In contrast to the scarcity of literature on the social acceptance of Power-to-X, the social acceptance of hydrogen specifically has received far more attention in the last 20 years, evidenced by a vast number of scientific papers of which some are presented in this chapter. The public perception of hydrogen is generally positive as shown by (Schönauer and Glanz 2022) and (Schmidt and Donsbach 2016). According to Hujits et al. the formation of a strong resistance as it was the case with other new technologies such as for instance carbon capture and storage (Terwel et al. 2012) is rather unlikely (Huijts and van Wee 2015).

Zimmer et al. for instance found a very positive attitude towards hydrogen-powered cars with 80% of the German respondents being in favor of introducing hydrogen vehicles. This under the condition that the hydrogen used is produced sustainably (Zimmer and Welke 2012). The request for green hydrogen is further emphasized in the study by (Lambert und Ashworth 2018). In (Huijts and van Wee 2015) it is found that the Dutch population is in favor of hydrogen fuel stations, however, this is accompanied by the so-called NIMBY effect. This describes the phenomenon that citizens are positive to the general idea of, in this case, hydrogen fuel stations but when it comes to the implementation of one close to their home, they oppose it. Interestingly the factor of proximity of a planned infrastructure to people's homes was controversial over different studies. Both (O'Garra et al. 2008) and (Thesen und Langhelle 2008) found that proximity to the hydrogen fuel station enhanced the support of the infrastructure. According to Schönauer et al. NIMBYism further comes into play when looking at large-scale infrastructure in the neighborhood. In this case the general acceptance of hydrogen technologies decreased (Schönauer and Glanz 2022). Schönauer et al recommend addressing this challenge through a transparent communication and an active participation of the community.

Providing adequate and sufficient information in general is of great importance. (Schmidt and Donsbach 2016) and (Thesen und Langhelle 2008) showed that a higher knowledge on H_2 correlated positively with a higher social acceptance. Storage of hydrogen too is perceived rather positively (Schmidt and Donsbach 2016). However, there is uncertainty around the possible risks and security issues especially regarding hydrogen storage close to residential areas (Zaunbrecher et al. 2016), as well as underground storage solutions. Opinions about the installation of hydrogen pipelines were equally positive and negative (Schmidt and Donsbach 2016).

6.4.2 Public acceptance of CCS

CO_2 is the other educt involved in the process used in USC-FlexStore. The public opinion on capture of CO_2 as well as other infrastructure such as pipelines and storage facility are therefore investigated in this chapter.

As mentioned before, CCS demonstration projects have had to deal with a lack of social acceptance which even led to the cancellation of different CCS projects e.g. (Jane Desbarats), (Terwel et al. 2012). It became clear that it is not only a question of economic hurdles or limited technological knowledge which led to a stagnation of CCS but also the low social acceptance (Sara et al. 2015). This was now addressed by numerous studies to fill this gap in information. L'Orange Seigo et al. reviewed and discussed a total of 42 research articles (majority is from Europe, a few from the US, Australia, Japan, Canada, and one from China) about the public perception of CCS and concludes: Generally, CCS is reluctantly accepted. Few people exhibit an extremely positive nor an extremely negative attitude. "The technology is rarely categorically rejected because people see the need for reducing CO_2 emissions into the atmosphere. At the same time, they object to the fact that it is an "end-of-pipe" solution, which does not reduce the production of CO_2 from fossil fuels, and they want to see it embedded in a comprehensive energy strategy that addresses the problem of climate change from multiple angles. » (L'Orange Seigo et al. 2014)

The social acceptance of CCS in Switzerland was explored in a set of different studies by Wallquist et al. between 2009 and 2012. In the scope of the very first study investigating the public perception of CCS in Switzerland in-depth interviews were conducted with a group of 16 laypeople. From this relatively small sample size 6 persons believed CCS was worth a try while 7 were fundamentally against it and the remaining 3 persons were not decided. 8 people would accept a field test in their municipality. 8 people saw a risk in rebound effects meaning that more efficient technologies lead to an increased consumption. The most prominent concern of the questioned people was the fundamental lack of sustainability of CCS. Deployment of CCS was perceived as a risk to a sustainable development of the energy economy (Wallquist et al. 2009).

This is consistent with the representative survey conducted by Wallquist et al. in the following year with a total of 654 Swiss people. Again, the most influential factor on the perceived benefits and risks of CCS technology was the concern about its unsustainability. (Wallquist et al. 2010) The third study on CCS acceptance by Wallquist et al. resulted in the following recommendations about the communication of this complex subject to laypeople.

Although provision of knowledge could, in some cases, lead to a decreased risk perception it was also seen to lead to confusion in specific knowledge domains. Wallquist et al. conclude: "Due to the public's limited attention, CCS communication should focus on information that quickly helps non-experts to improve their understanding and should avoid information that might increase the perception of dread concepts at first glance." (Wallquist et al. 2011).

In a last survey Wallquist et al. conducted an online survey with 139 Swiss citizens focusing on the three elements in the CCS chain: capture, pipeline and geological storage. It was found that CO_2 transport by pipelines lead to stronger opposition than the storage itself. A not in my backyard (NIMBY) phenomenon was detected both for pipelines and storage. However, the NIMBY effect disappeared when the CO_2 used stemmed from a biogas-fired plant, bioenergy with carbon dioxide capture and storage (BECCS). (Wallquist et al. 2012)

6.4.2.1. Public acceptance of CCU

The further utilization of the captured carbon by conversion into CH_4 is a key element in the USC FlexStore project, thus the following chapter reviews the existing literature about social acceptance of CCU. As numerous studies on the topic in recent years show the public awareness of CCU in countries such as Germany and the UK is very low ((Jones et al. 2017b), (Jones et al. 2017a), (Jones et al. 2014), (Perdan et al. 2017), (Arning et al. 2019a)). For instance (Jones et al. 2014) found in a pilot study with 16 participants only one person indicating that they have heard of CCU before. Not very different is the finding of Perdan et al. in a survey with 1213 participants whereof only 9% indicated to knowing what CCU is. On one hand the indeed low familiarity with this new technology may be a barrier for its fast deployment, on the other hand it also entails a potential to actively shape public perception by the involved stakeholders (Perdan et al. 2017).

At the same time the social acceptance for CCU was found to be neutral to positive by all the reviewed studies. Arning et al. found a slightly positive acceptance for CCU infrastructure and for CO_2 derived products (Arning et al. 2020), while Jones et al. state a tentative support towards CCU by the 28 interviewed laypeople (Jones et al. 2017a). In a preceding study by Jones et al 4 out of 16 respondents were fairly or very positive towards the technology (Jones et al. 2014). In another study conducted by Arning et al. a total of 313 German laypeople were questioned about their perceptions of alternative fuel production plants. Generally, the alternative fuel production plants were perceived positively. The well-known phenomenon of decrease in acceptance when looking at the local installation of such powerplants was observed (Arning et al. 2019b) and (Arning et al. 2018). The elevated acceptance level of CCU compared to CCS is obvious. CCU is perceived significantly more positively than CCS (Linzenich et al. 2019) and (Arning et al. 2019a).

The perception of CO_2-based fuels by laypeople was assessed by Engelman et al. and Linzenich et al. and in summary it is viewed more positively than conventional fuels and as an acceptable and beneficial technology respectively (Engelmann et al. 2020; Linzenich et al. 2022).

The perceived benefits of CCU are environmental benefits such as the potential of saving fossil resources (Arning et al. 2020; Jones et al. 2017a; Arning et al. 2019a; Arning et al. 2018) and the idea of moving towards a more circular economy (Jones et al. 2017a). The potential for climate mitigation effects of CCU was perceived controversial. While the participants of the study by Arning et al. perceived CCU's contribution to climate change mitigation as a benefit (Arning et al. 2019a) participants of other studies criticized the technologies myopic character as it only delays the release of CO_2 into the atmosphere without the potential for tackling climate change in the long run. However, CCU's potential to "buy time" by slowing the problem until more efficient measures are developed was expressed (Jones et al. 2014; Jones et al. 2017a). In the study by Jones et al. the idea of looking at the concept as a "bridging technology" to face climate change was supported. Respondents of the latter study were additionally sceptic about the high energy related and financial cost which could be invested in more efficacious technologies. Furthermore, the concern was expressed that CCU would draw funding from other technology addressing climate change (Arning et al. 2020; Jones et al. 2014). This falls in line with the here expressed opinion that CCU should not be a sole focus for investment in tackling climate change (Jones et al. 2017a). In another study by Jones et al. the perceived benefits were of economic nature instead of environmental (Jones et al. 2014).

A further concern that arose around CCU is its character as an end-of-pipe solution (Jones et al. 2017a). Also, the concern that industry would use it as a pretense to continue emitting climate damaging CO_2 and that people would use it as an excuse to continue with their wasteful lifestyles respectively (Arning et al. 2020; Jones et al. 2014) are raised and discussed.

Risks the public perceived as negative environmental risks caused by CCU entailed environmental pollution (Linzenich et al. 2022) CO_2 leakage (Arning et al. 2019a) and general ecological harmfulness (Linzenich et al. 2019). Contrary to that in other studies it was found that CO_2-based fuels were perceived to be a clean energy source and more eco-friendly compared to conventional fuels (Engelmann et al. 2020) and "sustainability" was attributed to the technology in (Linzenich et al. 2019).

In several studies the public expressed concerns about negative health risks. Arning et al. report the fear of allergies, headaches and accidents caused by suffocation during CO_2 storage, transport to CCU production sites, or the interaction with CO_2 derived products. (Engelmann et al. 2020; Arning et al. 2020). Fears about toxic effects were expressed in (Linzenich et al. 2022) and (Arning et al. 2019a). (Engelmann et al. 2020) in contrast found that CO_2-based fuels were perceived to be safe, rather harmless, and non-toxic posing less risks regarding types of exposure and properties leading to toxic effects compared with conventional fuels. In (Arning et al. 2019b) respondents were not too concerned by potential health risks from an alternative fuel production plant.

It was found that economic considerations impacted the social acceptance strongly. In (Linzenich et al. 2022) it was shown that alternative fuels are only an acceptable option under the condition that their price is comparable to conventional fuels. In (Arning et al. 2018) different CCU scenarios were compared and profitability had the highest impact on the scenario preferences. The preferred supply energy of the CCU scenarios for the production of alternative fuels were surplus energy followed by renewable energy resources (Arning et al. 2019a). Regarding CO_2 source, a comparison of CCU site deployment scenarios conducted in a previous study showed that taking CO_2 from a chemical and/or steel industry is preferable. And the comparison of the derived product showed that fuel production was preferred due to the highly valued individual motorized mobility (Arning et al. 2018).

6.5 Experience in public acceptance of deep drilling in Switzerland: an exploration industry perspective

Authors: Daniela van den Heuvel & Larryn Diamond, Institute of Geological Sciences, University of Bern

To complement the above review of literature on public perception of gas-storage projects in Switzerland and nearby countries, the following chapter summarizes experience from the geological exploration industry in dealing with public acceptance of deep drilling projects in Switzerland. The experience was documented in six personal interviews with expert professional geologists who have undertaken exploration and deep drilling projects (> 500 m depth) in Switzerland over the past two decades. The projects in question were primarily related to exploitation of geothermal energy but also to radioactive waste disposal, natural gas production and salt-solution mining. A separate report on the deep drilling project at St. Gallen (Muratore 2016) provides additional valuable insights. The industry perspective of interest, because it highlights the public acceptance issues that an exploration company would have to consider in finding and validating an underground site for geo-methanation in Switzerland.

The opinions of the interviewed experts are not distinguished by person in the following text. Instead, their points have been grouped into topics that cover different aspects of the public acceptance theme.

6.5.1 Public acceptance aspects for consideration by exploration companies

6.5.1.1. Reason for drilling

The type of subsurface application has a major impact on public perception and hence on its degree of support or opposition. Most of the projects discussed during the interviews were related to the exploitation of geothermal energy. As a local source of green and renewable energy, geothermal is relatively well-viewed, both by the public as well as the cantonal and federal authorities. Permitting and communication are thus relatively easy – at least as easy as is possible within the current legal and social framework of Switzerland.

Hydrocarbon projects on the other hand are in a very difficult position in Switzerland, encountering strong opposition from the local public and, in some cases, from cantonal authorities and even cantonal parliaments (e.g., Vaud where hydrocarbon exploration is banned). The opposition is strong enough (and the chances for success based on previous exploration too small) that very little exploration for hydrocarbons has been undertaken in recent years and international investors have largely terminated their projects in Switzerland. The primary motivation behind the opposition are the CO_2 emissions and the non-renewable nature of fossil fuels. In addition, in the absence of confirmed conventional hydrocarbon resources, unconventional resources (e.g., shale gas) have received increasing interest. In order to exploit shale gas deposits, fracking is necessary which raises additional concerns such as pollution of (sub)surface waters and induced seismicity.

Similarly to hydrocarbon exploration, exploration for storage sites for natural gas often encounters opposition. The main concerns are again the non-renewable nature of the resource and the CO_2 released during burning. Other concerns are the potential of leaks and consequent groundwater contamination, as well as induced seismicity. Underground storage of other gases (e.g., hydrogen) are less affected by the negative perception of fossil fuels despite similar technical challenges and they are therefore viewed more favourably. Establishing underground storage for gas has seen renewed interest in the wake of the Ukraine crisis (2022 and ongoing), especially at the level of federal authorities.

The exploration industry views the lay population as having a poor understanding of the geological subsurface. This means that public opinion on deep drilling projects, whether in support or opposition, is largely based on emotions rather than facts. Emphasis on the qualities of the subsurface technologies, such as “renewable”, “green” or “CO_2-neutral”, are more effective in ensuring public support –or at least in avoiding opposition– than lengthy explanations of how the technologies actually work. Success of green gases, especially geo-methane, will thus strongly depend on whether or not the public accepts the “renewable”, “green” and “CO_2-neutral” labels or not.

6.5.1.2. Political considerations

Apart from geological considerations, which define the technical feasibility of underground projects, political considerations are the most important criteria for site selection – especially for companies operating (inter)nationally. If there is little to no interest from local politicians, it is nearly impossible to start a project in certain Cantons or regions, as there will be no support to overcome any administrative hurdles or to deal with issues of social acceptance. Some cantonal authorities even take active steps to ban certain subsurface projects. The most well-known examples are the ban on exploration and production for hydrocarbons in Canton of Vaud and the lobbying against the Haute-Sorne project in the Canton of Jura. On the other hand, if there is a strong political will, there is usually a way to drive a project forward. This can go as far as amending laws and regulations or creating an entire legal framework (e.g subsurface law) specifically for the project. Strong political support also often goes hand in hand with a charismatic person or group of people who drive the project forwards and thus increase the trust in the general public and facilitate communication. This strong local political support was the reason for the execution of the deep geothermal projects in Basel, Triemli, St. Gallen and Geneva.

The political willingness to host and support deep drilling projects within a given Canton or region should be reassessed during the planning stage of each new project, as it can change relatively quickly depending on who is in charge of the local administrative offices and their agenda as well on as the national mood on energy topics.

6.5.1.3. Considerations regarding residents directly affected by drill sites

One of the primary objections to all of the projects experienced by the experts was exposure of the residents in the immediate vicinity of the drill site to noise, vibrations and night-lighting over the course of the drilling operations (typically 24 hr per day, 7 days per week for weeks to months). This issue must therefore be taken into account during site selection. Sites with the smallest number of people affected and/or the largest distances to neighbours are generally preferred. This makes site selection in densely populated areas (e.g., city of Geneva or Basel) much more difficult compared to the more sparsely populated countryside. For projects in cities, however, areas can often be found which already suffer from high levels of noise pollution (e.g., industrial sites). These can be favourable sites for drilling, as people in the vicinity are already used to noise and are thus potentially less likely to complain. In rural areas on the other hand, noise levels are often very low, traditional or regulated periods of quiet are more strictly enforced, and people are much less willing to put up with disturbances. The distances between drilling sites and the nearest neighbours are thus to be maximised during site selection if possible. Transparent communication with directly affected people at any stage of the project can greatly improve acceptance.

6.5.1.4. Communication with interest groups and the general public

Communication with interest groups and the general public is crucial throughout the duration of the project. It starts as soon as the permitting process with the cantonal authorities starts. Care has to be taken to involve everybody at the local level at the same time, from the mayor of the local community to the neighbours directly adjacent to the chosen site. Communication with interest groups and the public are not legal requirements but they are widely accepted as being important to establish transparency and trust early on in the planning and permitting processes.

6.5.1.5. Non-governmental organisations (NGO’s; Pro Natura, WWF etc.)

Generally speaking, Swiss environmental groups are in favour of geothermal projects or other projects supporting de-carbonisation of the energy sector. These groups may raise environmental concerns but they can be satisfactorily addressed if an exploration project demonstrates a plan to deal with the expected and potential issues. Depending on the question, the environmental groups can be tough but not unreasonable discussion partners. Talking to NGOs means conversing at a very high technical level, as they typically have clever, well-educated people in their communication teams.

6.5.1.6. General public

Communication with the general public is challenging for any project. Firstly, only a small proportion of the local population (around 10 to 20%) tends to be actually interested in the project and willing to be informed to a certain degree. The remaining 80 to 90% are relatively oblivious to the ongoing project, at least as long as it runs smoothly. Secondly, communicating to this small portion of the population willing to listen is made difficult by the highly variable backgrounds and degrees of technical and scientific understanding among the public. Even people well-versed in the natural sciences often have very little understanding of the subsurface, as they are rarely exposed to geological topics. For people with a less scientific background, opinions are often based more on emotions than facts, which requires an adapted form of communication. For such people, trust in the company behind the project is a crucial factor. Once trust is established, locals often become willing to be informed and potentially have their emotions replaced by facts. Uncertainty in geology is of course one of the important topics to try and convey.

Trust is also important for the public at large as well as for the media, because it fosters publicity and acceptance of the project. Local energy providers or other well-established local companies are often perceived as trustworthy. They must only maintain the trust they already have to gain support for new subsurface projects. A new company or one coming in from the outside needs to establish trust first, which is much harder and more time-consuming. Gaining or maintaining trust is something that cannot be done through a communication department or press releases alone. It requires members of the project team to go out and interact with the public at town hall meetings, open days and site visits.

Experience in Geneva has shown that the interested and well-informed members of the public can become part of the communication team. In more than one case, members of the public spontaneously defended SIG and their exploration program against attacks from individuals attempting to spread fake news (e.g., cracking of walls during initial stages of 3D seismic campaign) at town hall meetings and via social media. This example also shows why communicating in real time (e.g., via social media) is crucial for projects. In today's internet, out-of-date information and delayed communication are poorly received. In addition, fake news spreads rapidly. Damage control generally requires a published reaction from the company before the fake news has gone viral and become embedded in the minds of the public.

Owing to the apparently disinterested majority described above, obtaining public acceptance is a dynamic process which can take very unexpected turns, especially if charismatic advocates or opponents enter the scene or unexpected problems occur. The 80 to 90% of people who do not have an opinion on the ongoing project are much more likely to change their views from "Not that interested" to "Against the project" than becoming passionate supporters. Social science studies conducted within the exploration program in the Geneva Basin have shown that trust is very easily lost and hard to regain. Thus, once the scales have tipped, returning to the pre-crisis state of acceptance situation is viewed as being nearly impossible.

6.5.1.7. People directly affected by the project

During the site selection phase of project execution, sites with the fewest neighbours at the greatest distance are preferred, so as to avoid objections to project-related disturbances (see chapter "Considerations regarding residents directly affected by drill sites"). Nevertheless, some people in the immediate vicinity of the drill site may be affected by the operations over weeks to months. Communication with those people needs to start at the very beginning of the project to identify their concerns. The biggest ones are generally drilling noise followed by light pollution, traffic to and from the site, groundwater contamination and the aesthetic changes to the landscape. It is important to assess the situation (e.g., noise levels) before drilling operations start and then again during operations to show the actual changes and not just the ones perceived by the people affected. Several projects have opted for specific mitigation strategies such as noise barriers (their effectiveness depends on the height of the derrick), scheduling noisiest work during the day whenever possible, and designing specific access routes for site traffic which minimise the impact on the public.

The concerns of neighbours are found to be the same, irrespective of the kind of subsurface application for which a well is being drilled. The public's general lack of knowledge of the geological subsurface means that, understandably, locals usually cannot grasp the real risks of a given project. However, they can be concerned by things with which they have had personal experience. Conversely, they can worry about geological issues of no concern for a given operation simply because they have heard about the topic before, e.g., the perceived danger of radon release during recent drilling of the Nagra TBO wells through radon-poor sedimentary rocks Northern Switzerland. Actual geological risks like induced seismicity are often only perceived later in the project as the degree of understanding of the subsurface and the project increases. This is why steady and prolonged communication from the project team is crucial. It is not enough to involve the public during the permitting process alone. During drilling it is important to explain via site visits and town hall meetings etc., which project operations are currently taking place and how and why they might differ from those originally planned.

It has been observed (e.g., during the Basel project) that the concerns from the neighbours are often highest when the project is first announced. They diminish as the concerns are addressed and mitigation strategies are presented by the project company. However, once the actual drilling phase starts, complaints increase again as only then can residents experience how loud or bright and incessant the drilling operations truly are.

Concerns from the public directly affected by the project have to be taken seriously. This is especially true in the countryside where people are generally more connected and where unhappy neighbours can mobilise other potential opponents to the project rapidly and efficiently. This was observed at Haute Sorne, where concerns voiced by local neighbours regarding noise and aesthetics (not just during drilling but also during future long-term operation) ignited widespread opposition against the project. This included additional fears of contamination and seismicity induced by the project, and it first involved the more distant residents of the locality and then it eventually spread across the Canton of Jura.

6.5.1.8. Communication strategies

A large number of different approaches to communicate with the public as well as interest groups (politicians, environmental groups etc.) have been employed in the different projects. Most projects chose conventional ways of communicating: town hall meetings, information pamphlets, site visits, open days, press releases, social media, etc. The following two examples highlight two approaches which go above and beyond what is generally done regarding communication, both of which were very well received by the public.

Town hall meetings specific for different interest groups: As part of the site selection process for a deep engineered geothermal system (EGS), the company GeoEnergie Suisse organised town hall meetings in Haute Sorne (JU), Etzwilen (TG), Avenches (VD) and Triengen/Pfaffnau (LU). Rather than just information events with Q&A sessions for the participants, separate meetings were organised for people with different primary concerns. The first meeting was for residents in the immediate surroundings of the planned drill sites. In these meetings, the major concerns addressed were noise and light pollution, vibration, and traffic to and from the site. The second group consisted of people whose primary concern was groundwater pollution, whereas the last group focused on concerns regarding natural and induced seismicity. Both groups were also attended by members of NGOs (primarily WWF). Participation in any of the groups was voluntary, but only residents living within a prescribed distance from the planned drill sites were permitted to participate (i.e., a few hundred metres for the first group of directly affected residents; a few kilometres for the ground-water contamination group; and a few tens of kilometres for the seismicity group). The primary aim of these meetings was to deliver the information in which the different groups were interested and, due to the more specific nature of the topics discussed, have more time to answer questions in detail. Similarly to the Nagra TBO project, not all concerns raised by the interest groups made sense to the geological experts (e.g., potential of radon release) but they were addressed nevertheless. A number of individuals, generally voicing very strong opinions, left the interest groups after only a few meetings but continued to write more or less strongly worded letters to the project team. The feedback from the rest of the population was positive. Feedback from the public showed that

they felt they had been taken seriously and they applauded the transparency of the project. However, many still rejected a deep geothermal project in their vicinity -– they had evidently gained trust in the company but not in the technological application which the company aimed to implement.

Visitor centres at drill sites: While most companies offer site visits to interest groups or the general public on open days, Nagra went one step further and installed visitor centres and viewing platforms at each drill site. The visitor centre contained information on the TBO drilling programme and the search for a final repository as well as reports and pamphlets to browse through. Oftentimes, scientific or technical staff were present at the visitor centres to answer additional questions. The visitor platform allowed people to see the drilling operations up close while maintaining a safe distance. Together, these measures aimed to show the public that the site exploration for nuclear waste disposal is fully transparent. This was crucial as, despite the years of communication with the public and building of trust, some members of the public still believe that the exploration wells were a cover-up for secret disposal of radioactive waste. Around 3000 people visited the visitor centres and viewing platforms on the 9 drill sites. Most of the visitors were invited interest groups, primary and high school students from the surrounding area but also day trippers who dropped in spontaneously while passing by on foot or bicycle. Overall, the glimpses into the work of Nagra that these site visits allowed were well appreciated by the public.

6.5.1.9. Importance of local geological knowledge and experience

Over the decades of hydrocarbon exploration in Switzerland, it was common for Swiss companies to enter partnerships with foreign companies for exploration projects. The foreign companies would primarily bring assets and technical capabilities while the Swiss would act as local partners who understand the regulations and expectations of the authorities and the public. As the permitting process varies substantially between different cantons, this local knowledge was invaluable. In addition, habits and customs can vary noticeably between different regions and also between towns and country. This means that, depending on the area, a different way to communicate with the population was needed. This need for local partners also applies to other subsurface applications, e.g., geothermal.

Even for Swiss companies a local partner can be beneficial during development of a project. The local population, especially in the countryside, is often wary of companies coming from big cities. It is also important to be responsive to the local customs and conditions rather than simply push a planned project ahead regardless of the public resistance. This is exemplified by a number of projects initiated by the local energy providers (e.g., IWB at Basel, Stadtwerke St. Gallen in St. Gallen, SIG in Geneva Basin and ewb at Bern Forsthaus). None of these projects had to struggle for acceptance. It seems that the trust of politicians, authorities and the general public in these well-established companies was sufficient to prevent large-scale objections. This was confirmed by (Ejderyan et al. 2019) who studied social acceptance of the geothermal exploration project in Geneva. That study even found that bad news is perceived less negatively if presented by a trustworthy company and that this effect is more beneficial to trust than the presentation of solutions and mitigation strategies. Local partners also often provide another important liaison: a spokesperson who is respected by the communities. That person can be from the energy provider or also be a local politician (e.g., Fredy Brunner at St. Gallen). Care has to be taken for companies coming from outside Switzerland or outside the canton in question. Such companies can engage local communication specialists, but this is often perceived by the public to be a warning sign rather than something positive. Thus, communication should be done by the project team itself but with local support behind the scenes.

6.6 Development of possible plant concepts

In collaboration of RAG AG, Energie 360° and OST, different plant concepts were developed, three of which are considered in the following evaluation. These best practice cases were developed from learning out of the field tests and with a maximum on facility flexibility in mind. The following three ideas were evaluated in detail:

1. Geo-methanation
2. Geo- and aboveground methanation
3. Underground hydrogen storage and above-ground methanation

Concepts 1 and 2 use the underground reservoir for geo-methanation. Concept 2 includes direct above-ground methanation for the period when hydrogen production and methane demand overlap. This also makes it possible, should the educts not be sufficiently converted in the geo-methanation, for this to be done subsequently above ground. Concept 3, on the other hand, uses the underground only for storing the hydrogen and thus enables seasonal bridging, with methanation taking place above ground afterwards (see Figure 6-3). The elements of the three variants are similar but differ in their linkage.

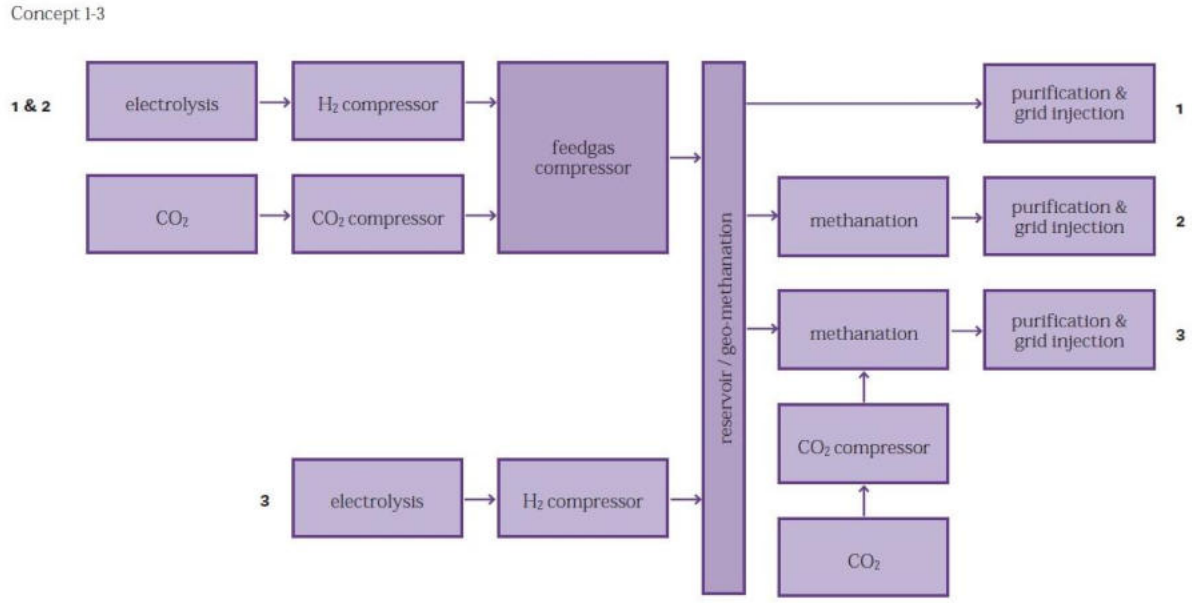

Figure 6-3: Concepts one to three for using a reservoir as a geo-methanation or hydrogen storage facility.

All concepts developed share some similarities that are necessary to allow the geo-methanation to function but do defer from a classic storage design. The first thing is, that additional wells will be needed as the volume capacity of the facility needs to be larger compared to classic natural gas storage. The reason is, that apart from injection and withdrawal of feed-gas circulation of the same is very important as the microbes in the reservoir are stationary and so their “food” needs to find its way to them. In addition, hydrogen and carbon dioxide are not injected alone into the reservoir but need a carrier gas (such as biomethane) due to microbial preferences described in Chapter 2. Furthermore, additional subsurface monitoring will be needed to control the geo-methanation process by injecting the right gas composition in the proper wells. The monitoring data is also needed as input for reservoir software that should predict the speed and efficiency of the process in the reservoir. The most important component here is a gas chromatography that needs to be installed for every well so the composition and distribution of the gas mixture in the reservoir is known and the geo-methanation can be stirred towards ideal conditions. The taking of water samples needs to be standardized so the microbial consortia in the reservoir are known and development of unwanted microbial consortia (e.g., SRB’s) can be prevented.

RAG Austria AG has started developing a monitoring tool during with the experience gained from this project that will be tested in the follow-up project C-CED.

6.6.1 Software requirements for operation of a geo-methanation facility

In order to anticipate how the reservoir will react to certain gas mixtures and injection rates and in order to know how long conversion will take in which region of the reservoir a proper forecasting software is needed. It must have the capabilities of classic reservoir simulation software packages such as pressure temperature simulations and mixing/equilibration/dissolution models that can predict aqueous and gaseous fluid flow in the reservoir. On top of that a strong microbial model needs to be included to forecast how the conversion is propagating within the reservoir. This must also include models that predict changes in pH and microbial consortium to prevent unwanted processes in the subsurface. Finally, a geochemical software such as Phreeqc used by Shell needs to be part of the package as the influence of carbon dioxide on the reservoir needs also be forecasted.

From such a software package forecasting on reservoir behaviour and gas mixing would be possible. The forecasting would allow the injection of the right gas compositions in the right wells of the reservoir and would also allow to anticipate how fast the conversion would happen in these regions. In the end this should enable subsurface engineers to predict when gas can be withdrawn from the reservoir and when the operation of the surface methanation unit is most efficient.

6.6.2 Concepts

6.6.2.1. Concept 1: Geo-methanation

In this basic concept, hydrogen and carbon dioxide are feedstock and pumped underground. The present methanogenetic microbiology will metabolise the available feedstock and convert it to methane. The methane can be extracted, processed and fed into the natural gas grid.

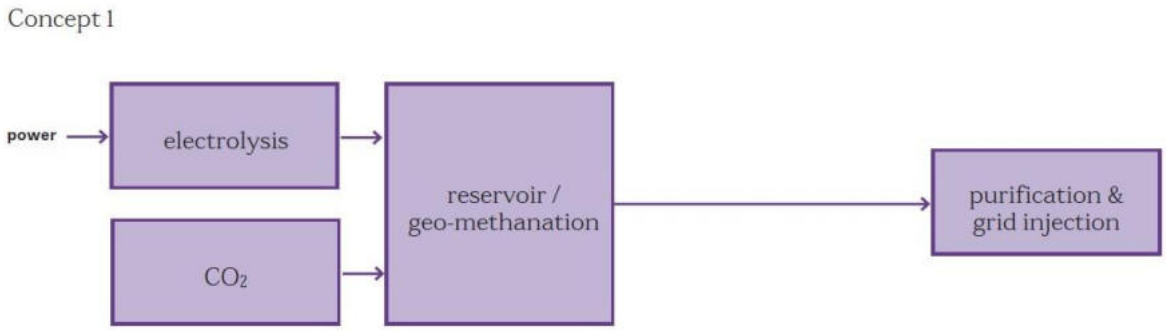

Figure 6-4: Concept 1 with geo-methanation.

In this concept, hydrogen and carbon dioxide are mixed, compressed and stored underground. The present microbiology converts these two educts into methane. The carbon dioxide can be added stoichiometrically or off-stoichiometrically, depending on the flexibility of the geo-methanation. The extraction of the methane can be done either via the same well or via other geo-methanation wells. Multiple wells are required to switch between injection and extraction, and for recirculation operation to mix the gas.

Such mixing is important, as an ideal-flow reactor would ensure the highest possible contact area of the feedstock with the available microbiology. Thus, regular movement of the gas mixture in the geo-methanation would boost the methane production capabilities of the plant.

After conversion to methane, the gas is extracted, dehydrated and H_2S (if present) removed. Afterwards, the methane will be purified, separating residual CO_2 and H_2 and returns these residuals into storage. The purification is needed to meet the gas grid standards as previously discussed.

If the plant is run in a loop, injection and withdrawal would be operated simultaneously, so it might be worthwhile to recover heat from cooling the compressed feed gas to preheat the recycle gas from storage. To ensure optimal metering in the desired stoichiometric ratio, the gas quality must be measured before it is fed into the storage reservoir. Chromatographs are usually used for this purpose.

When the gas is withdrawn from the storage reservoir for end use it needs to be dehydrated and purified in order to meet gas quality regulations. However, in case of gas-cycling it is beneficial to keep the gas wet as the microbes only live in the aqueous phase and constant drying of the reservoir would therefore be a problem. For end use the product gas must be freed from hydrogen sulphide before further use. This can be done e.g., with an amine scrubber, which in this case can also separate excess carbon dioxide. This seems advantageous assuming that underground methanation works very well or also with the prospect that higher hydrogen concentrations will probably be allowed in the gas grid in the future. In both cases, further purification would become unnecessary and could be bypassed.

6.6.2.2. Concept 2: Geo- and aboveground methanation

The second concept is similar to the first concept, adding only an aboveground methanation unit. Firstly, this would add methane generation capacity to the plant and increase its flexibility in always providing gas for end users. Secondly, the additional methanation is useful, when not fully converted gas mix needs to be extracted from the underground storage in order to meet customer demands. From operational experience it has been monitored that a full conversion of all components does not happen in the reservoir as the process runs into educt limitations at some point. Thus, the gas mix will always contain some amounts of hydrogen and CO_2. And a surface methanation unit will therefore increase the efficiency of the facility and decrease the necessity of gas purification.

In contrast to concept 1, concept 2 can also be used in such a way that the focus of the implementation is on the aboveground methanation, and the reservoir mainly serves as a storage for the reactants. The advantage of such a mode of operation is that less consideration must be given to the conditions necessary for the methanogenic archaea and the operation is thus much more flexible.

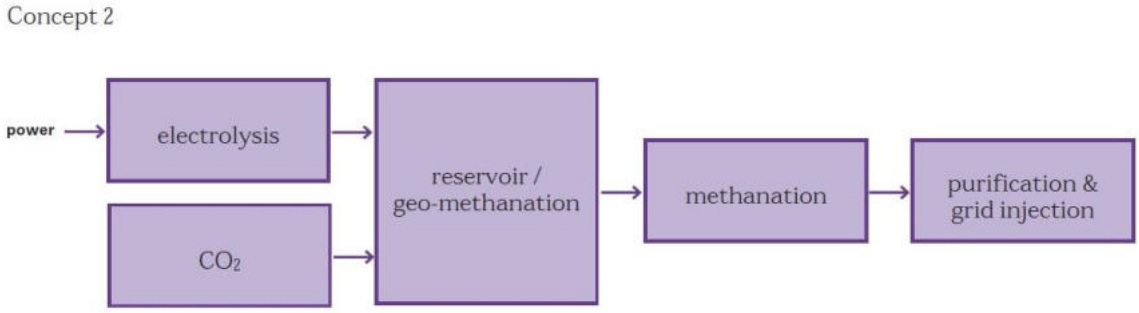

Figure 6-5: Concept 2 with underground and aboveground methanation.

In this concept, CO_2 and hydrogen are either mixed with the carrier gas and added to the geo-methanation after compression or added directly (or via compression) to the above-ground-methanation. As in concept 1, the methane is dried, desulphurized (if necessary) and purified after geo-methanation. In the purification process, CO_2 and hydrogen are separated as retentate, compressed again if necessary and fed into the above-ground-methanation or back into the storage reservoir. The separated methane is purified and fed into the grid or used as a carrier gas.

The peak of surplus energy is expected in summer, where the electrolyser could operate uninterrupted. The smallest loads will occur in spring and autumn, resulting in many more start-up and shutdown

cycles. The electrolyser used in this concept must be flexible to cope with the requirements. An optimal operational schedule is needed to maximize the number of hours of hydrogen generation. The feedstock can be provided in the same flexibility as in concept 1.

6.6.2.3. Concept 3: Underground hydrogen storage

The third concept goes without the geo-methanation but uses its underground capacities to temporarily store hydrogen. This makes it possible to produce hydrogen when surplus electricity is available and at the same time to operate the methanation continuously as feedstock is always available.

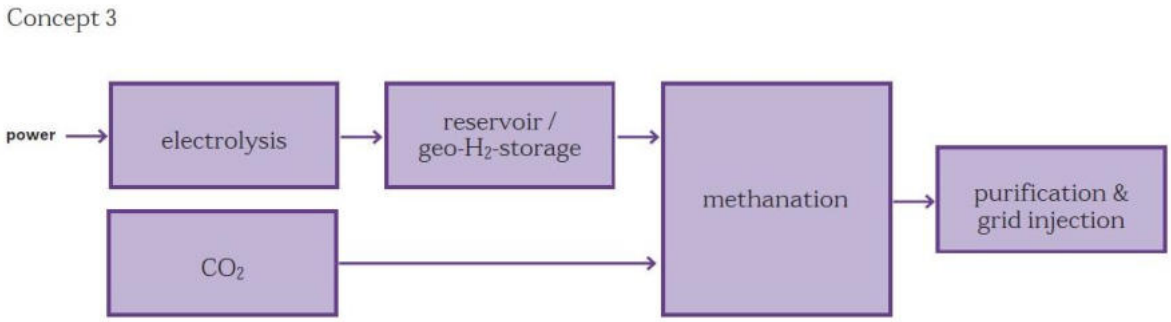

Figure 6-6: Concept 3 with underground hydrogen storage.

In concept 3, only compressed hydrogen is injected into the storage reservoir, using the subsurface as a hydrogen storage facility. Hydrogen is produced and stored when surplus electricity is available, thus using the vast underground capacities compared to their smaller/more expensive above-ground counterparts. This concept is evaluated in case the geo-methanation process does not take place sufficiently or its conditions are too complex for economic operation. Such restrictions could be in blending rates or low flexibility in management (investigated by IFA Tulln).

The CO_2 source for the above-ground-methanation is assumed to be constant throughout the year (e.g., from a waste incineration plant). A small buffer storage is used for short-term balancing and maintenance. The concept allows constant operation of the above-ground-methanation unit all year round, which is expected to have a positive economic impact. The hydrogen from the underground storage is purified for this purpose and fed into the methanation process with the compressed CO_2. Afterwards, the methane is purified, compressed, and injected into the gas grid. Alternatively, the hydrogen can also be directly utilized for industrial or transport purposes.

During the project, the idea of storing both hydrogen and CO_2 separately underground (and not only hydrogen as envisaged in this concept) was also discussed. Based on the assumption that CO_2 is available at a relatively constant level throughout the year (e.g., in waste incineration plants), this more complex variant was abandoned and only a buffer storage (above ground) for the CO_2 was included. As the findings of Empa indicates, CO_2 will likely not be a limiting factor. However, the storage of pure hydrogen underground is further investigated in “Underground Sun Storage 2030” conducted in the immediate vicinity of the project.

6.6.3 Plant sizes

In this chapter, the concepts from the previous section are mapped with a selection of evaluated site models from Empa. There, various future scenarios for the Swiss energy system were considered, based on the perspectives for the three upcoming decades of the Swiss Federal Office of Energy. With regard to these scenarios and by taking the currently used energy infrastructure into account, possible locations for geo-methanation project were defined on the basis of the technical framework conditions. It was found that there are generally two economically feasible options, either near CO_2 sources or on the site of a power plant. Municipal waste incineration plants (MWIP) have both sufficient on-site renewable electricity generation and CO_2 to capture. They are therefore among of the most promising candidates for geo-methanation next to run-of-river power plants (RoR), which have their peak production of renewable electricity approximately at the same time as the largest photovoltaics electricity surpluses occur in summer.

The top ten sites of RoR power plants as well as five MWIPs were evaluated based on their modelled annual net surplus electricity in 2050 and are listed in Table 6-7. Besides the total available electricity, the corresponding size of the electrolysis and the annual hydrogen production are registered. Furthermore, the table contains information on the closest CO_2 source and the nearest distance for a connection to both high and low-pressure gas grid. The second column indicates whether the site is located within a feasible area from geological point of view.

Table 6-7: Summary of the top USC-FlexStore sites at RoR and MWIP power plants in Switzerland and their most relevant characteristics (Duplicated and identical as Table 4-5).

#	USC site			Net surplus Electricity						H2		CO2 source				Gas grid	
	Geology	Power Plant	Name	used	used	total gen.	total gen.	hours	eq. FLH	ELYSE	Yield	needed	#	Type	Name	Distance	HD	LP
				GWh / year	GWh / summer	GWh / year	GWh / summer	hours	h	MW_el	t H2 / year	t CO2 / year				km	km	km
1	outer	RoR	Laufenburg	320	313	519	323	4368	3427	95	5484	30162	1	CEM	Würenlingen	15	2.1	4.2
2	inner	RoR	Verbois	277	261	384	278	4368	2898	89	4733	26032	1	MWIP	Aire-La-Ville	0	4.2	0.9
3	outer	RoR	Albbruck	274	265	435	284	4224	3425	80	4683	25756	1	CEM	Würenlingen	11	7.0	8.3
4	inner	RoR	Eglisau	163	159	257	165	4368	3150	53	2792	15357	1	MWIP	Dietikon	18	3.1	4.8
5	outer	RoR	Reckingen	132	129	213	133	4368	3509	38	2259	12427	1	CEM	Würenlingen	9	1.6	0.3
6	inner	RoR	Rheinau	126	123	196	127	4368	3523	36	2164	11903	1	MWIP	Winterthur	19	2.8	3.8
7	inner	RoR	Gösgen	108	103	248	107	4368	3247	42	1853	10192	1	MWIP	Oftringen	9	1.2	0.0
8	outer	RoR	Wildegg-Brugg	94	91	237	95	4368	2567	45	1611	8863	1	CEM	Möriken-Wildegg	6	4.6	0.6
9	inner	RoR	Mühleberg	93	91	132	97	4368	3106	31	1598	8789	1	MWIP	Bern	10	3.8	5.0
10	outer	RoR	Schaffhausen	90	87	141	91	4368	3571	25	1548	8512	1	MWIP	Winterthur	24	1.5	0.0
22	inner	MWIP	Zürich Hagenholz	55	50	111	56	4368	4368	13	948	5212	1	MWIP	Zürich Hagenholz	0	3.2	0.0
28	inner	MWIP	Zuchwil	49	44	97	49	4368	4368	11	832	4575	1	MWIP	Zuchwil	0	2.1	0.4
30	inner	MWIP	Aire-La-Ville	48	44	96	48	4368	4368	11	818	4500	1	MWIP	Aire-La-Ville	0	3.8	1.1
35	inner	MWIP	Hinwil	40	37	81	40	4368	4368	9	689	3792	1	MWIP	Hinwil	0	2.6	0.1
39	outer	MWIP	Monthey	38	34	75	38	4368	4368	9	643	3539	1	MWIP	Monthey	0	0.3	0.7

One unit of each type was chosen for the full techno-economic analysis, namely the RoR plant in Verbois (#2) and the MWIP in Zuchwil (#28). Both of them are located in the inner part of the geology belt, where information on subsurface temperatures and geology are available and they would operate one of the largest electrolysis sizes of their types, too. Furthermore, the potential of using the net surplus power of the entire country of Switzerland is analysed

To operate a geo-methanation system, the CO_2 must be added from another source. Since CO_2 sources usually exist all year round, a geo-methanation operation could be operated stoichiometrically or off-stoichiometrically. in the former, the CO_2 is used elsewhere or released into the atmosphere at the time when there is no excess flow. In the case of off-stoichiometric operation, the CO_2 is added when it occurs and corresponds in total to the annual demand of geo-methanation.

6.6.3.1. Size 1: Municipal waste incineration plant (MWIP)

Waste incineration has a constant energy production profile and constant waste gases, which are produced during the process and can serve as a source of carbon dioxide. For this reason, neither of the feed gases (CO_2 and H_2) requires intermediate storage before being injected underground for the conversion process. In addition, no major load fluctuations are to be expected throughout the year, as the feed from the MWIP is also relatively constant. The operation of a geo-methanation system at an MWI plant obtains electricity for electrolysis at a constant output when surplus electricity is available. In the case of Zuchwil, a power output of 11 MW_{el} is available. With the expected quantities of renewable gas produced with this system, an injection into a regional transport network (<5 bar) is considered.

6.6.3.2. Size 2: Run-of-River (RoR) hydro powerplant

In the case of the Verbois RoR power plant, the peak of surplus energy is expected in summer, while the smallest loads occur in spring and autumn, as well as increased start-up and shutdown processes. According to chapter 4, a CO_2 source is available nearby. With the expected quantities of renewable gas produced with this system, an injection into a national transmission network (>16 bar) is considered.

6.6.3.3. Size 3: Total Swiss potential

The largest size considered in this project for a possible geo-methanation is if the total amount of surplus electricity available throughout Switzerland in the future. The data for this is taken from chapter 4 and shows which amount of surplus electricity will be generated in Switzerland and when. Their calculations show that a maximum of 10'050 MW_{el} power will be available.

6.6.3.4. Parameters of the three scenarios

Initial models of the underground storage reservoirs were developed for the three scenarios in order to simulate the annual process of the filling level. The maximum surplus energy for each case is summarized in the table below and corresponds to the size of the electrolysis.

Table 6-8: Modelled electrolysis sizes of the plants from the data of Empa for different reference years.

	Size Electrolysis [MW_{el}]		
	2016	***2017***	***2018***
MWIP Zuchwil	11	11	11
RoR Verbois	87	98	89
Switzerland	8’964	10’050	9’590

In a first step, only the filling of the underground storage was considered for a whole year. Figure 6-7 shows the system boundaries and parameters of the model.

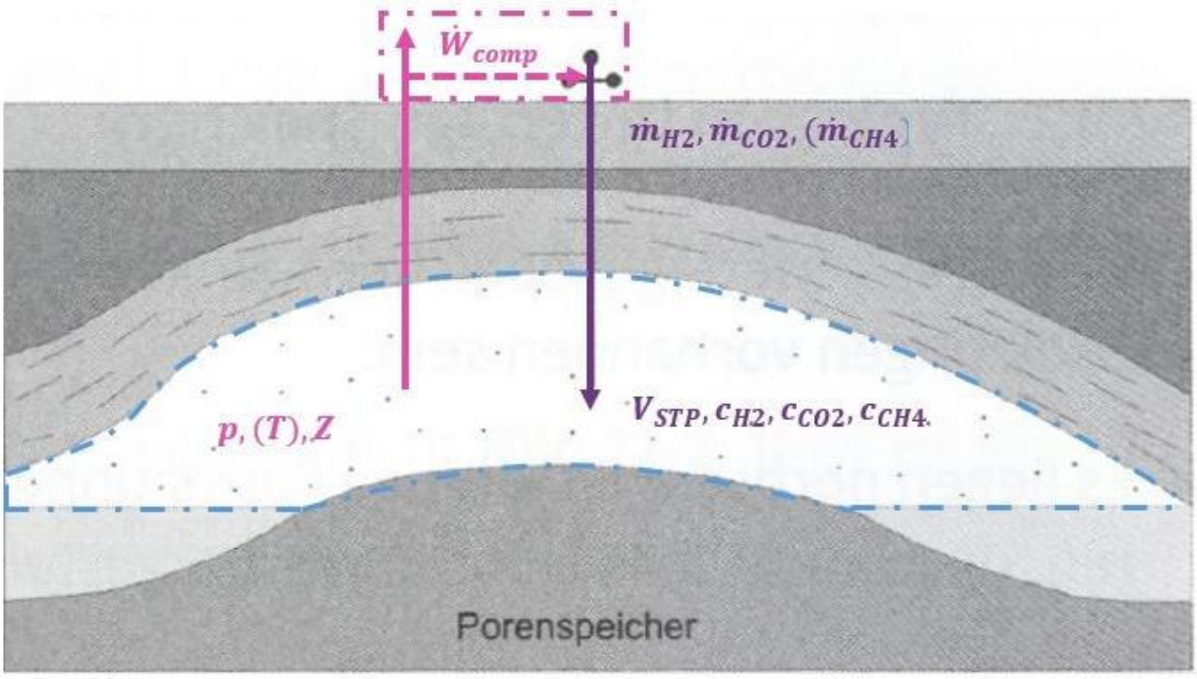

Figure 6-7: System boundaries and parameters of the initial USC -FlexStore model (purple), as well as the planned extensions of the model (pink) upon the development of the use cases. Source: (Kadner, 2015)

Presently, it is based on the mass flows of the feed gases, the gas volume at standard temperature and pressure (STP[2]) in the underground storage, as well as the concentration of the gases. Furthermore, both stoichiometric and off-stoichiometric injection has been modelled for all cases. In the former, hydrogen and carbon dioxide are always added in a ratio of 4:1, while in the off-stoichiometric filling a constant CO_2 mass flow is fed throughout the year. Moreover, the following boundary conditions were defined:

- Electrolysis efficiency as a function of partial load operation
- Conversion rate independent of temperature, pressure or gas composition
- Homogeneous mixing of all gases in the storage system

6.6.3.5. Cushion and carrier gas

According to Chapter 5, only aquifer reservoirs can be considered as gas storage facilities in Switzerland. To develop an aquifer reservoir, cushion gas is needed. According to (Kadner, 2015), the proportion of cushion gas in aquifer storage varies between 50 and 70 %. In the present project, 50% is assumed. In a conventional natural gas storage facility in an aquifer, the ratio of working gas to cushion gas is therefore around 50:50.

In geo-methanation, the working gas consists of the reactants hydrogen and CO_2 and a carrier gas, ideally methane. The carrier gas is necessary so that the partial pressure of the CO_2 in the subsurface does not become too high and does not disturb the microbiology. Methane is used as a carrier gas because this is also the desired product of geo-methanation and thus the process of this methanation is not disturbed. Because of the critical partial pressure, CO_2 cannot be used as a carrier gas (see chapter 2), and the use of hydrogen would probably be economically difficult.

[2] 15.6 C° and 101'325 Pa

In the calculations, a share of 80% carrier gas is assumed for the feed-in of hydrogen and CO_2 as a standard value, if not stated otherwise. This ensures that the partial pressure of CO_2 is not exceeded.

6.6.3.6. Resulting storage sizes

As already mentioned in previous chapters, various models of the geo-methanation were developed. On the one hand, both stoichiometric and off-stoichiometric feed gas injection was taken into account for each plant, with no difference in the amount of renewable working gas produced. In addition, two scenarios were calculated with regard to carrier gas:

- Model A: No additional carrier gas is provided by the natural gas grid.
- Model B: Carrier gas is obtained from the natural gas grid and amounts to a constant 80 vol.-% CH_4 in the feed gas volume flow.

The results are summarised in Table 6-9:

Table 6-9: Summary of the simulations of the storage filling process for two different models (A+B). For each model, the approximate amount of working gas stored, and the maximum level of the total gas (incl. cushion gas) attained in a year are specified. The geological volume was calculated with a pressure of 160 bar (maximum filling level) and the conversion rate according to Figure 6-8.

Site	Size electrolysis	Model A: No carrier gas			Model B: 80 % Carrier gas from grid		
	In MW	Max. storage volume [Mio. m^3, STP]	Max. storage volume incl. 50% cushion gas [Mio. m^3, STP]	Geological storage volume at max. filling level incl. cushion gas, 160 bar [Mio. m^3]	Max. storage volume [Mio. m^3, STP]	Max. storage volume incl. 50% cushion gas [Mio. m^3, STP]	Geological storage volume at max. filling level incl. cushion gas, 160 bar [Mio. m^3]
MWIP Zuchwil	11	1.75	3.50	0.023	8.7	17.5	0.114
RoR Verbois	89	14.1	28.3	0.184	70.7	141.4	0.919
all CH	9’590	1’524	3’048	19.8	7’619	15’238	99.0

For comparison reasons, the gas consumption of Switzerland is mentioned here. In 2018, approx. 35.6 TWh of heating energy was provided by natural gas, which corresponds to about 3'200 million m^3(STP) of methane. Between 5 and 13% of today's demand could be provided by geo-methanation if only the working gas volumes of model A are considered. Taking into account the expected future reduction in gas demand – Empa assumes a gas demand of 14 TWh in 2050 (-60% compared to today's level) - the potential of all RoR-operated USC plants is significantly greater, namely up to 32%. With the total Swiss surplus, the potential likely surpasses the requirements of the yearly national gas demand in 2050.

For further potential analyses, particularly the search for suitable sites in Switzerland, the relationship between the ratio of the geometric storage volume (VStorage) and the amount of gas to be stored (VGas,(STP)) as a function of the working pressure is shown in Figure 6-8. The pressure is limited by the drilling depth. The plotted area is limited by the temperature, 30 °C at the bottom and 60 °C at the top and the following gas composition has been modelled:

- c_CH_4 = 80 vol.-%
- c_H_2 = 16 vol.-%
- c_CO_2 = 4 vol.-%

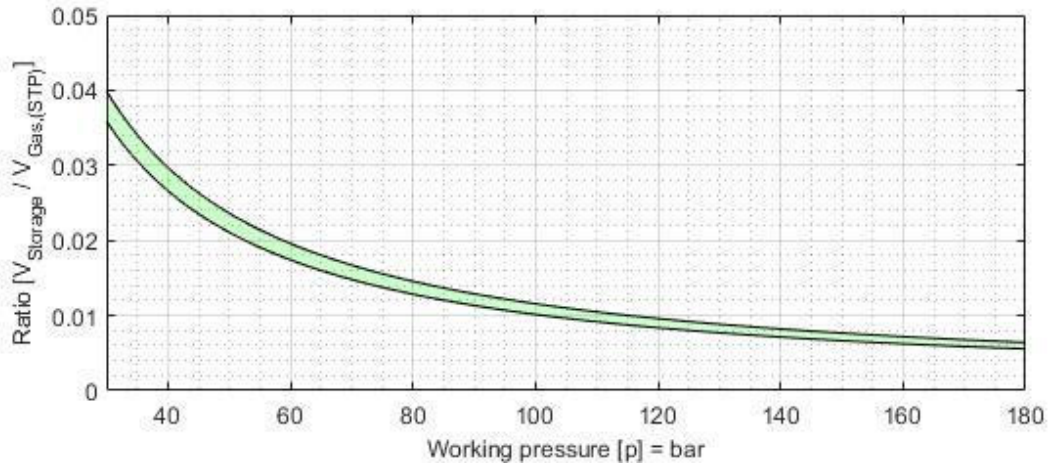

Figure 6-8: Correlation between the ratio of the geometric storage (VStorage) and the gas volume to be stored (VGas,(STP)) as a function of the working pressure.

6.6.3.7. Gas composition in the geo-methanation

As it may be possible to draw better conclusions around the conversion rate in the geo-methanation with more operational experience and whilst it seems to largely depend on the predominant gas composition, the annual change of the volume fractions in the developed models are briefly discussed.

Figure 6-9 shows the gas composition in Verbois with both feed gas injection alternatives for the model without additional carrier gas from the gas grid. Although considerable changes can be seen, the methane concentration never drops below 70% due to the cushion gas. Achieving optimal mixing would pose the major difficulty at this point.

With the constant feed of 80% methane in the feed gas (model B), the changes in the concentrations in the storage are marginal in the small single-digit percentage range, as shown in Figure 6-10.

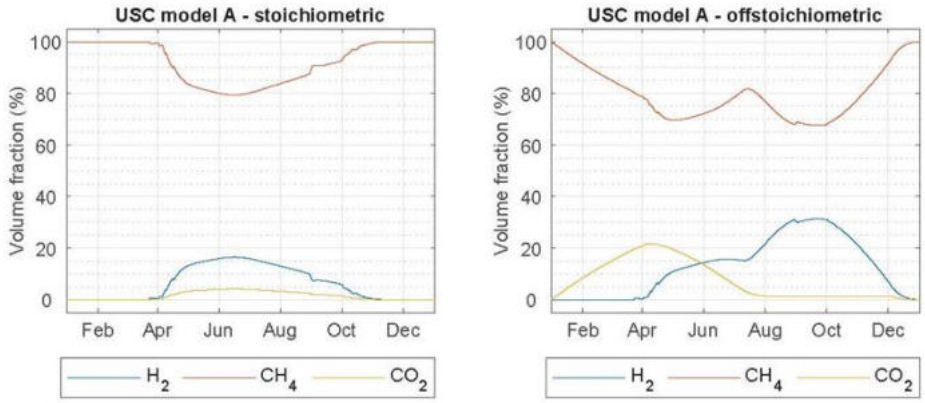

Figure 6-9: Seasonal gas composition in underground storage according to the USC model A of Verbois. Left: stoichiometric, right: off-stoichiometric feed gas dosing

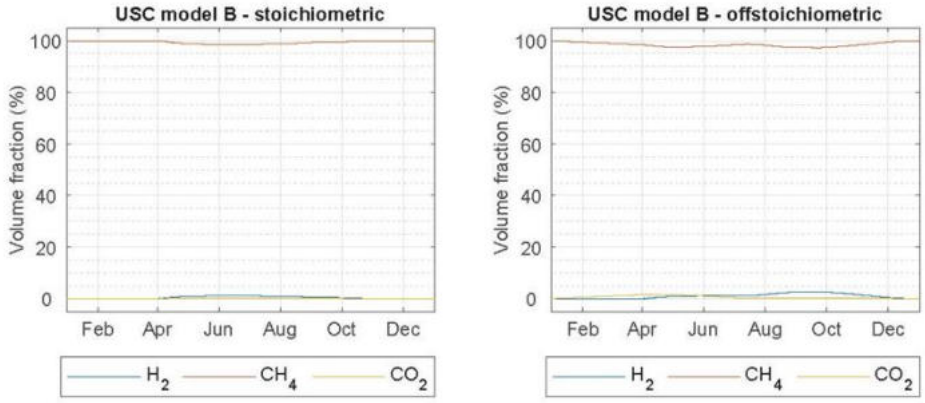

Figure 6-10: Seasonal gas composition in underground storage according to the USC model B of Verbois. Left: stoichiometric, right: off-stoichiometric feed gas dosing

6.6.3.8. Requirements for locations

In order to be able to define one or more sites that are suitable for geo-methanation, geological, technical and economic considerations are necessary. The siting requirements are strongly determined by the geological findings from University of Berne, but also by the availability of energy infrastructures such as electricity, gas and - due to tariffs for the electricity grid - the local energy generation potential as determined by Empa.

- Other important requirements are listed below:
- Plant location (land management)
- Soil protection laws
- Water rights
- Noise pollution
- Air pollution

- Hazardous substances
- Waste management
- Access authorisation (fencing)
- Safety issues (fire protection)
- Planning permission
- Operating permit

6.6.3.9. Geological requirements

The main component of geo-methanation is the storage space to be developed in the ground. In order to determine possible storage sites in Switzerland, the Geological Institute of the University of Bern conducted appraisals of the suitability of geological formations for USC in Switzerland based on available data across the Swiss Molasse Basin.

In general, in order to prevent the gas from escaping vertically or laterally, an aquifer reservoir must be sealed by an impermeable formation at the top and hydrodynamic traps should be present to prevent gas escaping laterally. In addition, the conditions (temperature, pH and pore water composition) have to be in the range where microbial methanogenesis is possible. These requirements are outlined in depth in chapter 5.

6.6.3.10. Techno-economic considerations

Next to defining ideal locations for a geological storage, enough power and connections to both power and gas grids are necessary. With a geo-methanation plant, electricity and gas grids are connected via electrolysis and underground storage. CO_2 and (renewable) electricity are used as input to produce hydrogen. In general, waste gases from biogas plants, wastewater treatment plants, incineration plants and cement plants are suitable as CO_2 sources (Meier et al., 2017). The methane gas produced is seen as a product of the node and connects the system to the gas grid.

Various parameters influence the technical and economic possibilities:

- Reservoir development: To build a geo-methanation plant, exploration, cushion gas and probes are needed, which incur significant costs. The amount of cushion gas needed depends on the system and operating concept. The larger the reservoir for geo-methanation, the more cushion gas is required, and the number of probes increases. The purchase of the cushion gas counts as an investment cost, as it remains in the reservoir for the entire life of the system and cannot be used elsewhere. If the reservoir is dissolved, part of the cushion gas can be sold.
- Carrier gas: If the reactants are brought into the reservoir with carrier gas, this must also be procured. In this project, methane is used as the carrier gas. Since this gas is obtained from the gas grid and fed back into it, the economic calculations assume cost neutrality. This means that it is assumed that the gas can be purchased and resold at the same cost and therefore has no influence on the business case, with the exception of the larger storage facility required.
- Recognition of the methane produced as a renewable gas: Hydrogen must come from a renewable source (renewable electricity source)
- Operating hours: In the previous research project Store&Go on power-to-gas plants, it was shown that in early applications, power-to-gas plants will need to run at high full-load hours (>5,000 h/a) to achieve low SNG production costs (Zauner et al., 2019). Later (as from 2030), the lowest costs will be achieved at fewer full-load hours (2,000–4,000 h/a) when the plant is operated only at the lowest electricity prices. The higher the full-load hours of the Power-to-Gas plant, the lower is the share of investment costs. However, the share of electricity costs is dominant. Therefore, higher operating

time requires that the Power-to-Gas plant be operated when electricity prices are comparatively high. The advantage of the declining share of investment costs at high full-load hours cannot be offset by the increase in the proportion of electricity costs.

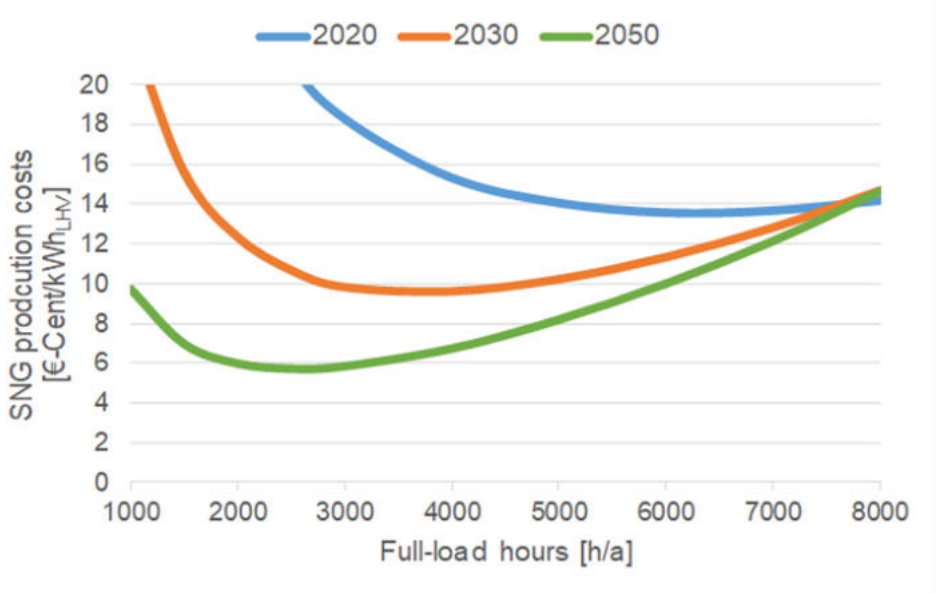

Figure 6-11: Specific SNG production costs in relation to the full-load hours for the scenarios PtG-Grid in 2020, 2030 and 2050. Note: The development of power-to-gas technology is subject to fundamental energy and climate policy decisions; thus, assumptions made about the future can change significantly. This has a major impact on the future SNG production costs calculated. Source: (Zauner et al., 2019)

- Larger electrolysis with higher hydrogen output generally have lower gas production costs than small electrolysis. It can therefore be advantageous to install a larger electrolysis and resell part of the excess hydrogen.
- Electricity source: The electricity price is a critical factor for economic viability. If it is too high, the hydrogen cannot be produced economically.
    - A sufficiently high and available power at the transformer is necessary.
    - Electricity directly from production leads to better economic efficiency (no grid fees).
    - If electricity production is high throughout Switzerland but demand is low, electricity costs fall. With an increasing installation rate of solar cells, this will often be the case in summer in the future. The operation of electrolysis at such times can have a major economic impact. However, attention should also be paid to a suitable number of operating hours.
- Grid fee exemption: The threshold for grid-beneficial electrolysis is optimally steered by the market. Whenever the market-price for electricity is below a defined benchmark, which is to be set below the levelized cost of energy per unit of the applicable non-renewable energy production asset, the assumption for electrolysis to be systemically beneficiary seems valid. The benchmark therefore must be kept above a level at which the levelized cost of energy of renewables is set. Such a mechanism would make use of the levelized cost of energy for renewable energy production compared to non-renewable plants and would incentivize to invest in flexible consumers (electrolysis) as well as in renewable assets by fostering a price floor for renewable electricity. Within the abovementioned price-spans, the production of hydrogen furthermore could be assumed to be entirely green.

- CO_2 source: the available CO_2 quantity should correspond to the planned plant size.
    - Ideally, a CO_2 source is available nearby so that the CO_2 can be transported by pipeline (cheaper than compression and transportation by truck).
    - The CO_2 is available in pure form or mixed with methane (biogas).
    - The CO_2 source should be constant or available in the same period as the hydrogen.
    - In the case of flue gas with different components or air as CO_2 source: High energy demand for filtration.
    - If wastewater treatment is used as CO_2 source, it can be checked whether the oxygen from electrolysis can be used for wastewater treatment (ozonation).
- Water source: Sufficient water of suitable quality must be available (electrolysis).
- Natural gas grid:
    - Proximity to gas grid for feed-in or local consumers.
    - Capacity in the network is large enough for additional gas feed-in.
    - The gas quality must meet the requirements of the gas grid; feed-in in accordance with G-18 regulations Directive
    - With aboveground methanation: Gas network with low pressure level advantageous (no compressor after methanation)
- Waste-heat: Heat must be dissipated from the process (electrolysis).
    - The higher the temperature, the better it can be utilised
    - Local consumers increase the overall efficiency of the plant
    - Feeding waste heat into a district heating network is recommended if the heat is generated at the same time as it is needed. For example, in winter the heat can be used to heat buildings, in summer for industrial processes.
- Space conditions: There must be sufficient space available at the site for the plant, including safety clearances.
- Building permit: An underground gas storage facility is unusual in recent Swiss history. This leads to uncertainty. The affected population and businesses must be informed and consulted from the outset.
    - Early contact and involvement of the relevant authorities
    - Proactive participation processes

6.6.4 Use cases of geo-methanation

In this chapter, the focus is on possible ways to integrate geo-methanation in our energy and economy system.

In two professionally moderated workshops, the project partners involved in the USC-FlexStore jointly developed new applicable ideas for a company working with geo-methanation technology in 2038. The timeframe was chosen in order to liberate the participants from hindering knowledge on restrictions of either regulatory, social or market-related nature during the ideation phase. The year 2038 was agreed upon since it is far enough for considerable changes in the general environment of the project and soon enough, so the majority of participants will not yet be retired. This approach left the participants the degrees of freedom to set their ideas in a very permissive environment and unbothered of a potential lack of sudden increases in the seasonal patterns of today's energy production due to conventional thermal power plants.

The result of the workshops were three possible applications:

1) "Strategic reserve" = storage as strategic reserve
2) "U-Store" = privately bookable seasonal electricity storage
3) "Power valley" = providing geographically regions or industry clusters with a higher level of energy security

Figure 6-12 describes the principle of geo-methanation and illustrates the three identified applications:

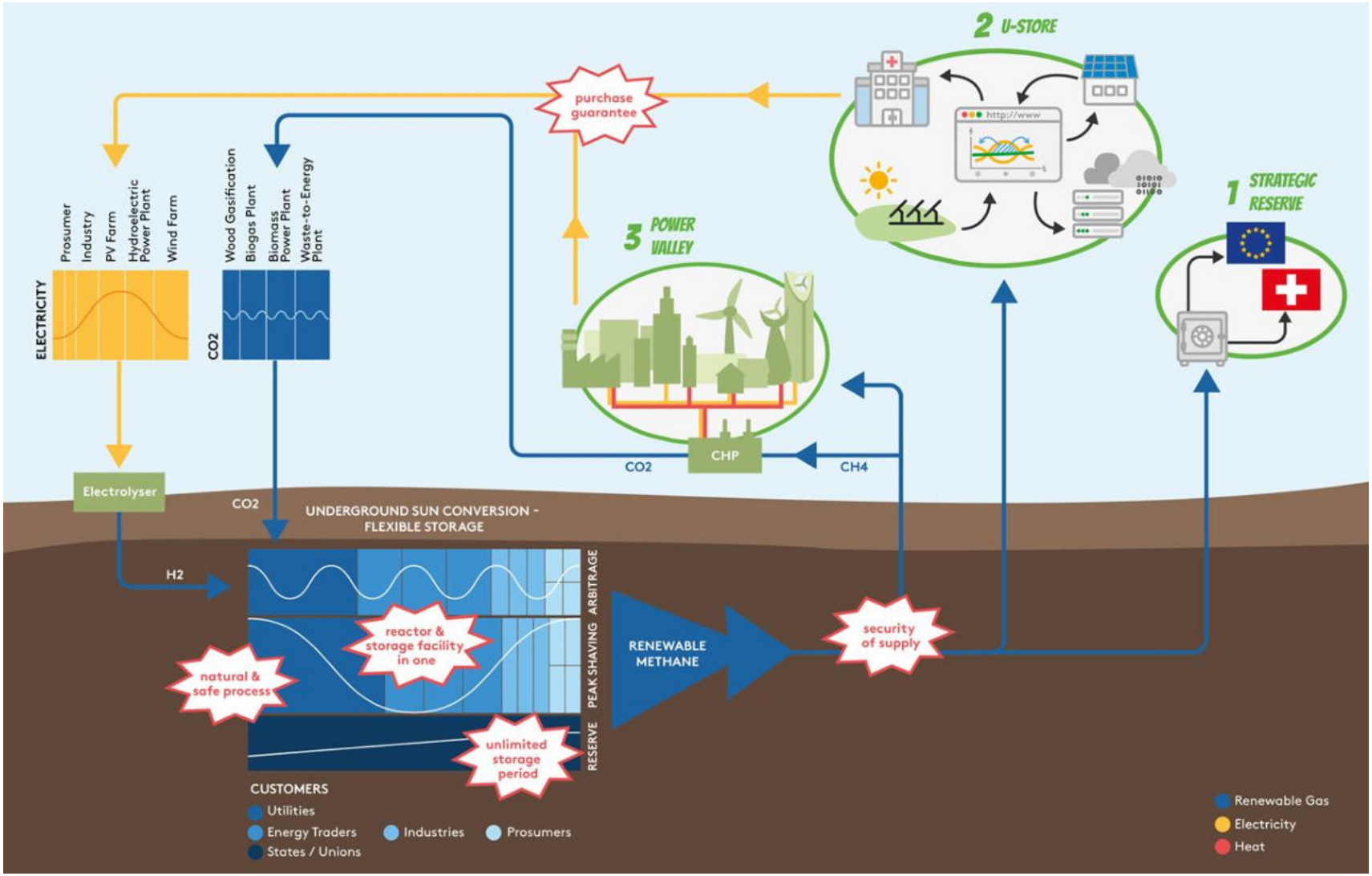

Figure 6-12: Principle of geo-methanation and illustration of the three identified market opportunities. Illustration by: Meret Boggiano, Energie 360°.

6.6.4.1. Key Elements of the geo-methanation process

Figure 6-13 illustrates the key elements, around which Underground Sun Conversion is set up and upon which the use cases are set.

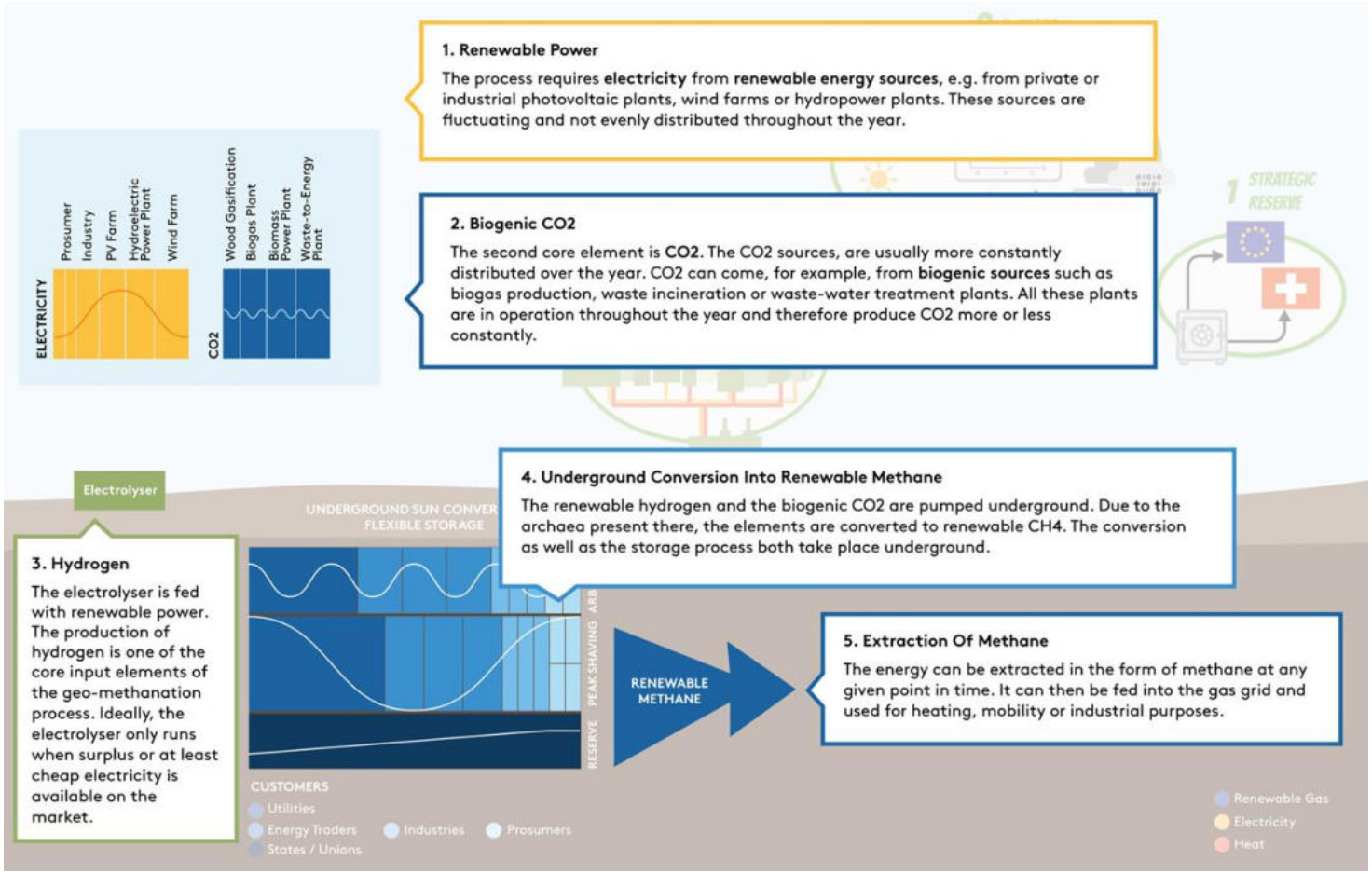

Figure 6-13: Key elements of the geo-methanation process with the different sources for power, hydrogen and CO_2. Illustration by: Meret Boggiano, Energie 360°.

6.6.4.2. Types of usage

Due to its large volume and high capacity, Underground Sun Conversion offers three of the main basic functions of a storage option, as illustrated in Figure 6-14:

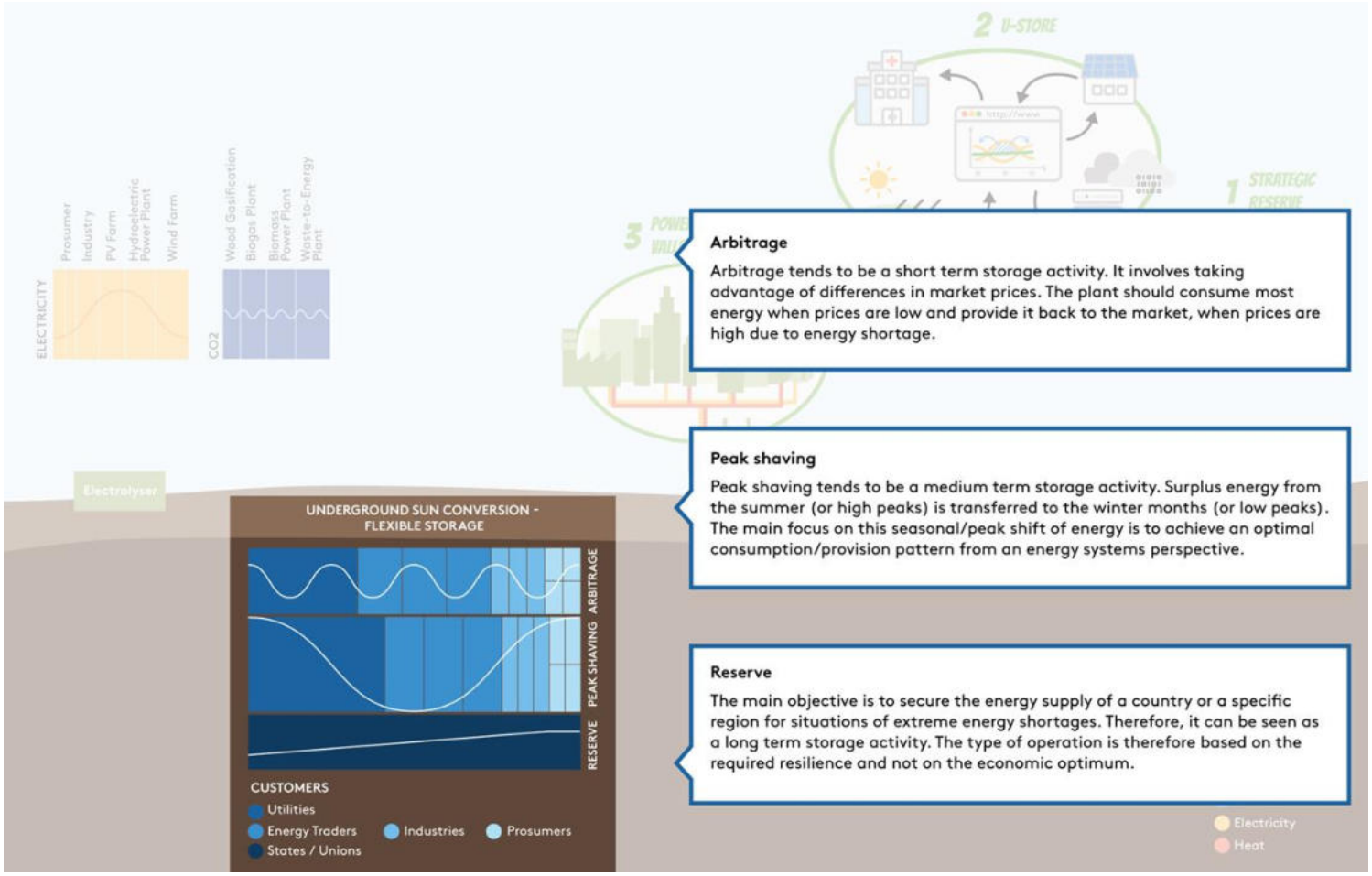

Figure 6-14: Different possibilites to use the Underground Sun Conversion - Flexible Storage. Illustration by: Meret Boggiano, Energie 360°.

6.6.4.3. Unique Selling Propositions

As Figure 6-15 demonstrates, the unique offerings towards different need-owners have been identified for the further development of use cases:

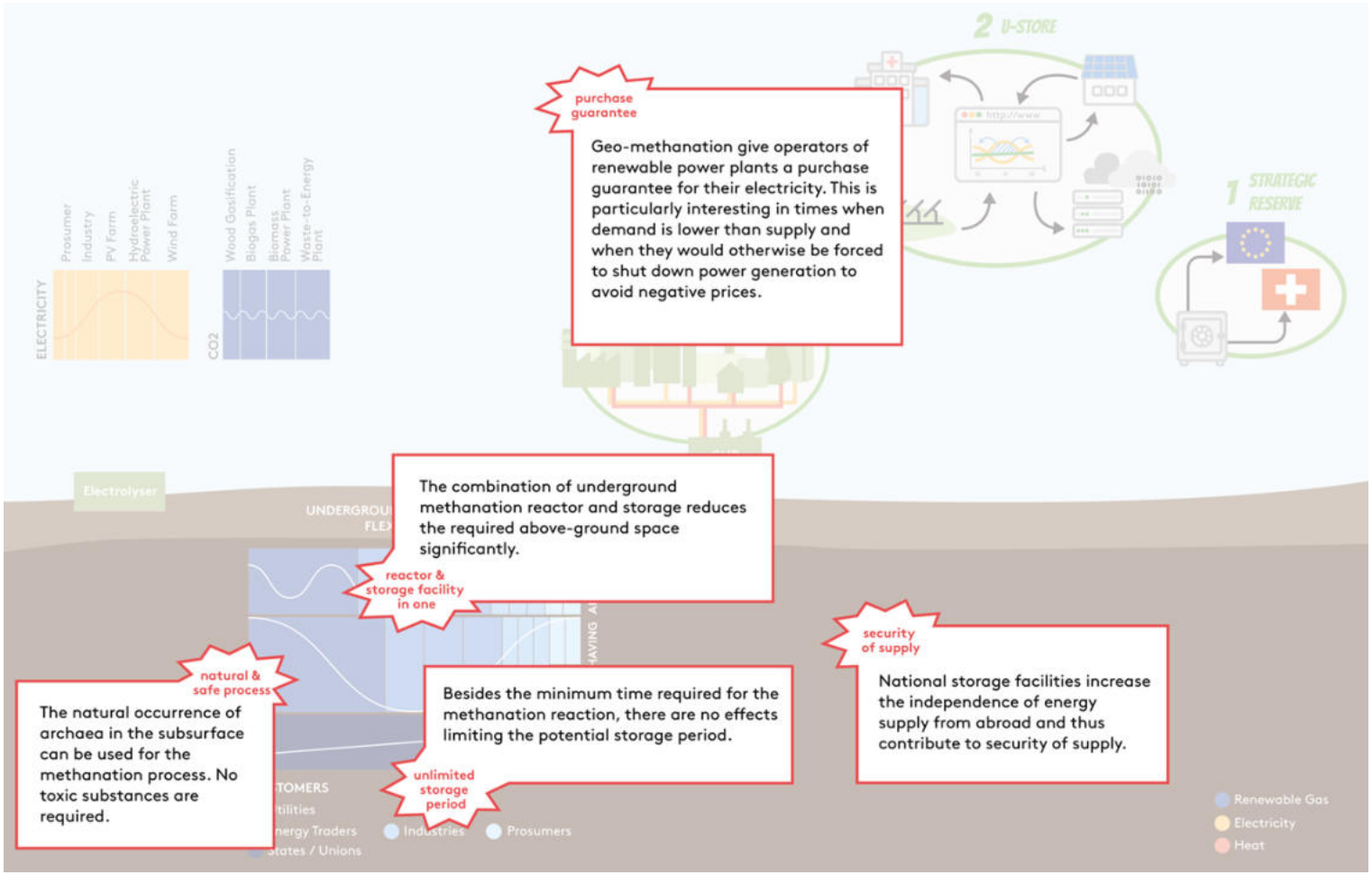

Figure 6-15: Benefits of the use of geo-methanation. Illustration by: Meret Boggiano, Energie 360°.

6.6.4.4. Identified Applications

1 - “Strategic Reserve”

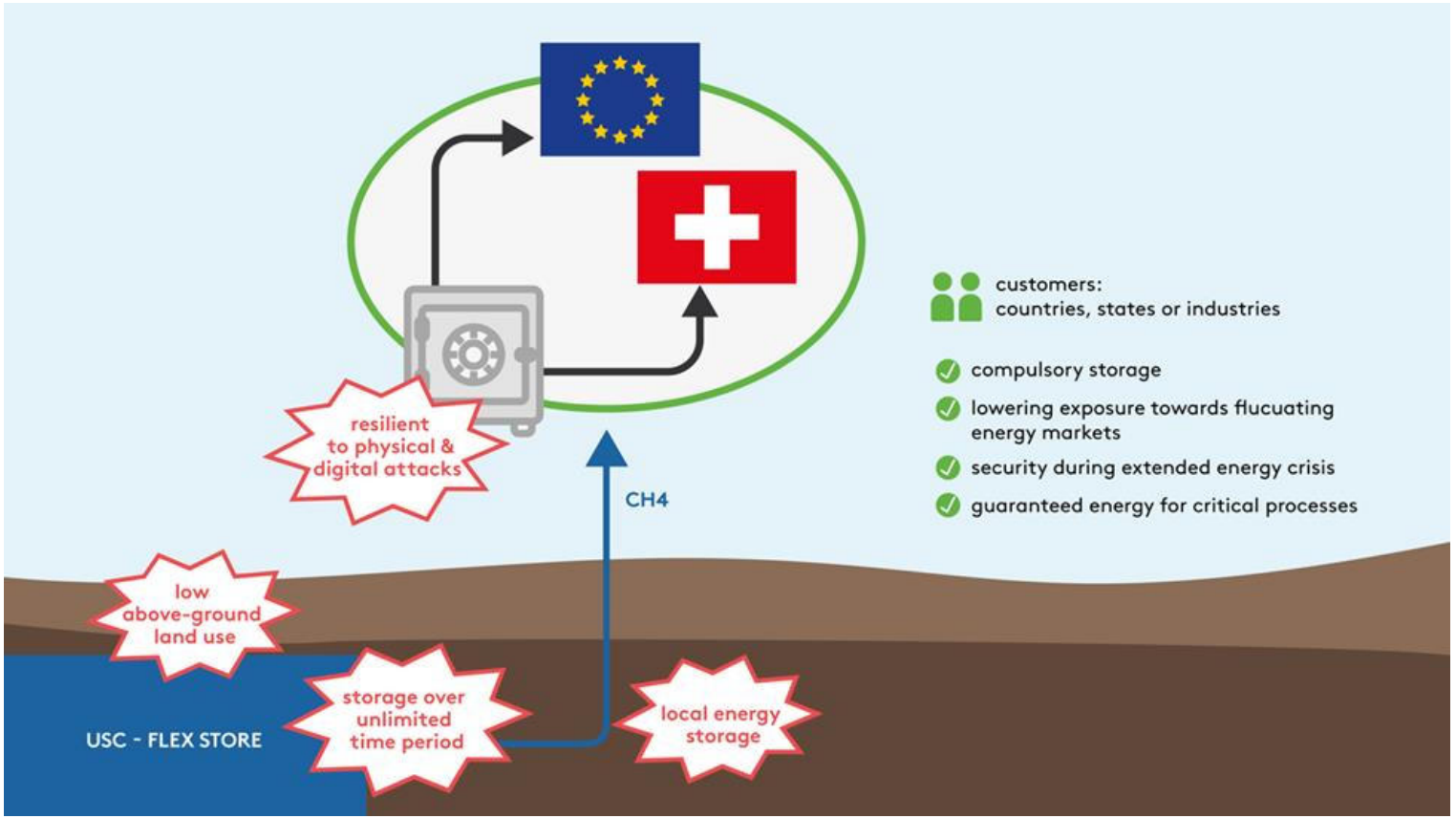

Figure 6-16: Benefits of the market opportunity to use geo-methanation as a "strategic reserve". Illustration by: Meret Boggiano, Energie 360°.

The concept of the “strategic reserve” is designed for countries, states or industries who are either obliged to keep a certain amount of energy stored in the form of a «compulsory storage», or who want to lower their exposition towards everyday energy market. The “strategic reserve” provides

governments with more independence related to foreign affairs. Furthermore, it ensures that critical processes don't need to be shut down due to energy supply shortage.

USPs of the "strategic reserve":

- A local renewable energy storage over an unlimited time periods.
- Significant size energy storage with low above-ground land consumption, therefore easy to monitor and secure. Critical processes don't need to be shut down due to energy supply shortage.
- Storage largely resilient to physical and digital attacks and acts of sabotage.
- Maintaining decision-making sovereignty of political leadership and maintaining economic and social functions during an extended energy crisis.
- Extensive independence from other countries/regions. Filling exclusively through national/local resources.
- Since the energy is stored in gaseous form, operation in an emergency is largely mechanical and the electronic control components can be isolated from wider networks, if necessary.

2 - “U-Store”

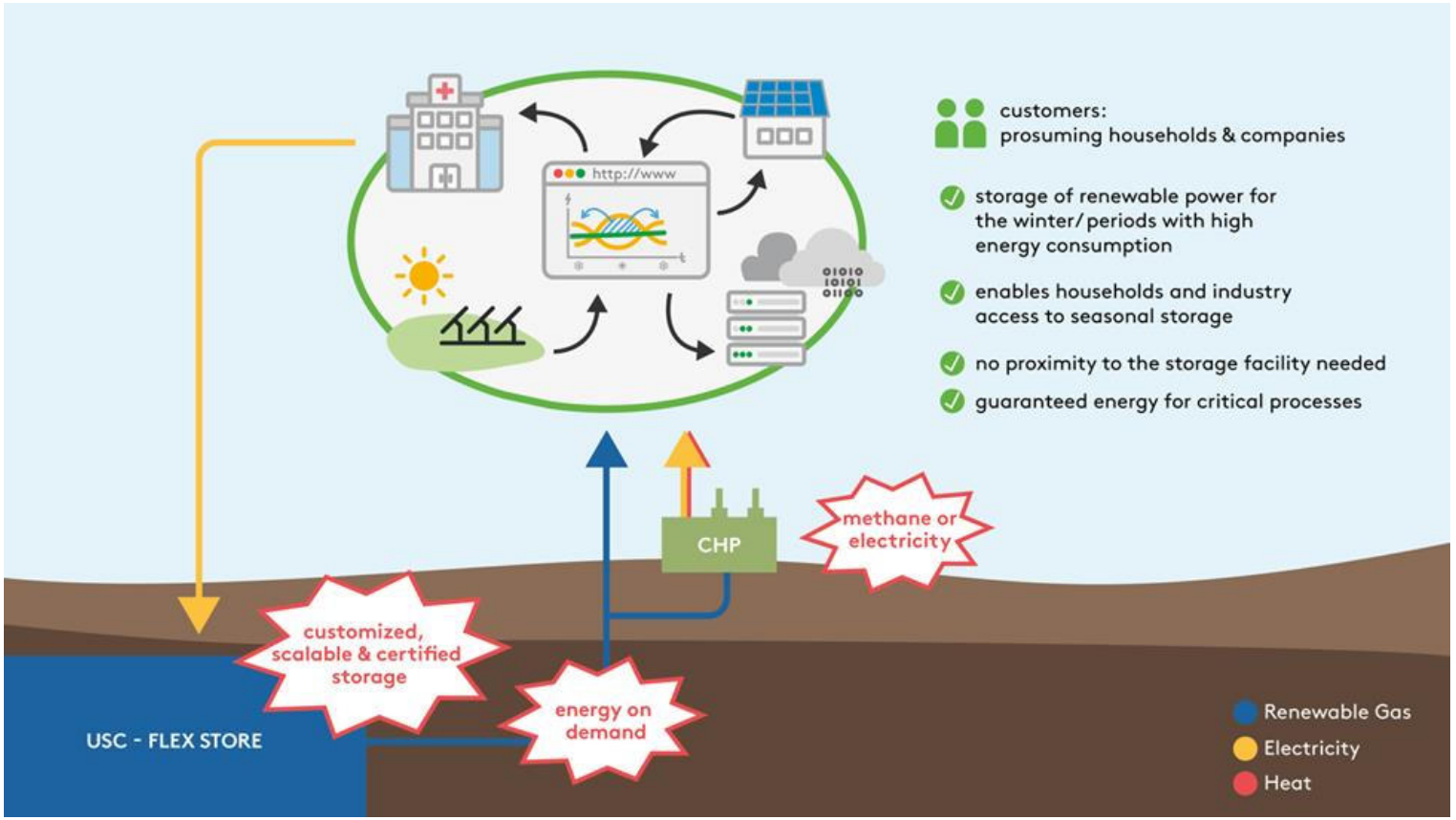

Figure 6-17: Benefits of the market opportunity to use geo-methanation as a "U-Store". Illustration by: Meret Boggiano, Energie 360°.

“U-Store” is aimed at private households producing energy, so called «prosumers», and at companies who want to store their renewable power for the winter/low peak months. Customers can connect their PV systems with the geo-methanation plant via an online platform/storage-market-place. They specify how much electricity they want to consume directly, how much they want to sell to the market and how much they want to store for the winter months. The goal is to offer customized, scalable and certified storage, that delivers and stores energy on demand for a wide range of prosumer types.

The prosumers can choose whether they want to obtain winter energy such as methane or if they want to receive the energy in the form of electricity, provided the transformation losses.

USPs of the “U-Store”:

- Private households and industry can store their own energy without having to deal with the storage itself.
- The approach enables also very small private and business-prosumers to access a seasonal storage solution and to become more energy independent.
- The participating prosumers do not need a close proximity to the storage facility. The physical transmission of the energy is decoupled from the “virtual” book keeping.

3 - “Power valley”

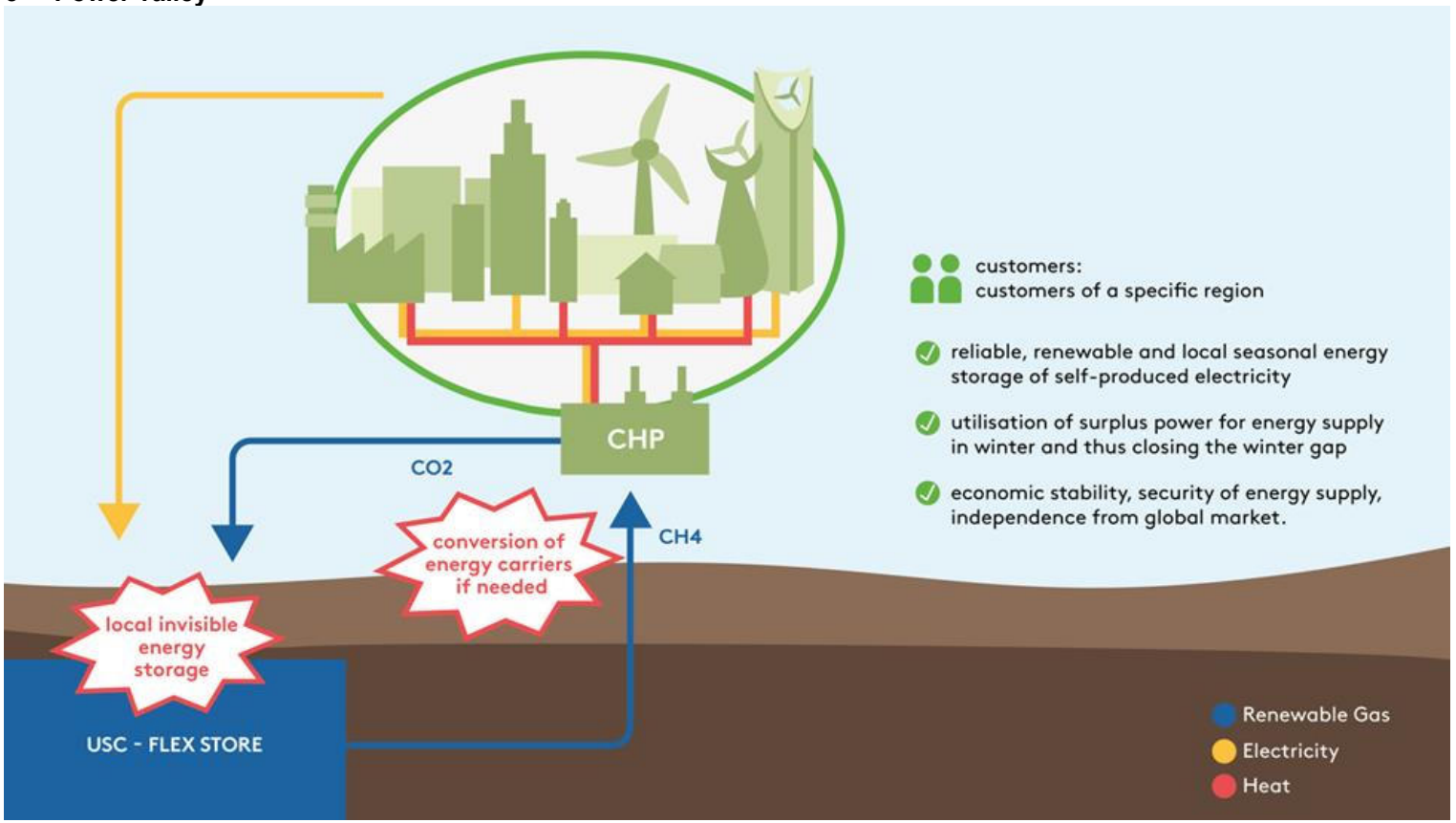

Figure 6-18: Benefits of the market opportunity to use geo-methanation as a "power valley". Illustration by: Meret Boggiano, Energie 360°.

“Power valley” is a concept that provides customers of a specific region with a range of locally, renewably produced energy carriers, throughout the year. The region produces the electricity it needs locally and stores it underground. After the geo-methanation process has taken place, the region either uses the produced methane directly as renewable biomethane or converts it to other energy carriers or into electricity and heat.

USPs of the “power valley”:

- Ensures a reliable, renewable and local seasonal energy storage of self-produced electricity for the population, small and medium-sized enterprises and industry: utilisation of surplus power for energy supply in winter and thus closing the winter gap.
- Energy remains invisibly stored in the region.
- Economic stability, resilience, security of energy supply, independence from global market.
- Could be of benefit for industries that need absolute energy security for their production processes.
- Provide regions with the security of always having the energy they need at a fixed price level.
- Provides regions a sense of communality and pride for being highly independent.
- Conversion of energy carriers: The energy sources are available to customers in the form in which they are needed.

6.6.5 Carbon neutrality of geo-methanation process

Every kWh of geo-methane can replace one kWh of fossil natural gas. The great advantage of renewable methane is that no additional CO_2 is released into the atmosphere when it is used. However, the CO_2 footprint of renewable methane also differs depending on the production method and the input materials. To quantify the CO_2 savings compared to conventional fossil natural gas, it is therefore important to consider the hydrogen used, the CO_2 source and the conversion process. In the project, the first point in this context was the certification of green hydrogen production. The certification of the electrolysis plant was based on the TÜV SÜD CMS70 standard, which is currently the most common standard in Europe. This standard specifies a greenhouse gas reduction of 90% for this application compared to conventional H_2 production using steam reforming. This corresponds to a maximum value for green hydrogen of 9 g CO_{2eq}/MJ H_2. The greenhouse gas balance includes electricity production and its upstream chains as well as other input materials such as chemicals for the water treatment of the electrolysis or the use of nitrogen to purge the pipes. The use of 100% renewable electricity is a basic prerequisite and is further enhanced by technology-specific requirements. It was possible to obtain this certification in the course of the project. In this case, electricity is purchased from a local run-of-river power plant. With a value of 4 g CO_{2eq}/MJ H_2, the greenhouse gas balance clearly meets the requirements. This certification openly and comprehensibly demonstrates the renewable nature of the electrolytically produced H_2 at the field test site and its greenhouse gas emission reduction compared to conventionally produced H_2. The CO_2 was sourced from a biogenic CO_2 source and the transport was also designed to be CO_2 neutral, so there is no additional carbon footprint here.

Now that the green property of the input gases is known, this should also apply to the product gas geo-methane. The exact definition of the requirements for certification of the resulting renewable methane have not yet been finalized, neither by a certification body nor by legal regulations. As things stand at present, the geomethane produced in the course of the field tests meets all the conditions for this. Even if it was not possible in the course of this project, a certification of the green properties of the geo-methane will be pursued further as soon as the framework for this has also been established.

6.6.6 Techno-economic evaluation

The techno-economic assessment includes, on the one hand, an evaluation of sensitivities: which elements of the plant have the greatest influence on the gas production costs. On the other hand, the total costs of a possible project can be roughly estimated and thus the different plant concepts can be compared with each other.

As pointed out in the conclusion of chapter 2, the supply of substrate gases needs to be balanced properly to achieve and maintain high methanation efficiency, the since several microbial processes are competing for the same substrates. For the techno-economic evaluation, this statement has above all the significance that the composition of the gas that is brought underground is essential for the optimal conditions for methanation. In concrete terms, this means that the partial pressure of CO_2 must not be above 4 bar. Since in Switzerland only one aquifer storage facility can be used for geo-methanation, the pressure is already relatively high anyway (between 80 and 160 bar, depending on filling level), so that carrier gas is needed to prevent the partial pressure from being exceeded. In the techno-economic evaluation, a share of carrier gas of 80 % is assumed, if not otherwise stated.

The technical-economic assessment is carried out using the figures from Chapter 6.2, among others. The cost assumptions used refer to the year 2030.

6.6.6.1. Costs concept 1 – Geo-methanation

The costs for such a geo-methanation according to concept 1 are as follows.

Table 6-10: Costs of concept 1 for different plant sizes, the cost assumptions refer to the year 2030.

Size of Electrolysis	in MW_{el}	10	50	90	100	500	1000
Capex of electrolyser	in Mio. €	6.3	31.5	56.7	63.1	315.3	630.5
Capex of compressors	in Mio. €	2.0	10.0	18.0	20.0	99.8	199.6
Capex of reservoir incl. exploration	in Mio. €	44	97	150	163	693	1’355
Capex of cushion gas	in Mio. €	12	60	107	119	596	1’192
Capex of purification and grid injection	in Mio. €	4.1	12.2	20.2	22.2	103.6	203.0
Additional costs	in Mio. €	19.2	58.9	98.6	108.6	505.8	1002
Salvage value	in Mio. €	4.9	13.6	22.4	24.6	112.2	221.7
Capex total	**in Mio. €**	**82.8**	**255.6**	**428.5**	**471.7**	**2’200**	**4’361**
Opex of electrolyser	in Mio. €	1.4	6.9	12.4	13.8	68.8	137.6
Opex of compressors	in Mio. €	0.5	2.5	4.5	5.0	24.9	49.9
Opex of reservoir	in Mio. €	3.9	10.8	17.7	19.4	88.7	175.3
Opex of purification and grid injection	in Mio. €	1.3	4.0	6.7	7.4	34.7	68.9
Costs for water	in Mio. €	0.3	1.4	2.5	2.8	14.1	28.1
Costs for CO_2	in Mio. €	2.1	10.7	19.3	21.5	107.3	214.6
Costs for electricity	in Mio. €	6.8	33.9	61.0	67.8	339.0	678.0
Opex total	**in Mio. €**	**16.2**	**70.2**	**124.1**	**137.7**	**677.6**	**1’352.4**
Methane production cost	EUR/MWh	410	270	255	253	239	237
Yearly methane production	in Mio. Nm3/a	1.6	7.9	14.3	15.9	79.4	158.9
NET PRESENT VALUE (NPV)	in Mio. €	-55	-116	-178	-193	-806	-1573

If the ratio of gas production costs is plotted against annual methane production, the following graph is derived.

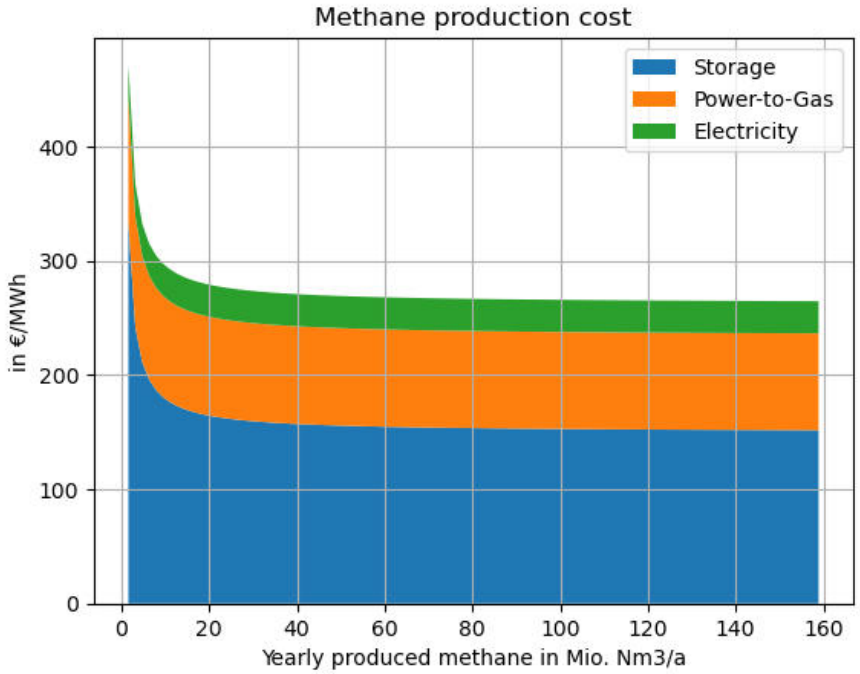

Figure 6-19: Methane production cost of concept 1 in €/MWh depending on the plant size and therefore the amount of the yearly produced methane (with a maximum of 20 % of educt gas (hydrogen and CO_2) in the geo-methanation). In the figure, the production costs are divided into the costs incurred for the storage facility (exploration, wells, cushion gas), the electricity, and the remaining costs, which are allocated to the conventional power-to-gas operation.

The different system components account for different shares of the total costs. This is broken down in the following diagram, which shows the shares of the individual expenses in the gas production costs (sum results in 100%).

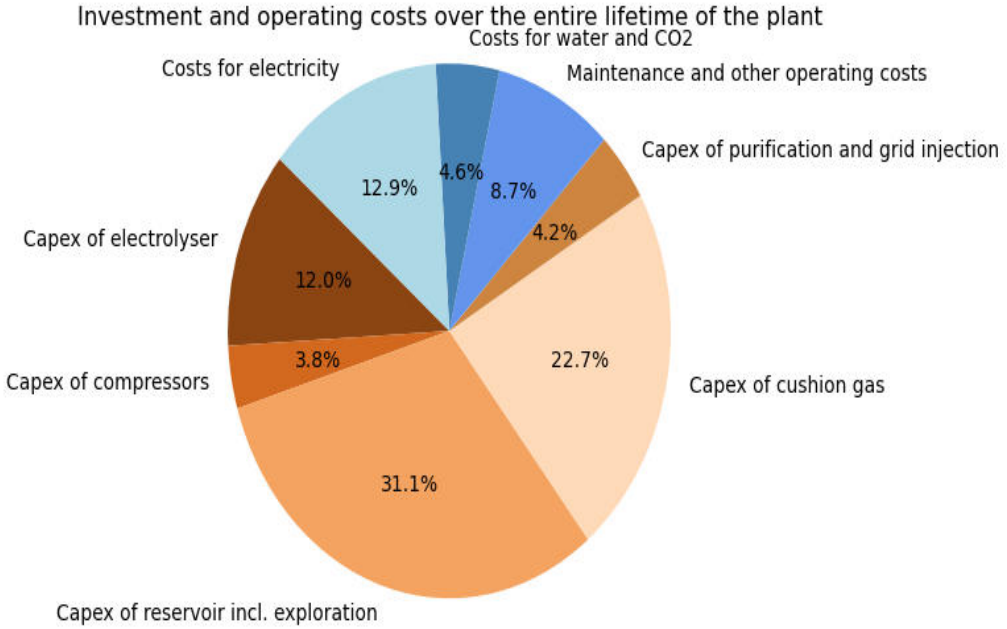

Figure 6-20: Distribution of investment and operating costs for a 100 MW_{el} plant according to concept 1, with a maximum of 20 % of educt gas (hydrogen and CO_2) in the geo-methanation.

6.6.6.2. Costs concept 2 – Combination of geo- and aboveground methanation

Concept 2 includes the possibility of an overground methanation, so that in times when there is both surplus electricity and demand for methane, the methane can be produced directly from hydrogen and CO_2.

There are different ways to operate concept 2. On the one hand, geo-methanation can continue to be pursued, with the associated conditions for operation. As a result, especially due to the necessary carrier gas for operation, the costs are similar to those of concept 1. On the other hand, with concept 2, methanation can be relocated to above-ground methanation. The reservoir is then mainly used as storage for CO_2 and hydrogen. A reaction to methane may still happen, but the operating conditions are not designed to be optimal. No carrier gas is necessary for this mode of operation. While the latter case is regarded as unattainable and is not tested, the case is corroborated nevertheless, for being able to establish a clear comparison and therefore outline the costs caused by the conditions in an aquifer and the additional need for the development of an aquifer storage site.

If the plant is operated according to the first mode, i.e., with geo-methanation and carrier gas, the costs are outlined in table 6-11:

Table 6-11: Costs of concept 2 for different plant sizes, with a maximum of 20 % of educt gas (hydrogen and CO_2) in the geo-methanation. The cost assumptions refer to the year 2030.

Size of Electrolysis	in MW_{el}	10	50	90	100	500	1000
Capex of electrolyser	in Mio. €	6.3	31.5	56.7	63.1	315.3	630.5
Capex of compressors	in Mio. €	2.0	10.0	18.0	20.0	99.8	199.6
Capex of reservoir incl. exploration	in Mio. €	44	97	150	163	693	1'355
Capex of cushion gas	in Mio. €	12	60	107	119	596	1'192
Capex of purification and grid injection	in Mio. €	4.1	12.2	20.2	22.2	102.6	203.0
Capex of aboveground methanation	in Mio. €	1.5	7.3	13.1	14.6	73.0	146.0
Additional costs	in Mio. €	19.6	60.9	102.3	112.6	526.3	1'043
Salvage value	in Mio. €	4.9	13.6	22.4	24.6	112.2	221.7
Capex total	**in Mio. €**	84.6	265.0	445.3	490.4	2'294	4'548
Opex of electrolyser	in Mio. €	1.4	6.9	12.4	13.8	68.8	137.6
Opex of compressors	in Mio. €	0.5	2.5	4.5	5.0	24.9	49.9
Opex of reservoir	in Mio. €	3.9	10.8	17.7	19.4	88.7	175.3
Opex of purification and grid injection	in Mio. €	1.3	4.0	6.7	7.4	34.7	68.9
Opex of aboveground methanation	in Mio. €	1.0	5.0	9.0	10.0	50.2	100.5
Costs for water	in Mio. €	0.3	1.4	2.5	2.8	14.1	28.1
Costs for CO_2	in Mio. €	2.1	10.7	19.3	21.5	107.3	214.6
Costs for electricity	in Mio. €	6.9	34.3	61.8	68.7	343.5	686.9
Opex total	**in Mio. €**	17.3	75.7	134.0	148.6	732.3	1'462
Methane production cost	EUR/MWh	423	282	267	265	251	249
Yearly methane production	in Mio. Nm3/a	1.6	7.9	14.3	15.9	79.4	158.9
NET PRESENT VALUE (NPV)	in Mio. €	-58	-131	-204	-223	-954	-1869

If the ratio of gas production costs is plotted against annual methane production, the following graph is derived:

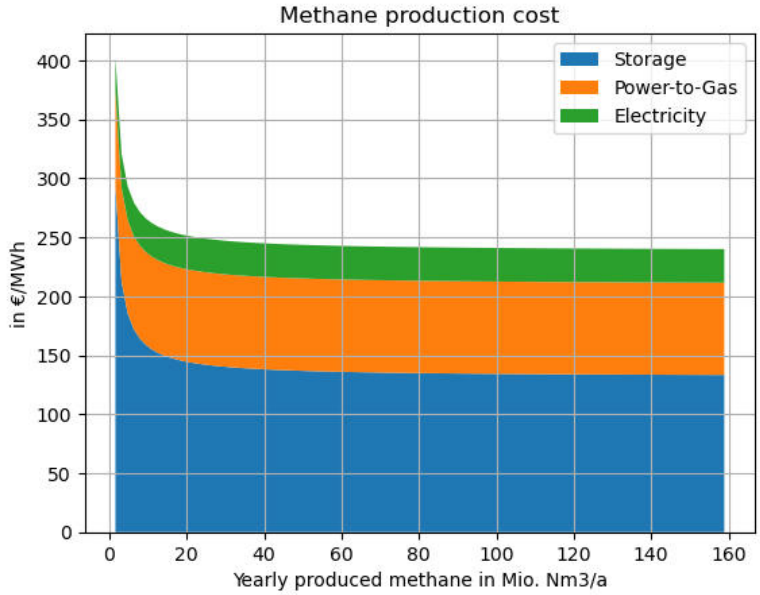

Figure 6-21: Methane production cost in €/MWh depending on the plant size and therefore the amount of the yearly produced methane (with a maximum of 20 % of educt gas (hydrogen and CO_2) in the geo-methanation). In the figure, the production costs are divided into the costs incurred for the storage facility (exploration, wells, cushion gas), the electricity, and the remaining costs, which are allocated to the conventional power-to-gas operation.

The different system components account for different shares of the total costs. This is broken down in the following diagram (Figure 6-22).

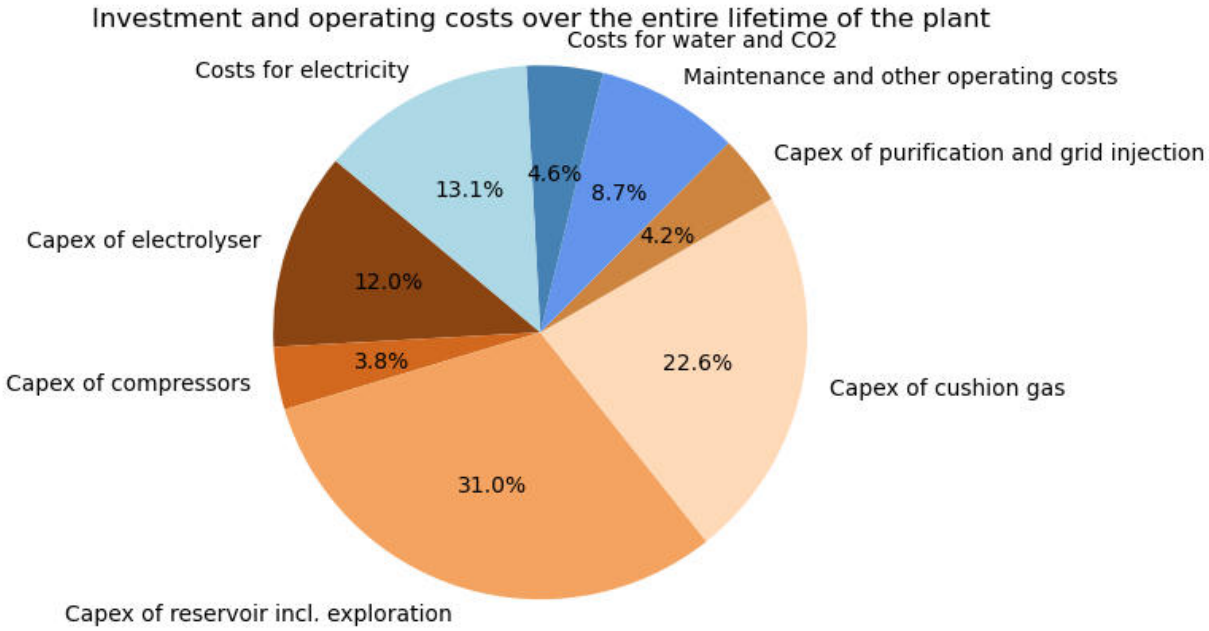

Figure 6-22: Distribution of investment and operating costs for a 100 MW_{el} plant according to concept 2, with a maximum of 20 % of educt gas (hydrogen and CO_2) in the geo-methanation.

It can be seen that the cushion gas and the development of the reservoir account for the largest part of the costs. This is due, among other things, to the high proportion of carrier gas that is injected into the reservoir with the reactants.

If the plant is not dependent on geo-methanation, the carrier gas can also be omitted, and the CO_2 and hydrogen can be directly injected underground. This reduces the amount of cushion gas required and thus the size of the reservoir.

Table 6-12: Costs of concept 2 for different plant sizes, with no carrier gas, i.e. a pure CO_2 and H_2 mixture, is inserted into the geo-methanation. The cost assumptions refer to the year 2030.

Size of Electrolysis	in MW_{el}	10	50	90	100	500	1000
Capex of electrolyser	in Mio. €	6.3	31.5	56.7	63.1	315.3	630.5
Capex of compressors	in Mio. €	2.0	10.0	18.0	20.0	99.8	199.6
Capex of reservoir incl. exploration	in Mio. €	33.5	44.1	54.7	57.4	163.3	295.7
Capex of cushion gas	in Mio. €	2.4	11.9	21.5	23.8	119.2	238.3
Capex of purification and grid injection	in Mio. €	4.1	12.2	20.2	22.2	102.6	203.0
Capex of aboveground methanation	in Mio. €	1.5	7.3	13.1	14.6	73.0	146.0
Additional costs	in Mio. €	13.9	32.8	51.6	56.3	244.5	479.7
Salvage value	in Mio. €	3.1	4.9	6.6	7.1	24.6	46.5
Capex total	**in Mio. €**	**60.6**	**144.9**	**229.2**	**250.3**	**1'093**	**2'146**
Opex of electrolyser	in Mio. €	1.4	6.9	12.4	13.8	68.8	137.6
Opex of compressors	in Mio. €	0.5	2.5	4.5	5.0	24.9	49.9
Opex of reservoir	in Mio. €	2.5	3.9	5.2	5.6	19.4	36.8
Opex of purification and grid injection	in Mio. €	1.3	4.0	6.7	7.4	34.7	68.9
Opex of aboveground methanation	in Mio. €	1.0	5.0	9.0	10.0	50.2	100.5
Costs for water	in Mio. €	0.3	1.4	2.5	2.8	14.1	28.1
Costs for CO_2	in Mio. €	2.1	10.7	19.3	21.5	107.3	214.6
Costs for electricity	in Mio. €	6.9	34.3	61.8	68.7	343.5	686.9
Opex total	**in Mio. €**	**15.9**	**68.7**	**121.6**	**134.8**	**663.0**	**1323**
Methane production cost	EUR/MWh	317	177	162	160	146	144
Yearly methane production	in Mio. Nm3/a	1.6	7.9	14.3	15.9	79.4	158.9
NET PRESENT VALUE (NPV)	in Mio. €	-34	-13	9	14	228	496

If the ratio of gas production costs is plotted against annual methane production, the following graph is derived:

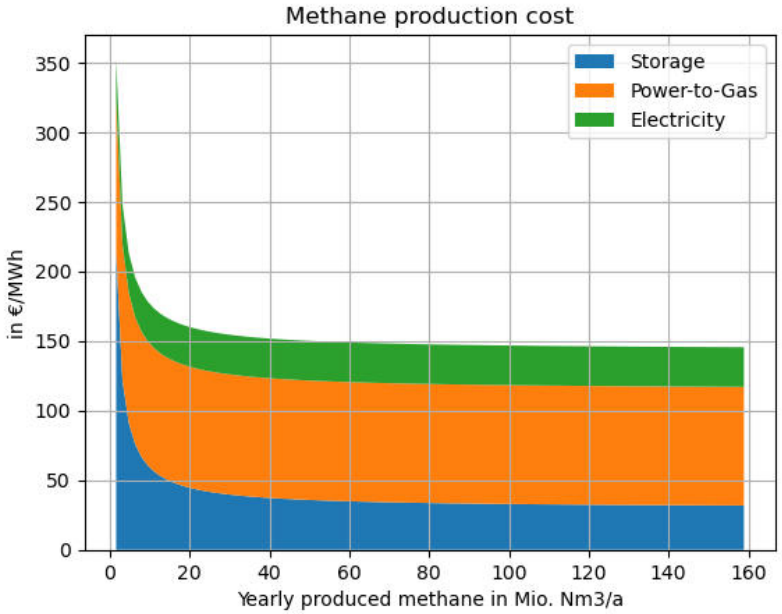

Figure 6-23: Methane production cost in €/MWh depending on the plant size and therefore the amount of the yearly produced methane, with no carrier gas, i.e., a pure CO_2 and H_2 mixture, is inserted into the geo-methanation. In the figure, the production costs are divided into the costs incurred for the storage facility (exploration, wells, cushion gas), the electricity, and the remaining costs, which are allocated to the conventional power-to-gas operation.

Figure 6-24 shows the cost shares when no carrier gas is used.

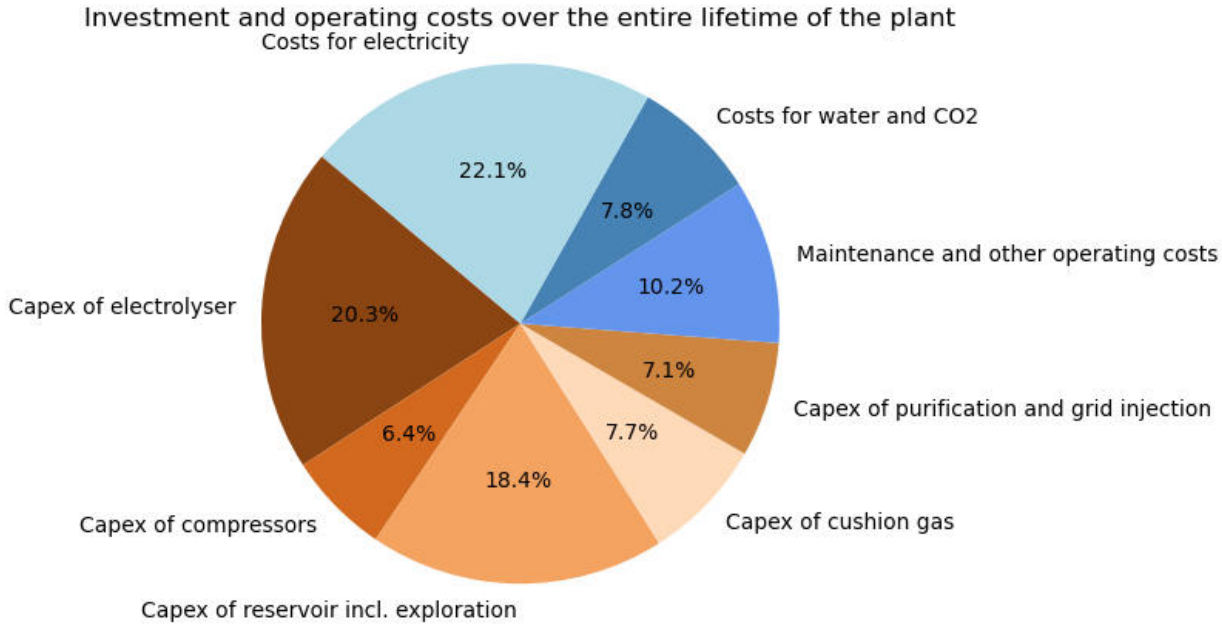

Figure 6-24: Distribution of investment and operating costs for a 100 MW_{el} plant according to concept 2, in which no carrier gas, i.e., a pure CO_2 and H_2 mixture, is inserted into the geo-methanation.

If no carrier gas is used in concept 2, the costs for electrolysis (investment costs as well as electricity costs) dominate. This concept therefore serves as an exemplification of the cost of the limitations of the

geo-methanation process, as outlined in chapters 2 and 3 and by extension the cost of CO_2 within the process in a high pressure environment of an aquifer storage formation.

6.6.6.3. Costs concept 3 – Storing hydrogen underground methanation aboveground

In concept 3, the hydrogen produced is stored underground, thus enabling seasonal storage. Methanation then takes place above ground as needed.

Table 6-13: Costs of concept 3 for different plant sizes. The cost assumptions refer to the year 2030.

Size of Electrolysis	in MW_{el}	10	50	90	100	500	1000
Capex of electrolyser	in Mio. €	6.3	31.5	56.7	63.1	315.3	630.5
Capex of compressors	in Mio. €	1.3	6.6	11.8	13.1	65.6	131.1
Capex of reservoir incl. exploration	in Mio. €	45.9	45.9	49.9	52.1	136.8	242.7
Capex of cushion gas	in Mio. €	1.9	9.5	17.2	19.1	95.3	190.7
Capex of purification and grid injection	in Mio. €	3.1	7.2	11.2	12.2	52.4	102.6
Capex of aboveground methanation	in Mio. €	1.5	7.3	13.1	14.6	73.0	146.0
Additional costs	in Mio. €	16.8	30.2	44.8	48.7	206.7	404.2
Salvage value	in Mio. €	4.2	4.8	5.8	6.2	20.2	37.7
Capex total	**in Mio. €**	**72.6**	**133.3**	**198.9**	**216.6**	**924.8**	**1'810**
Opex of electrolyser	in Mio. €	1.4	6.9	12.4	13.8	68.8	137.6
Opex of compressors	in Mio. €	0.3	1.7	3.1	3.5	17.4	34.7
Opex of reservoir	in Mio. €	3.3	3.8	4.6	4.9	16.0	29.8
Opex of purification and grid injection	in Mio. €	1.1	3.0	5.0	5.5	25.0	49.4
Opex of aboveground methanation	in Mio. €	1.0	5.0	9.0	10.0	50.2	100.5
Costs for water	in Mio. €	0.3	1.4	2.5	2.8	14.1	28.1
Costs for CO_2	in Mio. €	2.1	10.7	19.3	21.5	107.3	214.6
Costs for electricity	in Mio. €	6.0	30.2	54.3	60.3	301.7	603.4
Opex total	**in Mio. €**	**15.6**	**62.8**	**110.3**	**122.3**	**600.4**	**1'198**
Methane production cost	EUR/MWh	366	163	142	141	126	125
Yearly methane production	in Mio. Nm3/a	1.6	7.9	14.3	15.9	79.4	158.9
NET PRESENT VALUE (NPV)	in Mio. €	-45	5	49	59	454	948

If the ratio of gas production costs is plotted against annual methane production, the following graph is derived:

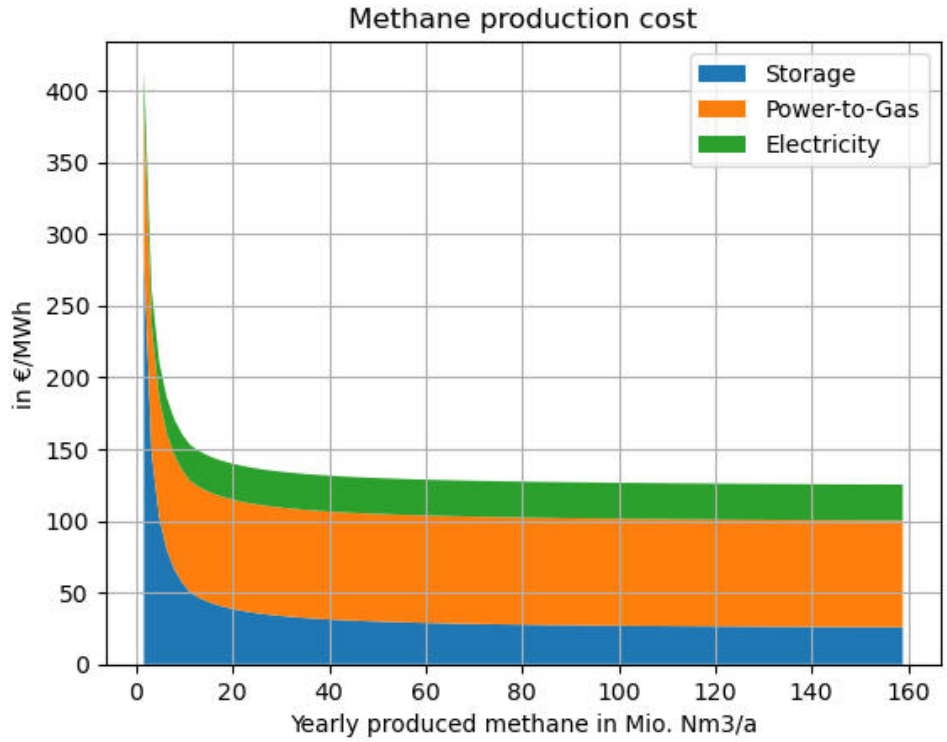

Figure 6-25: Methane production cost of concept 3 in €/MWh depending on the plant size and therefore the amount of the yearly produced methane. In the figure, the production costs are divided into the costs incurred for the storage facility (exploration, wells, cushion gas), the electricity, and the remaining costs, which are allocated to the conventional power-to-gas operation.

The different system components account for different shares of the total costs. This is broken down in the following diagram.

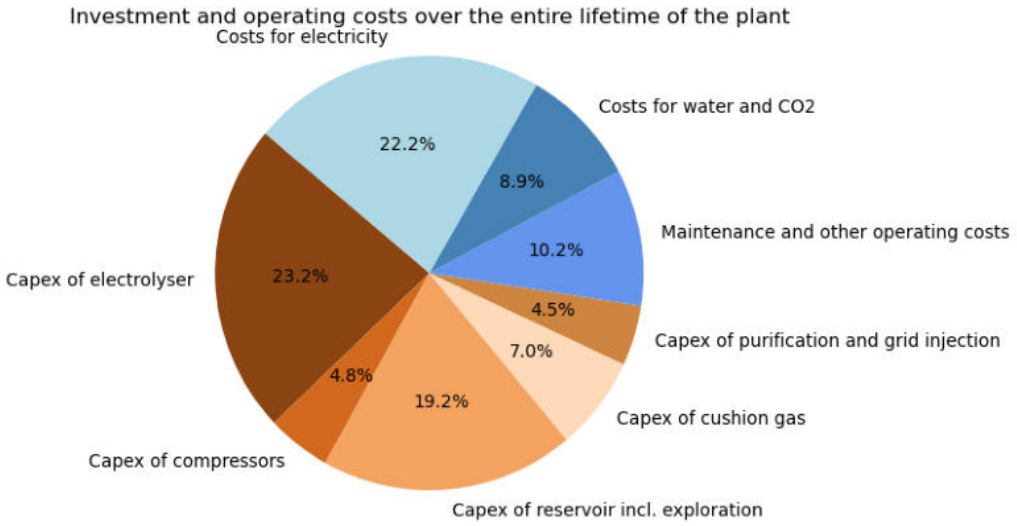

Figure 6-26: Distribution of investment and operating costs for a 100 MW_{el} plant according to concept 3.

6.6.6.4. Sensitivity

Storage volume: The analysis of the cost sensitivity of methane production with geo-methanation shows a large influence of the required storage volume, which influences both the number of wells and the volume of buffer gas. Since an aquifer reservoir is considered in this project, the share of the cushion gas must be 50% of the total gas. This means that when the storage is filled to the maximum, there is as much cushion gas in the storage reservoir as working gas. If the educts CO_2 and hydrogen require a carrier gas to be able to react (which is necessary in concept 1 and, depending on the mode of operation, also in concept 2), the amount of carrier gas influences the necessary storage volume. The more carrier gas is required, the more wells are needed and the amount of cushion gas increases. Since both wells and cushion gas account for a not inconsiderable proportion of the total costs, this is a major influencing factor. In figure 6-27 the influence of the amount of the necessary carrier gas on the net present value is shown.

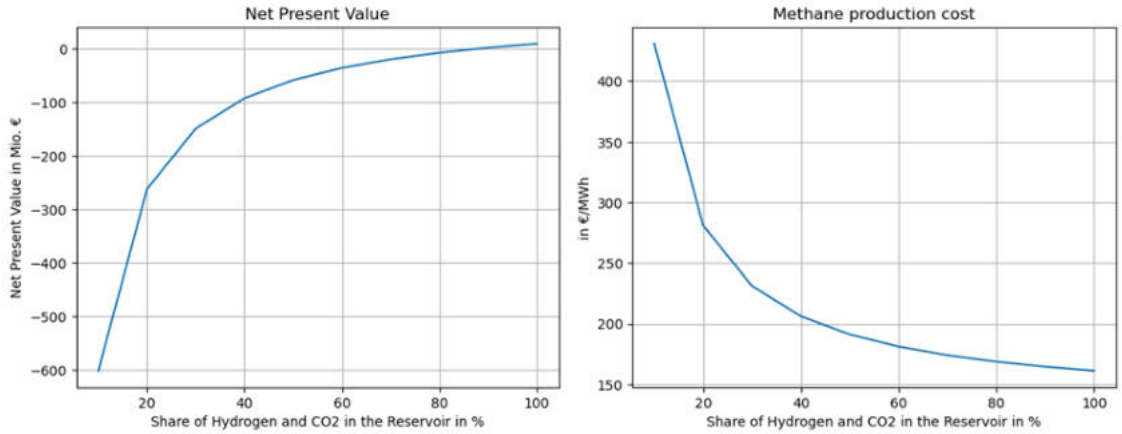

Figure 6-27: A comparison of the costs for geo-methanation according to concept 2 with an electrolysis size of 100 MW_{el} shows the influence of the necessary carrier gas on the net present value of the plant (left) and on the methane production cost (right). The smaller the range of H_2 and CO_2 in the reservoir the larger the necessary amount of the carrier and therefore the cushion gas is.

Concept 1 is based on geo-methanation and therefore needs carrier gas for geo-methanation to work. Concept 2, which focuses on using the underground for storage and the methanation takes place above-ground, does not require carrier gas. Consequently, the reservoir can be built smaller.

6.6.6.5. Costs of electricity

Power-to-gas technology is electricity-based, this also applies to USC technology. The higher the electricity prices, the higher the costs for hydrogen production and thus the methane production costs.

Looking at the influence of electricity prices on concept 3, for a plant with 100 MW_{el} input capacity, it becomes apparent that the tipping point between positive and negative NPV lies between 25 and 30 €/MWh electricity price.

In concepts 1 and 2, as mentioned above, the proportion of carrier and cushion gas has a major influence on economic efficiency. If no carrier gas is used in concept 2, the NPV is positive up to an average electricity price between 15 and 18 €/MWh. If the carrier gas share is increased to 50 %, the electricity price must remain below 3 €/MWh to achieve a positive net present value. With higher shares, no positive NPV can be achieved, based on the assumed price values and costs.

Since grid usage fees in Switzerland are between 20 and 70 €/MWh (depending on the location), an exemption of the grid usage fee for such a plant is necessary.

6.6.6.6. Discussion of the economic analysis

The development of the reservoir with the necessary exploration, wells, and cushion gas entails large but one-time costs. Once the storage facility has been developed, its use is no longer so cost-intensive and the longer the storage facility can be used and the more frequently gas can be produced, the smaller the impact of the investment costs on the total costs. It can also be assumed that a repurposing of an existing storage facility would bring a significant cost reduction, as both some wells as well as the cushion gas are already available and can be further used, and there are no exploration costs. As this project looked at possible locations for a reservoir in Switzerland, no conversion of an existing reservoir was investigated, as no such reservoir exists. However, it would be imaginable for Switzerland to rent a storage volume in a neighbouring country and use the geo-methanation technology there. Since it would then presumably no longer be an aquifer storage facility, the necessary operating pressures and thus the energy input for the compressors would also be lower.

Due to the high investment costs for underground storage, the gas production costs are lower for large plants than for small ones. This is partly because the exploration costs were assumed to be the same for all plant sizes. In Switzerland, a geo-methanation plant would only be interesting in the vicinity of large run-of-river power plants.

If a way can be found to operate the plant in such a way that the reactants are injected into the subsurface without any carrier gas or with only a small amount, the total costs are greatly reduced, and economical operation would be possible. If, on the other hand, the requirement is that a significant amount of carrier gas is needed, economic implementation is likely to be difficult.

Looking at the different operating concepts 1-3 in the context of the developed use cases "Strategic reserve", "U-Store" and "Power valley", concept 1 would come into question for the strategic energy reserve, or concept 3, if the hydrogen can be used directly and does not need to be converted to methane (based on the assumption, that a very large amount of energy supply is needed in a very short period of time in an emergency). For “U-Store” and “Power valley” all three concepts would be suitable. In the case of the strategic energy reserve, however, it must be considered that there is no annual gas exchange, but that the storage facility is filled with reactants once and the gas would only be produced in an emergency. This means that very little gas can be sold over the entire lifetime of the plant. This makes it very difficult to operate the plant economically. This plant concept is therefore only suitable as an emergency reserve, and the associated high costs would have to be borne by the institution or state that needs this security measure.

The second major influencing factor is the cost of electricity. If electricity can be produced regionally in a "U-Store" or "Power valley" operation and used without additional charges such as grid fees, the price sensitivity can be well controlled by the own plants. This takes advantage of the fact that the electricity cannot be used elsewhere in the summer and that geo-methanation can provide a purchase guarantee. Thanks to the integrated seasonal storage of the technology, price differences between summer and winter can be exploited.

With geo-methanation, methane production costs between 250 and 275 €/MWh can be achieved (concepts 1 and 2). If the current biogas production costs (which are around 140 €/MWh, based on internal information) are added to the costs for a rented storage cycle (around 2 €/MWh for injection and withdrawal, excluding rental costs, according to internal information), the costs are almost twice as high. This is calculated with a high share of carrier gas (whereby the calculations do not include the cost of the carrier gas, but a high carrier gas content increases the amount of cushion gas and number of wells, which leads to higher costs).

In summary, economic implementation is conceivable if a) the carrier gas is kept as low as possible, b) low-cost electricity is used without additional charges, and c) the gas produced can be sold as renewable gas (i.e., at a higher price).

6.7 Conclusion

An economic implementation is conceivable if a) the carrier gas is kept as low as possible, b) low-cost electricity is used without additional charges, and c) the gas produced can be sold as renewable gas (i.e. at a higher price).

The sites identified by Empa as possible locations (with electricity and CO_2 sources) in combination with the results of the University of Bern can be classified as follows:

- Very interesting location (zone 5), but reserved by Nagra: Eglisau (53 MW), Rheinau (36 MW)
- Interesting location (zone 4): Wildegg (45 MW), Gösgen (42 MW)
- Possible location (zone 1 or 2): Verbois (89 MW), Mühleberg (31 MW), Zürich Hagenholz (13 MW), Zuchwil (11 MW), Aire-la-Ville (11 MW), Hinwil (9 MW)
- Next to the boarder of a very interesting zone (zone 4 or 5): Laufenburg (95 MW) und Schaffhausen (25 MW)
- Not possible because for geological reasons: Reckingen, Monthey

The two sites of greatest interest for geo-methanation are currently reserved for Nagra. If it releases one site, that would certainly be a good option for a geo-methanation plant. Other interesting sites are Wildegg and Gösgen, where plants with electrolysis capacities of between 42 and 45 MW would be possible. According to the above calculation, methane production costs are still relatively high in this order of magnitude, a larger plant size would therefore be preferable.

Regardless of the size of the plant, early and transparent communication must be ensured for any potential project. Social acceptance in the planned area must be given for implementation. Since the choice of possible areas is relatively limited, special attention must be paid to ensure that the project does not fail due to social acceptance. In order for the project to be accepted by the population and stakeholders, information must be provided early and transparently, and open issues must be addressed. This applies to the above-ground plant, the underground development and the operation of geo-methanation.

6.8 Abbreviations

BECCS	Bioenergy with Carbon Capture and Storage
Capex	Capital Expenditure
CO_2	Carbon Dioxide
CCS	Carbon Capture and Storage
CCU	Carbon Capture and Utilization
CO_2	Carbon-Dioxide
H_2	Hydrogen
MWIP	Municipial Waste Incineration Plant
NIMBY	Not In My BackYard
OP	Operating Pressure
Opex	Operating Expediture
p	Pressure
PSA	Pressure Swing Adsorption
ROR	Run-of-Rivers-Powerplant
SNG	Synthetic Natural Gas
STP	Standard temperature and pressure
SOEC	Solid Oxide Electrolysis Cells
USC	Underground Sun Conversion

6.9 References

Arning, K.; Offermann-van Heek, J.; Linzenich, A.; Kaetelhoen, A.; Sternberg, A.; Bardow, A.; Ziefle, M. (2019a): Same or different? Insights on public perception and acceptance of carbon capture and storage or utilization in Germany. In Energy Policy 125, pp. 235–249. DOI: 10.1016/J.ENPOL.2018.10.039.

Arning, K.; Zaunbrecher, B.; Sternberg, A.; Bardow, A.; Ziefle, M. (2018): Blending Acceptance as Additional Evaluation Parameter into Carbon Capture and Utilization Life-Cycle Analyses. In : Proceedings of the 7th International Conference on Smart Cities and Green ICT Systems. 7th International Conference on Smart Cities and Green ICT Systems. Funchal, Madeira, Portugal, 16.03.2018 - 18.03.2018: SCITEPRESS - Science and Technology Publications, pp. 34–43.

Arning, Katrin; Offermann-van Heek, Julia; Sternberg, André; Bardow, André; Ziefle, Martina (2020): Risk-benefit perceptions and public acceptance of Carbon Capture and Utilization. In Environmental Innovation and Societal Transitions 35, pp. 292–308. DOI: 10.1016/j.eist.2019.05.003.

Arning, Katrin; Zaunbrecher, Barbara; Borning, Maximilian; van Bracht, Niklas; Ziefle, Martina; Moser, Albert (2019b): Does Size Matter? Investigating Laypeoples' Preferences for Roll-out Scenarios of Alternative Fuel Production Plants. In : Proceedings of the 8th International Conference on Smart Cities and Green ICT Systems. 8th International Conference on Smart Cities and Green ICT Systems. Heraklion, Crete, Greece, 03.05.2019 - 05.05.2019: SCITEPRESS - Science and Technology Publications, pp. 91–99.

Azarova, Valeriya; Cohen, Jed; Friedl, Christina; Reichl, Johannes (2019): Designing local renewable energy communities to increase social acceptance: Evidence from a choice experiment in Austria, Germany, Italy, and Switzerland. In Energy Policy 132, pp. 1176–1183. DOI: 10.1016/j.enpol.2019.06.067.

UVEK (2019): Bundesrat bekräftigt vollständige Öffnung des Strommarktes. (https://www.uvek.admin.ch/uvek/de/home/energie/oeffnung-strommarkt.html, checked on 05/26/2023.

Ejderyan, O.; Ruef, F.; Stauffacher, M. (2019): Geothermal energy in Switzerland: highlighting the role of context. In Geothermal Energy and Society, pp. 239–257.

ElCom: Warum sind Elektrizitätstarife in der Schweiz unterschiedlich hoch? Available online at https://www.elcom.admin.ch/elcom/de/home/themen/strompreise/elektrizitaetstarife.html, checked on 10/27/2021.

Engelmann, Linda; Arning, Katrin; Linzenich, Anika; Ziefle, Martina (2020): Risk Assessment Regarding Perceived Toxicity and Acceptance of Carbon Dioxide-Based Fuel by Laypeople for Its Use in Road Traffic and Aviation. In Front. Energy Res. 8, Article 579814. DOI: 10.3389/FENRG.2020.579814.

Graf, Frank; Schoof, René; Zdrallek, Markus (Eds.) (2021): Power-to-Gas. Grundlagen – Konzepte – Lösungen. Vulkan-Verlag GmbH. 1. Auflage. Essen: Vulkan Verlag (Edition gwf Gas + Energie).

Huijts, N.M.A.; van Wee, B. (2015): The evaluation of hydrogen fuel stations by citizens: The interrelated effects of socio-demographic, spatial and psychological variables. In International Journal of Hydrogen Energy 40 (33), pp. 10367–10381. DOI: 10.1016/j.ijhydene.2015.06.131.

Jane Desbarats: REVIEW OF THE PUBLIC PARTICIPATION PRACTICES FOR CCS AND NON-CCS PROJECTS IN EUROPE. Available online at https://ieep.eu/uploads/articles/attachments/5c201afe-77de-42c3-960e-e00e95534e86/Review_of_the_public_participation_practices_for_ccs_and_non-ccs_projects_in_Europe.pdf?v=63664509725, checked on 10/10/2022.

Jones, Christopher R.; Olfe-Kräutlein, Barbara; Kaklamanou, Daphne (2017a): Lay perceptions of Carbon Dioxide Utilisation technologies in the United Kingdom and Germany: An exploratory qualitative interview study. In Energy Research & Social Science 34, pp. 283–293. DOI: 10.1016/J.ERSS.2017.09.011.

Jones, Christopher R.; Olfe-Kräutlein, Barbara; Naims, Henriette; Armstrong, Katy (2017b): The Social Acceptance of Carbon Dioxide Utilisation: A Review and Research Agenda. In Front. Energy Res. 5, Article 11. DOI: 10.3389/FENRG.2017.00011.

Jones, Christopher R.; Radford, Rebecca L.; Armstrong, Katy; Styring, Peter (2014): What a waste! Assessing public perceptions of Carbon Dioxide Utilisation technology. In Journal of CO2 Utilization 7, pp. 51–54. DOI: 10.1016/j.jcou.2014.05.001.

Kadner, Kathrin (2015): Aufbau und Funktion von Gasspeichern. In: gas2energy.net Systemplanerische Grundlagen der Gasversorgung. 2. überarbeitete und erweiterte Auflage.

König, Sebastian; Bchini, Quentin; McKenna, Russell; Köppel, Wolfgang; Bachseitz, Michael; Entress, Jörg et al. (2018): Analysing the regional potential and social acceptance of power-to-gas in the context of decentralized co-generation in Baden-Württemberg. In Journal of Energy Storage 16, pp. 93–107. DOI: 10.1016/j.est.2017.12.011.

Lambert und Ashworth (2018): The Australian public's perception of hydrogen for energy. With assistance of Professor Peta Ashworth. Queensland. Available online at https://arena.gov.au/assets/2018/12/the-australian-publics-perception-of-hydrogen-for-energy.pdf, checked on 10/11/2022.

Linzenich, Anika; Arning, Katrin; Offermann-van Heek, Julia; Ziefle, Martina (2019): Uncovering attitudes towards carbon capture storage and utilization technologies in Germany: Insights into affective-cognitive evaluations of benefits and risks. In Energy Research & Social Science 48, pp. 205–218. DOI: 10.1016/J.ERSS.2018.09.017.

Linzenich, Anika; Engelmann, Linda; Arning, Katrin; Du, Miaomiao; Heger, Sebastian; Roß-Nickoll, Martina; Ziefle, Martina (2022): Harmful or Beneficial to Humans and the Environment? An Empirical Study on the Social Acceptance and Risk Perception of CO2-Based Fuels. In Front. Environ. Sci. 10, Article 737070. DOI: 10.3389/fenvs.2022.737070.

L'Orange Seigo, Selma; Dohle, Simone; Siegrist, Michael (2014): Public perception of carbon capture and storage (CCS): A review. In Renewable and Sustainable Energy Reviews 38, pp. 848–863. DOI: 10.1016/j.rser.2014.07.017.

Meier, B., Ruoss, F., & Friedl, M. (2017): Investigation of Carbon Flows in Switzerland with the Special Consideration of Carbon Dioxide as a Feedstock for Sustainable Energy Carriers. Energy Technology, 5(6). https://doi.org/10.1002/ente.201600554

Muratore, S. et. al. (2016): Tiefengeothermie: Das Projekt St. Gallen. USYS TdLab, ETH Zurich. Switzerland.

O'Garra, Tanya; Mourato, Susana; Pearson, Peter (2008): Investigating attitudes to hydrogen refuelling facilities and the social cost to local residents. In Energy Policy 36 (6), pp. 2074–2085. DOI: 10.1016/j.enpol.2008.02.026.

Perdan, Slobodan; Jones, Christopher R.; Azapagic, Adisa (2017): Public awareness and acceptance of carbon capture and utilisation in the UK. In Sustainable Production and Consumption 10, pp. 74–84. DOI: 10.1016/J.SPC.2017.01.001.

Sara, Juliana; Stikkelman, Rob M.; Herder, Paulien M. (2015): Assessing relative importance and mutual influence of barriers for CCS deployment of the ROAD project using AHP and DEMATEL methods. In International Journal of Greenhouse Gas Control 41, pp. 336–357. DOI: 10.1016/j.ijggc.2015.07.008.

Schmidt, Adriane; Donsbach, Wolfgang (2016): Acceptance factors of hydrogen and their use by relevant stakeholders and the media. In International Journal of Hydrogen Energy 41 (8), pp. 4509–4520. DOI: 10.1016/j.ijhydene.2016.01.058.

Schönauer, Anna-Lena; Glanz, Sabrina (2022): Hydrogen in future energy systems: Social acceptance of the technology and its large-scale infrastructure. In International Journal of Hydrogen Energy 47 (24), pp. 12251–12263. DOI: 10.1016/j.ijhydene.2021.05.160.

Terwel, Bart W.; Mors, Emma ter; Daamen, Dancker D.L. (2012): It's not only about safety: Beliefs and attitudes of 811 local residents regarding a CCS project in Barendrecht. In International Journal of Greenhouse Gas Control 9, pp. 41–51. DOI: 10.1016/j.ijggc.2012.02.017.

Thesen und Langhelle (2008): Awareness, acceptability and attitudes towards hydrogen vehicles and filling stations: A Greater Stavanger case study and comparisons with London. In International Journal of Hydrogen Energy 33 (21), pp. 5859–5867. DOI: 10.1016/j.ijhydene.2008.07.006.

Wallquist, Lasse; Seigo, Selma L'Orange; Visschers, Vivianne H.M.; Siegrist, Michael (2012): Public acceptance of CCS system elements: A conjoint measurement. In International Journal of Greenhouse Gas Control 6, pp. 77–83. DOI: 10.1016/j.ijggc.2011.11.008.

Wallquist, Lasse; Visschers, Vivianne H. M.; Siegrist, Michael (2010): Impact of Knowledge and Misconceptions on Benefit and Risk Perception of CCS. In Environ. Sci. Technol. 44 (17), pp. 6557–6562. DOI: 10.1021/es1005412.

Wallquist, Lasse; Visschers, Vivianne H.M.; Siegrist, Michael (2009): Lay concepts on CCS deployment in Switzerland based on qualitative interviews. In International Journal of Greenhouse Gas Control 3 (5), pp. 652–657. DOI: 10.1016/j.ijggc.2009.03.005.

Wallquist, Lasse; Visschers, Vivianne H.M.; Siegrist, Michael (2011): Antecedents of risk and benefit perception of CCS. In Energy Procedia 4, pp. 6288–6291. DOI: 10.1016/j.egypro.2011.02.643.

Zaunbrecher, Barbara S.; Bexten, Thomas; Wirsum, Manfred; Ziefle, Martina (2016): What is Stored, Why, and How? Mental Models, Knowledge, and Public Acceptance of Hydrogen Storage. In Energy Procedia 99, pp. 108–119. DOI: 10.1016/j.egypro.2016.10.102.

Zauner, A., Böhm, H., Rosenfeld, D. C., & Tichler, R. (2019): Analysis on future technology options. Project STORE&GO. Deliverable 7.7

Zimmer, René; Welke, Jörg (2012): Let's go green with hydrogen! The general public's perspective. In International Journal of Hydrogen Energy 37 (22), pp. 17502–17508. DOI: 10.1016/j.ijhydene.2012.02.126.

6.10 Contact Details

OST – Ostschweizer Fachhochschule

Zoe Stadler

Oberseestrasse 10, CH-8640 Rapperswil

+41 58 257 43 03

zoe.stadler@ost.ch

www.ost.ch/iet

Authors:

Zoe Stadler, Fiona Hauser and Imre Antalfy, Institute for Energy Technology, OST

Benedikt Hasibar and Markus Pichler, RAG

Daniela van den Heuvel and Larryn Diamond, Institute of Geological Sciences, University of Bern

Daniel Sidler and Meret Boggiano, Energie 360°

7 Overall Results, discussions, and conclusions

The demonstration of geo-methanation in field built on the results of previous projects. In the course of this project, it could be confirmed, that the storage and conversion of H_2 and CO_2 in a porous reservoir neither influences the quality nor the integrity of the reservoir. Furthermore, the evaluation of the corrosion coupons showed that the use of the gases mentioned does not cause any deviation in the corrosion rates compared to the use of conventional natural gas. Besides the information about integrity the field tests give an insight into the microbial processes occurring in the underground. However, options for monitoring these processes in the reservoir are limited to gas measurements and sporadic microbial and chemical analyses of water samples from the two wells. Due to this limitation, great emphasis was placed on continuous comparison with laboratory experiments. And it turns out that changing input parameters such as the H_{2in}/CO_{2in} ratio in both systems - field and lab - leads to comparable changes in the processes taking place. A H_{2in}/CO_{2in} ratio of 4:1 equals the stoichiometrically correct ratio for methanogenesis, in an underground reservoir. Starting with this H_{2in}/CO_{2in} ratio, methane is the main end-product in both field and lab. On the other hand, it could be shown that with a H_{2in}/CO_{2in} ratio too low, homoacetogenic bacteria are thermodynamically preferred over methanogenic archaea, which can lead to an unwanted reduction in the desired product generation and the production of acetate, thus an acidification of the system. With increasing acidification, the dominance of homoacetogenic bacteria over methanogenic archaea also increases further. To avoid this effect, an H_{2in}/CO_{2in} ratio of at least 4:1 must always be maintained. Besides the H_{2in}/CO_{2in} ratio the favoring of homoacetogenesis or methanogenesis depends on the partial pressure of CO_2 (pCO_2) and the pH associated with it. While methanogenic archaea operate best in a range from 6.5 – 7.5, the optimal pH range for homo-acetogenic bacteria is located between 5 – 5.5. With a high pCO_2, the pH decreases depending on the available buffer system. Therefore, a high pCO_2 is unwanted. A clear statement about which pCO_2 is still tolerable, before homoacetogenesis takes over, depends on the underlying buffer system. Since homoacetogenesis can never be ruled out in the system considered, it is important to develop strategies for dealing with acetate that has already formed. In order to guide the process back to the desired course, even if acetate formation has undesirably occurred, a method was tested to break down the acetate formed again. It was shown that at a low CO_2 addition rate, the acetate formed can be further converted to methane. In this way, not only is the production of CH_4, which was desired from the beginning, made up for, but acidification is also counteracted. This concept was tested in lab and confirmed in field and may be a basis for a promising strategy to deal with undesired acetate formation in an underground reservoir.

Enhancing methanogenesis by suppressing other microbial reactions such as homoacetogenesis is an important issue in upscaling the underground sun conversion process. Another important point is the conversion rate. In order to scale and plan the process, the reaction rate and its influencing factors must be known. For this purpose, various laboratory tests were carried out with different input parameters and varying run times. In experiments without feed gas limitation and maintaining a minimum H_{2in}/CO_{2in} ratio of 4, a methane evolution rate (MER) of 0.1-0.2 $Nm^3\ CH_4 * m^3$ pore space $volume^{-1} * day^{-1}$ could be determined. This value was measured independently of the reactor type used, the presence of reservoir rock and applied gas pressure, thus describes the optimal MER so far. In field the MER varies in tests under optimal conditions applied between 0.01 and 0.04 $Nm^3\ CH_4 * m^3$ pore space $volume^{-1} * day^{-1}$. This difference to the laboratory tests can be explained by the more complex system of the underground reservoir compared to lab conditions.

The outlined findings also provide reasonable estimations for the suitability of geological formations for an underground sun conversion plant. While there is little restrictions in a depleted gas field, due to a wide tolerance towards pressure differentials during any storage cycle, porous storage formations created within an aquifer need another operation regime. Storages in aquifers generally need a much higher minimal pressure in order to obtain the porous volume required for storage against the hydraulic pressure of the aquifer. Having the restrictions concerning pCO_2 in mind, all inputs of CO_2 would need to be accompanied by a sufficient amount of carrier-gas in order to remain within the tolerable limits and

to prevent a drop of pH within the storage. This in turn results in a significant higher volume needed for such a storage, with the resulting increasing invest for the installation of the storage.

Both in the field and in the laboratory, attempts were made to map the demands of a flexible energy system. Since H_2 and CO_2 will not always be present at the same time and in the correct ratio - related to the conversion to CH_4 - in the future, different mixing ratios of the input gases were investigated for their influence on the overall system. As mentioned before, it could be shown both in lab and field, that with a high H_{2in}/CO_{2in} ratio (over-stoichiometric) – in other words a surplus on H_2 – methanogenesis stays the main microbial reaction. This has a significant effect on the operation of an underground sun conversion plant. As renewable energy will be mainly available for the production of green H_2 during summer months, H_2 can be produced and stored directly inside the reservoir. From time to time – depending on the source – CO_2 can be admixed, until a minimum H_{2in}/CO_{2in} ratio is reached. This fits well to the developed operational concepts 1 and 2 described in chapter 6.

Operational concept 1 describes the “classical” underground sun conversion approach by using geo-methanation and the advantages of a large storage facility. Concept 2 is an extension of the previous one to include an aboveground methanation plant. This can increase the flexibility of the system by converting H_2 and CO_2 that have not yet been converted into CH_4 when they are withdrawn from the reservoir. The extension in the form of the above-ground methanation facility adds operational flexibility, for instance by not having to store the input gases in the storage in times where current gas-demand and simultaneously supply in electricity and CO_2 would allow for direct methanation.

Operational concept 3 describes the possibility for storing exclusively H_2 underground and performing methanation exclusively above ground. The biggest advantage of this option is the comparatively lower storage volume needed. This finding might be contra intuitive, since H_2 does have a significantly lower energy density per volume than CH_4. Due to the found restriction on the partial pressure and flexibility in stoichiometry, the total storage volume increases, since each injection of CO_2 requires vast amounts of carrier gas. This carrier gas and the produced geo-methane forms the working gas, which in turn determines the amount of needed cushion gas. As outlined in chapter 6, the increasing amount of cushion gas (as a reaction to the increased amount of working gas), means a significant increase in investment and hence capital expenditure during operation. Storing only H_2 underground does not require the same amount of cushion gas due to the described limitations as chapter 1 has summarized, and therefore can be built more economically. Concept 3 would require a methanation capacity above ground, either with the ability to produce methane in the amount of the highest demand peak of customers or combined with underground methane storage.

Depending on their use, each of these concepts has its advantages and disadvantages. It is important to embed the operational concepts in the overall energy system and its requirements.

Based on projected and/or mandated changes to the respective national energy-architecture in Austria and Switzerland, the future demand and supply situation on the electric sector in these two countries have been modelled. For the models, existing projections by state agencies and ENTSO-E were consulted, checked for consistency and plausibility, and, where necessary, adapted. At the same time, the future gas demand was modelled as well. For this sector, the demand-pattern over a modelled year had to be more detailed for Switzerland than for Austria, given the already present Austrian capacities for gas storage independent of geo-methanation.

As the model show, without the possibility for import and export electricity, both countries will produce in the year 2050 high amounts of electricity, which do not match a demand at time of production and cannot be used or stored through load-shifting or existing storage capacities as pumped hydro. As it is shown further, both domestic energy production and demand patterns, even after optimization and load-shifting, there are extended time periods without enough production to meet demand. While the Austrian energy system seems to have a more diverse production mix and through higher stakes of wind- and run-of-river-hydroelectric production may keep the total amount of electricity demand without a corresponding supply at the same time, the deficit still amounts to a worrying amount. For Switzerland, the same conclusions are present at the same periods but more pronounced. In both countries, however,

the surplus of electricity that probably will be needed to be curtailed is more prominent. The impact of these amounts of curtailed electricity puts the economic viability of following the outlined paths for the increasing installment of renewable electricity production assets in question, since for producers, these curtailments either will need to be reimbursed by someone or the incentive for investing in such capacities is not economic viable.

The overall need for inter-seasonal storage options for large volumes of energy and with high capacity is therefore proven in chapter 4, concerning both sides of the supply and demand equation.

As geo-methanation requires CO_2 as well as electricity without a consumer at the time of production for H_2, the locations of possible plants are limited to respective point sources for CO_2 and electricity to limit the cost for transportation. The results are outlined, and all factors have been summarized in a map in chapter 4.

The projections for the future energy system of Switzerland largely bases on official scenarios as performed by Prognos for the Swiss Federal Office for Energy. The increase in renewable energy production capacity in this data relies mainly on expansion in PV-production until 2050. Accordingly, a seasonal pattern in production is distinct in the models outlined in chapter 4. At the same time, heating is projected to be provided increasingly through heat-pumps. This demand-side effect shows in increased demand for electricity in winter months. As gas is substituted for the use of domestic heating, the demand will decrease overall and the demand curve throughout the year will flatten due to the increasing portion of industrial applications on the total consumption. These factors mainly contribute to a strongly season-related mismatch between electricity production and demand. A standardized year therefore accumulates to a total of approximately 12 Terrawatthours (TWh) deficits in electrical power, while a surplus of approximately 17 TWh is accumulated over the course of the same year. CO_2 point sources are cumulatively abundant and mainly placed in highly industrialized areas like the cantons of Aargau and Solothurn as well as parts of Zurich.

For Austria, the TYNDP 2022 model had to be adjusted, due to larger inherent inconsistencies. The resulting amalgamation of different sources nevertheless allowed for a model to reach results with the needed confidence. Also in Austria, PV will be the main driver in the push for a renewable energy production environment until 2050. In contrast to Switzerland, there are larger shares of wind and hydro production capacity foreseen and/or already installed. This leads to a somewhat more favorable distribution of the supply side and the push for the electrification of heating application is less pronounced. Still, the model shows an accumulated deficit throughout a standardized year of c.a. 6.5 TWh, while there is a total of approximately 15 TWh electricity production without a corresponding demand throughout that year. CO_2 point sources are despite a considerable decarbonization effort high enough in 2050 for the technical demand to produce approximately 50 TWh methane through geo-methanation. This would require about 110 TWh renewable electricity, what is clearly above the expected amount to be available. CO_2 therefore is not a limiting factor.

The suitability for geo-methanation outside the tested conditions in a depleted gas field was researched by a survey of data of the Swiss geology (chapter 5). Switzerland has no known active or depleted gas fields in a geological formation which cannot be ruled out instantly due to cautionary indicators as the reservoir temperatures. Therefore, the development of an inter-seasonal storage as proposed within this project, would require a suitable formation that forms presumably an aquifer. The mountainous character of the geography channels potentially promising formations between the alps and the jura mountain range. The knowledge of the deep underground of Switzerland is poor due to a lack of commercial activities in this area (which is sparked historically by findings of hydrocarbons). Therefore, the study was constrained largely to the area of the Swiss Molasse Basin, roughly below the plain between Lake Geneva and Lake Constance, even though a potentially promising area just north to northwest of the alps must be left out due to an almost complete lack of data. Table 5-1 gives an overview of the decisive selection criteria, which include, for example, the optimal temperature window (35 °C to 70 °C) and pH range (6-9) for microbial methanogenic activity.

Though this given limitations and difficulties urged by a lack of data, several geological units containing the characteristics of defined positive indicators have been identified and located. In some areas, more than one of these units probably fulfills the catalogue of positive indicators. In these areas it therefore would be possible to explore more than one unit with a single probe and are prioritized accordingly. The hence most promising of these areas are to be found south of the jura chain roughly between Oensingen (Canton of Solothurn) in the west and Birr (Canton of Aargau) in the east as well as the region north of the hill chain of Lägern (Cantons Aargau and Zurich). There is no certainty on the size of a reservoir, if any, that actually would prove to be eligible for seasonal storage underground Swiss ground. The formations considered nevertheless were selected so that a minimal capacity of 4.5 Mio. m^3_{STP} seems to be realistic and at least 400 Mio. m^3_{STP} are possible.

A successful exploration campaign in these areas requires about 6 years and for each completed campaign about 40 million Swiss Francs, without any guarantee of success at any stages of such a campaign. The necessary conditioning of the future underground storage then would take another 6 years.

The installation costs for the intended all-purpose Underground Sun Conversion site (as outlined in operational concept 1), as a result of the increased demands for storage volume, are estimated at 4.4 billion Euros for one large site for the total potential in Switzerland as outlined in chapter 5 and 6. With the intended operations and the supply needs for renewable gas in 2050 within a year, this would result in costs per MWh gas produced of 237 Euros. This is well above the currently accepted prices for natural gas or renewable gas. During August 2022, in midst of the highest uncertainties on natural gas availability in the winter of 2022/2023, the price for natural gas briefly touched the historical high-water-mark of 320 Euros per MWh, what is not seen as a viable benchmark going forward.

Operational Concept 2 adds operational flexibility by adding an above-ground methanation plant to the site. This allows to directly produce methane in times, when supply of electricity and demand for gas occurs at the same time and therefore can omit the need for a storage cycle. In addition, this operational concept is not limited by storage times of the input gases, due to the redundancy in methanation. The stoichiometry and pressure conditions would need to be adhered to in this concept. Therefore, the need for carrier gas increases in this scenario, what leads to a higher storage volume necessary and by extension also the investment. Increases. Due to the additional methanation plant above-ground, the cumulated capex exceeds the needs of operational concept 1. Hence the estimate for the cumulated capex at 4.5 billion Euros and the resulting costs at approximately 249 Euros per MWh..

The concept also allows to compare scenarios with and without the need for carrier gas in order to calculate the price, inflicted by limitations of CO_2 within the storage. If no carrier gas is used (in a fictional scenario), both investment and costs per MWh are reduced significantly (2.1 billion Euros and 144 €/MWh respectively). From there, the additional costs by using an aquifer, due to the limitations urged by the restricted use of CO2, can be defined. These costs are estimated to be at 2.4 billion Euros in investment and 105€/MWh produced. This finding also hints towards feasibility of geo-methanation when using a depleted gas field as it is the case in Austria.

Operational concept 3 deviates from the initially stated goals of the project but highlights high potential. Without the need for injecting CO_2 in an Underground Sun Conversion site, the requirements towards the volume for the total potential in Switzerland decrease significantly, as the need for carrier gas is decreased to a great extent, even though the gas volume in this concept consists of H_2 with a lower energy density per volume compared to CH_4. This results in investment requirements of about 1.8 billion Euros. Produced gas is estimated at a cost of 125 Euros per MWh in this operational concept. This concept requires either a constant supply of CO_2 throughout the year, sufficient for methanation at peak demand, or a separate storage site for either CO_2 or methane and therefore defies a key advantage of the concept of geo-methanation.

The results of chapter 6 show the limits of the potential for a domestic Swiss Underground Sun Conversion site. The estimations therein do have a limited validity for Austria and its potential for sites installed in depleted gas fields, as the restrictions on the content of CO_2 at any time are less prevalent.

Nevertheless, the findings of the project strongly indicate the viability of the installation of a pure H_2-storage site.

For the identified use cases in chapter 6, “strategic reserve” still would greatly benefit of the operational concept 1. This use case allows for a slow and methodical replenishment (or initial storing) of CO_2 and H_2. In this case, the importance of a pure domestic sourcing of the energy stored as well as the higher capacity of methane vis à vis H_2 is of equally big importance for the concept. The increased costs for the resulting gas is more neglectable, since the stored energy would be used in a case, where economics are of second importance. This use case also implies the need for a national or supra-national institution with regulatory power to take the lead for the concept.

The use case “U-Store” requires extensive further research concerning regulation, grid structures on regional and even local levels, and more granular geological data are an imperative not given so far. Furthermore, the future policy and technical necessities on curtailment for grid operators would need to be researched as well. Furthermore, the impact of state subsidies and remuneration schemes intended for accelerating the implementation of prosumer-based power plants have a big impact on the viability and necessities for the use case. The economic viability ties the use case to operational concepts 2 or 3.

Use case “power valley” aims for the implementation off regional Underground Sun Conversion sites. The regional approach of the concept focus on price stability and regional autonomy in energy matters. This also limits the feasible operational concepts to concepts 2 and 3., as concept 1 lacks the necessary economic viability and the operational parameters require a high amount of flexibility. Adaption of concept 2 is also depending on the achievable scale of the site, while concept 3 would reach break-even at a smaller size. The use case furthermore relies on aspects outside the scope of the project, mainly the economics of re-electrification of the energy stored.

Considering the factors outlined in the chapters 4 – 6, the most promising area for commencing the search for a suitable site in Switzerland would be the region stretching between Aarau (Canton of Aargau) and Olten (Canton of Solothurn). In this Area, close renewable electricity energy production from RoR power plants is present, due to the vicinity to the river of Aare. CO_2 supply is equally close, due to the strong presence of the cement industry and MWIP and geology looks to be suitable as well. The electricity- and natural gas grids are also strongly built in this area, due to the dense population and strong industrial history of the region.

8 Outlook and next steps

The need for inter-seasonal storage became more apparent and pressing during the project. Aside from the geo-political developments, also the structural electricity deficits during the winter in Austria and especially Switzerland was put to public attention. The findings of this research-project clearly highlight the systemic need for inter-seasonal storage in Switzerland as well as Austria.

The findings of this project also have shown methanation rates and adoption rates of the microbiological consortium that exceeded expectations. Cost-estimations for a green-field storage facility show costs well above the established energy prices, but are, seen in the big picture, comparatively close to the benchmark when considering the novelty of the technology. The findings concerning the limitations of the partial pressure of CO_2 in the reservoir limit the potential of geo-methanation outside of depleted gas fields and well-established aquifer-storage-sites. The geological survey, as an amalgamation of the existing knowledge on the Swiss molasse basin, has shown promising formations for further examination. These formations constitute the most feasible possibilities for geo-methanation, aside from largely unknown potentials in the Sub-Alpine Molasse in Switzerland. All these formations are Aquifers, and the conversion to a gas-storage therefore would require higher reservoir pressures than the storage sites of RAG Austria. Given the identified limitations constituted by the maximum partial pressure of CO_2, such a storage seems to be not feasible for geo-methanation from an economical perspective. Developed use cases are highlighting potential unique selling propositions that are not yet priceable. This especially applies to the concept “Strategic Reserve” as outlined in 6.3.7. The necessary consensus for enabling building such a storage concept is to be reached in politics and society. On the other hand, the results also show the potential for hydrogen storage in the same locations instead would decrease the costs significantly. This potential requires further examinations though and would open up the possibilities for the Swiss geology beyond the restrictions of the positive indicators for geo-methanation.

In addition, green hydrogen as a future energy-carrier and mean to decarbonize industries gained considerable traction since the planning of the project. Carbon Capture and Sequestration became more acceptable, while emission-rights are taken more serious than even three years ago. These developments influence the outlook and possible commercialization of geo-methanation. The availability of CO_2 to produce renewable gas will likely become increasingly scarce and therefore expensive. The political push for a hydrogen infrastructure in Europe diminishes the perceived value of methane over hydrogen with regard to the use of existing infrastructure. During this transitional period of methane becoming less and less demanded, while hydrogen, though on the rise, is not yet established to a point where it is feasible to switch infrastructure and industrial processes, geo-methanation could shine. With the achieved data and a further potential in enhancing the capacity and ability of the methanogen microbiome, geo-methanation might be the ultimate bridge-technology. Since geo-methanation works in depleted gas field, which makes up significant portions of the European gas storage capacities and is through the feed-rate of CO_2 very well controllable, the existing infrastructure could be, piece by piece, steered towards hydrogen. Gas storage sites with geo-methanation in this scenario handle the hydrogen to methane ratio in the adjacent gas grids, while producing at the same time renewable gas (given the use of green hydrogen and accordingly certified CO_2).

For the adaptation of the use cases “U-Store” and “power valley”, more granular energy projections would be needed, for each considered region or even down to single prosumers. In addition, the future electricity grid down to the lowest level and the policy of each regional or local grid operator would be needed to be researched. In Switzerland therefore, further information on the geology and/or political discussions about the value of security of supply of energy is needed, as the purely economic consideration of an inter-seasonal gas storage always will conclude in more economic options in the neighboring countries. In Austria and potentially further countries with a history of domestic natural gas production in Europe, the situation is different. The restricted flexibility in gas-mixtures by the restrictions on CO_2-ratios probably can be reduced in further research, which is already ongoing. Once the possibilities for further adaptations of the microbiome are better understood, the further course of action must be determined.